



HAL
open science

Influence of the fresh state properties of 3D printable concrete on the steel-concrete bonding and durability

Bilal Baz

► **To cite this version:**

Bilal Baz. Influence of the fresh state properties of 3D printable concrete on the steel-concrete bonding and durability. Civil Engineering. Ecole nationale supérieure Mines-Télécom Lille Douai; Université de Balamand (Tripoli, Liban), 2020. English. NNT : 2020MTLD0003 . tel-03229425

HAL Id: tel-03229425

<https://theses.hal.science/tel-03229425>

Submitted on 19 May 2021

HAL is a multi-disciplinary open access archive for the deposit and dissemination of scientific research documents, whether they are published or not. The documents may come from teaching and research institutions in France or abroad, or from public or private research centers.

L'archive ouverte pluridisciplinaire **HAL**, est destinée au dépôt et à la diffusion de documents scientifiques de niveau recherche, publiés ou non, émanant des établissements d'enseignement et de recherche français ou étrangers, des laboratoires publics ou privés.



THESE

**Préparée dans le cadre d'une cotutelle entre
IMT Lille Douai et L'Université de Balamand**

Présentée en vue d'obtenir

le grade de

DOCTEUR

en

Génie Civil

par

Bilal BAZ

Titre de la thèse :

**Influence of the fresh state properties of 3D printable concrete on
the steel-concrete bonding and durability**

Directeur de thèse: **Sébastien REMOND**

Co-directeur de thèse: **Georges AOUD**

Soutenu le 19 Novembre 2020 devant le jury d'examen

Président : **M. Roger LTEIF, Professeur**, Université Saint Joseph, Liban

Rapporteur : **M. Eric GRACIA-DIAZ, Professeur**, IMT Mines Alès, France

Rapporteur : **M. Ammar YAHIA, Professeur**, Université de Sherbrooke, Canada

Examinatrice : **Mme. Naima BELAYACHI, Maître de Conférences HDR**, Université d'Orléans, France

Examinatrice : **Mme. Khadija EL-CHEIKH, Docteur**, CSTC, Belgique

Examineur : **M. Didier LESUEUR, Docteur**, IMT Lille Douai, France

Co-directeur de thèse : **M. Sébastien REMOND, Professeur**, Polytech Orléans, France

Co-directeur de thèse : **M. Georges AOUD, Professeur**, University Of Balamand, Liban

Invité: **M. Philippe LEBLOND, Chef de pôle division structure, maçonnerie, partition**, CSTB, France

Ecole Doctorale SPI 072 (Lille I, Lille III, Artois, ULCO, UVHC, Centrale Lille, IMT Lille Douai)

ACKNOWLEDGMENTS

There are many people that I would like to thank for their direct and indirect contributions to this thesis. First and foremost, I would like to sincerely thank my thesis committee, represented by Pr. Roger LTEIF (Président, Université Saint Joseph, Liban), Pr. Eric GRACIA-DIAZ (Rapporteur, IMT Mines Alès, France), Pr. Ammar YAHIA (Rapporteur, Université de Sherbrooke, Canada), Dr. Naima BELAYACHI (Examinatrice, Université d'Orléans, France), Dr. Khadija EL-CHEIKH (Examinatrice, CSTC, Belgique), Dr. Didier LESUEUR (Examineur, IMT Lille Douai, France), and Mr. Philippe LEBLOND (Invité, CSTB, France), for giving their valuable time to guide and review this work. Their insight, feedback, and advice were influential and essential to get the best out of this thesis report.

To my thesis directors, Pr. Georges AOUAD and Pr. Sébastien REMOND, it is said that *“Better than a thousand days of diligent study is one day with a great teacher”*. Well!! Imagine how blessed I am for spending a three years journey, under your supervision, of nonstop learning and continuous guidance. Thank you from the deepest of my heart for your motivation, enthusiasm, immense knowledge and expertise in what is seen to be an uphill task, substantial effort, and most importantly your confidence in me. Thank you for creating such a supportive and cherishing educational environment that stimulated the best out of me.

I would like also to express my deepest gratitude to all people and colleagues who helped me in any manner, who have shared the effort and knowledge in order to make this work achievable.

Besides, it is my pleasure to strongly acknowledge IMT Lille Douai and the University of Balamand who offered me, together, the opportunity to purchase a PhD in Civil Engineering, under the Cotutelle program. Yet, a special thanks goes for the University of Balamand, who has embraced me since 2012, and from which I earned my Bachelor and Master Diplomas in Civil Engineering as well.

More than anything else, this thesis is dedicated to my parents, Adnan and Hilda, my sister Dima, and my future wife Yara, as well as to my extended family and family in law. I have to thank you for your love, support and endless sacrifices. Thank you all for giving me the strength to reach for the stars and chase my dreams. Thank you for being always by my side through all ups and downs. Thank you for bearing and tolerating my tense character and bad attitude during the past years. For my father and mother in particular, I am speechless in front of the greatness of your contributions. I know that there is no way to reward you. However, I believe that seeing your first lifelong project “me” holding a PhD makes it good. Yet, you and I as well, will be gladder and totally satisfied when your second one “Dima” gets to an end. Here is when you can say, with pride, that you have successfully made it. Which is why, I admit that I am where I am because of you.

As for the love of my life, Yara, from the day you walked into my life, you made me realize it was you who I was missing. You are my soulmate, my closest, truest friend, and the person I know that I can blindly count on. You were always my motivation, you stayed by my side to support me and lift my spirit up whenever I was down. Because of you I dared to dream big, and here it is, the dream became true. Truth be told, this is “our” achievement, and not only mine.

Last but not least, to all my friends, thank you for supporting and encouraging me throughout my journey. Your friendship makes me feel lighthearted. I cannot list all the names here, but you are always on my mind. However, there is an exceptional friend, although as a mentor, who I cannot move on without mentioning him. Georges AOUAD, not my thesis director, but my big brother and “Godfather” as my mother likes to call him. I had the privilege to meet you and ask for your academic guidance, without realizing that I was getting to know a forever friend. Your exceptional kindness and compassion can be rarely found in someone else. I can never repay you for what you have done, and still doing for me. Your supervision, advices, support and motivation are the reasons behind my success. Now, it is time to proudly say that our late nights and early mornings have paid off.

Success is no accident.

*It is Hard Work, Commitment,
Perseverance, Learning, Studying,
Sacrifice and most of all, Love of what you
are doing or learning to do.*

TABLE OF CONTENTS

LIST OF FIGURES	VI
LIST OF TABLES	X
GENERAL INTRODUCTION.....	1
CHAPTER 1: LITERATURE REVIEW.....	5
1.1- Evolution of The Construction Field.....	5
1.2- Future of Construction	6
1.3- 3D Printing Techniques in Construction.....	8
1.4- Current Situation of 3D Printing Applications.....	11
1.5- Materials Properties and Requirements.....	12
1.5.1- Fresh properties of Cementitious Materials	12
1.5.1.1- Description of The Material’s Physical Origin	12
1.5.1.2- Common Flow Behaviors and Rheological Models of Cementitious Materials	14
1.5.2- Rheometry	17
1.6- General Properties of 3D Printable Materials	17
1.7- Fresh State Requirements of 3D Printable Mortars.....	18
1.7.1- Flow Behaviour of 3D Printable Mortars.....	19
1.7.2- Rheological Requirements and States Transition of 3D printable Mortars.....	19
1.7.3- Thixotropic Models and Characteristics of 3D Printable Mortars	21
1.7.4- Measuring and Qualification of Mortars Early Age Properties and Printability.....	24
1.7.5- Rheological Problems and Object Failure During Manufacturing.....	25
1.7.6- Methods to Control The Rheological Properties.....	26
1.7.7- Effect of The Mix Composition on The Rheological Behavior of Printable Mortars.	27
1.8- Hardened State Properties of 3D Printed Elements.....	31
1.8.1- Mechanical Properties of 3D Printed Elements	31
1.8.2- Durability Properties of 3D Printed Elements.....	36

1.9- Reinforcement Approaches of 3D Printed Elements	37
1.9.1- Reinforced 3D Printed Elements.....	38
1.10- Sustainability and Life Cycle Assessment of 3D Printed Structures	42
1.11- Research Significance and Objectives	43

CHAPTER 2 : RHEOLOGICAL CHARACTERIZATION OF 3D PRINTABLE MORTARS47

1-Introduction.....	51
2-Materials and Methods.....	55
2.1- Raw Materials.....	55
2.2- Mix Design	56
2.3- Methods	57
2.3.1- Mixing Procedure	57
2.3.2- Printability Test	57
2.3.3- Fall-Cone Test	58
2.3.4 – Mechanical Performance.....	59
3-Results and Discussion.....	59
3.1- 3D Printing performance	59
3.2- Effect of High Range Water Reducer (HRWR).....	61
3.3- Effect of Viscosity Modifying Admixture (VMA).....	64
3.4- Effect of Limestone Filler.....	65
3.5- Effect of Water Content.....	67
3.6- Mechanical Performance	69
4-Conclusion	71

CHAPTER 3 : STRUCTURAL PERFORMANCE OF 3D PRINTED ELEMENTS IN FUNCTION OF THE MATERIAL’S RHEOLOGY AND PRINTING CONDITIONS 77

Part 1:

1-Introduction.....	81
2-Materials and Methods.....	83
2.1-Material Properties	83
2.2-Pull-Out test.....	87
2.2.1-Specimens preparation.....	86
2.2.2-Test setup preparation.....	89
3-Results.....	90
3.1-Material Results.....	90
3.2-Pull-Out Results	93
4-Conclusion	96

Part 2:

1-Introduction.....	101
2-Materials and methods	104
2.1- Mix design and material characterization.....	104
2.1.1- Mortar's composition.....	104
2.1.2- Mixing procedure.....	104
2.1.3- Printability assessment.....	104
2.1.4- Flow table test.....	105
2.1.5- Fall cone test.....	105
2.2- Specimen preparation for the pull-out test	106
2.2.1- Bar's geometry.....	106
2.2.2- Mixing procedure.....	106
2.2.3- Samples manufacturing.....	107
2.3- Mechanical characterization of the bond strength and testing procedure.....	111
3-Results and discussion.....	112
3.1- Flow table and fall cone results	112
3.2- Pull-out results	113

4-Conclusion	121
--------------------	-----

**CHAPTER 4 : DURABILITY ASSASSMENT OF 3D PRINTED
ELEMENTS IN FUNCTION OF THE MATERIAL’S RHEOLOGY AND
EXPOSED ENVIRONMENTS..... 127**

1-Introduction	130
2-Materials and Methods	132
2.1- Mix design and material characterization	133
2.1.1- Raw Materials	133
2.1.2- Mortar compositions	133
2.1.3- Mixing procedure	134
2.1.4- Printability assessment	134
2.1.5- Mechanical performance of mortars	134
2.1.6- Rheological characterization using the fall-cone test.....	134
2.2- Specimens preparation for the submersion in sulfuric acid solutions.....	135
2.2.1- Mixing procedure	135
2.2.2-Samples manufacturing.....	136
2.3- Sulfuric acid exposure.....	138
2.4- Macroscopic characterization.....	138
2.5- Microscopic characterization	139
2.5.1- Mercury Intrusion Porosimetry (MIP)	139
2.5.2- Scanning Electron Microscopy (SEM).....	139
3-Results and discussion	140
3.1- Mechanical performance of mortars	140
3.2- Fall-cone and thixotropy results.....	141
3.3- Macroscopic analysis and results.....	142
3.3.1- Shape deterioration and visual assessment.....	142

3.3.2- Mass loss	143
3.4- Microscopic analysis and results.....	146
3.4.1- Mercury Intrusion Porosimetry results.....	146
3.4.2- Scanning Electron Microscopy results.....	151
4-Conclusion and perspectives	158

List of Figures:

CHAPTER 1: LITERATURE REVIEW.....	V
Figure 1: Evolution of the Construction Field.....	6
Figure 2: 3D Printing Process and Model Translation [16]	7
Figure 3: Topology Optimization [24]	8
Figure 4: (Left) CyBe Construction (Right) XteeE Printers [29].....	9
Figure 5: (Left) COBOD (Right) Be More 3D Printers [29].....	9
Figure 6: (Left) Apis Core (Right) Construction 3D Printers [29].....	10
Figure 7: (Left) WASP [29] (Right) Cable Robot Printers [33].....	10
Figure 8: Difference Between (Left) Extrusion-Based [38] and (Right) D-Shape [39] AM approaches	11
Figure 9: Scheme of Couette flow [61]	13
Figure 10: Rheological Behavior of Non-Newtonian Fluids [66].....	14
Figure 11: Bingham vs Herschel–Bulkley Models [79].....	16
Figure 12: Variation of Shear Stress With Time [57]	16
Figure 13: Yield Stress Evolution Over Time [99]	21
Figure 14: Example of the yield stress evolution with time [102]	22
Figure 15: Yield Stress Evolution With Time: Perrot's Model Vs Roussel's Model [93].....	23
Figure 16: (Left) Layers Discontinuity and Surface Defects [120] (Right) Nozzle Blockage.	25
Figure 17: (Left) Plastic Collapse (Right) Elastic Buckling [121].....	26
Figure 18: Effect of W/C on the Yield Stress and Plastic Viscosity of Fresh Mixes [128]	27
Figure 19: Effect of of Silica Fume on The Material's Rheology [57]	28
Figure 20: Effect of Limestone on The Material's Rheology [127]	29
Figure 21: Effect of HRWR on The Material's Rheology [127]	30
Figure 22: Effect of VMA on The Material's Rheology [145].....	31
Figure 23: Applied Load With Respect to the Layers Orientation.....	32
Figure 24: Correspondence of All Printing and Material Parameters [156].....	33
Figure 25: Effect of the Layers Direction on The Compressive Strength of 3D Printed Elements [164].....	34
Figure 26: Effect of Time Gap on The Interlayers Strength [157].....	35

Figure 27: Effect of Surface Moisture on The Strength Between Layers [166]	35
Figure 28: (Left) River Revetment Wall [170] (Right) Coral Reef [171]	36
Figure 29: Flexural Strength of Fiber Reinforced 3D Printed Elements [50]	39
Figure 30: Bond Strength in Cast and Printed Concrete [179].....	40
Figure 31: Maximum Bearing and Deflection Capacity of 3D Printed Elements [188]	41
Figure 32: Comparision Between Printed and Full Solid Reinforced Concrete Beams [189].	41
Figure 33: Comparision of CO2 Emission Between Printable and COventional Concrete [200]	43

CHAPTER 2 : RHEOLOGICAL CHARACTERIZATION OF 3D

PRINTABLE MORTARS.....47

Figure 1: Particle Size Distributions for Sand, Cement, and Limestone Filler	56
Figure 2: Fall-Cone Test	59
Figure 3: Printed element using the Lab. Gun	60
Figure 4: Printed element (b, c) using the actual printer (a)	61
Figure 5: Yield stress variation for different HRWR concentrations	63
Figure 6: Effect of HRWR on the Structuration Rate.....	63
Figure 7: Yield stress variation for different VMA concentrations	65
Figure 8: Effect of VMA on the Structuration Rate	65
Figure 9: Yield stress variation for different filler concentrations	67
Figure 10: Effect of Limestone Filler on the Structuration Rate	67
Figure 11: Yield stress variation for different W/C	68
Figure 12: Effect Of W/C on the Structuration Rate	69

CHAPTER 3 : STRUCTURAL PERFORMANCE OF 3D PRINTED

ELEMENTS IN FUNCTION OF THE MATERIAL’S RHEOLOGY AND

PRINTING CONDITIONS 77

Part 1:

Figure 1: (top) printed beam (bottom left) Perpendicular loading (bottom right) Parallel loading.....	85
Figure 2: Casting molds for Pull-Out samples.....	87

Figure 3: Different printing methods	88
Figure 4: Printed Pull-Out sample before (left) and after (right) being confined.....	89
Figure 5: Non-printed sample with scraped surfaces before (left) and after (right) being confined.....	89
Figure 6: Pull-Out test set up	90
Figure 7: Compressive Strength at 3 Days	92
Figure 8: Compressive Strength at 28 Days	92
Figure 9: Pull-Out strength variation for all mixes.....	95
Figure 10: Bond profile when printing over the bar (left) and when inserting the bar after printing (right).....	96

Part 2:

Figure 1: Illustration of an indented bar [50]	106
Figure 2: 3-axis gantry printer	108
Figure 3: Conceptual printing path and bars layout	108
Figure 4: 3D printed Pull-out samples.....	109
Figure 5: Parallel and Perpendicular printed samples after being Cut.....	110
Figure 6: Confined Pull-out samples.....	110
Figure 7: Setup illustration	111
Figure 8: Pull-out testing system.....	112
Figure 9: Yield stress variation in function of time.....	113
Figure 10: Graphical presentation of the average and relative pull-out strength	115
Figure 11: Load-displacement relationship for non-printed samples.....	116
Figure 12: Load-displacement relationship for parallel samples	117
Figure 13: Load-displacement relationship for perpendicular samples	117
Figure 14: Broken printed element showing macroscopic voids	118
Figure 15: Schematic illustration of the voids creation.....	118

Figure 16: Nozzle's standoff distance variation.....	119
Figure 17: Pressure gradient over steel bars.....	120

**CHAPTER 4 : DURABILITY ASSASSMENT OF 3D PRINTED
ELEMENTS IN FUNCTION OF THE MATERIAL’S RHEOLOGY AND
EXPOSED ENVIRONMENTS..... 127**

Figure 1: 3-axis gantry printer.....	136
Figure 2: Printed sample of each mix.....	137
Figure 3: Testing sample	137
Figure 4: Specimens of the same mix placed inside a plastic container	138
Figure 5: Schematic illustration of SEM samples	140
Figure 6: Yield stress variation in function of time for Mix A	141
Figure 7: Yield stress variation in function of time for Mix B.....	142
Figure 8: Yield stress variation in function of time for Mix C.....	142
Figure 9: Progressive damage of printed and non-printed samples in 1% acidic solution.....	143
Figure 10: Progressive damage of printed and non-printed samples in 3% acidic solution ...	143
Figure 11: Mass loss of printed and non-printed concrete samples exposed to a solution containing (a) 1% and (b) 3% sulfuric acid	145
Figure 12: Pore size distribution of printed and non-printed elements Mix A	148
Figure 13: Pore size distribution of printed and non-printed elements Mix B	149
Figure 14: Pore size distribution of printed and non-printed elements Mix C	150
Figure 15: Microstructure of the non-degraded / non-printed sample Mix A	152
Figure 16: Microstructure of the non-degraded / printed sample Mix A	153
Figure 17: Microstructure of the degraded / non-printed sample after 56 days of exposure Mix A	155
Figure 18: Closer view of the zone attained by the acid and the gypsum precipitation Mix A	156
Figure 19: Microstructure of the degraded / printed sample Cut side 1 after 56 days of exposure Mix A	157
Figure 20: Microstructure of the degraded / printed sample Cut side 2 after 56 days of exposure Mix A	157

List of Tables:

CHAPTER 2 : RHEOLOGICAL CHARACTERIZATION OF 3D PRINTABLE MORTARS	47
Table 1: Mixes compositions (mass in grams).....	57
Table 2: Compressive strength of all mixes	70
CHAPTER 3 : STRUCTURAL PERFORMANCE OF 3D PRINTED ELEMENTS IN FUNCTION OF THE MATERIAL’S RHEOLOGY AND PRINTING CONDITIONS	77
Part 1:	
Table 1: Mixes compositions	84
Table 2: Workability Characteristics.....	91
Table 3: Pull-Out results.....	94
Part 2:	
Table 1: Surface geometry specifications of the indented bars.....	106
Table 2: Detailed pull-out results	114
CHAPTER 4 : DURABILITY ASSASSMENT OF 3D PRINTED ELEMENTS IN FUNCTION OF THE MATERIAL’S RHEOLOGY AND EXPOSED ENVIRONMENTS.....	127
Table 1: Chemical and mineralogical composition of cement	133
Table 2: Relative mixes compositions.....	134
Table 3: Total Porosity.....	146
GENERAL CONCLUSION.....	165
PERSPECTIVES.....	169
REFERENCES.....	171

GENERAL INTRODUCTION

In the shade of the population growth and construction practices evolution since the early ages, different techniques have been developed and adopted to properly serve the growing needs for habitats. Hence, the construction sector has been one of the most challenging sectors facing the growing economics across the globe. Indeed, there was an urgent need to further improve this field, especially on the environmental and socio-economical levels. Accordingly, an outstanding shift has been done towards the automation in construction, for all the benefits that it could bring to the field. Some of these benefits displays a higher and faster supply of housing, a reduction in the construction cost, and most importantly a higher resource efficiency by reducing the number of workers, and amount of wastage produced.

Nowadays, the latest automated construction technique is known as Additive Manufacturing or 3D printing. Though, this technique is still under development, and it brought attention in both academic and industrial applications. However, the most important challenges that encounters 3D printing are the fresh and hardened state properties of the cementitious material used for printing; and the reinforcement strategy to provide ductility and tensile capacity for structural elements. Hence, these issues must be fully addressed, and continuously developed in order to keep up the success earned by this technology.

Concerning the challenges imposed by the material used for 3D printing applications when still in its fresh state, it must present two prime characteristics in order to be considered printable. These characteristics are extrudability and buildability. Extrudability is the ability of the material to circulate inside the system and get out of the nozzle without blocking it, or exhibiting segregation problems. Meanwhile, buildability refers to the ability of the material to preserve its shape after being printed, in addition to being capable of withstanding the imposed loads coming from superposed layers. In this regard, printable materials require a better understanding of their rheological properties, especially those related to the buildability characteristic. This is said because buildability is the most fundamental aspect that makes a successful printing process. Consequently, it should be accurately monitored in order to avoid any deformation or failure during printing. Technically, the corresponding rheological phenomenon that describes

buildability is referred to by thixotropic behavior, which accounts for the material's shear stress evolution with time, responsible of its hardening and early strength.

Another issue that has to be investigated is the reinforcement of 3D Printed elements used for structural applications. This issue can no longer be omitted, and it has to be extensively investigated. This is said because the lack of reinforcement makes it harder for this technology to locate itself among conventional construction methods. Therefore, many approaches have been developed, and different reinforcing techniques were exploited to determine the most convenient method that suits more the constraints imposed by 3D printing. However, conventional reinforcement using steel bars can never be surrendered. Though, despite the procedure used to incorporate reinforcing steel inside the elements, a proper interaction between the reinforcement and printed layers should be provided. In this context, a strong link between both materials (steel and mortar) should be ensured in order to achieve a coherent and monolithic response against externally imposed structural loads.

Apart from the material's rheology and reinforcing adequacy, the durability performance of 3D printed concrete elements must be taken into consideration as well. Owing to the exponential increase of 3D printing applications, printed elements became more subjected to aggressive environments due to their field of applications, such as for underground and infrastructure constructions, in addition to many other uses. Thus far, the concept of layers stacking, and the fact of creating interfaces between successive layers might create weak planes, giving rise to additional paths for the intrusion of substances from the surrounding environment. Certainly in such cases, the degradation of concrete and corrosion of reinforcement might be further accelerated, leading to the whole deterioration of the printed element. Therefore, the durability behavior of printed elements, exposed to aggressive environments must be carefully assessed.

This thesis covers certain topics related to the fresh and hardened state properties of 3D printed elements. Precisely, it deals with the fresh state properties of the material and their effects on the hardened state and mechanical response of 3D printed elements. Thus, as a first step, the rheological characteristics of different printable mixes was assessed, and the effect of some chemical and mineral additives was considered. The rheological parameter studied in this research corresponded to the yield stress of the material, and it has been measured using the Fall-Cone test

over a specific period of time. Then after, the equivalent structuration rates were derived, and the proper thixotropic model was fitted to each category of mixes.

Afterwards, a research campaign was performed to study the influence of the material's fresh state properties on the structural capacity of 3D printed elements. On this subject, an initial study has been performed concerning the effect of the material's workability on the link developed with printed mortar. A series of pull-out tests has been conducted first over manually printed concrete elements. In the same perspective, a different set of samples printed using an automated 3-axis gantry printer were tested similarly. In this context, the effect of the printing method and the layers direction with respect to steel bar were thoroughly investigated.

On top of that, this research targeted the effect of the material's fresh properties on the durability performance of 3D printed elements. Hence, a proper experimental campaign has been established to characterize the ability of printed elements to resist chemical attacks. Therefore, samples having different compositions were exposed to sulfuric acid environments. Later on, all samples were characterized on a macro and micro scale levels.

CHAPTER 1 : LITERATURE REVIEW

1.1- Evolution of the Construction Field

Thousand years ago, people roamed from place to place looking for animals to hunt and plants to feed on. They did not build houses or shelters since they were always moving. They slept under the stars, got wet under the rain, sweated under the sun and cooked their meals over open wood fires [1]. Much later on, the early humans began to put up shelters, tents made of animal skins, and tried to protect themselves from the weather. A few more thousand years, humankind had discovered agriculture, and people slowly began to learn a new way of getting food. Once they found ways letting them stay in one place, they started thinking about building shelters that were larger, stronger and more comfortable [2]. In this context, building materials and construction methods started to develop consecutively [3].

“Technology is rooted in the past, dominates the present and extends to the future” [4]. Until now, the continuous evolution of all construction techniques in terms of technical and technological developments, implicitly includes the knowledge and experience inherited from early humans as the ancestors passed them down to descendants for the future [2]. In other words, the development of all modern construction techniques and new materials are always related to the traditional ones (Fig. 1). Thus, building technology will constantly develop, and it will never stop or disappear [5]. Previously, all construction procedures were naturally acquired by experience and the lessons learned from practice. By that time, craftsmen had inborn ways to solve engineering problems [6]. However, meanwhile the only driving forces behind the development of construction techniques are science and technology. Many new possibilities are found to enhance the conceptual design of concrete structures, as well as their detailing and production. On top of that, the implementation of digital technologies in the construction field allowed overcoming most of the typical constraints imposed by traditional processes. However, digital construction for large-scale application and mass-market production is still a persisting challenge [7][8]. The arising obstacles are analogous to those previously found after each invention of a new concept. Though, it is expected that before putting into service any newly developed technique, and before the concept reaches maturity, several decades of research and small scale applications must elapse [9].

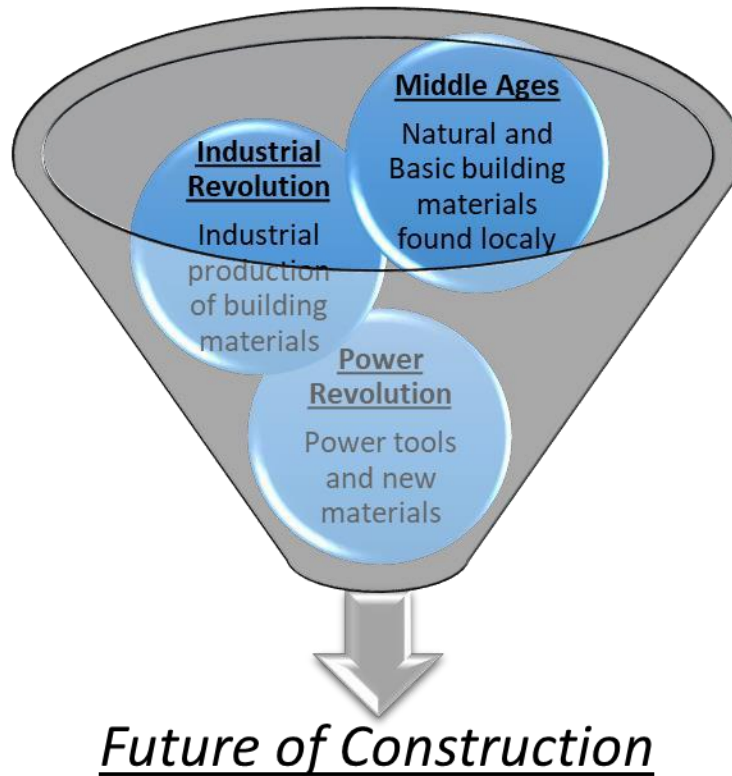


Figure 1: Evolution of the Construction Field

1.2- Future of Construction

The construction sector is currently taking advantage of the digitalization and automation of different building techniques. The major benefits of bringing automation to the field are to reduce the construction time, labors work, environmental impact and energy consumption, and improve the quality of the product. In addition, it eliminates all geometrical constraints imposed by traditional construction practices [10]. In light of that, a new concept has been introduced based on the principle of Additive Manufacturing (AM). This principle also known as 3-Dimensional Printing (3DP) is defined as the process of adding materials to make objects from 3D model data by laying down successive layers on top of each other [11]. Though, 3DP became a revolution by itself, not only for its manufacturing concept, but for its endless production conditions that can be only limited by imagination [12][13]. More specifically, a new chapter in building technology has started since 2014 as the first house was completely printed [14].

Normally, the printing process involves several steps. These steps start by converting the 3D-CAD model showing the object to be created into a Standard Triangulation Language (STL) format, in a process known as slicing. The STL file contains all the information needed to represent the digital

model in 2D Cartesian coordinate layers. Then after, a list of commands that the printer can understand is established, and fed to the printer through a proper data system to launch the printing process. At the end, a physical model is produced [15] (Fig. 2).

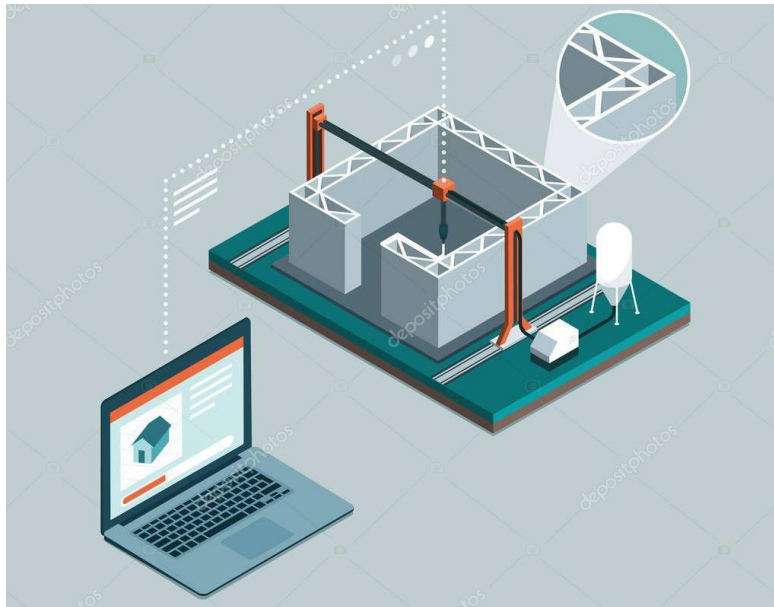


Figure 2: 3D Printing Process and Model Translation [16]

While 3DP is growing rapidly, there are many concerns about the properties of the printed object, because the manufacturing process is completely different from other conventional methods. In conventional construction techniques, concrete is poured inside a customized mold in order to give it the desired shape. Whereas, 3DP do not require any formwork to support concrete layers. This fact disclosed endless possibilities for architects, which makes them totally free of any typical geometrical design constraints. 3DP opened a new realm of design by offering the ability to use curvilinear forms, rather than being restricted to rectilinear forms due to several limitations [17][18][19]. Apart from aesthetics, it is commonly known that straight edge forms are one of the weakest structural forms. However, curvilinear shapes are the strongest. For example, the humble egg having a simple and consistent curve is one of the most efficient structures in nature [18]. Put differently, 3D printing provides optimization in the design which can further help designing efficient structures, and therefore saves materials. One method is the topology optimization which results in a complex geometrical form (Fig. 3). Accordingly, 3D printing is the most suitable

technique to implement the corresponding design. It is used to distribute a limited amount of the material in a predetermined design space. Precisely, the material is deposited in a way that the resulting structure complies with the boundary conditions, such as the acting loads and the resulting load bearing capacity. Thus, 3DP allows the use of less material in a smarter approach, only where it is needed [20][21][22][23].

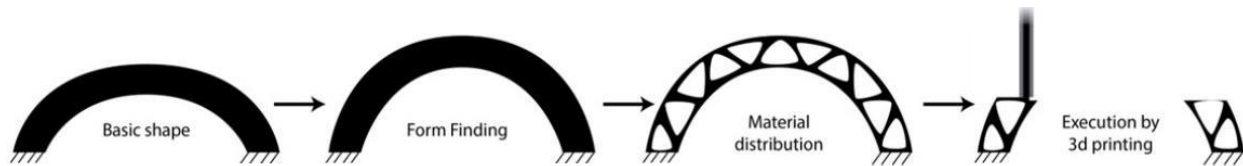


Figure 3: Topology Optimization [24]

As a matter of principle, a successful 3D printing application in the construction field would lead to more sustainable structures, as well as notably decrease the total cost of the project. This is said because 3DP does not use neither formworks, nor too many labors, which makes worth 50% of the total cost, apart from the reduction in waste material and energy consumption [25]. In addition, time is money as well, thus 3DP is an extremely fast process that takes only several hours/days due to the continuous work of the printer.

1.3- 3D Printing Techniques in Construction

Different printing technologies have been developed to print concrete elements and structures having different sizes, and under different conditions [26]. Different robotic technologies are used depending on the size and function of the element to be printed [27]. The size of a printed object might vary between small elements inside a building, moving to a fully functional construction such as a small family home, straight up to a large-scale multi-level building. For the case of printing independent elements or small houses, the most commonly used technologies are multi-axis robotic arm, gantry frame, or overhead bridge, involving external pumping system having a maximum capacity of several cubic meters [28]. For example, the Dutch company CyBe Construction, and the French company XtreeE are able to print small concrete structures using a 6-axis robotic arm (Fig. 4). Besides, the Danish-based 3D printing company COBOD, and the Spanish company Be More 3D, use a gantry frame and overhead bridge to make their printings (Fig. 5).



Figure 4: (Left) CyBe Construction (Right) XtreeE Printers [29]



Figure 5: (Left) COBOD (Right) Be More 3D Printers [29]

Yet, scaling-up towards printing multi-story buildings still needs development. Such volume of constructions requires adaptation of equipment. Even so, several alternative solutions are being developed, such as the use of fixed cranes or crane trucks [30], and robot with cables [31][32]. For example, the Russian company Apis Cor developed a 3D printer that could build a house in just 24 hours, and in extreme weather conditions. The printer covers initially a printing surface of 132 m² and it can be easily transported on a mobile crane. Apis Core was able to print a building located in Dubai of 640 m², reaching a height of almost 10 m, in 17 days. Similarly, the French company Construction 3D, uses the concrete crane printer to print large structures (Fig. 6). In the same

context, the Italian manufacturer WASP has developed one of the largest 3D printers called the Crane WASP that is 12 m tall and 7 m wide. On the other hand, German researches displayed a show-case cable-driven robot that moves over long distances across four cables (Fig. 7).

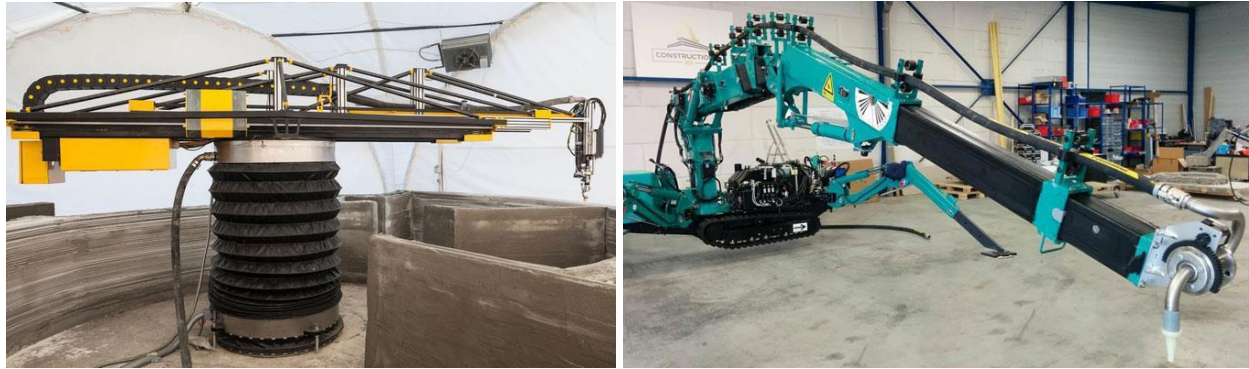


Figure 6: (Left) Apis Core (Right) Construction 3D Printers [29]

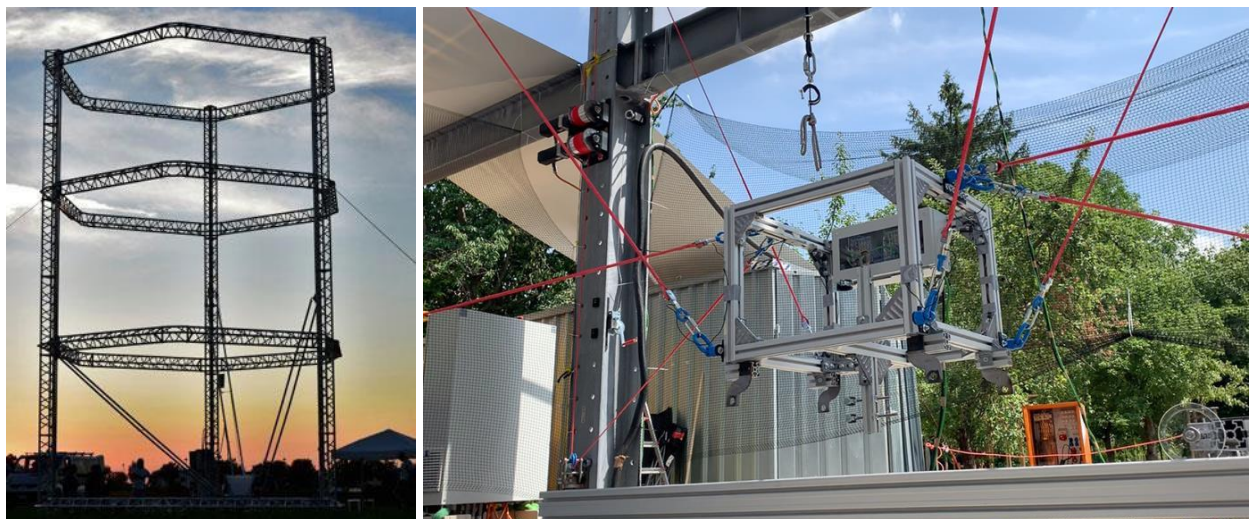


Figure 7: (Left) WASP [29] (Right) Cable Robot Printers [33]

Currently, there are two major additive manufacturing processes using concrete materials, applied in the construction and architectural industry. These approaches are the Extrusion-Based Technique known as Fused Deposition Modelling (FDM), and the Powder-Bed / D-Shape printing (Fig. 8). The common feature between both of them is the production of 3D objects additively [34][35]. However, each method has been developed for distinct application purposes. These processes print objects either through pumping and extrusion of concrete, or by powder deposition and selective binding. Precisely, the Extrusion-Based technique consists of extruding concrete material out of a nozzle mounted on a gantry frame. The printing process is done by continuously

depositing mortar filaments, one on top of other. Whereas, Powder-Bed printing consists of jetting a liquid binder selectively on an existing powder layer [36][37].



Figure 8: Difference Between (Left) Extrusion-Based [38] and (Right) D-Shape [39] AM approaches

In the year 2012, the development of 3D printing of concrete elements in the construction field has turned from being a linear progression to a quasi-exponential one [40][41]. Many showcases have been presented all over the world on a regular basis. Some noteworthy examples include: the office building in Dubai, measuring 250 m², the two-storey house measuring 400 m², the Five-Storey apartment building, and 1100 m² Villa, all in china, the Landscape house and Canal House in the Netherlands, the ProtoHouse in the United Kingdom, and much more [14][42].

1.4- Current Situation of 3D Printing Applications

Most of the Additive Manufacturing methods used for construction applications are still considered relatively new to the field. Though, a constant research effort is always in the process to illuminate the fundamental understanding of the new technology, and reach its maximum potentials [42]. Unsurprisingly, different techniques have been developed during the past years. Yet, 3D concrete printing cannot be considered as an isolated solution for conventional construction strategies [43][44]. Looking at the current state of 3D printing, there is still not enough understanding of all performance properties related first, to the rheological behavior of the printable material used; and second, to the mechanical and structural efficiency of a printed element [45][46][47]. For the time being, there is still a lack of normative regulations and performance testing protocols for the digital production of printable mixes, and printed structures [27][48]. Though, the current standards and regulations must be revised and further adapted to be

applied to 3D printing applications. Up to now, all construction codes consider that concrete elements are homogeneous [49]. However, this fact cannot be applicable for 3D printed concrete elements, due to their anisotropic behavior [50][51]. The layering concept affects the performance of a printed concrete element significantly. The interfaces between successive layers influence the mechanical performance, bond behavior, durability, and bearing capacity of the element used for structural applications.

1.5- Materials Properties and Requirements

1.5.1- Fresh properties of Cementitious Materials

The fresh state properties of mortars are the most essential parameters used to control the quality of the mixes. These fresh properties help in defining the purpose and mode of application of each mix [52]. Accordingly, each mix design has to meet certain requirements and specifications when still being in its fresh state, depending on its intended application. These characteristics are known as rheological properties. In its turn, rheology refers to the physics that studies the deformation and flow of matters. Though, rheology is paramount for all highly engineered cementitious materials, especially for those used in additive manufacturing and 3D printing applications [52][53][54][55].

The term rheology was found by Bingham in 1920, and it was considered one of the most important tools used to characterize the cement-based materials [56]. Mainly, the rheology of all cementitious materials entails different parameters, namely viscosity, plasticity, and elasticity, derived from the applied shear stresses [57]. In this regard, rheology has been considered as the most effective tool to characterize the workability and stability of the material, and to predict its flow behavior [57].

Besides, one of the principle rheological phenomenon for all cement-based materials is known as thixotropic behavior, which corresponds to the ability of the material to build-up an internal structure when being at rest [58]. Precisely, thixotropy is a time dependent process that accounts for the change in the microstructure of a colloidal suspension and particle agglomeration, whether at a constant or increasing shear stress [52][59].

1.5.1.1- Description of The Material's Physical Origin

In general, the mostly used techniques to evaluate the rheology of a material are based on the couette rheometry, to describe the relation between the shear stress (τ) and shear rate ($\dot{\gamma}$) (the shear rate is the derivative of the shear deformation (γ) in function of time (t), $\dot{\gamma}(x,t) = \frac{d\gamma(x,t)}{dt}$) [60].

Mainly, the couette flow describes the flow behavior of a viscous fluid being sheared between two surfaces of infinite extent, separated by a distance (h), one of which is stationary and the other is moving at a constant velocity (V). Herein, the velocity distribution follows a plane laminar movement, resulting in a linear law (Fig. 11). Theoretically, two particles infinitely adjacent, located at a distance (x) and vertically separated by a distance (d_x) at a given time (t), will have a displacement of $u_{(x,t)}$ and $u_{(x,t)} + du_{(x,t)}$ respectively after a certain period of time equal to $(t + d_t)$. The induced shear deformation (γ) of the material at time $(t + d_t)$, is calculated following Eq. 3:

$$\gamma_{(x,t)} = \frac{du_{(x,t)}}{d_x} \text{ (Eq. 3) [61]}$$

On the other hand, the resulting shear rate ($\dot{\gamma}$) is a function of the material's velocity (V), derived using Eq. 4:

$$\dot{\gamma}_{(x,t)} = \frac{dV_{(x,t)}}{d_x} \text{ (Eq. 4) [61]}$$

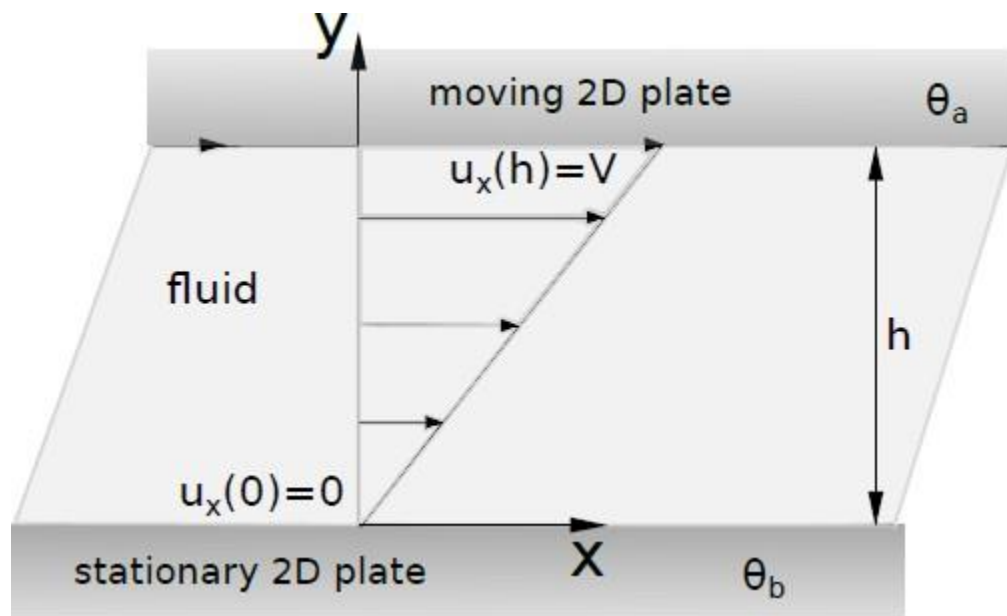


Figure 9: Scheme of Couette flow [61]

f o
C g
o i
u c
e a
t l
t B
e e
h
f a
l v
o i
o

1.5.1.2- Common Flow Behaviors and Rheological Models of Cementitious Materials

As mentioned earlier, rheology is also concerned by the flow behavior of the matters. However, the numerical description and prediction of the flow behavior of cement-based materials is complicated, due to the complexity of the material's composition. This is said because mortars contain not only particles having different sizes (ranging between μm to mm), but also experience chemical reactions, known as cement hydration, causing behavioral variations with time [57].

In fact, these materials are generally non-Newtonian fluids, and can exert different behavioral aspects (Fig. 9). Typically, non-Newtonian fluids do not present a linear variation of stresses with respect to the applied shear rates, and sometimes do not start from the origin ($\tau_0 = 0, \dot{\gamma}_0 = 0$) [62]. Precisely, in a Newtonian fluid, the viscosity is always constant across all shear rates, starting from the origin, but in a non-Newtonian fluid, the relation between the shear stress and the shear rate is different. Therefore, a constant coefficient of viscosity cannot be defined [63][64]. Hence, in order to make things easier, the corresponding flow behavior of any cement-based material can be estimated using different models approach [65].

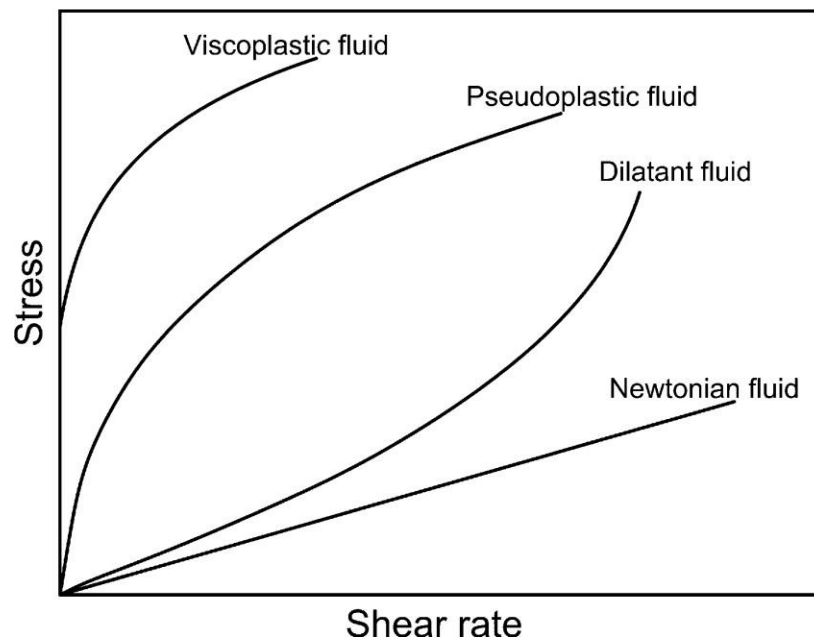


Figure 10: Rheological Behavior of Non-Newtonian Fluids [66]

Precisely, cement pastes are colloidal suspensions inside which the particles interactions form various microstructures. Different types of macroscopic flow behavior occur, depending on how such microstructures respond to an applied shear stress or strain rate [67][68][69]. There are

different ways of describing the steady state flow of fresh cement pastes, such as Bingham, Herschel–Bulkley, Ellis, Casson or Eyring rheological models [70][71]. However, it is demonstrated that the classical yield stress models (Bingham and Herschel–Bulkley) are the most adapted models [72] (Fig. 10). Though, the Bingham model is the most used one, and it was commonly agreed that the fresh mortar can be classified as a Bingham fluid in terms of their rheological properties [73][74]. With this assumption, the rheological performance of such materials is correlated to the yield stress and plastic viscosity uniquely, and they are the only parameters to characterize the flow curve within a range of shear rates [63].

However, apart from the Bingham model, the Herschel–Bulkley fluid model is characterized by three parameters: yield stress (τ_0), consistency factor (k), and an exponent (n) relating the shear stress to the corresponding shear rate [76]. This model is described in Eq. 2, and compared to the Bingham model in Fig. 10. Though, it is worth noting that the Herschel–Bulkley model can resume to the Bingham model, when the exponent (n) is equal to 1 [77][78].

$$\begin{cases} \dot{\gamma} = 0 & \text{if } \tau < \tau_0 \\ \tau = \tau_0 + k\dot{\gamma}^n & \text{if } \tau \geq \tau_0 \end{cases} \quad (\text{Eq. 2}) [76]$$

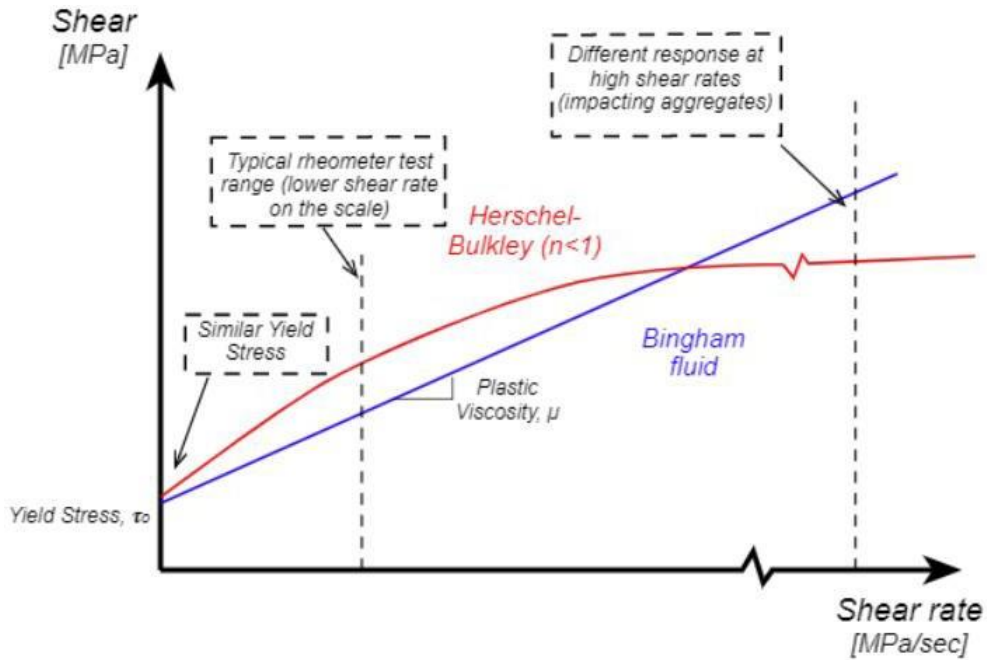


Figure 11: Bingham vs Herschel–Bulkley Models [79]

Apart from that, the yield stress prescribing the performance of the fresh materials is dictated by the static yield stress, dynamic yield stress and plastic viscosity. When the shear stress reaches the static yield stress, the material flows. Then after, when the material flows, the static yield stress decreases to the level of dynamic yield stress in order to preserve a constant flow rate (Fig, 12) [80]. Besides, plastic viscosity is the resistance against the flow of the material. Normally, the described response to the applied stresses applies over the material’s flow behavior initially at rest.

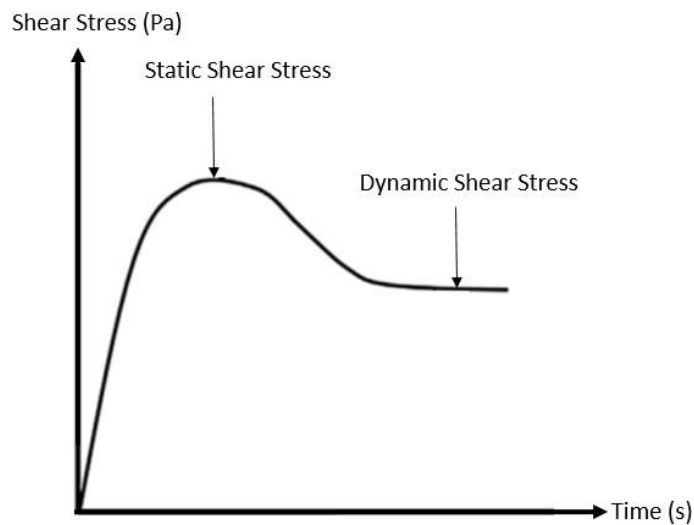


Figure 12: Variation of Shear Stress With Time [57]

Indeed, many factors affect the overall rheology of a material and its flow, mainly the interaction forces between colloidal particles, particles separation and effects such as jamming, spacing, surface area and roughness [57][81][82]. As well, the properties of fresh concrete are attributed to the inter-particle forces such as the van der Waals and electrostatic repulsive forces [83][84].

1.5.2- Rheometry

As previously describes, the rheological behavior of the Newtonian materials totally differs from that of non-Newtonian materials. It is more complicated for non-Newtonian materials to be characterized, and it is widely acknowledged to be far from straightforward. Nonetheless, the rheological measurements of cement-based materials are even more complicated due to their variations across time [66].

Rheological measurements are most commonly performed using rotational shear rheometers. Though, conventional rheometers have different geometries, but in all cases, the material gets sheared between two surfaces [85]. Several examples of these rheometers are the simple rotational viscometer Brookfield type, the parallel plate rheometer, the cone and plate rheometer, the capillary rheometer, and the concentric cylinders rheometer.

In general, rheometers are the most accurate devices used to measure the rheology of cement-based materials. However, they are not popular outside the laboratory. They are subject to many drawbacks, which are the cost, immobility (size and weight), and time consuming. In addition, rheometers are difficult to use, they need skilled operators. What is even more important is that rheometers are mostly designed for homogeneous materials, containing no particles [63]. They are not adapted for materials containing large aggregates, such as mortar and concrete [74]. In fact, there are still different methods that are much easier and practical to be performed over mortars and concrete, on-site, and without the need of skilled operators. Some of these methods are the slump slump-flow test [86] [87], and the inclined plane [88]. Though, in practice, these methods show certain shortcomings especially that they are not capable of directly measuring the intrinsic rheological parameters of the material.

1.6- General Properties of 3D Printable Materials

In general, all cementitious materials have a very sensitive physico-chemical behavior [27][89]. The evolution of the material's strength starts by the hydration reactions between anhydrous cement particles and water. This reaction generates C-S-H bridges between cement particles.

However, the physical aspect of the material's strength evolution refers to the setting of the material, which corresponds to the hardening and acceleration of the hydrates formation [89]. Particularly, when the material is used for 3D printing applications, this behavior has a major importance on the overall performance of a printed object [52].

The material used in 3D printing must provide a balance between different fresh properties, and therefore comply with very basic requirements in order to be considered printable [80][90]. The key properties for a printable mortar are extrudability, and buildability. Extrudability, is defined as the ability of the material to be workable and flowable enough to get out of a nozzle without blocking it or the conduits. It should maintain a smooth flow rate during the pumping process to allow a constant layer's printing [91]. Whereas, buildability is the ability of a printed layer to retain its shape after being printed, and to withstand the load coming from superposed layers without showing any deformation [91]. Buildability is considered as the first stiffening stage of the material, where it must present a fast setting rate, yet still be suitable to provide good bond between successive layers to form a homogeneous component without the risk of forming cold-joints between layers [27].

Over and above, the evolution rate of the material's stiffness over time makes a critical parameter as well. Indeed, it must be perfectly controlled in order to guaranty a smooth development of the printed structure [52]. Thus, the overall phenomenon involves not only the control of the material's behavior in its fresh state (printability), but also following up the changes over time, after being placed.

1.7- Fresh State Requirements of 3D Printable Mortars

As previously explained, 3D printing is considered as the most widely used digital construction method of concrete structures [92]. Precisely, this construction technique is divided into two major steps. The first step consists of pumping and extruding the material, whereas the second step depends on its deposition. Accordingly, in order to ensure a good flow of the material during the first step, and a strong stability during the second step, the material must have complete control over its rheological properties, and it must remain homogeneous all over the process. On one hand, the printable material must have sufficient fluidity during the first step to be pumped properly. On the other hand, it must be stiff and firm enough to allow its shape stability once deposited. These

contradictions in the behavior of the material require particular rheological properties in order to carry out a proper printing process [80].

Physically speaking, a transition must take place between the first and the second step of the printing process. The material must undergo a state transition from liquid-like behavior (during pumping) to solid-like behavior (after deposition). This transition is the core aspect that printable concrete must present [93][94]. Therefore, for an adequate understanding of the material's paradigm, it is necessary to provide a clear mechanical description of its fresh state directly after mixing, up-until a certain time after being printed.

1.7.1- Flow Behaviour of 3D Printable Mortars

Generally, this type of material displays an apparent viscosity that decreases with increasing shear rate [62]. Still, when it is at rest, it behaves as a plastic solid [95]. Alternatively stated, such material deforms elastically, and flows like a stiff body when the external stresses are smaller than the static yield stress. Therefore, the flow curve are most likely to be non-linear. As a consequence, such material do not level out (change its shape) under gravity. Even more, it was confirmed that when the material is at rest, it consists of three-dimensional structures of sufficient rigidity to resist certain externally applied load [62][96].

1.7.2- Rheological Requirements and States Transition of 3D printable Mortars

Unlike polymer printable material, the transition from plastic to solid behavior of cementitious mortars is not achieved by a sudden change of temperature [97][93]. Indeed, this state-transition completely relies on the kinetics of the mechanical structural build-up of the material, resulting from the chemical reactions and activity of cement in water.

The internal structure of cement-based materials goes through different modifications over different levels. Effectively, fresh mortars undergo a progressive change in their physical, rheological, and chemical characteristics [27]. In addition, the rheology of cement pastes is derived initially from the cement particles that flocculate and form a network of interacting particles. This phenomenon, so-called flocculation, allows for the material to display an initial yield stress, enabling it to resist external stresses just after being deposited [59]. At that instant, the material keeps on developing and organizing its internal structure for several tens/hundreds of seconds, before reaching its final configuration [59]. Simultaneously, when the material is still in its dormant phase, the nucleation of the hydrates occurs. This phenomenon corresponds to the

formation of more solid hydrate bridges. As a matter of fact, the structuration phase of the material takes place, coming from the increase of the size and numbers of hydrates bridges between percolated cement particles.

Particularly, in the case of 3D printing, when the layer has been deposited, an adequate yield stress must be reached. This stress must sustain first the gravity stresses, then after the additional stresses coming from subsequent layers. Though, by successively depositing layers, these stresses progressively increase. Accordingly, in order to prevent the collapse of the printed element, the yield stress of the material shall proportionally increase as well, during a critical timeframe. Therefore, in order to monitor the gravity-induced stresses over the most loaded layer (bottom layers), the yield stress must be correlated to the density of the mix used (ρ), the gravity constant (g), and to the current / final height of the printed element (h “ongoing height”, H “total height”), as described in Eq. 5.

$$\tau_{0,0} = \frac{\rho g H}{\sqrt{3}} \text{ (Eq. 5) [98]}$$

The overall phenomenon, since the deposition of the layer until the completion of the whole structure is further represented in Fig. 13:

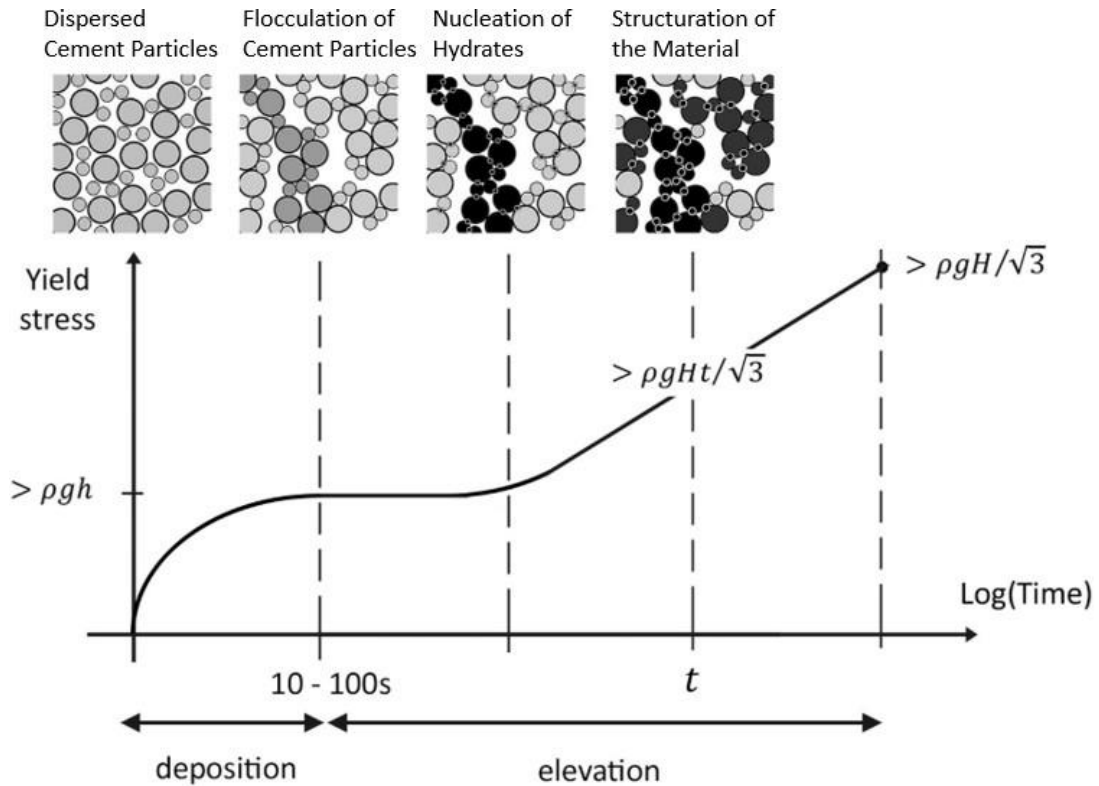


Figure 13: Yield Stress Evolution Over Time [99]

1.7.3- Thixotropic Models and Characteristics of 3D Printable Mortars

The controlling rheological phenomenon for printable mortars is their thixotropic behavior. When the material is deposited, it exhibits an initial yield stress, and a critical yield strain. However, at rest, the yield stress increases whereas the shear strain decreases. This fact makes the material stronger and more rigid with the increasing time, and it is attributed to the material's thixotropic behavior (Fig. 14) [100][101].

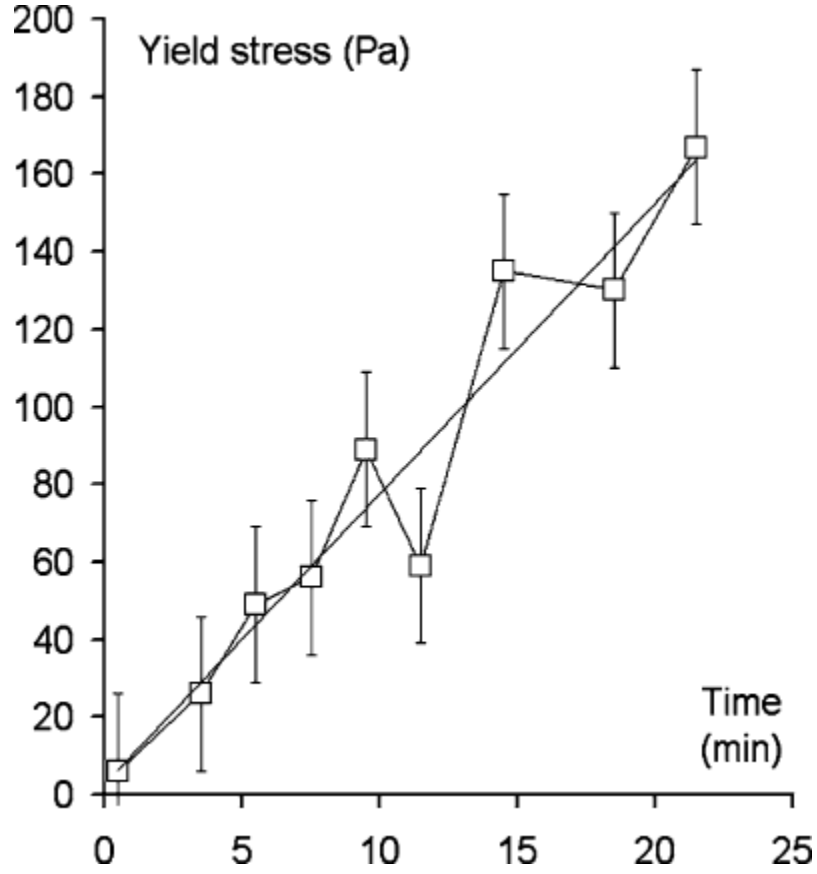


Figure 14: Example of the yield stress evolution with time [102]

The mechanical behavior of a freshly printed element is dictated by the structuration rate, corresponding to the increasing static yield stress of the material over time, after the layer's deposition, and it is designated by (A_{thix}) [52]. However, there are two prime models used to describe and predict the structuration rate of the material (Fig. 14). Roussel [103] explains that during the first hour, the increase is often considered to be linear, and can be written as shown in Eq. 6. Though, at $t = 0 \text{ sec}$, the initial stress $\tau_{0,0}$ is negligible ($\tau_{0,0} \approx 0 \text{ Pa}$) when compared to the shear stress developed when the mix is at rest [59][103][104]. Therefore, the static yield stress can be presented in a simplified form, as shown in Eq. 7.

$$\tau_0(t) = \tau_{0,0} + A_{thix}t \quad (\text{Eq. 6}) [103]$$

$$\tau_0(t) = A_{thix}t \quad (\text{Eq. 7}) [103]$$

However, Perrot et al. [105] offered a more elaborated model showing that beyond that period (first hour), the increase of the yield stress accelerates, and the kinetics of the structural build-up changes from linear to exponential (Fig. 15), as shown in Eq. 8. It is worth to mention that, Perrot's model tends to be linear over a short period of time as well (for $t = 0 \text{ sec}$). Though it further includes a critical time characteristic (t_c) used to describe the static yield stress evolution over longer periods. Physically, this change is attributed to the beginning of the setting process of the material, causing an increase in the solid volume fraction [93][105][106].

$$\tau_{0(t)} = A_{thix} t_c \left(e^{t/t_c} - 1 \right) + \tau_{0,0} \quad (\text{Eq. 8}) [105]$$

Indeed, these models can be used to set the optimal printing time (t_H) and speed (V) to guarantee the stability of the structure, as in Eq. 9 and Eq. 10 respectively [97].

$$A_{thix} = \frac{\rho g H}{\sqrt{3} t_H} \quad (\text{Eq. 9}) [97]$$

$$V < \frac{\sqrt{3} L A_{thix}}{\rho g h} \quad (\text{Eq. 10}) [97]$$

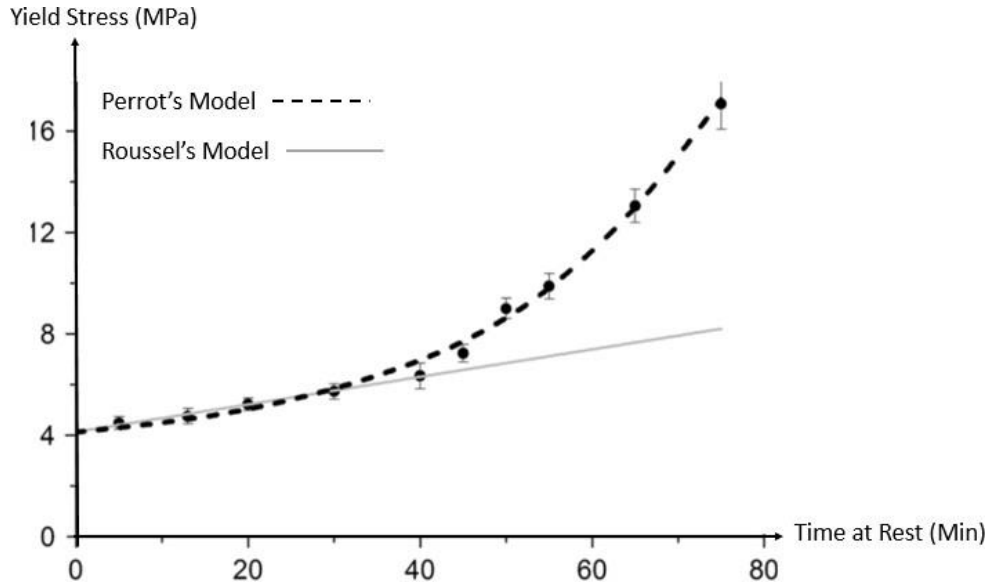


Figure 15: Yield Stress Evolution With Time: Perrot's Model Vs Roussel's Model [93]

1.7.4- Measuring and Qualification of Mortars Early Age Properties and Printability

In section 1.5.2, it was mentioned that despite the attractiveness of most rheometers, there is many drawbacks that cease their application for the characterization of mortars. Indeed, to assess the printability of cementitious materials, it is mandatory to follow up the material's stiffness and strength evolution with time, after the layers deposition [107], in order to estimate the adequate building rate [108]. In this regard, several attempts were made to monitor inline the evolution of the material's properties. For example, Leal Da Silva et al. [109] used the oscillatory rheometry and ultrasound test measurements to estimate the material's elastic modulus evolution over time. However, this technique requires expensive and very sensitive devices that are not easy to implement in 3D printing. On the other hand, to relieve this situation, instantaneous and continuous method are being developed in order to meet these needs. For example, the penetration test or gravity induced flow tests are being further adapted to be compatible with printable mortars [107]. Most importantly, these methods use simple tools, and they are fast enough to be used in line with the printing process. As an example of the penetration test, the cone plunger was used by Rubio et al [110], to investigate the effect of different mix composition on fresh and rheological properties of printable mortar. Whereas, Khalil et al. [84] used a Vicat plunger for standard consistency having a diameter of 10mm, to study the effect of Calcium Sulfo-Aluminate cement on the printability of pastes and mortars.

Notwithstanding, straightforward methods were used to assess the quality of printable mortars. For example, Zhang et al. [111] assessed the buildability of the material by visual inspections. They, simply noted the deformations of printed layers, or the collapse of the whole element. Le et al. [91] referred to the workability, extrudability, buildability and setting time of the material, as the essential parameters to qualify the material used. Herein, the workability, and the open time of the material were derived from the vane shear apparatus measurements. As for the extrudability and buildability, they were checked by visualizing the ability of the material to get out of a 9mm circular nozzle without any blockage of the nozzle, or discontinuity in the layer. Another example is attributed to Kazemian et al. [112] who considered that a good print quality corresponds to a good surface quality, square edges of the layers, dimensional consistency, and conformity to the CAD model.

1.7.5- Rheological Problems and Object Failure During Manufacturing

As previously discussed, the printability of a mortar is dictated by its extrudability and buildability properties. Herein, the extrudability characteristics of a material mostly affect the pumping and extrusion stages in the manufacturing of concrete elements. It should be always ensured that the material flows inside the system without excessive friction, because if happened, the material begins to scrape causing more defects to the surface and discontinuity of the printed layer. Even worst, this might causes interstitial fluid drainage within the material inside the conduits, mostly leading to a blockage [113][77][114][115] (Fig. 16). Nevertheless, it has been reported in earlier studies that material heterogeneities could appear during the flow of firm mortars [77][116][117]. In addition, it has been observed as well, that very concentrated suspensions are more subjected to liquid filtration and drainage during their extrusion [117][118][119].



Figure 16: (Left) Layers Discontinuity and Surface Defects [120] (Right) Nozzle Blockage

On the other hand, Printed structures are subjected to different buildability problems, after the layers deposition (Fig. 17). Two mechanisms were recognized as the major causes of collapse in 3D printed elements during the manufacturing process, which are the material failure, and loss of stability [107]. Each layer slightly deforms when a certain load is applied to it. Therefore, it is necessary to account for this deformation in order to perceive the exact number of layers that must be printed to construct a structure with the exact targeted height [93][100]. However, more serious events could happen leading to a total collapse of the structure [121]. For example, a plastic collapse might occur, corresponding to the breakage of the base layer (the most heavily loaded

layer). This type of failure is caused by the excessive stress exerted on the layer, overcoming its actual static yield stress, arising from the weight of the superposed layer. The mostly affected structures by this mode of failure are the non-slender ones [122]. Whereas, in the case of slender elements, an elastic buckling (structural buckling) is most likely to occur. In general, buckling failure is caused either by making cantilevers, or due to an incorrect alignment of the printed layers causing eccentricities [100][121]. Over and above, during the printing of a curved element, the layer is being bent. As a fact, the inner part of the curved layer gets compressed, while the outer part gets stretched. This elongation creates different cracks all over the curvature boundary which cause not only aesthetic problems to the element, but a strength and durability weakness in its hardened state [27].

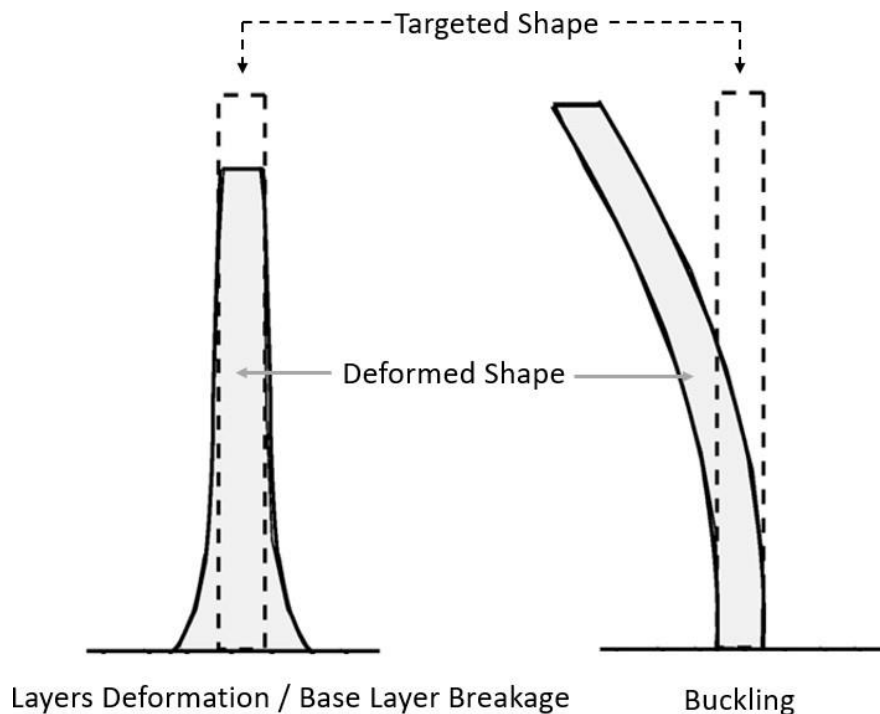


Figure 17: (Left) Plastic Collapse (Right) Elastic Buckling [121]

1.7.6- Methods to Control the Rheological Properties

Generally, the fresh properties of cement-based materials are highly affected by the mix composition, such as the use of admixtures, minerals, and the overall material proportions [123][124]. The rheological behavior depends on the quality of each constituent, their proportions in the mix, and their interactions [57]. Besides, an effective mixing procedure must be followed in order to have full control over these properties [27]. For example, it is possible to control the

rheological properties of the mix by delaying the addition of High Range Water Reducer admixtures. This can better increase the workability and decrease the viscosity of the mix [125]. Furthermore, using higher shear mixing could improve the material's workability by decreasing its viscosity [125]. On top of that, the yield stress of the material could be further decreased to about the half (for a short period of time) if vibrated [126].

1.7.7- Effect of the Mix Composition on the Rheological Behavior of Printable Mortars

Concerning the material's composition and proportions in the mix, initially, the volume of paste is an essential parameter that plays a key role in changing the material's rheology. A higher volume of paste, provides a better flowability [57]. Koehler [127] confirmed that any increase of the paste volume would result in an increase of slump, and a reduction of yield stress and plastic viscosity. Similarly, Banfill [128] found that a higher volume of paste decreases the yield stress of the mixture. Gołaszewski [129] found that the volume of paste would affect more the plastic viscosity of the material rather than its yield stress.

Besides, concerning the water to cement ratio, an increase of the water content, decreases dramatically the yield stress and plastic viscosity of the material [126]. Banfill [128] assured that a higher water content would decrease the yield stress of the mix (Fig. 18), and similarly did Hernández et al. [130].

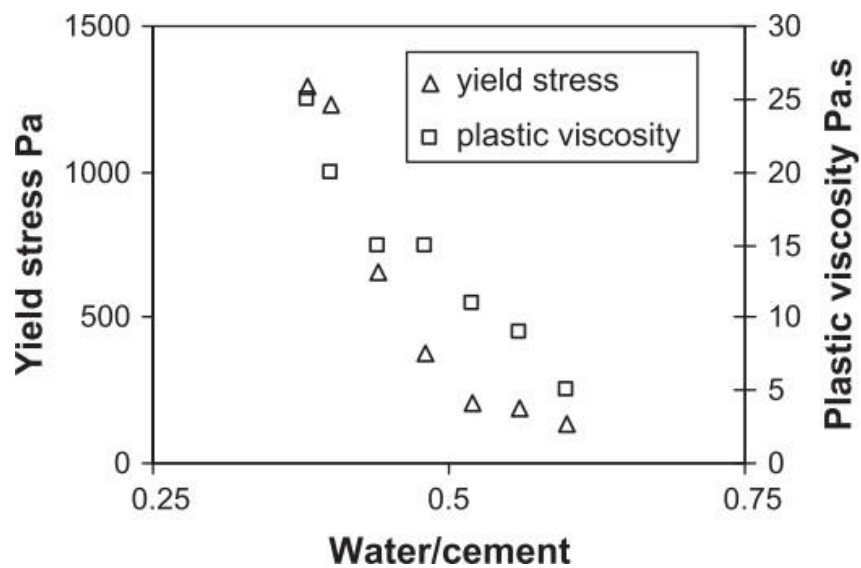


Figure 18: Effect of W/C on the Yield Stress and Plastic Viscosity of Fresh Mixes [128]

As for the addition of minerals such as silica fume and limestone powder, it is commonly known that silica fume is an extremely fine powder having a higher specific surface area than cement [57]. Therefore, silica fume particles can easily fill the voids between other particles, and improve the gradation and packing density [57]. Besides, silica fume increases significantly the flocculation rate of the material [131][132]. As a results, it can be added in mortars to provide better uniformity and cohesiveness of the material, as an inorganic viscosity modifying agent [57]. In this regard, Ahari et al. [132][133] found that silica fume increases the yield stress and plastic viscosity of the material, and therefore its overall thixotropic values. Similarly did Dengwun et al. [57] (Fig. 19). Furthermore, many studies found that the workability of the material increases when used at low replacement rates, and decreases if used at higher replacement rates [127]. Accordingly, Tattersal [134] stated that an addition of 2% to 3% of the cement’s weight could be used as a pumping aid.

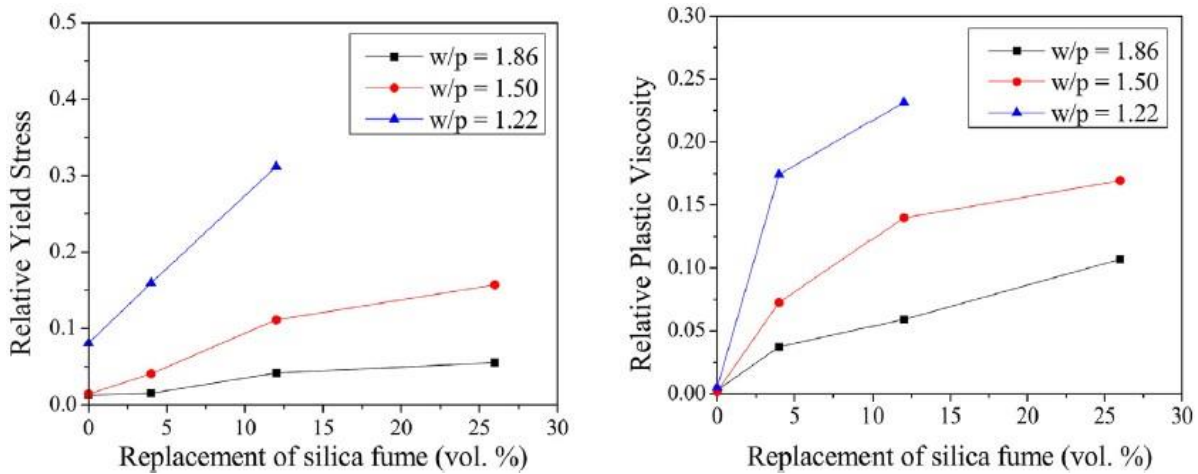


Figure 19: Effect of of Silica Fume on The Material’s Rheology [57]

Concerning the use of limestone powder as a mineral admixture, it increases the adhesion and friction between cement particles, mainly due to the irregular shape and roughness of the particles [135][136]. Limestone particles reduce the spacing between other particles and increase the inter particle contacts. In addition, limestone filler have high adsorption capacity of High Range Water Reducers, which helps in further dispersing the cement particles [57][137]. Some researchers found that limestone filler would increase the yield stress of the material, as well as its plastic viscosity. For example, Rahman et al. [131] stated that increasing the limestone portion in the mix leads to an increase of the flocculation rate. Koehler et al. [127] concluded that limestone addition contributes to an increase of the mix’s yield stress and plastic viscosity with time (Fig. 20).

Besides, Bonavetti-Irassar et al. [138], and Tsivilis et al. [139] showed that limestone filler increases the structuration rate of the mix with the increasing time.

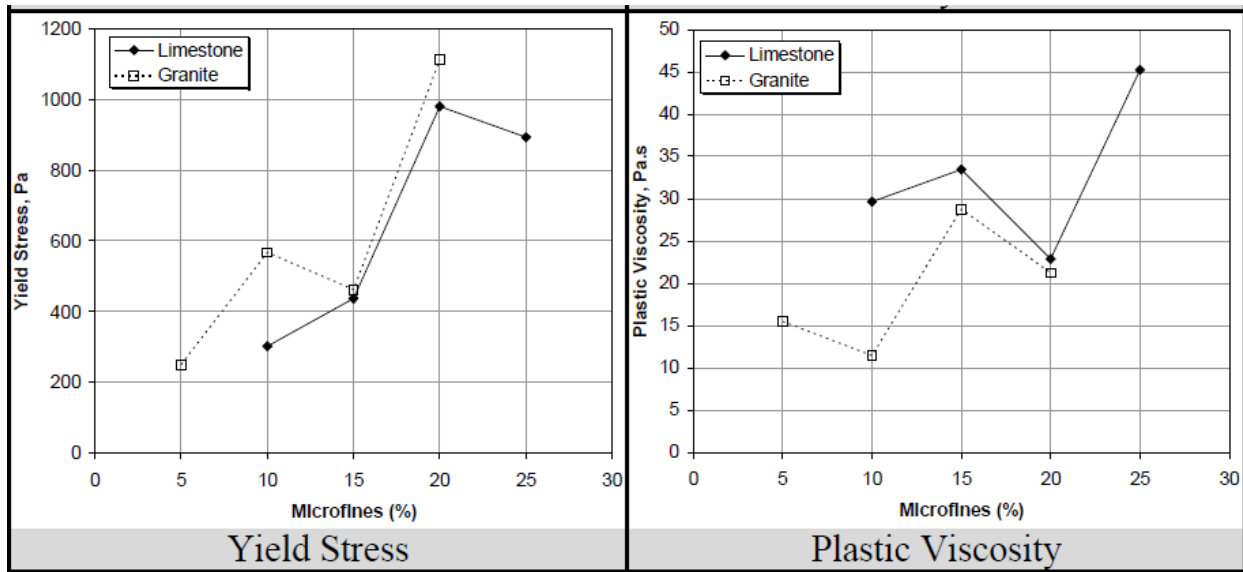


Figure 20: Effect of Limestone on The Material's Rheology [127]

Regarding the use of some chemical admixtures such as Polycarboxylate based High Range Water Reducers and Viscosity Modifying Agents, it is commonly known that HRWR are mostly used to decrease the yield stress and viscosity of cementitious materials. They have an extreme potential to disperse cement particles [140]. The effect of HRWR on the material's properties has been clearly shown by Koehler et al. [127] (Fig. 21). Furthermore, Khalil el al. [84] showed in their study that HRWR decreases linearly the yield stress of mortars, and their structuration rates as well. As well, Qian et al. [140] concluded that an addition of HRWR decreases the thixotropy.

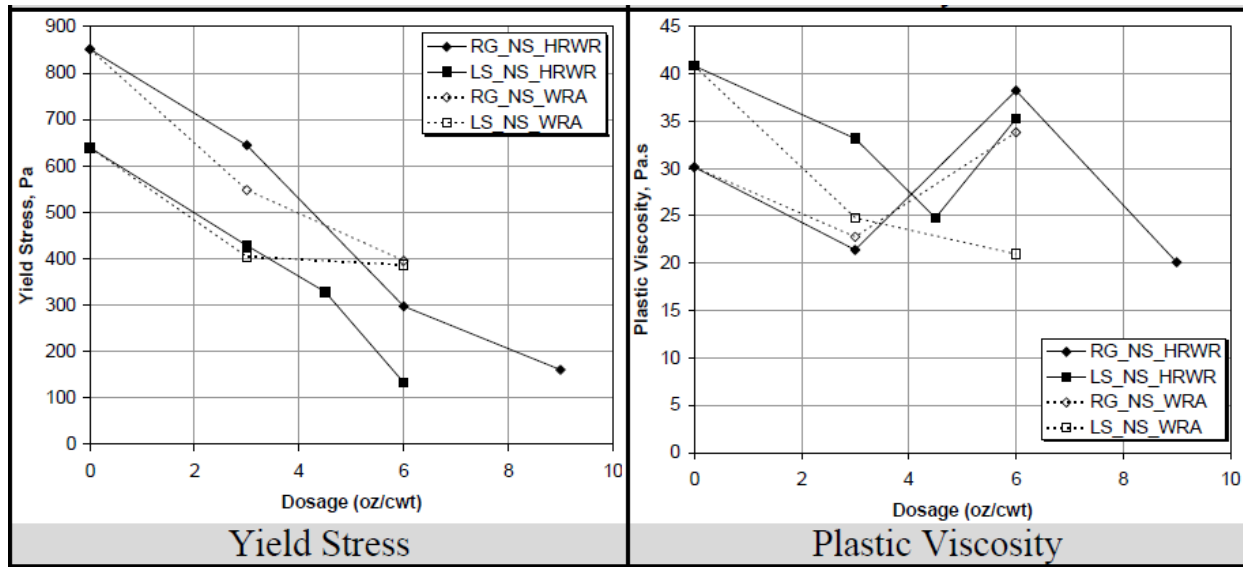


Figure 21: Effect of HRWR on The Material's Rheology [127]

Apropos the Viscosity Modifying Agents, their essential role is to improve the rheology of cementitious material by enhancing the uniformity and cohesiveness of the mix [141]. Though, few researches investigated its effect on the thixotropy of cement pastes [142]. VMA is often used in combination with the appropriate HRWR [143]. In general, the shear stress of the fresh mix including VMA is mostly affected [141][144]. This was confirmed by DauKsys et al. [145] who showed that VMA moderately increase the structuration rate of cementitious materials (Fig. 22). In addition, other researchers found that they do not evidently influence the yield stress of the materials, but its viscosity in particular [146]. Therefore, it can be pointed out that they do not have a considerable effect on the structuration rate increase.

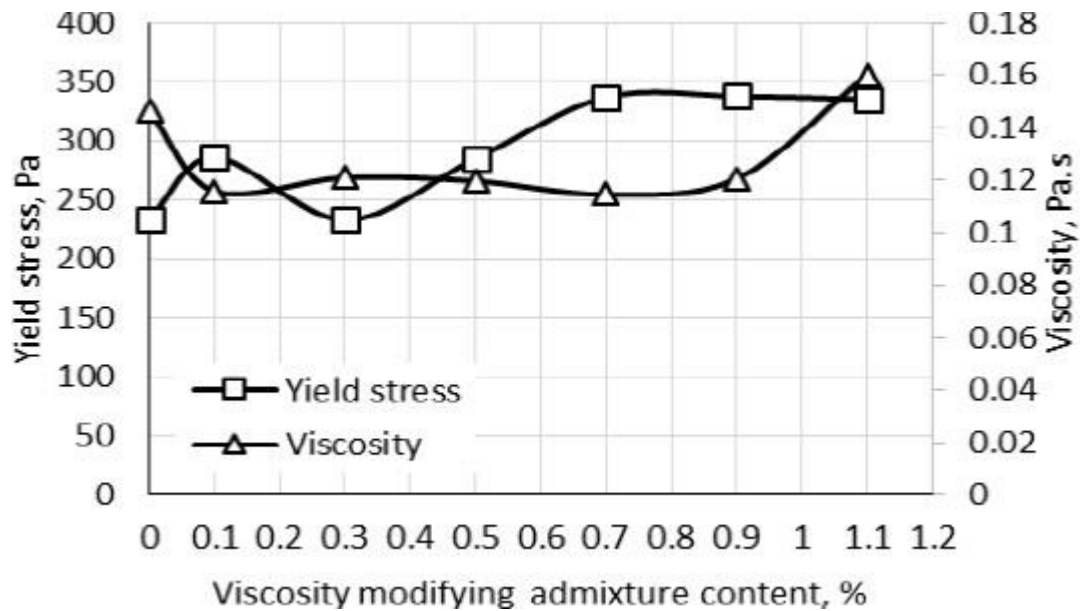


Figure 22: Effect of VMA on The Material's Rheology [145]

1.8- Hardened State Properties of 3D Printed Elements

1.8.1- Mechanical Properties of 3D Printed Elements

The layering process enabling the additive manufacturing concept, as well as the fresh properties of the material used, affects greatly the behavior and quality of the printed element in its hardened state (compressive strength, flexural strength, etc...). Indeed, a good bond between superposed layers is a key factor for providing a monolithic action of a printed element. Over and above, the mechanical properties of printed elements define the structural performance of the overall structure. Therefore, apart from the conformity to the designed geometry, it is the hardened state properties that give for the manufactured object its value [147].

The fabrication mode that do not use formworks, and the curing conditions influence the mechanical strength of the printed element. Practically, the continuous exposure to the surrounding environment increases the cracking resulting from the drying shrinkage [147][148][149]. Likewise, because of the layering concept, 3D printed elements exhibit anisotropic characteristics [50][51][150]. This happens because, the microstructure of the material inside the layer differs somewhat from its microstructure at the boundaries between layers, and because of the formation of unwanted voids between layers in contact [151]. As a matter of fact, the loading direction of the specimen with respect to the printed layers influences its mechanical properties (Fig. 23). Having

said that, it is possible to adjust the orientation of the printed layers for each element based on the applied loads when in service [147]. In other words, the bond generated between successive layers, corresponding to the interlayer strength, imposes a new parameter that must be taken into consideration.

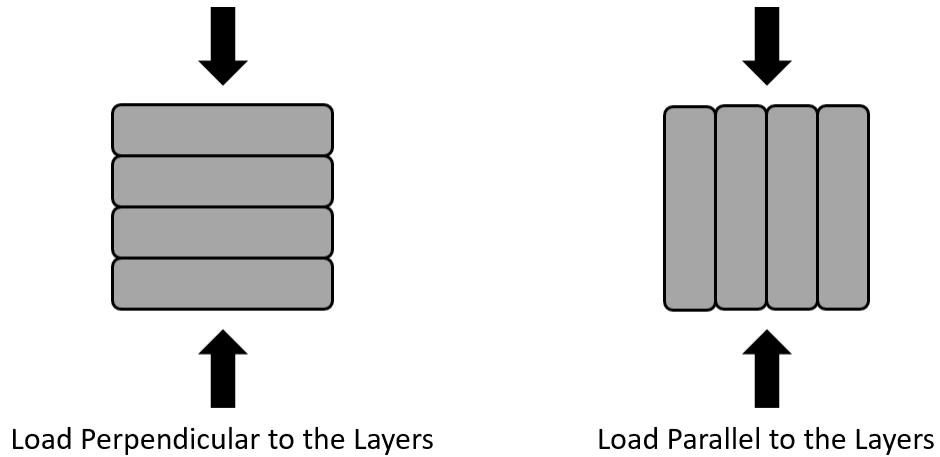


Figure 23: Applied Load With Respect to the Layers Orientation

Technically, the creation of the bond can be explained by the surface forces acting at the interface, controlled by three major adhesion characteristics which are mechanical interaction, chemical bonding, and thermodynamic linkage [152][153]. Implicitly, the adhesion between successive layers can be described as their interaction on a micro-scale, corresponding to the chemical reactions and cement hydration; and macro-scale corresponding to the interlocking and surface roughness of the layers [154][155]. Practically, the interfacial bond strength is determined by the material's rheology and printing parameters such as, printing speed and time gap between successive layers, nozzle standoff distance, contact area between layers, pumping pressure [156] (Fig. 24). For example, large time gap between layers deposition results in a cold-joint formation [97][157][158]. To avoid such incident, the optimum time gap between layers should be determined. Accordingly, the printing speed must be properly controlled. As for the other printing parameters, a balance should be always maintained based on the rheological properties of the material used. For example, a low printing quality induces a higher surface roughness. Correspondingly, a lower printing pressure amplifies the presence of voids by entrapping air bubbles between successive layers, instead of pushing the material being printed into these voids [37][159]. As well, these parameters might result in under-filling problems, caused by the

reduction of the effective density of each layer, causing a formation of additional voids [147]. On the contrary, a high printing pressure might enforce existing air bubbles inside the layer to escape and stay entrapped between layers [160]. Meanwhile, there is no predefined practice or approach to monitor these parameters altogether, they can be only determined instantaneously, for each situation separately [107].

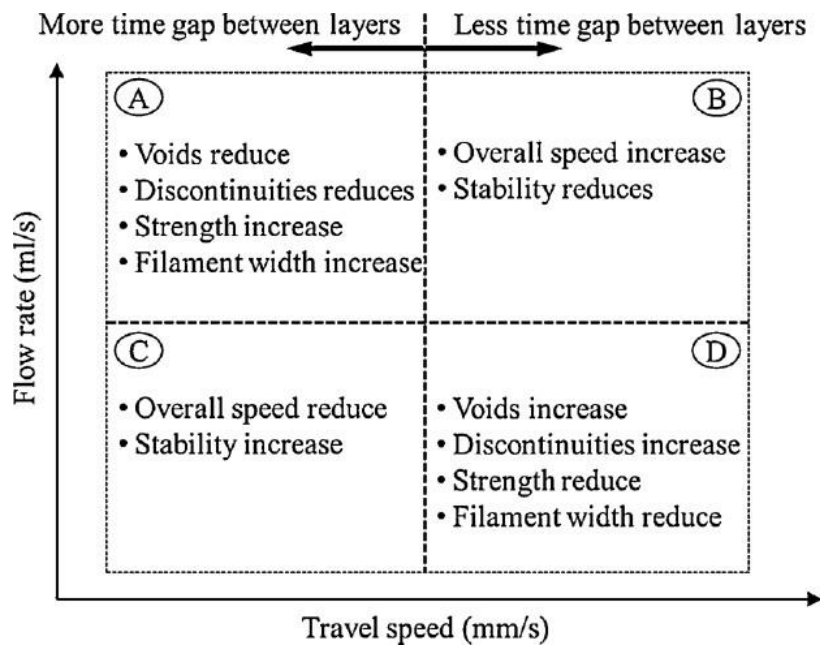


Figure 24: Correspondence of All Printing and Material Parameters [156]

Many researchers working on the development of additive manufacturing assessed the quality of the bond generated between printed layers, based on different variables and parameters. For example, Paul et al. [161], Feng et al. [162], and Nerella et al. [90] investigated the effect of the layers direction with respect to the applied load, on the bearing capacity of printed elements. In fact, they all found that the compressive and flexural strengths of 3D printed specimens are governed by the layers direction (Fig 25). Though, Koker et al. [163] found that in some cases, and depending on the printing parameters, the mechanical strength of printed elements is greater than for casted elements. This fact is attributed to the extra pressure exerted on the material during the printing process which reduces the voids inside the layer and at the interface making a denser matrix.

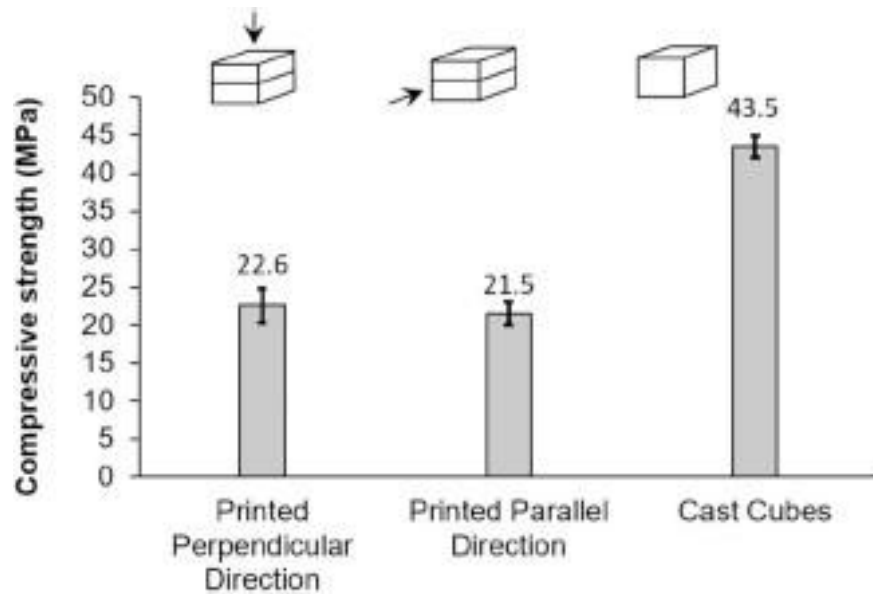


Figure 25: Effect of the Layers Direction on The Compressive Strength of 3D Printed Elements [164]

Wolfs et al. [165] investigated the effect of time interval between layers deposition, nozzle's height, and surface dehydration on the compressive and tensile strength of printed elements. Herein, they found a minor influence of the layers orientation with respect to the applied loads. However, the bond strength between layers decreases as the time interval between layers deposition increases. The negative effect of time delay was also confirmed by FalCon et al. [9] and Tay et al. [157] (Fig. 26). However, this time gap lead the layers surfaces to dry out, causing a further decrease in the bond strength. These results were in accordance with Sanjayan et al. [17] when studying the effect of surface moisture on the inter-layer strength of 3D printed concrete. These studies showed that for short time gaps, the bond generated between layers decreases due to the surface water evaporation. Yet, this bond regains strength at higher time gaps (up to a certain limit) due to the material's bleeding, moisturizing the surfaces. Here as well, Marchement et al. [166] were able to prove the exact same fact (Fig. 27). Yet, wolfs et al. [165] could not obtain a clear relation between the height of the nozzle and the interlayer strength.

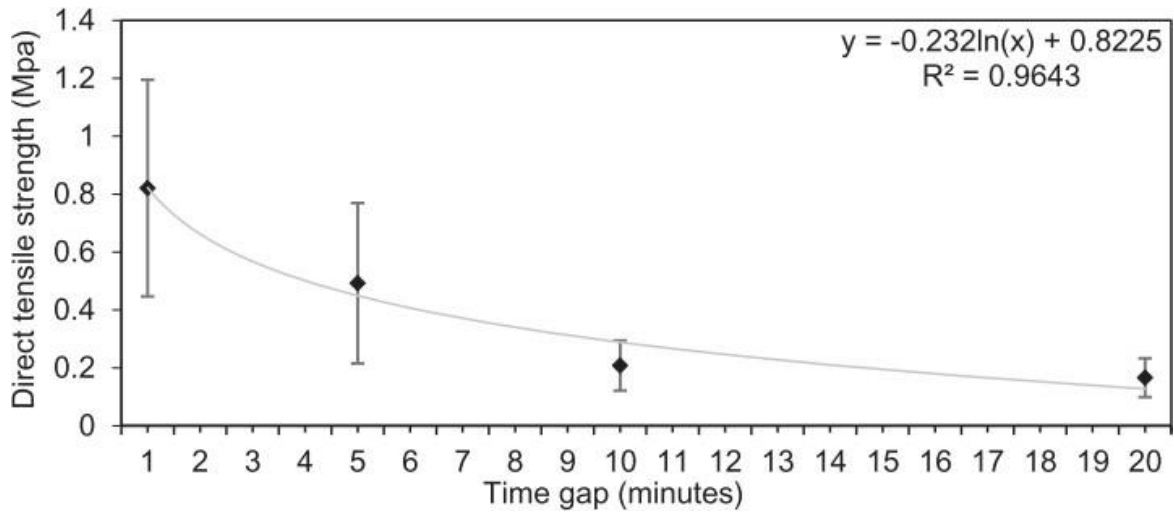


Figure 26: Effect of Time Gap on The Interlayers Strength [157]

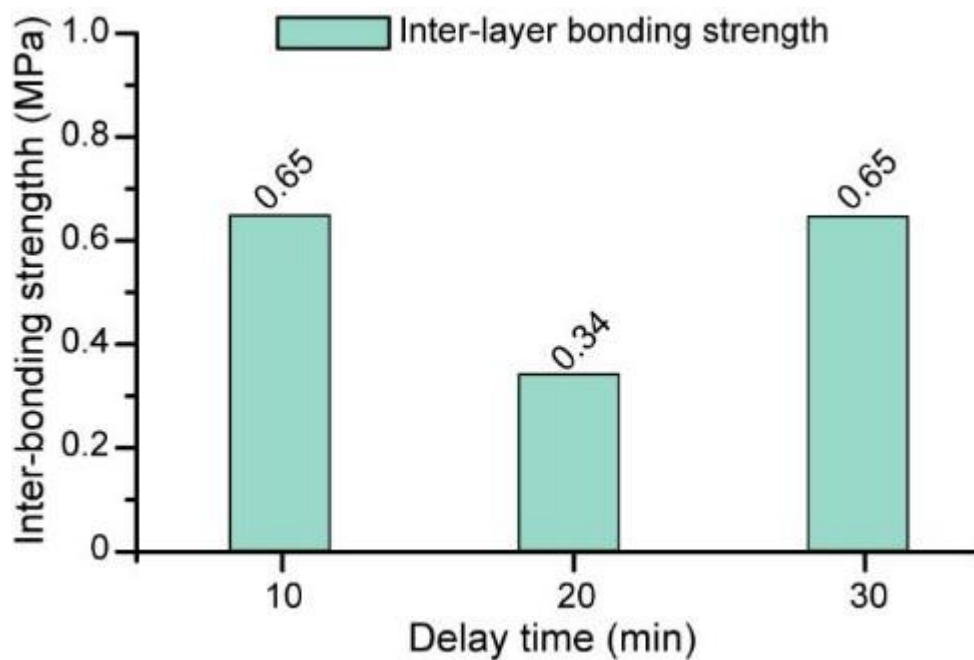


Figure 27: Effect of Surface Moisture on The Strength Between Layers [166]

Besides, Zareiyan et al. [154] studied the effect of the extrusion rate, aggregate size, and layer's thickness on the interlayer strength of printed elements. They found that when the aggregates size increased, the printed element became more subjected to cold-joint effect. This happened because large aggregates lead to less homogeneous layered structures. However, as the layer's thickness decreased, the compressive strength of the element increased. On the other hand, Lee et al. [167]

investigated the existing relation between pores and tensile bond strength of additively manufactured mortars, using X-Ray and computed tomography analysis. As a fact, they found that the voids were majorly positioned at the interface level, which caused a strength reduction.

1.8.2- Durability Properties of 3D Printed Elements

Recently, 3D printing of concrete objects became even more widespread and popular. 3D printing is gaining interest in the infrastructure industry and many other critical field of applications, such as water collectors, river revetment walls, and the reproduction of natural coral reefs [168][169][170][171] (Fig. 28). In such cases, 3D printed elements are continuously exposed to aggressive environments. Again, the same printing parameters and rheological properties affecting the mechanical strength of printed concrete elements, affect their durability characteristics. This is all attributed to the weak interfaces between successive layers. Indeed, these weaknesses threaten the overall durability of the concrete elements due to the formation of additional preferential ingress paths for aggressive substances and chemical from the surrounding environment. This is said because chemicals intrusion through weak interfaces would be much faster than in bulk material.

In the literature, most studies are concerned only by the early and long-term strength of mortars, mainly their rheological and physical behaviors [42][172]. However, they are rarely studied for their durability properties [10][173]. Therefore, some mechanical and physical properties are poorly observed [43].



Figure 28: (Left) River Revetment Wall [170] (Right) Coral Reef [171]

1.9- Reinforcement Approaches of 3D Printed Elements

In general, the tensile strength of concrete is 10 times weaker than its compressive strength, which is relatively low [37][48][174]. Therefore, when designing a structural element, it is commonly known to neglect the tensile strength of concrete itself. Hence, the use of reinforcement is essential to provide sufficient tensile capacity and ductility to the structural element. Apart from strength, a minimum reinforcement must be provided to fulfill several essential functions such as, avoiding brittle failures at cracking, ensure sufficient ductile behavior to equally redistribute stresses all over the element, and most importantly to limit the deformations and crack widths [9][48][175]. Alongside, exclusively for the case of 3D printed elements presenting weak interface strengths from the extrusion process, the interface itself can be considered as an artificial crack initiator used to have control over the cracks spacing and widths across the whole element [9].

The incorporation of reinforcements in 3D printed elements is still in its infancy stage. Though, if 3D printing technology wants to be considered as a competing construction method for conventional practices, it must be able to provide proper reinforcement. In other words, 3D printed elements must be able to tolerate the stresses imposed during their service life as integral structural parts of a building. Therefore, tensile strength beyond the mortar's capacity is mandatory.

Particularly, the distinctive characteristic of 3D printing is its ability to produce random shapes without geometrical constraints. It is a formwork-free method, enabling the construction of complex architectural and creative concrete structures [97]. However, as previously explained, 3D printed concrete exhibits tensile weakness that necessitates the addition of steel reinforcement, similar to conventional concrete [48]. Therefore, despite its attractiveness, when it comes to integrating reinforcement, 3D printing imposes specific challenges that can never be omitted if printed elements are used for structural applications [40][176][177]. The identity of this construction technique based on the superposition of layers, eliminates external vibration, undermining the link generated between steel reinforcement and printed concrete, and thereby the structural capacity and overall performance of the element. Apart from that, the layering process increases the risk of external fluid migration through the layer interfaces, causing reinforcement corrosion [40][43][178]. As a consequence, developing a comprehensive and appropriate reinforcing approach makes 3D printing technology more and more challenging.

Many academic and industrial institutions are currently developing several approaches to find the most appropriate reinforcing method of 3D printed concrete elements. Technically, these methods consist of either in-mixed fibers reinforcement or continuous steel bars. For the case of using traditional steel bars as in conventional concrete, this matter can be done manually by adding reinforcing bars during the printing process, or through the use of a robotic tool alongside. For example, reinforcement can be done by placing reinforcing bars between printed layers, at the interface level [176], or by extruding a metal cable simultaneously with the deposition of concrete layers [179]. This can also be done by printing an integrated formwork, and placing inside of it a structural steel cage, then after filling it using conventional concrete [34][176]. Over and above, pre-stressing tendons placed inside existing conduits, can be used [181]. Besides, reinforcement can be done by printing over a standing steel cage using a fork shaped printing nozzle that extrudes mortar on both sides of the cage [182]. Apart from all previously mentioned approaches, there is still several methods for reinforcement into service, but less circulated. These methods are the Mesh-Molding, the Sparce Concrete Reinforcement In Meshwork, and the Smart Dynamic Casting. The Mesh-Molding method is done by robotically printing and assembling the whole system including the steel mesh, which plays the role of a mold and reinforcing medium simultaneously [183], whereas the Sparse Concrete Reinforcement In Meshworks (SCRIM) is done by joining printed concrete to a textile reinforcing mesh to produce a reinforced element [184]. Though, the Smart Dynamic Casting (SDC) is done by shaping concrete using a flexible actuated formwork, over vertically placed reinforcing meshes [185].

1.9.1- Reinforced 3D Printed Elements

Different reinforcing methods were presented in the context of 3D printing of concrete elements. Certain approaches consist of adding fibers to the printed material, whereas others use conventional steel bars. Both methods have potentials, but for most applications rebars are required, since fiber reinforced elements are limited in strength and ductility [40] [48]. Additionally, the presence of fibers might generate a weakness between superposed layers, because they might not cross the horizontal joints properly, leaving extra voids at the interface level [40]. Farina et al. [186] found that the mechanical behavior of fiber reinforced 3D printed elements (shear capacity, flexural strength, and fracture toughness) greatly depends on the design and the material of the fibers used. Accordingly, they found that fibers having rough surfaces exhibit high interfacial bond strength, while smooth fibers induce limited interfacial strength.

Despite the fact, Panda et al. [50] studied the anisotropic mechanical performance of 3D printed fiber reinforced sustainable construction material, using different contents and lengths of glass fibers. As a matter of fact, they found that the mechanical performance of the fiber reinforced elements can be improved with the increase in the fiber content up to 1%. Yet, the results showed an obvious directional dependency caused by the layers directions (Fig. 29). Similarly, Bos et al. [187] studied the effect of steel fibers inclusion in a printed element. Herein, they found that fibers improve the flexural strength of printed elements, and eliminated the strength difference between casted and printed elements, which normally exists in the case of unreinforced elements.

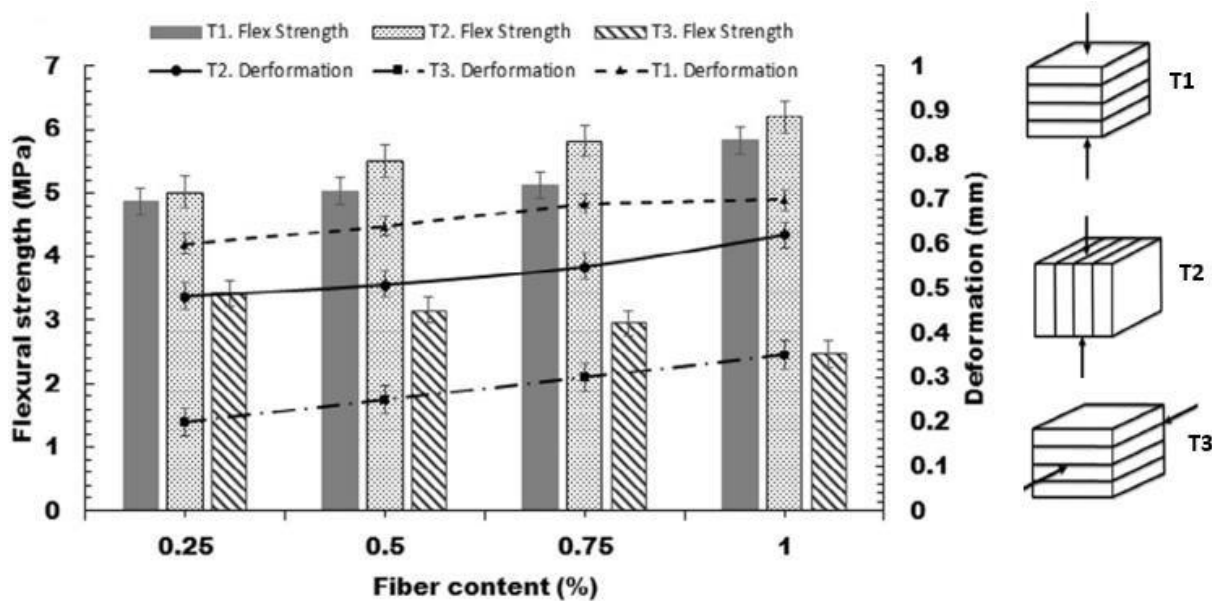


Figure 29: Flexural Strength of Fiber Reinforced 3D Printed Elements [50]

Concerning the use of continuous reinforcement, and regardless of the incorporation method of the reinforcing element (such as rebar, steel cables, filaments, and wires), many 3D printing variables come into play, and must be carefully addressed. In such cases, the diameter of the bar and the corresponding layer's geometry influence the structural capacity of the element. Over and above, the absence of vibration imposes further challenges regarding the bond between printed concrete and the bar. Besides, the influence of the anisotropic characteristics of a printed element affects the level of interaction between the bar and the layer. As for the material used for printing, it is evident that its rheological properties could sometimes affect the quality of the bond. In this context, Bos et al. [179] performed an experimental exploration on the ability of metal cables

having different diameters, to be used as reinforcements in 3D printed elements. Therefore, they conducted a series of pull-out and bending tests over casted and printed specimens. In their study, they found that in printed concrete, the bond strength of the cable with the layers is considerably lower than in cast concrete (Fig. 30). Moreover, they found that 3D printed reinforced beams exert a good flexural capacity and significant post-cracking resistance. In addition, this study showed that the cable's diameter influences the failure mode and capacity of the element, though a clear relation was not found. It is worth to mention that in this study, Bos et al. [179] did not take into consideration the effect of the layer's direction with respect to the cable, thus all printed layers were parallel to the cables.

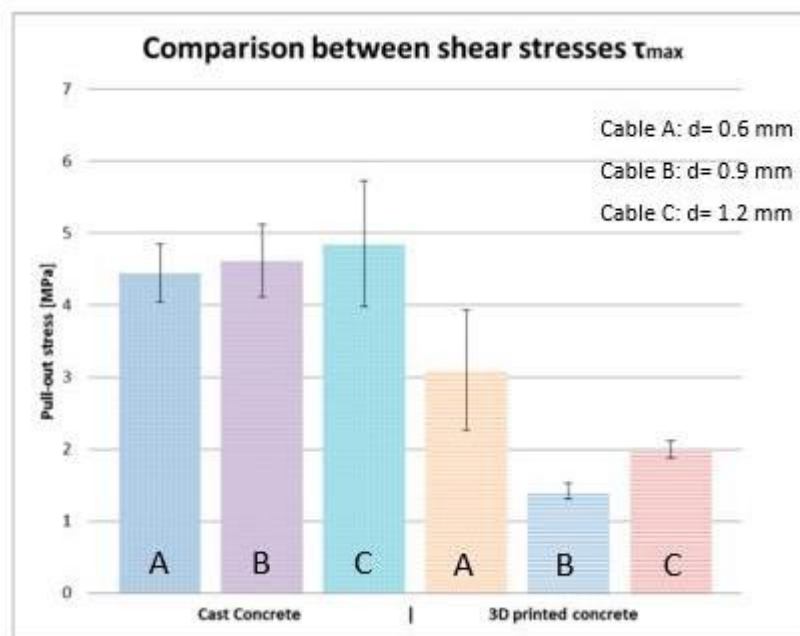


Figure 30: Bond Strength in Cast and Printed Concrete [179]

Similarly, Lim et al. [188] used different steel cables as well to reinforce 3D printed elements, and compared their performance based on 4-point bending test. Hereby, Lim et al. found that steel cables improve the flexural strength of 3D printed elements (Fig. 31).

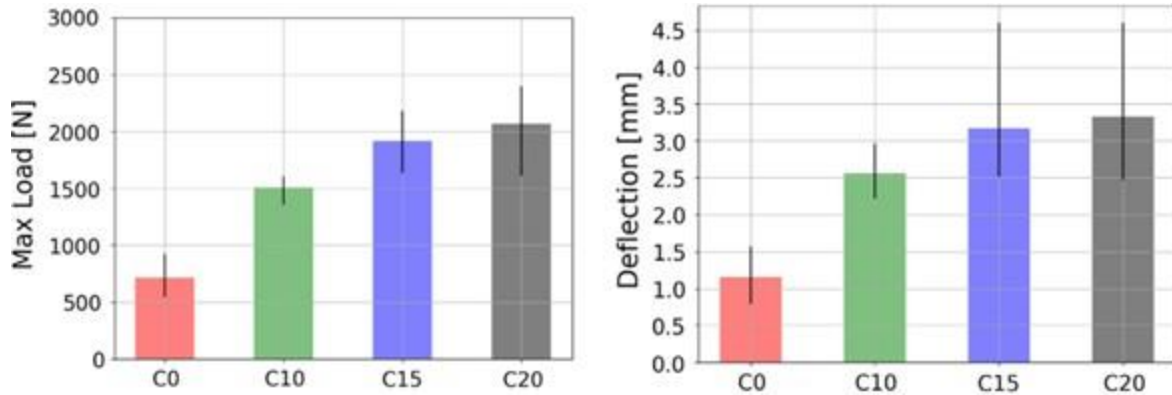


Figure 31: Maximum Bearing and Deflection Capacity of 3D Printed Elements [188]

From a different perspective, Asprone et al. [189] adopted a novel approach of reinforcement, based on printing separate segments, which are then assembled into a unique 3 m long beam element using an external steel system. The flexural strength of the beam is tested by 3-point bending test, and the results were comparable to that of an equivalent full solid reinforced beam. However, the deflection results of the printed beam were not credible because of the new manufacturing approach, therefore a remarkable difference was found (Fig. 32).

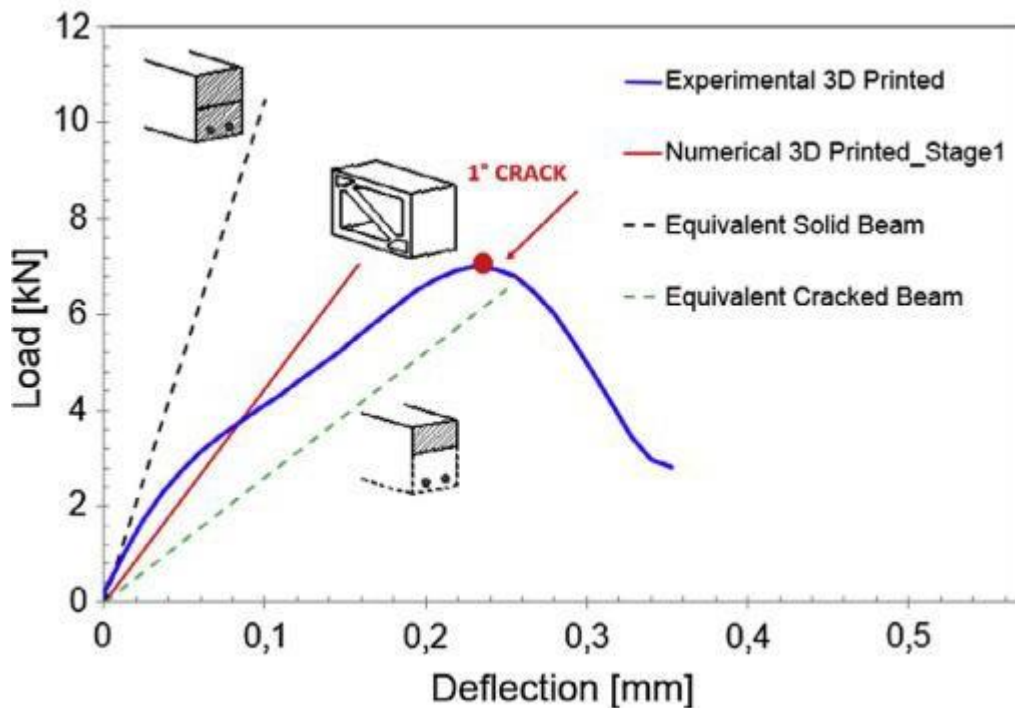


Figure 32: Comparison Between Printed and Full Solid Reinforced Concrete Beams [189]

1.10- Sustainability and Life Cycle Assessment of 3D Printed Structures

In general, the construction sector is an essential contributor to the world's economy, but in contrast, it has a significant impact on the environment. It is one of the largest users of energy, and material resources [190]. Though, the building industry is considered as one of the major contributors to the environmental pollution, and in particular for the CO₂ emissions [191][192][193], as well as a major consumer of raw materials with 40% of the global use [194][195].

Other way around, previous researches highlighted that the integration of AM in the construction field, have high sustainable benefits and potentials, such as Kohtala [196], and Ford et al. [197]. Similarly did Kreigner et al. [198] who argued that 3D printing has potentially fewer environmental impacts and lower energy demand when compared to the conventional construction techniques using molds and formworks. Additionally, Faludi et al. [199] stated that 3D printing reduces the amount of waste and it is an energy saving process. However, all these studies focused on small-scale processes and showcase structures. They were based on optimized theories and approaches. Yet, very few were quantitative. Therefore in their turn, Agusti-Juan et al. [200] conducted a detailed life cycle assessment over different sets of walls, to explicitly illustrate the difference between the conventional construction method and 3D printing. Both sets included straight, single curved, and double curved walls. The first set was conventionally casted and the second set was printed using the Mesh-Mold approach. Though, they found that the concrete used for 3D printing is much more demanding to meet the specific properties needed, and contributes to approximately 40% more CO₂ emissions than the conventional concrete due to the increased amount of Portland cement (Fig. 33). As for the reinforcement, Agusti-Juan et al. [200] did not found a remarkable difference in the reinforcement amount needed between Mesh-Molding and the conventional technique. Accordingly, they indicated that the environmental performance of digital fabrication depends majorly on the use of concrete materials.

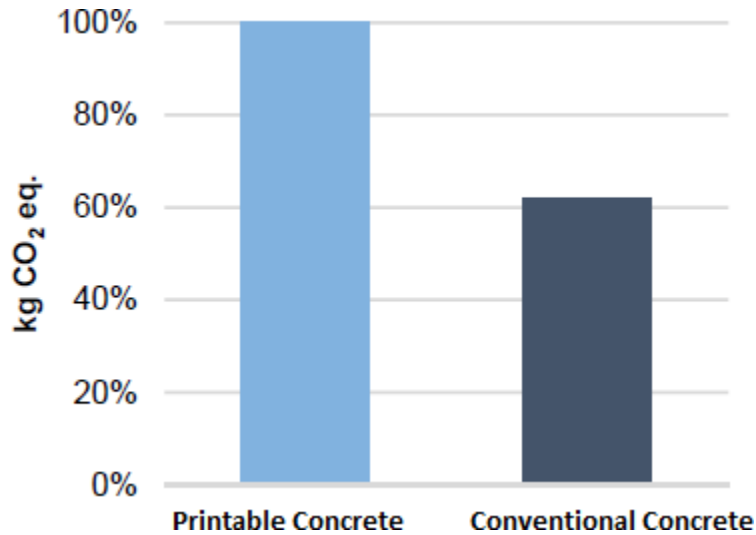


Figure 33: Comparison of CO₂ Emission Between Printable and Conventional Concrete [200]

In spite of that, the eco-toxicity and negative environmental effect induced by 3D printing, can be rectified with the increasing structural complexity, making a positive feedback loop. More precisely, 3D printing offers a better structural optimization which thereby can decrease the amount of materials used. In addition, it generates less wastes, especially in terms of material's utilization and formworks employment for conventional construction practices.

1.11- Research Significance and Objectives

After all the challenges imposed by 3D Printing in terms of fresh and hardened state properties of printable materials, and the structural behavior of printed elements; several subjects must be continuously addressed and developed in order to further promote its application in the construction field. In particular, two major problematic were identified, the first one related to the development of a practical formulation method of printable mortars that comply with the buildability requirements of the material, and second, corresponds to the performance characterization of 3D printed elements in terms of the quality and adequacy of the interaction between printed concrete layers and reinforcing bars, and the durability of the printed elements. However, knowing that there are many methods adopted for the formulation of printable mortars, for example by using accelerators or some other chemical admixtures, it was decided to develop a different approach that can be systematically implemented using some predefined graphs based on the structuration rate of the material needed for its good buildability. As for the structural reinforcement of 3D printed elements, all what has been presented in the literature show the strategies used for the incorporation of reinforcement in a 3D printed element. However, it is not

the reinforcement approach that only matters. Indeed, the structural behavior of the reinforced elements and the interaction between printed layers and the reinforcement is what mostly counts.

Hence, it was of our interest to cover both fields through relevant experimental campaigns. Accordingly, this research covered the whole production process, starting by the mix design and formulation up until the product's delivery and evaluation. In this regard, the common thread of this thesis was to understand the effect of the material's rheology and fresh state properties on the hardened state quality and structural performance of 3D printed elements. Particularly, the aims and objectives were the following:

- Understanding the effect of several mostly used chemical and mineral additives in the mix design, on the rheological and thixotropic behavior of fresh printable mortars, and correspondingly, their effect on the printability characteristics of the material used.

Subsequently, the outcomes were correlated to the performance of 3D printed elements, in order to answer three major questions concerning the effect of the material's fresh state properties and rheology on the hardened state properties of printed objects, which are:

- How could the material's fresh state properties affect the bond generated between steel reinforcement and printed concrete layers?
- How could the layers direction with respect to the steel bar affect the quality of the bond developed with printed concrete layers?
- How could the material's fresh state properties affect the durability performance of printed elements exposed to difference chemical environments?

A purely experimental program has been associated to this thesis, following the methodology chart below. A series of rheological, mechanical, and durability tests have been conducted to characterize the fresh and hardened state properties of printable materials. Respectively, each of the following chapters describes the proper experimental protocol adopted, as well as the resulting outcomes.

Fresh state properties of 3D printable concrete

❖ **Rheological and thixotropic characterization:**

Objective: *Investigating the effect of several chemical and mineral admixtures on the printability and structuration rate evolution of the printable material with time.*

- Printability (extrudability and buildability)
- Flow table test (Workability)
- Fall-cone test (Yield stress evolution)



Hardened state properties of 3D printed elements

❖ **Mechanical and structural characterization:**

Objective: *Investigating the effect of the material's rheology and fresh state properties on the hardened state properties of 3D printed elements.*

-
- **Bond strength with Rebar:**
 - Pull-out test

Particular Variable:

 - ✓ Printing technique:
 1. Manual printing using a lab gun device.
 2. Automated printing using a 3-axis gantry printer.
 - ✓ Printed layers direction:
 1. Parallel to the steel bar.
 2. Perpendicular to the steel bar.
 - **Durability assessment:**
 - Macroscopic analysis:
 - Visual inspections
 - Mass loss
 - Compressive strength variation
 - Microscopic analysis:
 - Mercury intrusion porosimetry (MIP)
 - Thermogravimetric analysis (TGA)
 - Scanning electron microscopy (SEM)
 - X-ray tomography.

Chapter 2 addresses the rheological characterization of newly developed printable mixes having different compositions. In particular, this study exploits the influence of certain chemical and mineral additives on the material's thixotropy, such as high range water reducer (HRWR), viscosity modifying agent (VMA), limestone filler, and water content. Accordingly, the rheological measurements associated to the yield stress, were estimated along a certain period of time using the Fall-Cone test. The results were then correlated to the material's structuration rate

evolution (A_{thix}). Further and beyond, a comprehensive understanding of the trend and mode of variation of the A_{thix} was provided for each category of mixes.

Chapter 3 deals with the effect of the material's rheology and fresh state properties on the mechanical behavior of 3D printed elements. Herein, a preliminary study has been done to characterize the effect of the material's workability on the link generated between the reinforcement and the printed layers. Therefore, a series of pull-out tests has been conducted over manually printed concrete elements under different printing conditions. Besides, a second study has been carried out in the same context. However, for this case, the samples were printed using an automated 3-axis gantry printer. In both studies, the effect of the printing method and layers direction, whether parallel or perpendicular to the steel bar, on the bond generated with steel bars have been broadly investigated.

Chapter 4 focuses on the durability assessment of three different mixes having different compositions, selected based on the findings of chapter 2 and 3. This chapter presents an opening study of the performance of 3D printed concrete elements when subjected to chemical attacks. It is ahead of most research topics concerning 3D printing of concrete elements. It was done to better understand the effect of the material's fresh state properties on the performance of 3D printed elements when exposed to severe environments, and in particular, the quality of the link generated between superposed layers. In this study, the samples were submerged in two different sulfuric acid solutions having concentrations of 1% and 3%. Herein, it was decided to use sulfuric acid attack as an accelerated process for the samples degradation, because of its strong impact against concrete. Mainly, a mechanical, macroscopic and microscopic characterizations have been addressed for the inspections of the corroded samples.

CHAPTER 2 : RHEOLOGICAL CHARACTERIZATION OF 3D PRINTABLE MORTARS

After understanding the fresh state properties of the developed printable mixes, and determining the effect of certain chemical and mineral additives on the thixotropic behavior of printable materials; the next two chapters present various experimental studies showing the effect of the material's rheology and thixotropy on the mechanical properties of 3D printed elements when in their hardened states, namely their structural and durability performances.

Chapter 1 went over a detailed literature review of 3D printing technology of cementitious materials, and its application in the construction field. Here in chapter 2, a detailed characterization of different printable mixes, when still in their fresh state, was done through penetration tests. The material's properties and rheology influence the quality of the printed elements in terms of structural stability, mechanical and durability performance. Thus, such sensitive materials must be highly engineered. Their rheological properties must be tailored to satisfy conflicting printability requirements, such as extrudability and buildability [201][202][203]. Particularly, 3D printable materials majorly exhibit several complex phenomena such as thixotropy [161]. On top of that, any minimal change in the formulation of such mixes leads to flow instabilities, product defects and functional disruption [204].

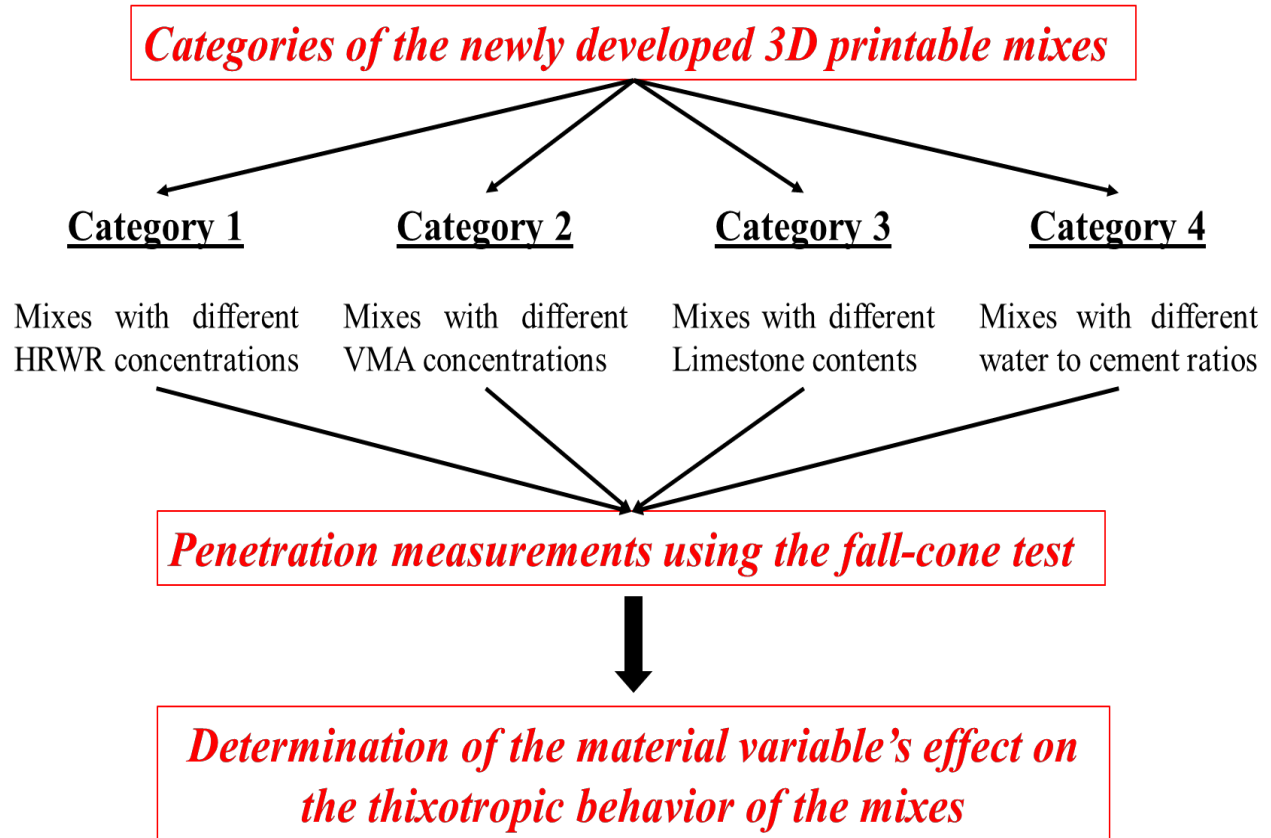
This chapter not only goes over the influence of the mix composition on rheology of the material in terms of shear stress variation with time, but also the trend and mode of variation of the structuration rate (A_{thix}) in function of the mix composition. This is actually done because the A_{thix} provides a crucial indication of the material's buildability. It reveals the stiffness of the printed material, which is directly related to the ability of the printed layers to withstand the loads coming from the subsequent ones. Thus, it provides an indication about the printing speed and building rate that should be adopted for each printable mix design independently. However, as mentioned before, developing 3D printable mixes requires precision and accuracy of the mix composition and material's proportions. Thus, in order to insure good printability of the developed mixes, laboratory testing must be carried out on a smaller scale, before producing large batches in order to ensure a high printing quality. In this context, four variable materials were considered for this

research, which are high range water reducer (HRWR), viscosity modifying agent (VMA), limestone filler, and water. These materials were chosen in particular because it is well known that HRWR and VMA make the most basic and practical combination to adjust the rheological properties of cement-based mixes. In addition Limestone powder has been included in this study because it counts as one of most pragmatic substitute of cement. Eventually, water content has been systematically considered because of its fundamental importance in any mix design.

Therefore, the aim of this chapter is to understand the effect of these chemical and mineral constituents on the rheological characteristics of 3D printable concrete mixtures. In particular, how the thixotropy of the material could be affected by varying independently the content of HRWR, VMA, limestone filler, and water in the developed mix?

Herein, the experiments were carried out over sets of newly developed 3D printable mixes, which were classified in four different categories, according to their compositions. The first category contained mixes having different HRWR concentrations. The second category contained mixes having different VMA concentrations. The third category included mixes with different limestone filler contents. The fourth category enclosed mixes having different water to cement ratios. Herein, the rheological measurements were done using the fall-cone test. This penetration approach was adopted due to its simplicity and practicality, in spite of most other rheometry. Technically, the penetration depth of the cone inside the material was related to the dynamic yield stress. These measurements were taken every 150 sec (2.5 min) over the course of 1320 sec (22 min) to follow up the variation of the static yield stress over the given period of time. The multiple measurements recorded for each mix independently were brought together within each category. Thus, the effect of the constituent variables on the structural build-up rates (A_{thix}) and thixotropic behavior of the materials were identified.

A representative methodology chart of the workflow is shown below.



The results of this work were accepted for publication in Magazine of Concrete Research as a journal article, entitled “Influence of the mix composition on the thixotropy of 3D printable mortars”, by Bilal BAZ, Sébastien REMOND, Georges AOUAD, and it is under edition.

The outcomes of this research showed that the variation of the static yield stress of 3D printable mortars can be considered linear during the first 22 min. Thus, in most cases, a linear relationship can be adopted in order to represent the structuration rate and predict the thixotropic behavior of the mixture. In particular, the structuration rate in function of the material’s variable shows a reasonable linearity for the mixes having different contents of HRWR, limestone, and water, except for the mixes having different VMA concentrations.

Influence of the mix composition on the thixotropy of 3D printable mortars

Bilal BAZ, Faculty of Engineering, University Of Balamand, UOB, Al Koura, Lebanon
IMT Lille Douai, LGCgE – GCE, F-59508 Douai, France

E-mail: bilal.baz@imt-lille-douai.fr

Sébastien REMOND, Univ Orléans, Univ Tours, INSA CVL, LaMé, EA 7494, France

E-mail: sebastien.remond@univ-orleans.fr

Georges AOUAD, Faculty of Engineering, University Of Balamand, UOB, Al Koura,
Lebanon

E-mail: Georges.Aouad@balamand.edu.lb

***Corresponding Author: Bilal BAZ**, Faculty of Engineering, University Of Balamand, UOB,
Al Koura, Lebanon

IMT Lille Douai, LGCgE – GCE, F-59508 Douai, France

E-mail: bilal.baz@imt-lille-douai.fr

Abstract

Digital fabrication of concrete elements requires a better understanding of the rheological behavior of the cementitious material used. Fresh concrete is known to be a thixotropic material having time dependent characteristics. Moreover, fresh mortars used in 3D printing should maintain a sufficient shear stress to avoid any deformation or failure during printing. This paper concentrates on the experimental investigation of the buildability properties of different printable materials, on the bases of shear stress, measured using the Fall-cone test. The effect of different constituents such as high range water reducer (HRWR), viscosity modifying agent (VMA), limestone filler and water content on the evolution of the yield stress in mortars, derived from the shear stress, are studied experimentally and discussed in details. Accordingly, the change of variables induces quasi linear relationship with the growth of the structuration rate and structural build-up (A_{thix}) of mortars, which corresponds to the variation of the yield stress with time. These findings enable the use of the A_{thix} concept and the proposed curves for

designing new printable mixes for what suits more the buildability properties of large scale 3D printed structures.

Key words: Mortar - Rheological properties - Admixtures

1- Introduction

In the last few years a lot of efforts have been carried out in the field of 3D printing of cementitious materials for buildings and construction. A lot of work is being done to develop adequate printing systems like extrusion based techniques, such as contour crafting (Khoshnevis, 2004; Khoshnevis et al., 2006), powder based techniques known as D-shape printing (Le *et al*, 2012a, 2012b; Nematollahi *et al*, 2017) and the Mesh Molding systems (Hack *et al*, 2015). Concrete is the most commonly used structural material worldwide, which has developed to a high level of engineering sophistication (Banfill, 2011). In highly engineered concrete applications such as 3D printing, rheology is paramount. The fresh state properties of printable mortars can be used as parameters to control the quality of the mixes and to define the purpose and mode of application of each mix. More specifically, the material used for printing has to meet certain rheological requirements and specifications, namely extrudability and buildability (Bos *et al*, 2016; El Cheikh *et al*, 2017; Khalil *et al*, 2017). This means that the ink (printable concrete) used must be fluid enough while inside the printer to be pumped and extruded, but once it gets deposited it must undergo a fast state transition to a material with enough strength to resist deformations. For example, in the case of Polylactic acid “PLA” printing, this transition is achieved by a sudden change of temperature. The polymer filament is heated inside the nozzle to above its melting point making it in a plastic state so it can be extruded. When printed, the rapid cooling causes a state transition of the material from plastic to solid behavior (Kirchmayer *et al*, 2015). This form of physical transformation is not the case of printing mortars. The state transition required for mortar after being printed imposes a new challenge. The challenge here is that mortar should preserve a yield stress higher than the stress caused by its self-weight, to overcome any deformation due to the imposed load. Further, the yield stress of the printed layer has to increase significantly with time to withstand the additional loads coming from superposed layers (Weng *et al*, 2016). Meanwhile, a balance has to be maintained between all rheological properties of printable mortar to enhance the printability characteristics. In general, pumpability and extrudability of mortars are monitored by the viscosity and dynamic yield stress of the material. Whereas, the performance of the fresh ink in terms of buildability properties is dictated by the static yield stress, which is the yield stress needed to initiate the flow/deformation of the material (Weng *et al*, 2016). Thus, the basics of developing a strong

and efficient print process depends on the ability to understand the material's technology and rheological signature.

Different methods were proposed to assess the quality of printable mortars. Generally, researches are either based on practical measurements or on theoretical calculations. For example, Le et al. (Le, Austin, Lim, Buswell, Gibb, *et al*, 2012) considered that workability, extrudability, buildability and setting time are the essential parameters for characterization. Where, extrudability is tested through the ability of the material to get out of a 9 mm circular nozzle and visually checking for any blockage or discontinuity. In addition, the workability is checked by measuring the shear strength of the mix using the vane shear apparatus, and the open time was determined accordingly. Kazemian et al. (Kazemian *et al*, 2017) considered the print quality in terms of surface quality, squared edges, dimensional consistency and conformity as the main parameters to evaluate the mix design. Consequently two test methods were adopted, the layer's settlement and the cylinder stability tests. Zhang et al. (Zhang *et al*, 2018) assessed buildability based on the visible deformation of printed layers or the collapse of the whole structure. Indeed, it is not sufficient to visually characterize buildability properties for 3D printing applications due to its substantial considerations that must be taken into consideration through physical measurements and calculations. Alternatively, in this paper, pumpability, workability and extrudability properties are visually evaluated based on extruded layers using a lab gun device, simulating the mechanism of an actual printer. Whereas, buildability properties of these mortars were further assessed, because of their crucial importance, by analyzing their thixotropic behavior.

Thixotropic behavior is a major rheological phenomenon that accounts for the change in the microstructure of a colloidal suspension and particle agglomeration at either a constant or increasing shear rate (Marchon and Flatt, 2015; Singh, Singh and Kumar, 2019) It also accounts for the recovery of the material when it goes back to rest. More specifically, when testing the rheology of cement-based materials, thixotropy is generally associated with the flocculation of particles and ongoing hydration reaction which is a time dependent process. Though, when the material is sheared, the links generated between particles are broken which leads to a decrease in the yield stress of the material (Roussel and Ovarlez, 2012; Roussel, 2018b). In addition, thixotropy is a reversible process that comes into dominance over a short timescale (Jarny *et al*, 2005), it occurs within several minutes up to 2h which is the typical time span of a printing process (Panda *et al.*, 2019a, 2019b).

Likewise, according to Roussel, when the material is at rest, the static yield stress starts to increase gradually, and it is known as structural build-up phase (Roussel, 2018a). This phase starts after the material rests for several tenth of seconds (Roussel and Ovarlez, 2012), and lasts for several tenths of minutes (Lootens *et al*, 2009; Perrot *et al*, 2015; Subramaniam Wang, 2010). The structural build-up is related to the formation of hydrates (e.g. C-S-H) bridges between cement grains (Wangler *et al*, 2016). Roussel *et al*. (Roussel and Ovarlez, 2012) proposed a linear model for the description of the structural build-up phase according to the structuration rate (A_{thix}), and it can be derived as in Eq. 1:

$$A_{thix} = \frac{\tau_0}{t} \quad (\text{Eq. 1}).$$

Where:

$$\tau = \text{Yield Stress (Pa)} \qquad t = \text{time at rest (sec)}$$

In 3D printing applications, a higher A_{thix} index provides an important indication of the stiffness of the ink used, and it is related to the ability of the layers to withstand subsequent ones. Following on, the yield stress of mortar must evolve faster than the weight application of superposed layers. This relation can be described by Eq. 2:

$$V < \frac{\sqrt{3} L A_{thix}}{\rho g h}$$

Where:

$$\begin{aligned} V &= \text{Maximum printing velocity (m/sec)} & L &= \text{Contour length (m)} \\ \rho &= \text{Density of the mix (Kg/m}^3\text{)} & g &= \text{Gravity constant (m/sec}^2\text{)} \\ h &= \text{Layer's height (m)} \end{aligned}$$

Further, a recent study introduced a specific process requirement for the evolution of the material's stiffness for a slender printed element (Suiker, 2018; Wolfs, Bos and Salet, 2018). This study demonstrated that a linear increase in the shear stress is more needed when the slenderness of the element increases. After all, it can be said that the optimization of concrete production can be easily predicted using the structural build-up properties of cement based material (Perrot *et al*, 2016).

Several rheometers have been developed to quantify the rheological behavior of cementitious materials, including their thixotropic behavior as a major characteristic. Beaupré et al. (Beaupré et al., 2003) compared the results taken from different rheometers and measuring techniques and found a constant correlation between all results, but the absolute values differed significantly (Beaupré *et al*, 2003; Banfill *et al*, 2017). For example, rotational rheometers (Qian and Kawashima, 2016) and plate rheometers (Mahmoodzadeh and Chidiac, 2013; Vance *et al*, 2015) are mostly used to test the thixotropy of cement pastes and quantify structural build-up, but they are not perfectly adapted for mortars or concrete, and this can be clearly found in the literature where most studies are conducted over mixes that do not contain aggregates. Nevertheless, rheometers are not widely used in spite of their attractiveness and accuracy. This is because they are less adapted for mortars, expensive, time consuming and need skilled operators.

Though, simpler and faster measuring techniques of the shear stress would be more adapted for 3D printing, because it is better to follow-up progressively and on site the variation of A_{thix} during the printing process. This has to be done in order to estimate the rate of buildability and layers deposition (Panda *et al*, 2019). As an example, the Fall-Cone test previously used by Estellé et al. (Estellé *et al*, 2012) when comparing the yield stress of the same paste material using different measuring techniques can be implemented for such measurements. The slump, slump flow and the flow time of the material can be also used to calculate the corresponding yield stress (Wallevik, 2006; Omran and Khayat, 2014), and the inclined plate approach can be used as well (Omran, Khayat and Elaguab, 2012). Until now, there is still no standard testing method to measure the structuration rate of fresh mortars (Chidiac, Habibbeigi and Chan, 2016; Nerella *et al*, 2019), especially for evaluating buildability properties for 3D printing applications (Tay, Qian and Tan, 2019). Knowing that, to date, the work done on quantifying structural build up and thixotropic evolution has been almost limited to normal / non-printable concrete mixes (Nerella *et al*, 2019).

Over and above, the yield stress of the fresh mix is majorly affected by the use of admixtures mainly HRWR and VMA, in addition to other mix components (Li, 2013). These additives are known for their ability to modify the rheological behavior of cementitious materials, and they are highly recommended for designing printable inks. Accordingly, the aim of this study is to give a better understanding of the early age physical properties of thixotropic printable mixes, for what suits more large-scale printing, and to demonstrate how critical are the mix proportions in the development of concrete systems for additive manufacturing in terms of structural build-up, using the Fall-Cone test.

In the literature, several researches focus on the influence of the mix compositions on the shear stress variation with respect to time, such as in (Huang *et al*, 2019). Whereas, in this paper we were more concerned by going beyond these limits, and understand the trend and mode of variation of the A_{thix} in relation to the mix compositions. Accordingly, the objectives of this paper are:

- Characterizing the effect of different constituents on the yield stress evolution of fresh printable mortars with time such as high range water reducer, viscosity modifying agent, limestone filler and water content independently.
- Establishing appropriate curves of the A_{thix} variation in relation to the material variables, which will help in formulating sustainable mortar mixes suitable for laboratory and large scale 3D printing application, based on the needed structuration rate.

2- Materials and Methods

2.1- Raw Materials

All developed mixes consist of an Ordinary Portland Cement Type 1 (CEM I 52.5 N), having a density of 3.1 g/cm^3 and $8.2 \text{ }\mu\text{m}$ median particle diameter “ D_{50} ”, CBCALC $80 \text{ }\mu\text{m}$ limestone filler with a density of 2.7 g/cm^3 and $5.7 \text{ }\mu\text{m}$ D_{50} , CHRYSO®Fluid Optima 100 HRWR having a phosphonate base with $31\% \pm 1.5\%$ dry content, commercially used BELITEX® ADDICHAP VMA powder, and a crushed limestone sand having a particle size distribution of 0 to 2 mm including 19% smaller than $63 \text{ }\mu\text{m}$ and a density of 2.7 g/cm^3 .

Fig. 1 shows the particle size distributions (PSD) of powder materials used. These distributions were determined using an LS 13 320 Laser Diffraction Particle Size Analyzer. PSDs of cement and limestone are compared to that of the sand used. It can be seen that the particle size of the cement and limestone filler are close.

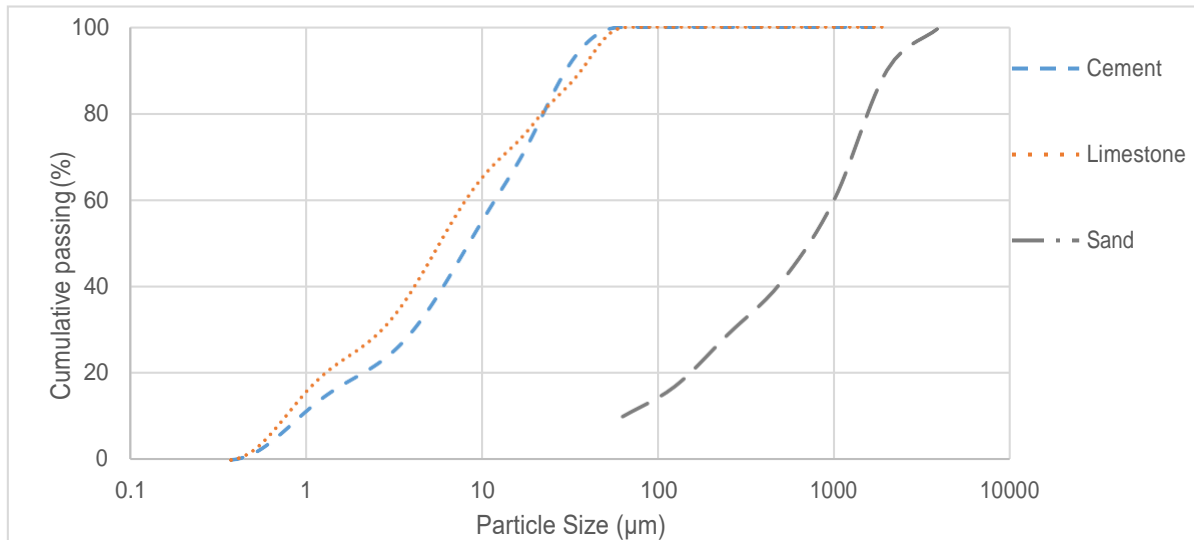


Figure 1 Particle Size Distributions for Sand, Cement, and Limestone Filler

2.2- Mix Design

In order to obtain the desired quality and performance of the printable mix, all constituents and their proportions have to be carefully determined (Klovas, 2018). In this paper, all mixes are designed so that all of them are printable (as discussed later on in section 2.3.2). Mixes are classified under four main categories according to their compositions. Table 1 shows all the mixes constituents by mass (grams). Category 1 includes mixes with different HRWR concentrations starting by a dry content concentration of 0.126% of the cement's mass which is equivalent to a liquid mass of 2 g, straight up to 0.25% that is equal to 4 g. An increment of 0.5 g (0.031% dry content) is maintained between all mixes. Category 2 includes mixes with different VMA concentrations with respect to the cement's mass. An initial mass of 1 g (0.2%) is adopted and it keeps on increasing by 0.5 g (0.1%) until a total mass of 3 g (0.6%). All the admixture concentrations that were adopted in these mixes fall within the allowable range specified by the manufacturer to overcome any adverse effect such as excessive retardation of the very early age hydration reactions. Category 3 contains mixes with different limestone filler contents, knowing that the total volume of the paste is maintained constant. The initial mix contains 100 g (15%) limestone filler of the total powder content. This fraction keeps on increasing by 32 g (5%) in each mix until it reaches 227 g (35%). Category 4 mainly contains a variation in the water to cement ratio (W/C) that starts by 0.41 with an increment of 0.02 up to 0.47. In order to simplify the design of printable materials of category 4, mixes are adapted by only increasing their water content, without keeping a constant volume of paste. Thus, a second but less influencing parameter comes into play which is the volumetric proportion of the paste that increased from 0.274 to 0.303 due to the addition of 10 cm³ of water in each mix.

Table 1 Mixes compositions (mass in grams)

	Sand	OPC	Filler	Water (W/C)	HRWR	VMA
Category 1						
Mix1	850	493	164	251	2	1
Mix2	850	493	164	251	2.5	1
Mix3	850	493	164	251	3	1
Mix4	850	493	164	251	3.5	1
Mix5	850	493	164	251	4	1
Category 2						
Mix5	850	493	164	251	4	1
Mix6	850	493	164	251	4	1.5
Mix7	850	493	164	251	4	2
Mix8	850	493	164	251	4	2.5
Mix9	850	493	164	251	4	3
Category 3						
Mix10	850	567	100	251	4	2
Mix11	850	530	132	251	4	2
Mix7	850	493	164	251	4	2
Mix12	850	457	196	251	4	2
Mix13	850	421	227	251	4	2
Category 4						
Mix14	850	493	164	202 (0.41)	7.5	2
Mix15	850	493	164	212 (0.43)	7.5	2
Mix16	850	493	164	222 (0.45)	7.5	2
Mix17	850	493	164	232 (0.47)	7.5	2

2.3- Methods

2.3.1- Mixing Procedure

A mixing procedure was adopted and always done at room temperature (≈ 22 °C) to minimize the difference between batches. A Hobart mixer N50CE was used. Firstly, all solid ingredients were dry mixed for 2 minutes at low speed (60 RPM). Then, water and HRWR were added within 30 seconds while keeping on mixing at low speed. The mixing process continued for 90 seconds at high speed (124 RPM), followed by 60 seconds of rest. At the end, 120 seconds of mixing at high speed were carried out before collecting the material.

2.3.2- Printability Test

All mixes are tested for printability by printing straight layers on top of each other using first a lab gun device having a circular nozzle of 1 cm diameter similar to the one previously used by El-Cheikh et al. (El Cheikh *et al*, 2017), Khalil et al. (Khalil *et al*, 2017) and Baz et al. (Baz *et*

al, 2020; Baz *et al*, 2020), and then using a gantry printer having a circular nozzle of 1.9 cm diameter (Fig. 4a).

2.3.3- Fall-Cone Test

In this study we adopted the Fall-Cone test as per the European standard “NF EN ISO 17892-6” (CEN, 2017) to quantify the thixotropic behavior of cement mortars. This test consists of measuring the penetration depth of a cone under an imposed load (Estellé *et al*, 2012). From a rheological perspective, the contact between the surface of the cone and mortar will increase as it penetrates more, thus the resisting forces induced by the shear stress will keep on increasing to reach an equilibrium point with the applied mass. In our case, in order to insure a significant penetration of the cone in the material, we used a cone having a 30 ° angle and we added 100 g to the initial mass of the system (80 g), so we ended up having a total mass of 180 g. After mixing, the material is collected and placed in a circular steel container having a depth of 5 cm and a diameter of 30 cm. The container is then placed over a jolting table for 30 jolts to ensure a uniform distribution and leveling of the material inside the bucket. The surface of the bucket is gently sawn to cut off the excessive material. The sample is left 120 seconds first at rest after finishing, because the vibration of the mortar has the potential to decrease its yield stress to about the half (Hu and Larrard, 1996). The cone is positioned so that its tip just touches the surface of the sample. Then after, the cone is released for around 5 seconds so that it has enough time to penetrate the material. A minimum distance of 5 cm is left between successive penetrations (Fig. 2). At the end, the penetration depth is recorded and the corresponding yield stress is calculated using Eq. 3:

$$\tau = \frac{F \cos \theta^2}{\pi h^2 \tan \theta}$$

Where:

τ = Yield Stress (Pa)

θ = Angle of the Cone used (30 °)

F = Force generated by the mass of Cone (180 g)

h = Penetration depth of the Cone (mm)

This procedure is repeated each 150 seconds (2.5 minutes) over the course of 1320 seconds (22 minutes) for all mixes, because for a longer duration the cone would no longer penetrate in most of the mixes, and the measurements would not be accurate anymore. Each mix is tested

three times, each on a different batch, and the final result of every mix corresponds to the average of all trials.



Figure 2 Fall-Cone Test

2.3.4 – Mechanical Performance

As previously explained, the core findings of this research are based on the fresh state properties of the developed mixes, in particular their thixotropic behavior. However, the varying parameters do also affect the hardened state properties, which are equally important as much as their fresh properties from a mix design standpoint.

In consequence, the mechanical performance of all prepared mixes was systematically evaluated by measuring their compressive strengths at 2 and 28 days. Tests are conducted over a set of 4×4×16 cm beams. Each mold is filled by 2 layers and each one is struck 60 times using a jolting table, according to the European standard placing method NF EN 196-1 (AFNOR, 2006). The samples are kept for 24h in the molds then they are de-molded and put to cure in 100% RH and 23°C until the testing date. After then, all samples are tested under compression at a load rate of 144 KN/min according to the European standard testing method NF EN 196-1 (AFNOR, 2006).

3- Results and Discussion

3.1- 3D Printing performance

Fig. 3 shows how a printed element looks like when produced using the laboratory (Lab.) gun device to assess for the printability properties. It also reveals the ability of using this device in anticipating the aspect of the material to be used for 3D printing. Thus, all developed mixes showed the ability to be used for 3D printing applications. As well, mix7 (from table 1) was randomly selected to be printed using the actual printer shown in Fig. 4 (a). Fig. 4 (b) shows an arbitrary shape being printed to ensure the performance of the developed mix. Then after, a cut was taken from the printed element to visualize closely the superposed layers Fig. 4 (c). The printed element consisted of 10 superposed layers, each 1 cm deep. The layers were able to keep on their predefined geometry without showing any deformation or shape instability due to the fact of superposition.

Any variable's concentration falling outside the specified ranges in the developed mixes would result in a non-printable material, either due an early collapse of the first deposited layer, or due to blockage and un-extrudability issues. In other words, if an HRWR concentration, W/C or limestone filler content is above 0.8%, 0.47 and 35% respectively, the material would be too fluid to carry on superposed layers. Whereas, a concentration of HRWR below 0.4% or a W/C and limestone filler content below 0.41 and 15% would result in a stiff material unable to be extruded. Oppositely, a VMA concentration below 0.2% gives an extremely fluid material, while a concentration above 0.6% makes it unprintable. Note that, these ranges apply only over the mixes developed for this study.



Figure 3 Printed element using the Lab. Gun



(a)



(b)



(c)

Figure 4 Printed element (b, c) using the actual printer (a)

3.2- Effect of High Range Water Reducer (HRWR)

Fig. 5 shows the variation of the yield stress with respect to time for all mortars with different HRWR dosages. It can first be seen that the yield stress increases with time, whatever the HRWR content is. Moreover, an increase of HRWR concentration in the mix, leads to a decrease in the thixotropy of the mortar (decrease in the slope of the curve). Besides, the mode of variation of the yield stress with respect to time can be reasonably described using a linear model with an acceptable correlation factor (R^2) varying between 0.89 and 0.97.

All over this study, we adopted the linear model proposed by Roussel et al. (Roussel and Ovarlez, 2012) because it is based on a single variable. This model is described as a function of the structuration rate (A_{thix}), defined in Eq. 4:

$$\tau_0(t) = \tau_{0,0} + A_{thix}t \quad (\text{Eq. 4})$$

The corresponding A_{thix} is equal to the slope of the resulting curve. However, the initial shear stress at time $t = 0$ ($\tau_{0,0}$) is neglected, because it is very small in comparison to the shear stresses developed when the mix is at rest. Thus, the results of this study are presented according to Eq. 5:

$$\tau_0(t) = A_{thix}t \quad (\text{Eq. 5})$$

However, Perrot et al. (Perrot, Pierre and Picandet, 2015) proposed an exponential model that implements a critical time characteristic (t_c) corresponding to the adjusted time needed to obtain the best exponential fit curve, in addition to the A_{thix} . This relation is described in Eq. 6:

$$\tau_0(t) = A_{thix}t_c \left(e^{t_{rest}/t_c} - 1 \right) + \tau_{0,0} \quad (\text{Eq. 6})$$

This model describes a smooth transition from a linear increase of shear stress at early age to an exponential evolution after a period of time. Still, all the results in this study were also examined using the exponential growth model, but most cases did not give better correlations than the linear one. For example, in this case the exponential model gave lower correlations varying between 0.85 and 0.95. Thus, for coherence with the objectives of our study aiming to characterize the buildability properties of different printable mixes, the A_{thix} is chosen as a simplified physical parameter representing the material's behavior.

Fig. 6 shows the variation of A_{thix} as a function of HRWR content for the mixes of category 1. The structuration rate of the mortar decreases linearly with the increase of HRWR concentration in the mix. The increase of HRWR content from 0.126% to 0.25% decreased the A_{thix} from about 6.9 Pa/sec to 2.93 Pa/sec (2.35 times) ($R^2=0.9474$). These results and mode of variation are in agreement with the study done by Khalil (Khalil, 2018) about the formulation and rheological characterization of mortars with Ordinary Portland Cement and Sulfoaluminate Cements. In her Study, Khalil found that the yield stress of pastes decreases linearly during the first 1500 seconds (25 minutes) as the dosage of HRWR in the mix increases. As well, Qian et al. (Qian *et al.*, 2018) concluded that an increase of HRWR decreases thixotropy through a corresponding relation between the yield stress and the steady-state equilibrium value at

constant shear rates. Precisely, this relation accounts for the initial peak value of the measured stress followed by a decay until reaching the steady state.

An increase in the HRWR concentration decreases the A_{thix} , because in general as the concentration of HRWR increases in the mix, the de-flocculation and dispersion of cement grains will also increase making it harder for the C-S-H bridges to be produced during the same period of time as for mixes having a lower dosage.

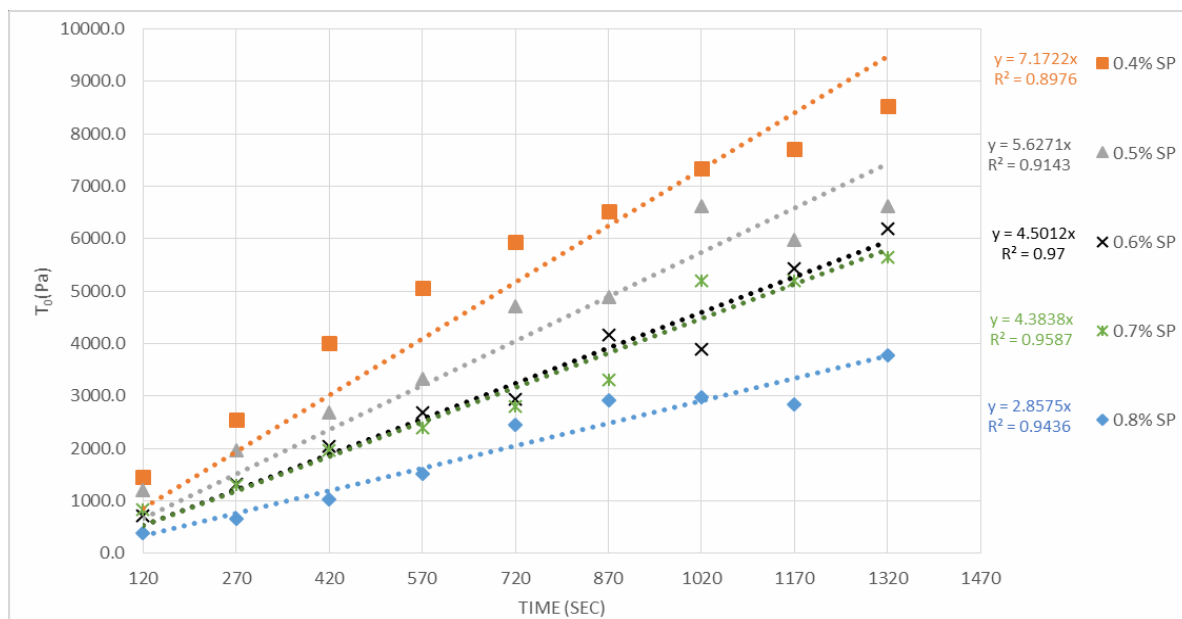


Figure 5 yield stress variation for different HRWR concentrations

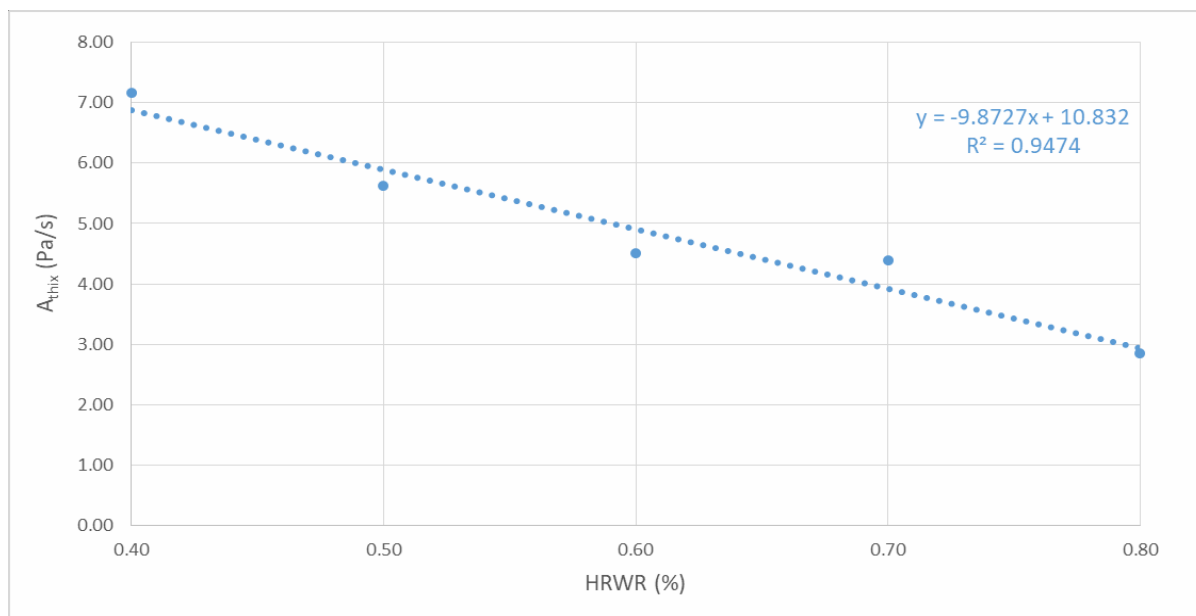


Figure 6 Effect of HRWR on the Structuration Rate

3.3- Effect of Viscosity Modifying Admixture (VMA)

Fig. 7 shows the yield stress variation for mixes having different VMA concentrations in function of time. An increase of yield stress is always maintained with time. Same as for the case of HRWR, a linear model is adopted to describe the variation of the yield stress with time. Accordingly, a reasonable correlation factor (R^2) is shown for all mixes varying between 0.93 and 0.97, knowing that the exponential model was not better since a lower correlation between the results was found ranging between 0.88 and 0.96.

Fig. 8 describes the variation of the structuration rate of all corresponding mixes. The results show that A_{thix} increases from 3.5 Pa/sec to 6 Pa/sec (1.7 times). An increase in the rate of structural build-up due to the thixotropy of the mixes follows the augmentation of VMA concentration until a certain limit. However, a concentration higher than 0.3% does not lead to a considerable increase in the structuration rate of the mortar, thus it is considered as a turning point. Hence, the variation cannot be presented as a linear increase. The same effect of VMA on the yield stress was found in the study done by Daukšys et al. (Daukšys and Klovas, 2018).

It is commonly known that VMAs play a key function in modifying the rheology of the cement paste, they increase the macroscopic yield stress to a certain extent (Nguyen, Remond and Gallias, 2011; Helnan-Moussa, Vanhove and Wirquin, 2013; Chen *et al*, 2019). There are few researches in the literature that studied the effect of VMA on the thixotropy of cement pastes but from a different perspective, such as in Rahul et al. (Rahul *et al*, 2019). They tested the setting time and rate of hydration of cement in the presence of a constant VMA concentration, and concluded its effect on the thixotropic variation. Even though, they found a similar conclusion, where the VMA increases the thixotropy.

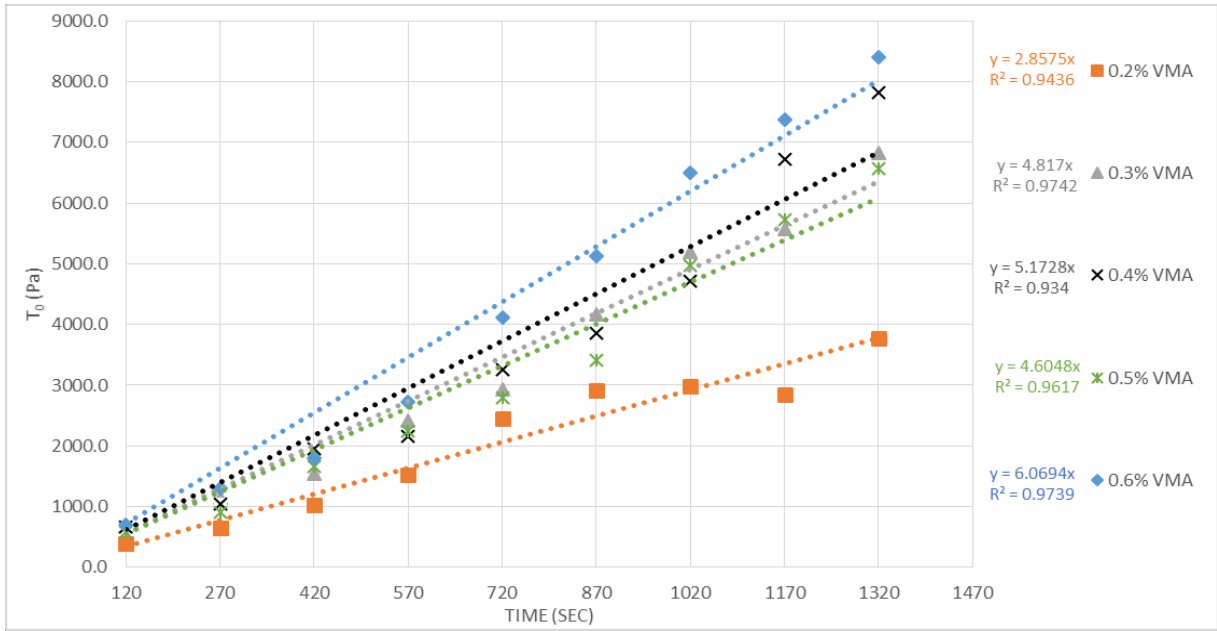


Figure 7 yield stress variation for different VMA concentrations

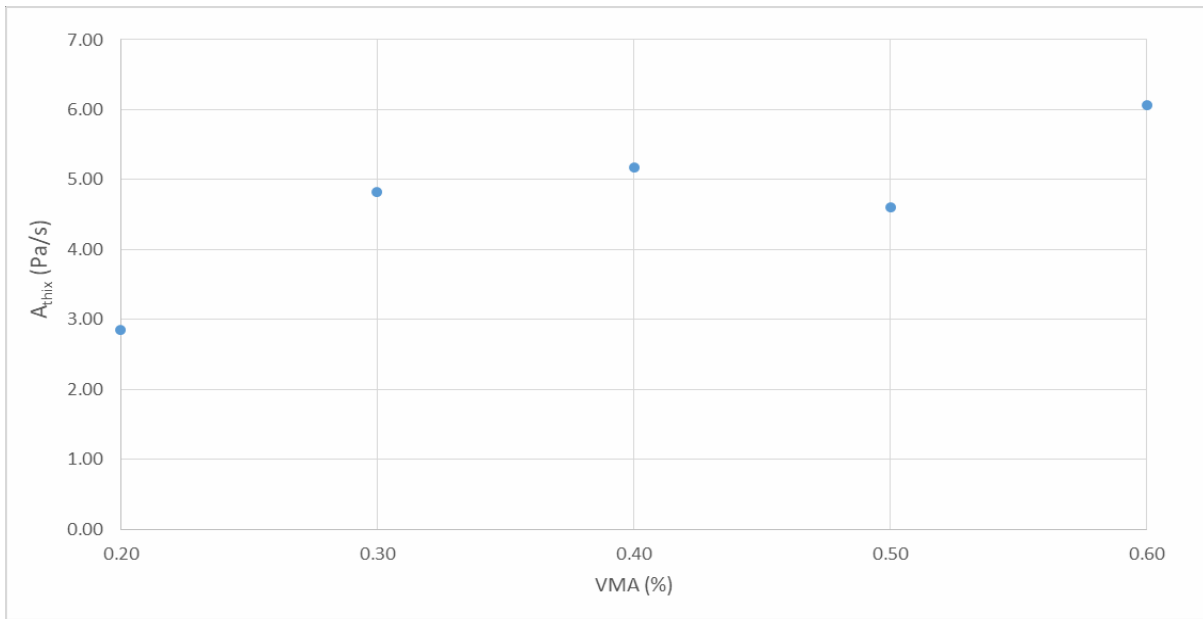


Figure 8 Effect of VMA on the Structuration Rate

3.4- Effect of Limestone Filler

Fig. 9 and Fig. 10 show respectively the yield stress evolution and the A_{thix} variation of mixes having different limestone filler proportions in the mix. The yield stresses induced in the material increase continuously with time. This variation is well represented by the linear model (R^2 varying between 0.93 and 0.97). However, the thixotropy decreases as the proportion of the limestone filler increases in the mix (Fig. 9), and this was also reported by Rahman et al. (Rahman et al., 2014) when studying the thixotropic behavior of self-compacting concrete with different mineral admixtures. Here also, Perrot's model cannot be considered

better because it showed an approximately similar correlation between results (R^2 ranging between 0.93 to 0.96). Although, the decrease in the thixotropy of the material shown in Fig. 9 can be expressed by a linear decrease in the A_{thix} (Fig. 10). A replacement of 20% of the cement powder by limestone filler decreases the A_{thix} 1.83 times ($R^2=0.9202$). This decrease happened because limestone powder do not generate C-S-H, it only plays the role of a nucleation site. Thus, the total production of C-S-H fraction would relatively decrease as well as the structuration rate, due to the reduced amount of cement particles enabling the formation of effective colloidal bridges between grains.

As mentioned previously in the literature, the structural build-up evolution is derived from the C-S-H formation between cement grains. In general, limestone is considered as an inert filler material that improves the hydration rate of cement at early age (Camiletti, Soliman and Nehdi, 2014), thus it increases the total volume of the hydration products. In the literature, some researches investigating the effect of limestone powder on the build-up rate of cementations material cared more to preserve a certain level of workability or flowability. For example Rahman et al. (Rahman, Baluch and Malik, 2014) managed to control the flowability of the developed mixes to a certain value by changing the dosage of Superplasticizer and the limestone content simultaneously. In that way, Rahman et al. (Rahman, Baluch and Malik, 2014) were able to conclude that the addition of limestone filler resulted in an increase of the structuration rate using the ICAR rheometer.

Contrarily, this is not the case of the study in hand, since we are keeping on the same effective water volume for all mixes, and the addition of limestone is done by a volumetric substitution of cement powder. The total volume of the mix is always maintained constant. In other words, we are preserving the same Water to Binder ratio (W/B). Limestone filler is the only increasing element in this category. Thus, this action gives a higher water to cement ratio (W/C) for each mix, contributing also to this decrease. In the same context, a relevant study done by El-Moussaoui et al. (El-Moussaoui, Dhir and Hewlett, 2019) went over the effect of partial substitution of cement by limestone and water to cement ratio (W/C), combined, on the strength development of the mix design.

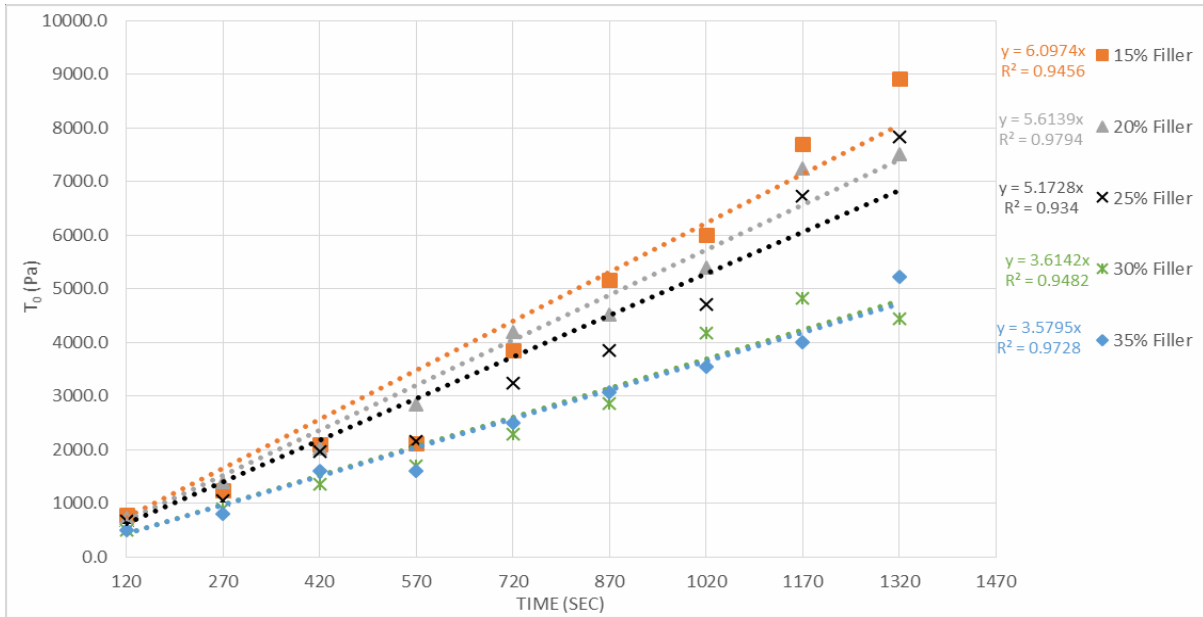


Figure 9 yield stress variation for different filler concentrations

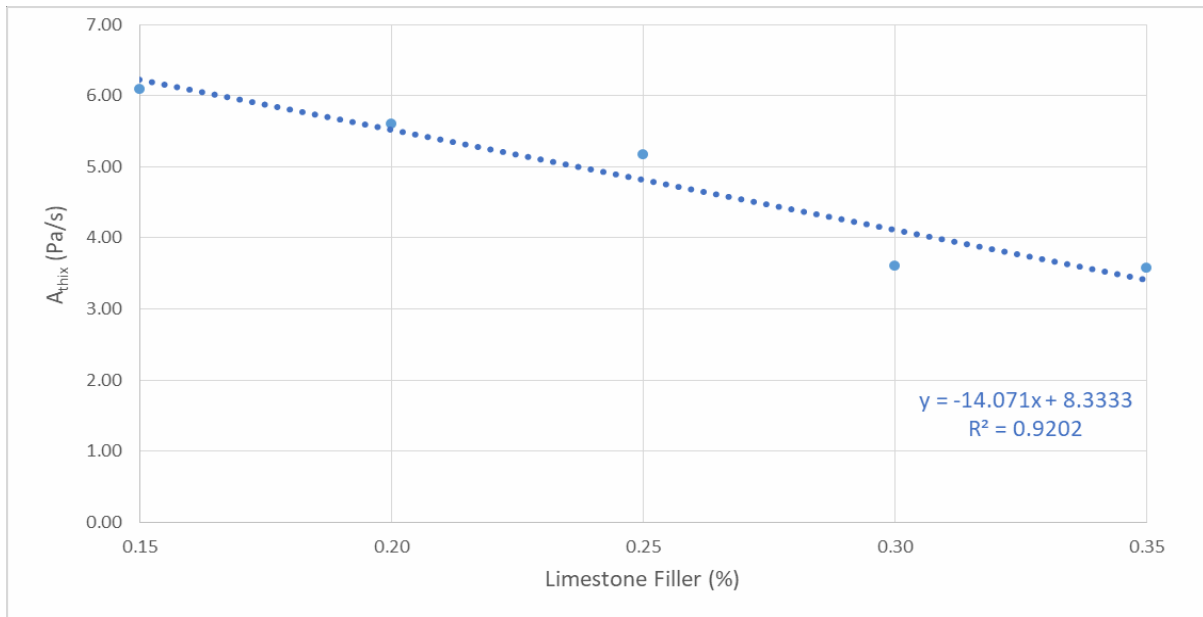


Figure 10 Effect of Limestone Filler on the Structuration Rate

3.5- Effect of Water Content

Fig. 11 shows the evolution of the yield stress for mixes having different water contents in function of time. The increase in the water content decreases considerably the thixotropy of the mix.

At first, it was noticed that the variation of the yield stress was more likely to be exponential rather than linear when going through the entire time scale (1320 seconds). Thus, the exponential growth rate model proposed by Perrot et al. (Perrot, Pierre and Picandet, 2015) was more representative, and it gave an R^2 ranging between 0.94 and 0.98, whereas, the linear

model gave an R^2 varying between 0.74 and 0.91. Thus, the growth rate of the shear stress can be divided into two stages. In the first stage defined between 120 seconds and 870 seconds, the shear stress variation was linear and quite slow. Then after, a fast development of the shear stress happened until the end of the testing time (1320 seconds), and this can be clearly observed in Fig. 11 for the mix having a W/C of 0.41. That is why, in order to keep on the same analysis method adopted for all previous measurements, we kept on Roussel's model but the results were limited to the first part of the variation (up to 870 seconds), in order to have a more relevant sequence with better correlations. In this case, the range of variation of R^2 with the linear model improved to an interval of 0.93 and 0.95.

Fig. 12 shows the effect of the water content on the structuration rate (A_{thix}) measured only for the first 870 seconds. It can be observed in both figures how severe the addition of water to the mix is. The results of our study showed that an increase in the W/C from 0.41 to 0.47 would dramatically decrease the A_{thix} 12.5 times in a linear fashion ($R^2=0.9003$). These results occurred because when the water content increases, the packing density decreases and a weaker internal friction is generated. Consequently, the excessive water separate further the cement grains from each other making it harder for C-S-H bonds to be formed, and therefore decrease the yield stress and A_{thix} . The results of our research are also coherent with those of Banfill (Banfill, 2011) when testing the additivity effects in the rheology of fresh concrete containing water reducing admixtures, and Khalil (Khalil, 2018).

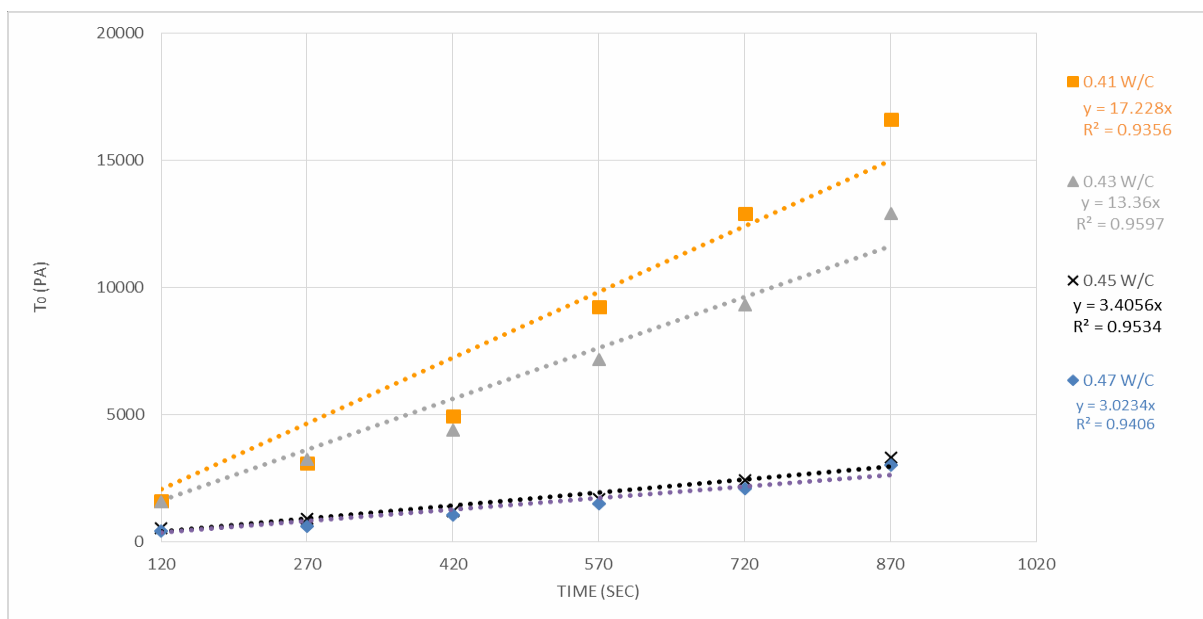


Figure 11 yield stress variation for different W/C

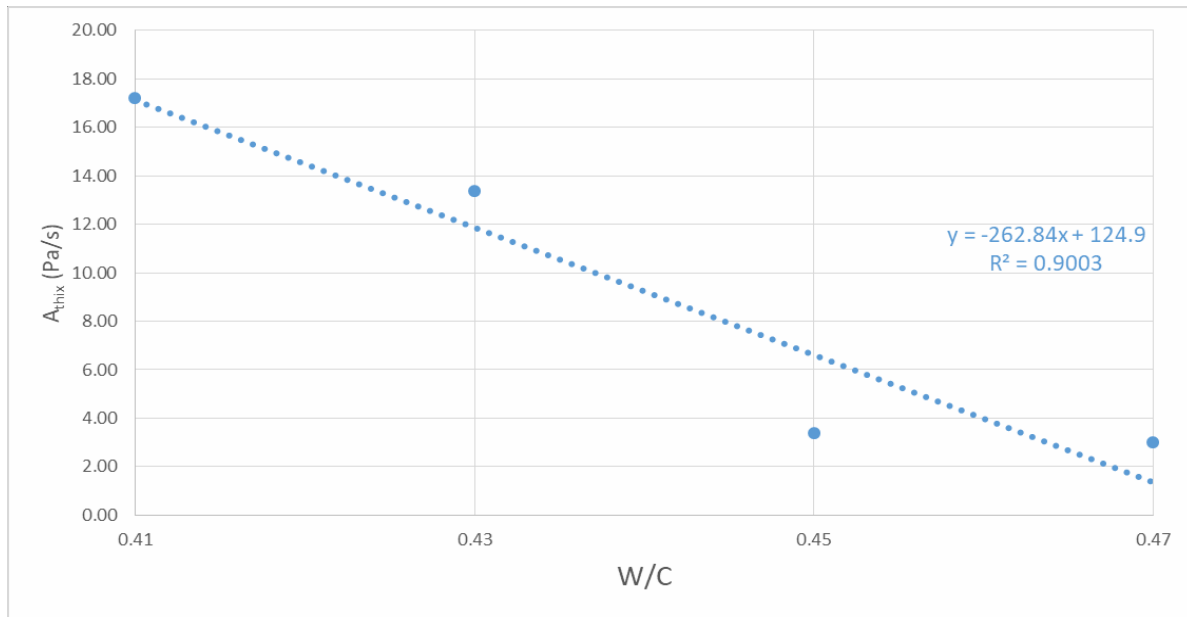


Figure 12 Effect Of W/C on the Structuration Rate

3.6- Mechanical Performance

The compressive strength of all mixes at 2 and 28 days are summarized in Table 5. Indeed, it is well known that the fresh state properties of cement-based mixtures influence the hardened state properties and mechanical performance of the material (Grazia *et al*, 2020). Herein, the results show that the compressive strength of mixes having different HRWR concentrations but a constant W/C were almost the same for all samples. These results comply with the literature, such as in Boudchicha et al. (Boudchicha, Zouaoui and Gallias, 2012) when studying the Influence of the formulation parameters on the compressive strengths of mortars with admixtures, as well as in Dhir et al. (Dhir and Andrew W. F. Yap†, 1983). As for the mixes having different VMA concentrations and a constant W/C, they approximately gave similar compressive strengths, which is also in alignment with studies on the mode of action and application guidelines for Viscosity Modifying Agents in concrete mixes (EFNARC, 2006). Thus, it can be said that these admixtures influence mainly the fresh properties of concrete, and they do not have any significant effect on the strength development when properly used. They physically affect the rheological properties of cement-based materials. Hence, for a successful development of 3D printable mixtures it would be more apposite to control their rheology through the use of the suitable combination of admixtures. On the contrary, replacing a portion of cement by limestone filler decreased the compressive strength of the mixes as the proportion of cement decreases due to its dilution effect. Similarly, increasing the water content decreased the compressive strength of the mixes. This happens due to the creation of additional pores that weakened the hardened material.

Table 2 Compressive Strength of All Mixes

Category 1 (MPa)			Category 2 (MPa)		
	2 days	28 days		2 days	28 days
0% HRWR (Ref.) <i>(std. dev.)</i>	33.14 <i>(2.07)</i>	47.05 <i>(2.25)</i>	0% VMA (Ref.) <i>(std. dev.)</i>	31.9 <i>(1.87)</i>	53.34 <i>(3.41)</i>
0.4% HRWR <i>(std. dev.)</i>	36.84 <i>(1.33)</i>	54.5 <i>(3.94)</i>	0.2% VMA <i>(std. dev.)</i>	39.44 <i>(1.03)</i>	55.32 <i>(3.8)</i>
0.5% HRWR <i>(std. dev.)</i>	38.52 <i>(1.74)</i>	55.57 <i>(3.14)</i>	0.3% VMA <i>(std. dev.)</i>	38.6 <i>(2.55)</i>	55.87 <i>(3.6)</i>
0.6% HRWR <i>(std. dev.)</i>	38.81 <i>(0.26)</i>	52.13 <i>(2.94)</i>	0.4% VMA <i>(std. dev.)</i>	38.19 <i>(1.87)</i>	60.19 <i>(2.6)</i>
0.7% HRWR <i>(std. dev.)</i>	40.47 <i>(1.15)</i>	55.95 <i>(3.04)</i>	0.5% VMA <i>(std. dev.)</i>	40.43 <i>(2.49)</i>	56.85 <i>(3.16)</i>
0.8% HRWR <i>(std. dev.)</i>	39.44 <i>(1.03)</i>	55.32 <i>(3.8)</i>	0.6% VMA <i>(std. dev.)</i>	41.69 <i>(2.73)</i>	54.55 <i>(3.34)</i>
Category 3 (MPa)			Category 4 (MPa)		
	2 days	28 days		2 days	28 days
0% Filler (Ref.) <i>(std. dev.)</i>	50.22 <i>(2.29)</i>	67.7 <i>(4.5)</i>	0.41 (W/C) <i>(std. dev.)</i>	48.55 <i>(3.5)</i>	73.12 <i>(3.76)</i>
15% Filler <i>(std. dev.)</i>	43.22 <i>(2.18)</i>	62.8 <i>(4.32)</i>	0.43 (W/C) <i>(std. dev.)</i>	47.54 <i>(1.86)</i>	66.23 <i>(4.21)</i>
20% Filler <i>(std. dev.)</i>	41.24 <i>(2.2)</i>	60.08 <i>(2.92)</i>	0.45 (W/C) <i>(std. dev.)</i>	43.25 <i>(2.08)</i>	63.87 <i>(4.21)</i>
25% Filler <i>(std. dev.)</i>	38.19 <i>(1.87)</i>	60.19 <i>(2.6)</i>	0.47 (W/C) <i>(std. dev.)</i>	42.23 <i>(1.45)</i>	61.99 <i>(3.96)</i>
30% Filler <i>(std. dev.)</i>	35.86 <i>(1.44)</i>	54.09 <i>(4.22)</i>			
35% Filler <i>(std. dev.)</i>	32.48 <i>(1.00)</i>	50.17 <i>(2.94)</i>			

4- Conclusion

The results presented in this paper showed the efficiency of the Fall-Cone test for measuring the thixotropic behavior of mortars. This method helps in improving the buildability of mortars, and preventing the deformation and collapse of fresh concrete during printing in case of any perturbation that could happen in real situations. Going further beyond, this rapid method of testing the fresh behavior of concrete would consequently help in identifying the size of concrete batches that should be prepared, and the exact building rate that should be adopted in order to avoid weak layer interface or cold-joints effect.

More technically, the results of this research show that the linear model applied over the experimental measurements taken from the Fall-Cone test is capable of simulating and depicting the actual thixotropic behavior of mortars, during a period of time close to 1320 seconds. Further, it can be seen that a reasonable linear relationship is found between the structuration rates (A_{thix}) and the variable's concentration in the mix except for the case of VMA. Consequently, the formulation of new mixes based on a predefined A_{thix} value became easier by using the appropriate proposed curves. However, the material variables influence the A_{thix} variation in a different order of magnitude.

Last of all, controlling the thixotropy of mortars should be done by adapting the concentration of the appropriate admixtures and chemicals, such as the HRWR and VMA because they do not influence its compressive strength. On the other hand, limestone filler and water content should be used only to modify the hardened state properties of the material.

For future work, the overall mix design should be tailored according to the element to be printed in terms of shape and time, and it would be highly interesting to investigate the failure mode of the freshly printed material.

Acknowledgment

The authors would like to acknowledge the financial support by Partenariats Hubert Curien (PHC) CEDRE program PROJET N° 42287YD, and the Supply of material from Carrières du Boulonnais, Eqiom, and Chryso.

Conflict of interest

We know of no conflicts of interest associated with this publication, and there has been no financial support for this work that could have influenced its outcomes. As a corresponding Author, I confirm that the manuscript has been read and approved for submission by all the named authors.

References

AFNOR NF EN 196-1, Methods of testing cement - Part 1 : determination of strength' (2006).

Phil Banfill, Denis Beaupré, Frédéric Chapdelaine, François de Larrard, Peter Domone, Laurent Nachbaur, Thierry Sedran, Olaf Wallevik, and Jon E. Wallevik (2017) 'Comparison of concrete rheometers : International tests at LCPC (Nantes , France) in October , 2000'.

Banfill, P. F. G. (2011) 'Additivity effects in the rheology of fresh concrete containing water-reducing admixtures', *Construction and Building Materials*, 25, pp. 2955–2960. doi: 10.1016/j.conbuildmat.2010.12.001.

Baz, B., Aouad, G., Leblond, P., Al-mansouri, O., Melody, D., and REMOND, S., (2020) 'Mechanical assessment of concrete – Steel bonding in 3D printed elements', *Construction and Building Materials*, 256, p. 119457. doi: 10.1016/j.conbuildmat.2020.119457.

BAZ, B., AOUAD, G. and REMOND, S. (2020) 'Effect of the Printing Method and Mortar's Workability on Pull-Out Strength of 3D Printed Elements', *Construction and Building Materials*, 230, p. 117002. Available at: <https://doi.org/10.1016/j.conbuildmat.2019.117002>.

Beaupré, D., Chapdelaine, F., Domone, P., Koehler, E., Shen, L., Sonebi, M., Struble, L., Tepke, D., Olafur, W., and Wallevik, Jon E. (2003) 'Comparison of concrete rheometers : International tests at MB (Cleveland OH , USA)', *National Institute of Standards and Technology*.

Bos, F., Bos, Wolfs, R., Ahmed, Z., Salet, T., (2016) 'Additive manufacturing of concrete in construction: potentials and challenges of 3D concrete printing', *Virtual and Physical Prototyping*, 11(3), pp. 209–225. doi: 10.1080/17452759.2016.1209867.

Boudchicha, A., Zouaoui, M. C. and Gallias, J. (2012) 'Influence of the Parameters of Formulation on the Mechanical Strengths of Cementing Materials with Admixtures and Super- plasticizers', pp. 17–19.

Camiletti, J., Soliman, A. M. and Nehdi, M. L. (2014) 'Effect of limestone addition on early-age properties of ultra high-performance concrete', *Proceedings of the Institution of Civil Engineers*, 167(CM2), pp. 65–78.

CEN (European Committee for Standardization) (2017) 'EN ISO 17892-6: Geotechnical investigation and testing - laboratory testing of soil - part 6: Fall cone test'.

El Cheikh, Rémond, S., Khalil, N., and Aouad, G. (2017) 'Numerical and experimental studies of aggregate blocking in mortar extrusion', *Construction and Building Materials*, 145, pp. 452–463. doi: 10.1016/j.conbuildmat.2017.04.032.

Chen, Y., Figueiredo, S., Yalçinkaya, Ç., Çopuroğlu, O., Veer, F., and Schlangen, E. (2019) 'The effect of viscosity-modifying admixture on the extrudability of limestone and calcined clay-based cementitious material for extrusion-based 3D concrete printing', *Materials*, 12(9). doi: 10.3390/ma12091374.

Chidiac, S. E., Habibbeigi, F. and Chan, D. (2016) 'Slump and Slump Flow for Characterizing Yield Stress of Fresh Concrete', *International Concrete Abstracts Portal*, 103(6), pp. 413–418.

El-Moussaoui, M., Dhir, R. K., and Hewlett, P. C. (2019) 'Concrete strength development and sustainability: the limestone constituent cement effect', *Magazine of Concrete Research*, 71(21), pp. 1097-1112.

Daukšys, S. and Klovas, A. (2018) 'Calculation of plastic viscosity of concrete mixture using the modified empirical formula', *FIB Conference: Sustainable Concrete:*

Materials and Structures, (442), pp. 012–018. doi: 10.1088/1757-899X/442/1/012018.

Dhir, R. K. and Andrew W. F. Yap† (1983) ‘Superplasticized high-workability concrete: some properties in the fresh and hardened states’, *Magazine of Concrete Research*, 35(125), pp. 214–228.

EFNARC (2006) ‘Guidelines for Viscosity Modifying Admixtures For Concrete’, European Federation of Concrete Admixture Associations.

Estellé, P., Michon, C., Lanos, C., and Grossiord, J.L. (2012) ‘De l ’ intérêt d ’ une caractérisation rhéologique empirique et relative’, *Rhéologie*, 21, pp. 10–35.

Grazia, M. T. De, Sanchez, L. F. M., Romano, R., and Pileggi, R. (2020) ‘Evaluation of the fresh and hardened state properties of low cement content systems’, *Magazine of Concrete Research*, 72(5), pp. 232–245.

Hack, N., Lauer, W., Gramazio, F., and Kohler, M. (2015) ‘Mesh Mould: Robotically Fabricated Metal Meshes as Concrete Formwork and Reinforcement’, *FERRO-11: Proceedings of the 11th International Symposium on Ferrocement and 3rd ICTRC International Conference on Textile Reinforced Concrete*, pp. 347–359.

Helnan-Moussa, B., Vanhove, Y. and Wirquin, E. (2013) ‘Thixotropic behaviour and structural breakdown of fresh cement paste: comparison between two types of VMA’, *Advances in Cement Research*, 25(4), pp. 235–244.

Hu, C. and Larrard, F. de (1996) ‘The Rheology of Fresh High-Performance Concrete’, *Cement and Concrete Research*, 26(2), pp. 283–294. doi: [https://doi.org/10.1016/0008-8846\(95\)00213-8](https://doi.org/10.1016/0008-8846(95)00213-8).

Huang, T., Yuan, Q., Huang, H., Peng, J., Deng, D., and Xie, Y. (2019) ‘The structural buildup of cement paste and its rheological characterization’, *15 th International Congress on the Chemistry of Cemen.*,

Jarny, S., Roussel, N., Rodts, S., Bertrand, F., Le Roy, R., and Coussot, P. (2005) ‘Rheological behavior of cement pastes from MRI velocimetry’, *Cement and Concrete Research*, 35(10), pp. 1873–1881. doi: 10.1016/j.cemconres.2005.03.009.

Kazemian, A., Yuan, X., Cochran, E., and Khoshnevis, B. (2017) ‘Cementitious materials for construction-scale 3D printing: Laboratory testing of fresh printing mixture’, *Construction and Building Materials*, 145, pp. 639–647. doi: 10.1016/j.conbuildmat.2017.04.015.

Khalil, N., Aouad, G., El Cheikh, K., and Remond, S. (2017) ‘Use of calcium sulfoaluminate cements for setting control of 3D-printing mortars’, *Construction and Building Materials*, 157, pp. 382–391. doi: 10.1016/j.conbuildmat.2017.09.109.

Khalil, N. (2018) Formulation et caractérisation chimique et rhéologique des mortiers imprimable en 3D a base de mélanges de ciments portland et sulfoalumineux., Ph.D thesis. IMT Lille Douai.

Khoshnevis, B. (2004) ‘Automated construction by contour crafting - Related robotics and information technologies’, *Automation in Construction*, 13(1), pp. 5–19. doi: 10.1016/j.autcon.2003.08.012.

Kirchmajer, D. M., Iii, R. G. and Panhuis, M. (2015) ‘An overview of the suitability of hydrogel-forming polymers for extrusion-based 3D-printing’, *Journal of Materials Chemistry B*, 3, pp. 4105–4117. doi: 10.1039/C5TB00393H.

Klovas, A. (2018) ‘The Influence of Fine Particle Content (Cement Together with Sand Particles up to 0 . 25 mm) on Rheological Properties of Concrete Mixture’. doi: 10.4028/www.scientific.net/SSP.276.97.

Le, T. T., Austin, S. A., Lim, S., Buswell, R. A., Law, R., Gibb, A.G.F., and Thorpe, T. (2012) ‘Hardened properties of high-performance printing concrete’, *Cement and Concrete Research*, 42(3), pp. 558–566. doi: 10.1016/j.cemconres.2011.12.003.

Le, T. T., Austin, S. A., Lim, S., Buswell, R. A., Gibb, A. G. F., and Thorpe, T.

- (2012) ‘Mix design and fresh properties for high-performance printing concrete’, *Materials and Structures*, 45(8), pp. 1221–1232. doi: 10.1617/s11527-012-9828-z.
- Li, L. (2013) ‘Book review: Understanding the Rheology of Concrete’, *Magazine of Concrete Research*, 65(2), pp. 137–137.
- Lootens, D., Jousset, P., Martinie, L., Roussel, N., and Flatt, R. J. (2009) ‘Yield stress during setting of cement pastes from penetration tests’, *Cement and Concrete Research*, 39(5), pp. 401–408. doi: 10.1016/j.cemconres.2009.01.012.
- Mahmoodzadeh, F. and Chidiac, S. E. (2013) ‘Rheological models for predicting plastic viscosity and yield stress of fresh concrete’, *Cement and Concrete Research*, 49, pp. 1–9. doi: 10.1016/j.cemconres.2013.03.004.
- Marchon, D. and Flatt, R. J. (2015) Impact of chemical admixtures on cement hydration, *Science and Technology of Concrete Admixtures*, doi: 10.1016/B978-0-08-100693-1.00012-6.
- Nematollahi, B., Xia, M. and Sanjayan, J. (2017) ‘Current Progress of 3D Concrete Printing Technologies’, *Proceedings of 34th International Symposium on Automation and Robotics in Construction*, pp. 260–267. doi: 10.22260/ISARC2017/0035.
- Nerella, V. N., Beigh, M.A.B., Fataei, S., and Mechtcherine, V. (2019) ‘Strain-based approach for measuring structural build-up of cement pastes in the context of digital construction’, *Cement and Concrete Research*, 115, pp. 530–544. doi: 10.1016/j.cemconres.2018.08.003.
- Nguyen, V. H., Remond, S. and Gallias, J. L. (2011) ‘Influence of cement grouts composition on the rheological behaviour’, *Cement and Concrete Research*, 41(3), pp. 292–300. doi: 10.1016/j.cemconres.2010.11.015.
- Omran, A. F. and Khayat, K. H. (2014) ‘Choice of thixotropic index to evaluate formwork pressure characteristics of self-consolidating concrete’, *Cement and Concrete Research*, 63, pp. 89–97. doi: 10.1016/j.cemconres.2014.05.005.
- Omran, A. F., Khayat, K. H. and Elaguab, Y. M. (2012) ‘Effect of SCC mixture composition on thixotropy and formwork pressure’, *Journal of Materials in Civil Engineering*, 24(7), pp. 876–888.
- Panda, B., Ruan, S., Unluer, C., tan, M. (2019) ‘Improving the 3D printability of high volume fly ash mixtures via the use of nano attapulgite clay’, *Composites Part B: Engineering*, 165, pp. 75–83. doi: 10.1016/j.compositesb.2018.11.109.
- Panda, B., Lim, J. H. and Tan, M. J. (2019) ‘Mechanical properties and deformation behaviour of early age concrete in the context of digital construction’, *Composites Part B: Engineering*, 165, pp. 563–571. doi: 10.1016/j.compositesb.2019.02.040.
- Perrot, A., Pierre, A. and Picandet, V. (2015) ‘Prediction of lateral form pressure exerted by concrete at low casting rates’, *Materials and Structures*, 48(7), pp. 2315–2322. doi: 10.1617/s11527-014-0313-8.
- Perrot, A., Rangeard, D. and Pierre, A. (2016) ‘Structural built-up of cement-based materials used for 3D- printing extrusion techniques’, *Materials and Structures*, 49, pp. 1213–1220. doi: 10.1617/s11527-015-0571-0.
- Qian, Y., Lesage, K., El Cheikh, K., and Schutter, G. (2018) ‘Effect of polycarboxylate ether superplasticizer (PCE) on dynamic yield stress, thixotropy and flocculation state of fresh cement pastes in consideration of the Critical Micelle Concentration (CMC)’, *Cement and Concrete Research*, 107, pp. 75–84. doi: 10.1016/j.cemconres.2018.02.019.
- Qian, Y. and Kawashima, S. (2016) ‘Flow onset of fresh mortars in rheometers: Contribution of paste deflocculation and sand particle migration’, *Cement and Concrete Research*, 90, pp. 97–103. doi: 10.1016/j.cemconres.2016.09.006.
- Rahman, M., Baluch, M. H. and Malik, M. A. (2014) ‘Thixotropic behavior of self

compacting concrete with different mineral admixtures’, *Construction and Building Materials*, 50, pp. 710–717. doi: <https://doi.org/10.1016/j.conbuildmat.2013.10.025>.

Rahul, A. V., Santhanam, M., Meena, H., and Ghani, Z. (2019) ‘3D printable concrete: Mixture design and test methods’, *Cement and Concrete Composites*, 97, pp. 13–23. doi: [10.1016/j.cemconcomp.2018.12.014](https://doi.org/10.1016/j.cemconcomp.2018.12.014).

Roussel, N. (2018a) ‘A thixotropy model for fresh fluid concretes : Theory , validation and applications’, *Cement and Concrete Research*, 36, pp. 1797–1806. doi: [10.1016/j.cemconres.2006.05.025](https://doi.org/10.1016/j.cemconres.2006.05.025).

Roussel, N. (2018b) ‘Rheological requirements for printable concretes’, *Cement and Concrete Research*, 112, pp. 76–85. doi: [10.1016/j.cemconres.2018.04.005](https://doi.org/10.1016/j.cemconres.2018.04.005).

Roussel, N. and Ovarlez, G. (2012) ‘The origins of thixotropy of fresh cement pastes’, *Cement and Concrete Research*, 42(1), pp. 148–157. doi: <https://doi.org/10.1016/j.cemconres.2011.09.004>.

Singh, R. B., Singh, B. and Kumar, N. (2019) ‘Thixotropy of self-compacting concrete containing recycled aggregates’, *Magazine of Concrete Research*, 71(1), pp. 14–25. doi: [10.1680/jmacr.17.00273](https://doi.org/10.1680/jmacr.17.00273).

Subramaniam KV, W. X. (2010) ‘An investigation of microstructure evolution in cement paste through setting using ultrasonic and rheological measurements’, *Cement and Concrete Research*, 40, pp. 33–44.

Suiker, A. S. J. (2018) ‘Mechanical performance of wall structures in 3D printing processes : Theory , design tools and experiments’, *International Journal of Mechanical Sciences*, 137, pp. 145–170. doi: [10.1016/j.ijmecsci.2018.01.010](https://doi.org/10.1016/j.ijmecsci.2018.01.010).

Tay, Y. W. D., Qian, Y. and Tan, M. J. (2019) ‘Printability region for 3D concrete printing using slump and slump flow test’, *Composites Part B: Engineering*, 174. doi: [10.1016/j.compositesb.2019.106968](https://doi.org/10.1016/j.compositesb.2019.106968).

Vance, K., Arora, A., Sant, G., and Neithalath, N. (2015) ‘Rheological evaluations of interground and blended cement-limestone suspensions’, *Construction and Building Materials*, 79, pp. 65–72. doi: [10.1016/j.conbuildmat.2014.12.054](https://doi.org/10.1016/j.conbuildmat.2014.12.054).

Wallevik, J. E. (2006) ‘Relationship between the Bingham parameters and slump’, *Cement and Concrete Research*, 36(7), pp. 1214–1221. doi: [10.1016/j.cemconres.2006.03.001](https://doi.org/10.1016/j.cemconres.2006.03.001).

Wangler, T., Lloret, E., Reiter, L., Hack, N., Gramazio, F., Kohler, M., Bernhard, M., Dillengurger, B., Buchli, J., Roussel, N. and Flatt, R. (2016) ‘Digital Concrete : Opportunities and Challenges’, *RILEM Technical Letters*, 1, pp. 67–75. doi: [10.21809/rilemtechlett.2016.16](https://doi.org/10.21809/rilemtechlett.2016.16).

Weng, Y., Tan, M. J. and Qian, S. (2016) ‘Rheology and Printability of Engineered Cementitious Composites-A Literature Review’, *2nd International Conference on Progress in Additive Manufacturing (Pro-AM 2016) 16-19 May 2016, Singapore*.

Wolfs, R. J. M., Bos, F. P. and Salet, T. A. M. (2018) ‘Early age mechanical behaviour of 3D printed concrete : Numerical modelling and experimental testing’, *Cement and Concrete Research*, 106, pp. 103–116. doi: [10.1016/j.cemconres.2018.02.001](https://doi.org/10.1016/j.cemconres.2018.02.001).

Yeh, B. K. H.-T. Y. (2006) ‘Mega-scale fabrication by Contour Crafting’, *International Journal of Industrial and Systems Engineering*, 1(3), pp. 301–320.

Zhang, Y., Zhang, Y., Liu, G., Yang, Y., Wu, M., Bo, P., (2018) ‘Fresh properties of a novel 3D printing concrete ink’, *Construction and Building Materials*, 174, pp. 263–271. doi: [10.1016/j.conbuildmat.2018.04.115](https://doi.org/10.1016/j.conbuildmat.2018.04.115).

CHAPTER 3 : STRUCTURAL PERFORMANCE OF 3D PRINTED ELEMENTS IN FUNCTION OF THE MATERIAL'S RHEOLOGY AND PRINTING CONDITIONS

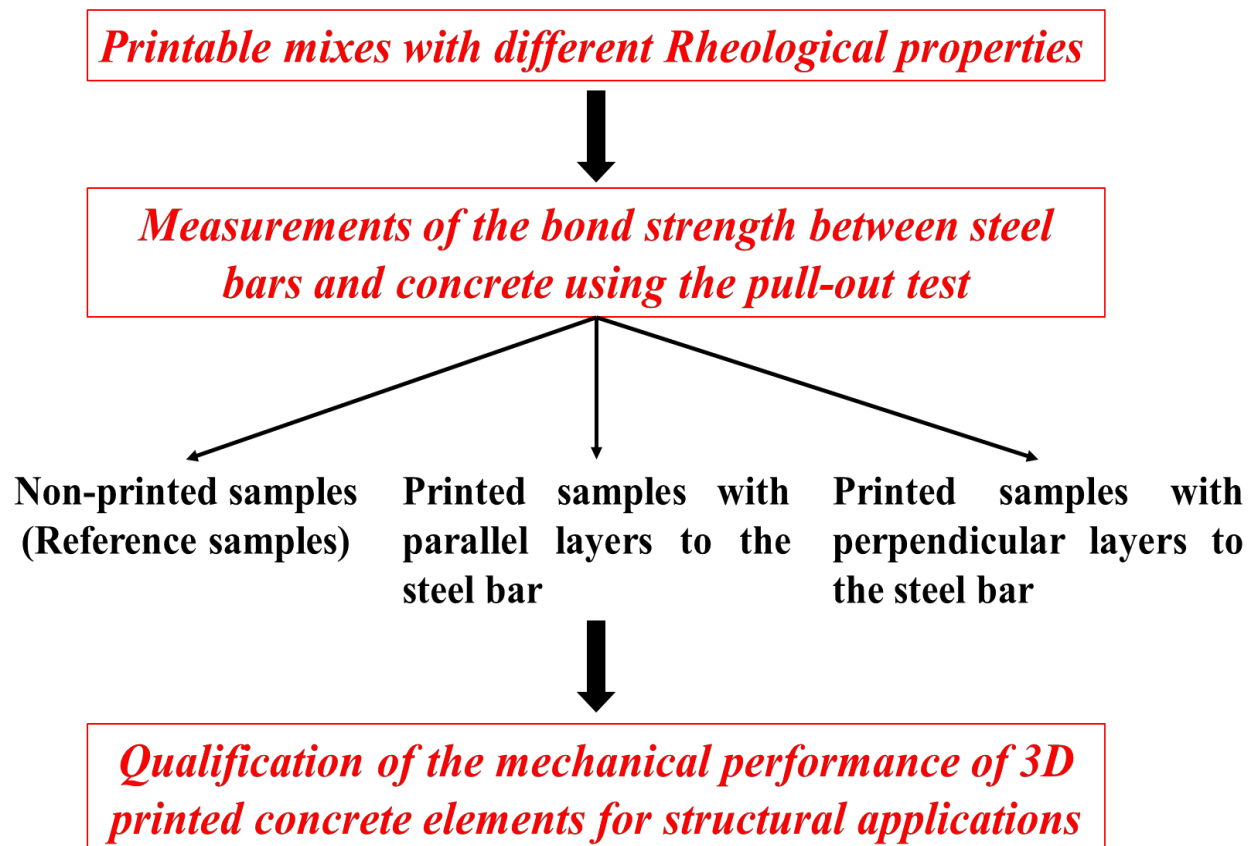
Reinforced concrete is considered by far the most widely used composite material in the construction field [205]. However, as extensively discussed in the literature, there is still a lack of viable strategies for the structural reinforcement of 3D printed concrete elements, as well as standardized regulations [27][45][46][47][48]. Indeed, not only the production technique of reinforced 3D printed elements ceases the progress of this approach, but also the fresh state properties of the printable material used impose further challenges. The rheological characteristics of the material influence the structural integrity of the printed element. They determine the ability of a composite element to behave homogeneously, as a monolithic conventional reinforced element. In principle, the rheological properties of the printable material affect the quality of the bond generated with the steel bars, which in turn affects the structural capacity and performance of the element when subjected to externally applied loads.

This chapter deals with the previously mentioned challenges, exhibited by the material's fresh state properties and printing techniques. It presents an initial attempt towards the effective implementation of reinforcement in a 3D printed concrete element, through examining the quality of the bond generated between printed concrete layers and the steel bars. Herein, the qualification process has been made based on a series of pull-out tests, performed over printed elements and compared to conventionally casted ones. In the same context, two different printing techniques were adopted to produce the printed elements, either using a manual technique or an automated 3-axis gantry printer. For both cases, the varying parameters were the material's composition, rheological and thixotropic properties and layers direction with respect to the steel bar, whether parallel or perpendicular to it.

Regarding the case of manually printed elements, the aims of this experimental investigation were to study first, the influence of the material's workability and second, the effect of the printing method, on the quality of the bond generated with steel bars. Thus, four different printable mixes

were developed, having each a distinct flowability and workability. Here, the manual printing process was done using a laboratory gun device, simulating the work performed by an actual printer. Besides, five different printing conditions were executed in total. Initially, two methods for each printing direction (parallel and perpendicular) were done by directly printing over the steel bar. Whereas, the fifth condition consisted of inserting the steel bar inside the element directly after being printed (when the material is still in its fresh state).

The proper methodology chart of the workflow is shown below.



The results of this work were published as a journal article in *Construction and Building Materials*, under the reference of:

B. BAZ, G. AOUAD, and S. REMOND, “Effect of the Printing Method and Mortar’s Workability on Pull-Out Strength of 3D Printed Elements,” *Construction and Building Materials*, vol. 230, 117002, 2020.

As for the printed elements produced by using an automated 3-axis gantry printer, the same framework and methodology have been applied, as in the earlier experimental program. The first objective here was to particularly investigate the ultimate consequences that a thixotropic material may lead to, on the quality of the bond generated with steel bars. Whereas, the second objective was to identify the effect of the layers direction with respect to the steel bar on the developed bond. Though, only one mix design was used to produce the pull-out samples, especially because of the complexity and toughness of the elements production. The mix was chosen out of the ones previously developed in chapter 2. It had a very high thixotropic behavior, but it was intentionally selected on this basis in order to cover the most detrimental outcomes that might grow out of.

The results of this work were published as a journal article in *Construction and Building Materials*, under the reference of:

B. Baz, G. Aouad, P. Leblond, O. Al-mansouri, D. Melody, and S. Remond, “Mechanical assessment of concrete – Steel bonding in 3D printed elements,” *Construction and Building Materials*, vol. 256, 119457, 2020.

In consequence, the results of this research showed that the implementation of conventional reinforcing steel bars, at the interface level between successive layers, is an efficient and practical method for the structural reinforcement of 3D printed concrete elements. In addition, it was confirmed that the installation of reinforcement is able to improve the overall strength of 3D printed components for better load bearing regimes. Therefore, they can be used as integral structural elements. More specifically, the outcomes showed that neither the rheological properties of the printable material used, nor the layers direction with respect to the steel bars, largely affect the quality of the bond generated between printed concrete layers and steel bars. However, despite the printing method whether manually or using the 3-axis gantry printer, the bond in conventionally mold casted samples mostly dominate. It gives better resistance against pull-out forces than printed samples. This happens because of the externally applied vibration, which is not practiced in printed elements due to their production approach. Nonetheless, for the particular case of printed elements using the actual printer, the variation of the bonding quality caused by layers direction was better exposed. Herein, the parallel printed samples outperformed the perpendicular printed ones. Though, the manual printing approach can still be used as a representative printing method for preliminary studies.

The current chapter presented the most relevant factors that affect the quality of the bond generated between printed concrete layers and steel bars, namely, the material's rheology and layers direction with respect to the bar. Though, the effect of the material's fresh state properties on the mechanical and hardened state of a printed body is also concerned by its durability performance, when exposed to harsh environments. Therefore, the next chapter will particularly assess the durability of certain 3D printed concrete elements when subjected to diverse chemical environments.

Effect of the Printing Method and Mortar's Workability on Pull-Out Strength of 3D Printed Elements

Bilal BAZ^{1,2}, Georges AOUAD¹, Sébastien REMOND²

¹Faculty of Engineering, University Of Balamand, UOB, Al Koura, Lebanon

²IMT Lille Douai, LGCgE – GCE, F-59508 Douai, France

Key words: Pull-Out – Bond Strength – 3D Printing – Additive Manufacturing – Mortar

Abstract

3D Printing of Concrete is gaining more attention with time as an alternative method for construction for its high degree of freedom. Until now, most of 3D printed elements are pre-printed then moved to their designated locations. The most practical method for moving printed elements is lifting them by means of implemented anchors. However, due to the nature of this construction method, it does not allow for any type of vibration, also due to the use of a special type of concrete mix, that do not flow by itself, there are still a lot of queries concerning the adherence of concrete with steel bars. The objective of this paper is to characterize the bond between steel and printed mortars as a function of mortar's workability and printing method. Pull-out tests of an 8mm steel bar embedded in either printed or non-printed mortars of varying workability have been performed after 3 days of casting. It is found that the workability of the ink does not affect the pull-out strength, neither the printing method nor layers direction affect the pull-out strength in respect to the steel bar.

1-Introduction

3D printing (3DP) is an additive manufacturing process (AM) defined by the ASTM for being “the process of joining materials to make objects from 3D model data, usually layer upon layer” [1]. 3D printing has become one of the fastest growing technologies, and it took place in the everyday life. It was introduced to all kinds of manufacturing industries [2], medical applications [3], and food preparation [4]. It is a sophisticated computer modeling technology, where physical objects are created using an automated process based on CAD models [2].

Since its emergence, 3D printing of concrete materials imposed a lot of challenges and opportunities to the construction sector [5][6]. Different additive manufacturing methods have been developed, and they rely on different systems [7]. The most commonly used methods are the Extrusion-Based systems, Powder-Based, or D-Shape techniques [8][9][10]. First, the Extrusion- Based systems consist of extruding a cementitious material from a nozzle mounted on

a robot or a gantry frame, and it prints the structure by depositing concrete filaments, having a constant cross section, on top of each other [9][10]. Whereas, the Powder-Based technique is capable of making complex shapes or structures by jetting selectively a liquid binder through a nozzle on an existing layer of printable powder to bind the particles together. Then, the remaining non-bonded particles are removed by means of a de-powdering process [11][12]. The Powder-Based technique is mostly used as an off-site process and that suits small scale building components [9][10]. For this research, the Extrusion-Based technique is adopted.

With all the techniques mentioned earlier, the incorporation of steel bars is hard to be done properly in a 3D printed element. This concern represents an evident obstacle for the maturity of 3D printing in the construction field [13][14]. Many alternative attempts have been performed to provide sufficient ductility for 3D printed elements. For example, fibers can be used in the 3D printing of concrete elements as a reinforcing agent [15][16][17][18][19]. However, fibers cannot be always used as a replacement for the structural steel because it is limited in terms of strength and ductility [14]. In most cases, to obtain the optimal structural performance, steel reinforcement has to be incorporated in order to improve the physical and mechanical properties of the 3D printed components [20]. Therefore, structural steel will improve the overall strength of the component and its integrity [21]. Several attempts have been taken by different companies and research institutes. For example, HuaShang Tengdam started by reinforcing 3D Printed structures by printing over an actual structural steel cage, where the printer has a fork shaped nozzle that eject concrete simultaneously on both sides of the steel cage [9][22]. Apis Cor and Win Sun introduced the reinforcement to their printed elements by producing a permanent 3D printed formwork and then placing inside of it the Rebar. Then after, the printed formwork is filled by conventional casted concrete [23]. Other novel methods of reinforcement are also applied such as the Mesh-Molding method, where the whole system is robotically printed and assembled, including the steel mesh [24], and the Sparse Concrete Reinforcement In Meshworks (SCRIM) that joins concrete printing and textile reinforcement meshes to produce a 3D printed reinforced element [25].

Besides, whatever the method used is, an important issue concerns the link developed between concrete and steel, because the ink used for printing is a particular material. This concrete material is different than any other one since it is allowed neither to flow by itself, nor to be vibrated. Thus, the performance of the link between steel and printed concrete has to be verified, especially when

working with materials that have different workabilities. A stiff printable material could end-up with a bad wrapping of the steel bar, while a more workable material would help in a better covering of all the surface of the bar leading to a better link by eliminating the chance of unintended voids. For the moment, regardless of the lack of ductility in 3D printed elements and its consequences on the structural behavior, the issue of putting reinforcement bars into printed concrete is certainly not mature enough to be fully addressed [26][27]. However, lifting printed elements and transporting them need an immediate solution, since until now most of the 3D printed elements are pre-fabricated then transported to their final destination, and eventually linked to an existing structural element. This paper deals with this specific question, by studying the effect of incorporating a steel bar inside the element during the printing process on the pull-out capacity at early age. This paper particularly investigates the bond strength generated between printed mortar and steel based on the workability of the used mortar. So the main objectives are:

- First, develop a conceptual method for measuring the bond between steel and printed mortar.
- Second, understand how the printing method and the layers direction with respect to the steel bar affect the pull-out strength at early age.
- Third, understand the effect of workability of the mortar on the bond developed with steel bars.

Section 2 first introduces the mixes used, in addition to the appropriate protocols for the evaluation of the fresh and hardened properties of the materials. Then after, a detailed description of the pull-out test used for evaluating the bond generated between concrete and steel is presented. Section 3 presents all the experimental results for both material properties and pull-out test.

2-Materials and Methods

2.1-Material Properties

There are two prime specifications for a mortar to be considered printable. Precisely, these characteristics are extrudability and buildability. Extrudability is the ability of a material to be workable and flowable enough to be pumped and printed without blocking the nozzle or the conduits. Buildability requires a fast setting and stiff material that can preserve its shape after being printed, and withstand the load coming from superposed layers. These requirements lead to a completely opposite performance when compared to the commonly used material that has the tendency to flow by itself when pumped, such as self-leveling concrete. The contradiction appears when a Zero slump material has to be flowable enough to be used for concrete printing. That is why the material's properties influence the link between steel and concrete. In this study,

four different printable mixes have been manufactured.

The developed mixes consist of ordinary Portland cement CEM I (PA L 42.5) from Holcim-Lebanon, Silica Fume from HOLDERCHEM-Lebanon and a high range water reducer poly carboxylate (PCE) based Super-Plasticizer. The sand used consists of crushed limestone with a particle size ranging between 0 and 1.5mm (Table. 1). In order to vary the mortar's workability, the super plasticizer contents were changed, except for mix4 where the water to binder ratio (W/B) was also increased. The mixing process and testing method of the mixes are done according to Khalil et al. [28]. In order to test the workability, a flow test is done for all mixes as per the Standard Test Method for Flow of Hydraulic Cement Mortar (ASTM C1437-15). In this standard, the spreading of a material is measured after 25 chocks on the flow table. In addition, the extrudability and buildability properties are tested by printing manually the largest number of superposed layers having a straight wall shape for each mix using a lab gun device having a circular nozzle of 1cm diameter previously used by El-Cheikh et al. [29] and Khalil et al. [28].

Table 1 Mixes compositions

	OPC (g)	SF (g)	Sand (g)	W/B	SP (%)
Mix1	614.47	68.28	850	0.4	0.26
Mix2	614.47	68.28	850	0.4	0.36
Mix3	614.47	68.28	850	0.4	0.4
Mix4	614.47	68.28	850	0.45	0.4

The compressive strength of all mixes has been measured at 3 and 28 days. This is done to determine whether the workability of the ink used has a major influence on the strength of the material when printed or not. Tests are conducted over a set of 4x4x16cm beams. Two sample categories are tested for each mix design. The first category consists of specimens simply poured in the appropriate molds in 2 layers. According to the standard placing method (ASTM C348), each layer is struck 60 times using a jolting table. The next set of samples consists of elements printed manually inside the same molds. In this case specifically, the molds are used only to produce perfectly plane surfaces so the compressive strength test can be performed accurately. Each printed beam is made out of 4 layers, 1cm thick each (Fig. 1), using a lab gun device having a rectangular nozzle of 1cmx3cm cross section similar to the device used by Sanjayan et al. [30]

to study the effect of surface moisture on inter-layer strength of 3D printed concrete and Marchment et al. [31] when studying the effect of delay time on the mechanical properties of extrusion-based 3D printed concrete. The layers are printed successively without any time gap, in order to avoid the formation of cold joints that affect the mechanical properties of the printed samples. The samples are kept for 24h in the molds, then they are de-molded and put to cure in a fully humid environment (RH=100%, 23°C) until the testing day. After then, all samples are tested under compression at a load rate of 2.5kN/sec according to ASTM C349. However, the printed beams are tested in two directions. The applied load is either parallel or perpendicular to the printed layers (Fig. 1).

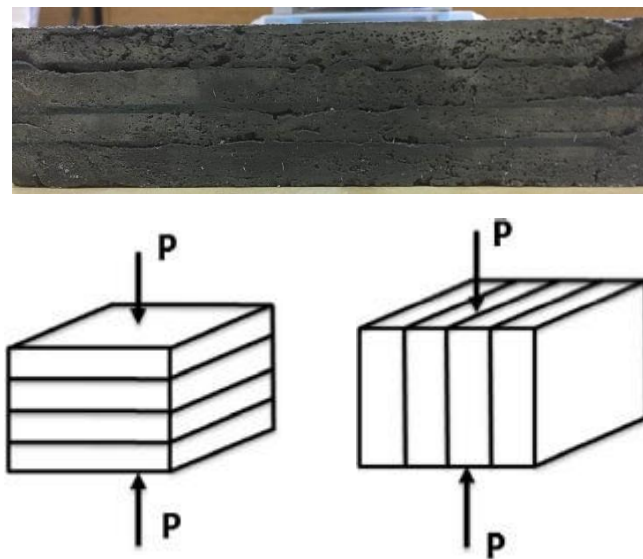


Figure 1 (top) printed beam (bottom left) Perpendicular loading (bottom right) Parallel loading

2.2-Pull-Out test

The pull-out test is generally applied to study the bond between steel and concrete. This research aims to specifically study the bond between a steel bar and the newly developed printable mixes. The reinforcing steel bars used in the pull-out experiments are T8 bars with 8.15mm nominal diameter, a yield strength “Fy” equal to 501Mpa and an ultimate tensile strength capacity “Fu” of 583Mpa.

It is well known that the bond strength developed between steel and concrete is directly related to the compressive strength of the material [26]. However, the failure mode of a sample differs between confined and unconfined boundary conditions. In the case of an unconfined sample, a concrete splitting failure occurs resulting from the longitudinal propagated cracks coming from the bar’s wedging action over the surrounding concrete. In confined condition, the failure

mechanism is generally governed by a de-bonding, resulting from the shearing action of the bar's ribs over the concrete, and therefore a slipping failure of the steel bar happens [27] [32]. For the purpose of this study, a bar slipping failure concerns us the most. In addition, there are many other factors that affect the failure mechanism such as the volume of concrete around the bar, the surface condition of the bar and its geometry [33].

In general, there are three major mechanisms that are resisting the pull-out of a conventional ribbed bar. These are mainly adhesion, dilatancy and friction. The combination between adhesion and dilatancy creates the bond resistance occurring before failure, and friction produces the resistance after failure [34].

2.2.1-Specimens preparation

The pull-out samples consisted of 16x16x20cm concrete cubes with an effective embedment depth of 8cm for the steel bar. The adopted sample's dimensions satisfy our aim for having a slipping failure of the bar, not a splitting failure of concrete cube nor a steel rupture. Two different types of samples are presented. The first set of samples consists of conventionally casted elements, and the second set consists of printed elements over a steel bar with different printing methods, both to be presented after. In order to cast the samples, a prismatic mold is made of wood with an open top. Because of the downward protruding reinforcing bar, the bottom cap is drilled at the middle to let the bar pass through (Fig. 2). In addition, an adhesive tape is applied on the free part of the anchor, for a depth of 1cm in order to break the adhesion, to set the exact embedment length and to decrease the stress concentration at the top of the anchor. Moreover, a stability support is added to the mold at its bottom to ensure that the bar remains rigid and vertical at all times, letting the applied forces be purely tensile. 24h after casting, the specimens are de-molded and placed in a 100% humid environment at 23°C until the day of testing.



Figure 2 Casting molds for Pull-Out samples

To proceed with the pull-out test of the printed elements, the same volume was adopted (16x16x20cm). For the printed specimens, the main variables that have to be defined are the layer's printing method and orientation with respect to the steel bar. This means that whether the layers are parallel or perpendicular to the steel bar, and if it is feasible to insert the reinforcing steel bar after printing and before the material's setting.

In this paper it was decided to print directly over the steel bar, which can serve the objectives more, knowing that there are different methods for incorporating steel bars in 3D printed elements, for example, printing steel bars simultaneously with concrete [35], printing over an actual steel cage, applying an external steel system after printing, and many other methods [36].

In this paper, printing is done using a lab gun device having a circular nozzle of 1cm diameter similar to the device used by El-Cheikh et al. [29] and Khalil et al. [28], simulating the printer's work. Each layer has a 1cm thickness. To print parallel layers to the steel bar, two different methods were adopted, and to print perpendicular layers, two other different techniques were also used. Fig. 3 shows a schematic description of the printing methods. The first perpendicular method (PerpM1) consists of printing layers in a circular manner all around the bar using a single gun, while the other method (PerpM2) is done by printing 2 adjacent layers at once surrounding the bar using 2 guns simultaneously. As for the parallel layers, also two different methods were used. The first method (ParaM1) consists of using two guns simultaneously in line along the steel bar. The bar is placed between the two devices so the printed layers can cover the whole perimeter. The second method (ParaM2) is made by first, printing the bed layer, then, simply placing the steel bar

on top of it. The bar is slightly pushed down in a way that half of its diameter is merged in the layer below, after that, a second layer is printed over it.

Regarding the reversed scenario where the printing takes place first, the layers are printed similarly to PerpM1, and then the steel bar is inserted directly after printing without any time gap. The insertion of the bar is done manually and very delicately with the help of a stabilization support to ensure a vertical penetration without perturbing the surrounding concrete.

The standoff distance of the nozzle is approximately 0.5cm apart of the bar, and the printed part exceeds the bar by 6cm to ensure a full and strong coverage. Thus, the overall printed part is 15cm long including the adhesive tape.

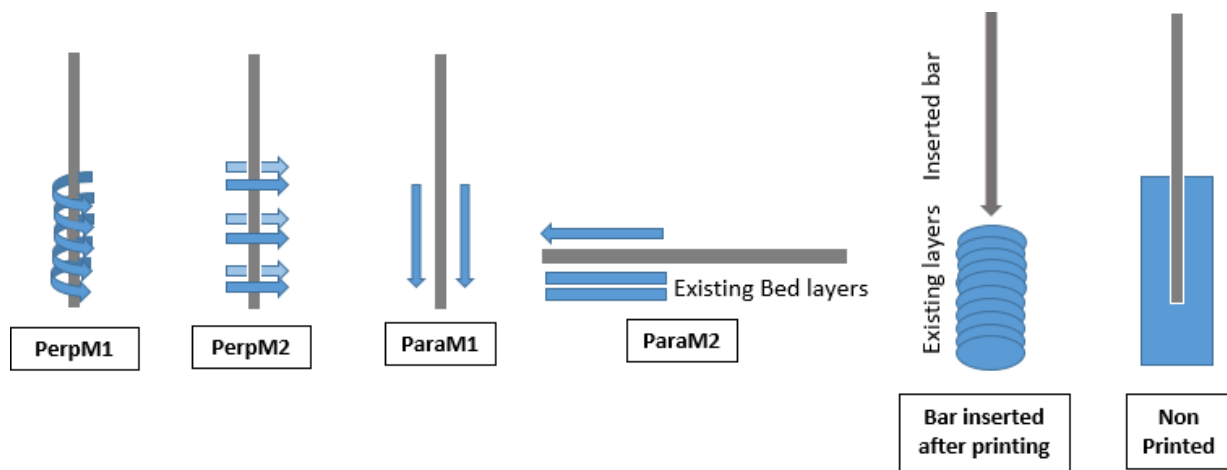


Figure 3 Different printing methods

For all samples and conditions, each printed element is placed inside a 16x16x20cm mold after 24h and a different mortar mix is used to fill up the remaining volume and ensure a strong encapsulation of the printed segment. It is not mandatory to use the printable mix to fill the mold since this research is only concerned by the link between the steel bar and the printed material, knowing that any failure at the joint between the two types of material would never happen. Fig. 4 shows an example of how the printed sample looks like before and after being wrapped by the filling mortar.

As for the non-printed samples, they are produced by pouring and vibrating printable concrete around the steel bar, inside a small mold. After de-molding, the smooth surfaces of the elements are scraped to ensure a better link with the filling material providing confinement (Fig. 5).

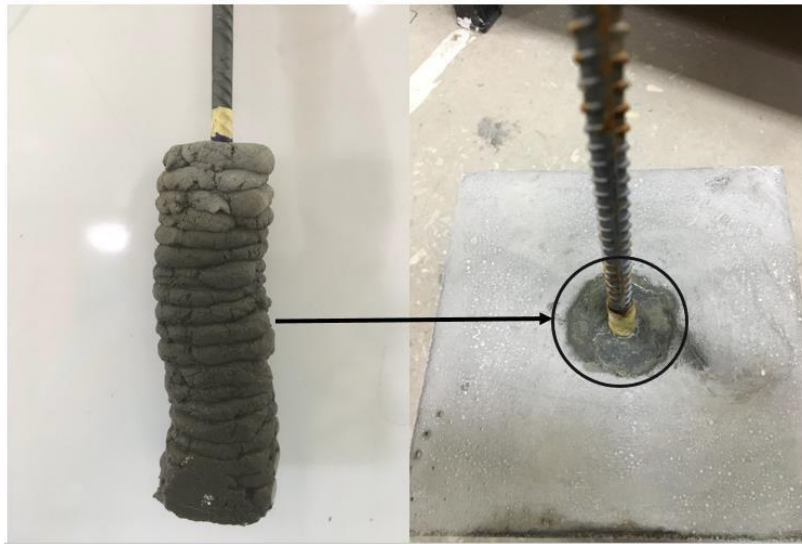


Figure 4 Printed Pull-Out sample before (left) and after (right) being confined

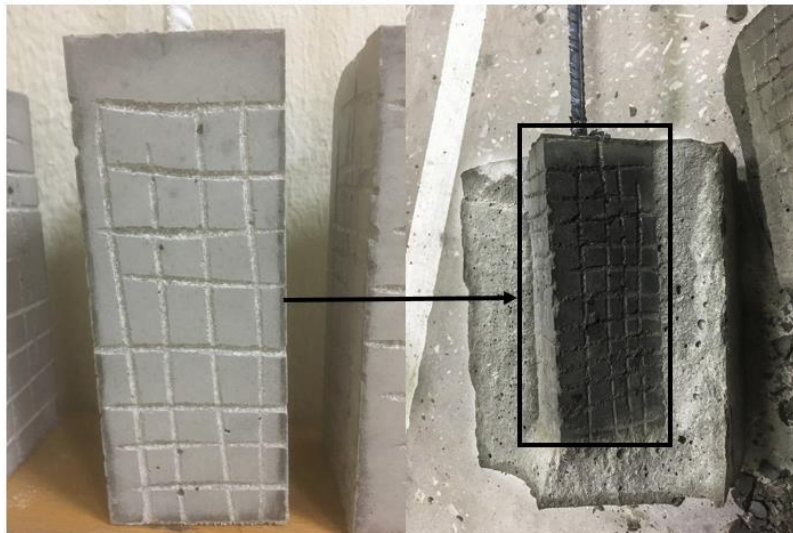


Figure 5 Non-printed sample with scraped surfaces before (left) and after (right) being confined

2.2.2-Test Set Up Preparation

The machine used to perform the pull-out test is a UTM machine. A customized steel setup is developed to serve the pull-out test (Fig. 6). This setup aims to hold the pull-out specimens inside. First, the system is made out of two large steel plates with 3cm thickness and 32x32cm surface area. Both plates are connected by means of bolts so the space between them can be fixed according to the specimen's size. The system forms a box with open sides. The top plate is grooved straight to the middle so it allows the steel bar coming out of the specimen to slide in. The bottom plate is drilled at its center and connected to a steel bar that is held by the testing machine. After that, the

sample is placed inside the setup and the steel bar that has to be pulled out is held by the UTM clamps. A rubber pad is placed between the specimen and the top plate of the setup in order to transfer a uniform stress distribution over the surface of the specimen in case of any making defects. The loading rate is set to be 1KN/sec, falling within the allowable range defined by the ASTM C234 standard.

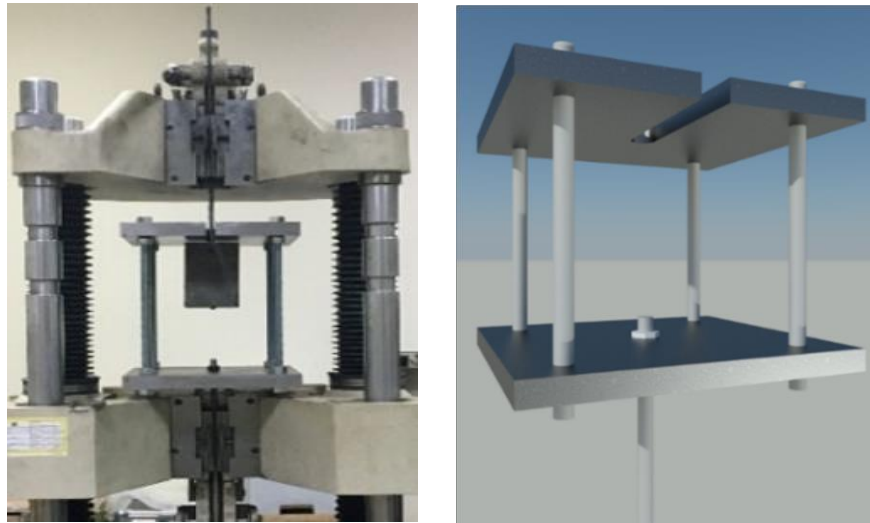


Figure 6 Pull-Out test set up

3-Results

3.1-Material Results

All mixes satisfy the Printability characteristics, even for different workabilities. All freshly printed elements failed by buckling, but the obtained results showed a good correlation between the maximum number of layers and the material's workability (Table. 2).

Fig. 7 and Fig. 8 show the compressive strength at 3 and 28 days respectively for all samples whether printed or not. The results for the non-printed samples showed approximately the same resistance for mix1, mix2 and mix3 at 28 days since they have almost the same compositions, while mix4 gave a lower resistance due to its higher W/B ratio. But when talking about 3D printing, an additional factor comes into play and influences the compressive strength of the elements, which is the direction of the printed layers whether parallel or perpendicular to the load imposed [37]. Indeed, the results of this research confirm that the 3D printed specimens are anisotropic elements.

The results showed that at 28 days the non-printed samples dominated, followed by the parallel samples that gave better results than the perpendicular ones. This happened because non-printed samples contain less voids than the printed ones due to the external vibration. However, printed samples contain voids mostly located between layers, this justifies the fact of having lower compressive strength than non-printed samples. But then, the voids found between layers are more vulnerable when the printed samples are loaded perpendicularly to the layers. This is said because these voids show up in a series form of weak points causing failure as soon as the chain breaks down. This results in having a lower resistance when compared to the samples loaded parallel to the layers. As stated earlier, the compressive strength of non-printed samples were almost the same for the first three mixes while being lower for mix4. In general, the variation between printed and non-printed elements diminishes as the workability of the mix increases, since the printed layers have higher tendency to merge together, decreasing the effect of superposition and voids formation. Concerning the case of perpendicular samples, all results were identical even for mix4. These results were in agreement with the results obtained by Feng et al. [38] and Nerella et al. [39]. Even though, based on the research done by Koker [40], it was found that the mechanical strength of extruded materials could be greater than the simply casted elements, and this is certainly due to the extra pressure exerted on the material in its fresh state reducing the voids inside the extruded layer itself which will end-up having a denser matrix. However, this is not always the case for 3D printed elements since many other factors come into play, mainly the nozzle shape, nozzle standoff distance and printing speed [37][41].

Regarding the compressive strength of the elements tested at 3 days, all results were almost the same for all mixes and loading directions. The variation between results cannot be clearly seen, thus a significant conclusion could not be drawn.

Table 2 Workability Characteristics

	Spreading (cm)	Maximum number of Superposed layers
Mix1	14.5	22
Mix2	16	16
Mix3	18	12
Mix4	20	9

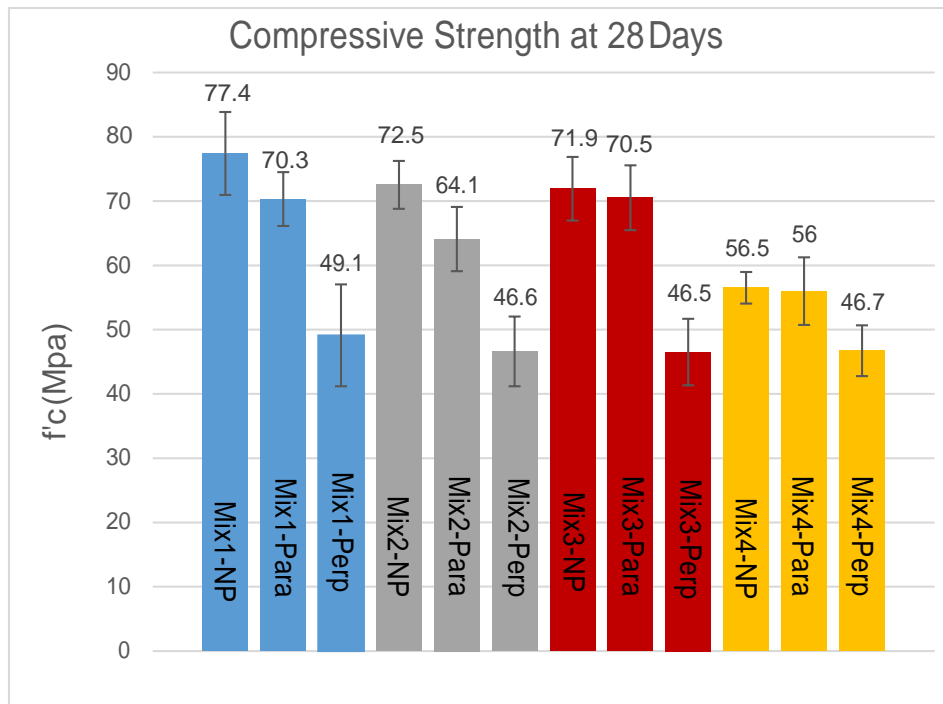


Figure 7 Compressive Strength at 28 Days

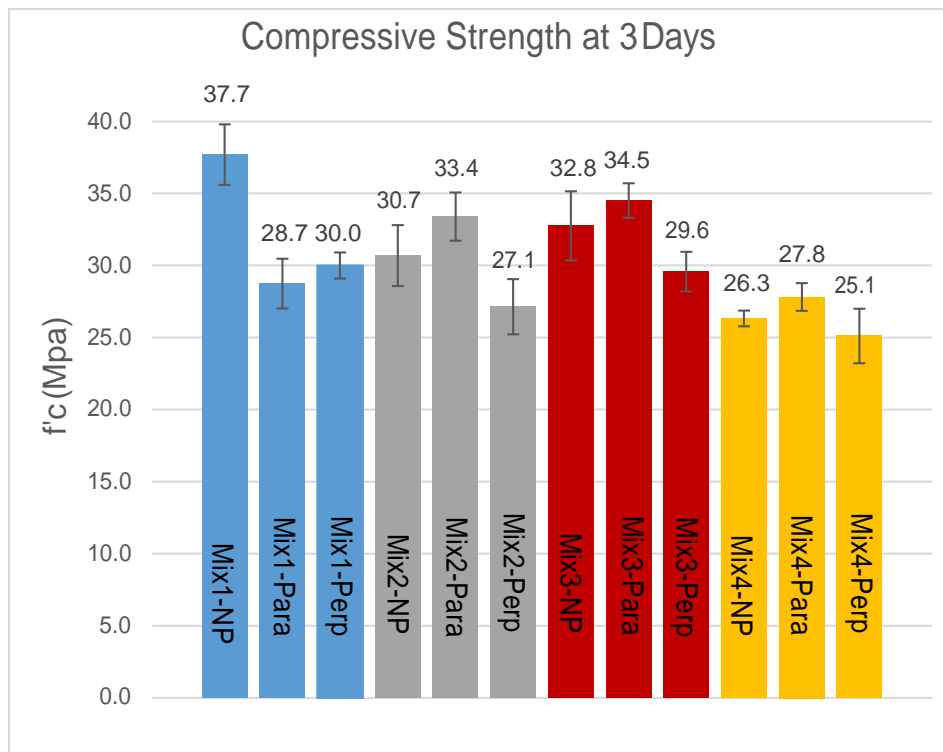


Figure 8 Compressive Strength at 3 Days

3.2-Pull-Out Results

Table 3 presents the pull-out test results for all mixes and conditions. All numbers show the bond stress corresponding to the actual force applied, calculated using the following equation:

$$T = \frac{F}{\pi \cdot db \cdot l_e} \text{ (Eq. 1)}$$

Where:

T = experimental bond stress (MPa)

F = ultimate axial tension force (N)

db = nominal rebar diameter (mm)

le = embedment length (mm)

In addition, Table 3 includes the average bond stress and standard deviation for each condition individually. Although, Fig. 9 shows how the relative pull-out strength (compared to non-printed sample) varies according to the printing method and the variation of workability for each mix.

Based on these results, it can be clearly seen that the pull-out strengths of most printed samples are close enough to the results of the non-printed ones relative to each mix. This is true except for the case where the bar is inserted after the printing takes place. It can be said that all mixes with different workabilities gave more or less the same pull-out results for all printing methods and conditions. This can be clearly indicated by the standard deviation bars shown on the curves of Fig. 9.

All standard deviations for pull-out results corresponding to either printed or vibrated samples are almost equivalent, altering in the same extent. Namely, all results fall in the same array, thus they also confirm that the manual printing technique adopted for this research is a reliable and consistent method.

Concerning the case of a steel bar inserted after printing, this method is neither practical nor efficient. Even though, as the workability of the material increases, the bond with the steel bar increases, because a more flowable material would fill more voids caused by the insertion of the bar. However, the relative pull-out strength of a steel bar that is inserted after printing is still behind when compared to any other method adopted in this study. In other words, whatever the mix properties were, the irregularities (voids, entrapped air, etc.) created around the inserted bar are more severe than any other case (Fig. 10).

Besides, according to the compressive strength results of printed samples, perpendicular samples showed the lowest bearing capacity for all mixes. Even though, this weakness did not affect the resistance of the perpendicular printed layer against the stresses generated by the pull-out forces when the layers are perpendicular to the steel bar.

In this study, all printing methods reflect different approaches for 3D printing. Yet, PerpM1 and ParaM2 are considered as the most suitable printing methods because they are the most practical, therefore reducing any chance for manufacturing defects such as voids formation.

However, from a global point of view, the manual printing method adopted in this paper is relatively different than what can be done using an automated 3D printer. But stills, even when using a robotized 3D printer, a large scatter between samples coming from different sources will always shows up, because all the developed 3D printing techniques until now have not been standardized and do not follow a predefined procedure for reproducibility. They majorly depends on the piloting of the operator and the material properties. In other words, 3D printing technology in all its aspects and applications is still a subjective technique until being standardized.

Table 3 Pull-Out results

	Mix1		Mix2		Mix3		Mix4	
	T(MPa)	Av. (S.D.)	T(MPa)	Av. (S.D.)	T(MPa)	Av. (S.D.)	T(MPa)	Av. (S.D.)
Non-Printed	15.1	15.23 (0.27)	15.5	15.33 (0.52)	14.9	14.91 (0.54)	14	13.6 (0.57)
	15.2		15.8		15.8		12.8	
	14.9		14.6		14.8		13.6	
	15.6		15.5		14.8		14	
	15.4		X		14.3		X	
PerpM 1	14.1	14.37 (0.73)	15	14.98 (0.3)	14.3	14.87 (0.68)	11.7	12.19 (0.45)
	15.5		15.4		15.2		12.3	
	13.5		15.1		14.5		12.1	
	14.3		14.8		15.9		12.9	
	14.5		14.6		14.4		12	
PerpM 2	11.8	11.98 (1.09)	14.6	14.29 (0.41)	14.8	14.32 (0.73)	15	14.34 (0.47)
	12.9		14.3		14.2		14.6	
	10.2		13.8		15.1		13.9	
	12.2		14		14.3		13.9	
	12.8		14.8		13.2		14.3	
	13.8	13.49	14.2		12.4		11.2	

ParaM 1	14.8	(1.26)	14.8	14.57 (0.58)	12.3	12.34 (0.15)	11.3	10.95 (1.51)
	12.5		14.6		12.5		13.2	
	14.5		15.4		12.4		9.5	
	11.9		13.9		12.1		9.6	
ParaM 2	14.6	15.0 (0.4)	14.2	13.69 (0.78)	15.2	15.35 (0.29)	15.1	15.13 (0.34)
	15.4		12.5		15.5		15.6	
	15.4		13.3		15.6		14.8	
	15		14.2		14.9		14.8	
	14.6		14.3		15.5		15.3	
Bar After	1.9	3.68 (1.21)	2.6	3.68 (1.39)	3.6	5.01 (1.01)	9.8	8.2 (1.0)
	3.4		5.9		5.8		7.5	
	5.2		2.4		5		7.3	
	4.2		3.7		6.1		7.9	
	3.6		3.7		4.5		8.5	

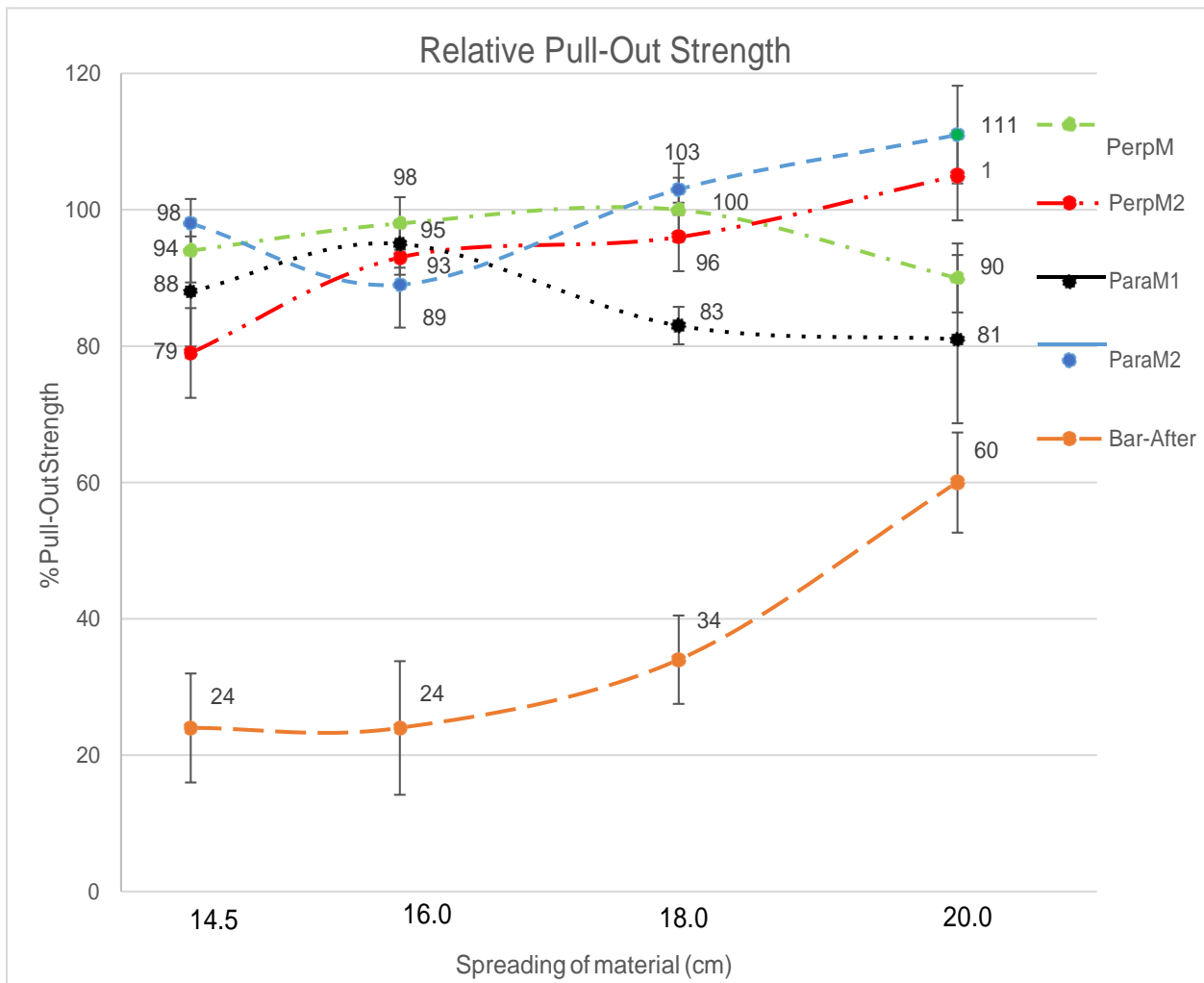


Figure 9 Pull-Out strength variation for all mixes

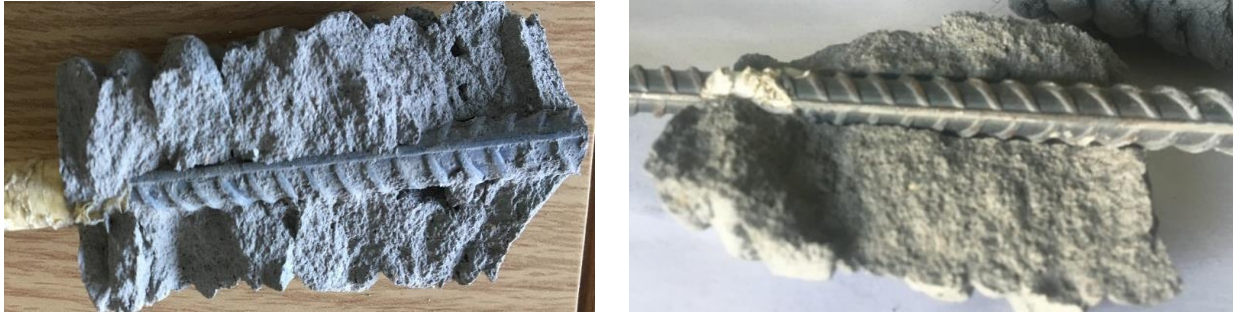


Figure 10 Bond profile when printing over the bar (left) and when inserting the bar after printing (right)

4-Conclusion

A pull-out test has been conducted on conventionally mold-cast and printed samples under different conditions. The factors that were studied in this research are the effect of workability on the link developed between steel and concrete, and the effect of the printing method and layers direction on the pull-out strength of a steel anchor. In addition, the compressive strengths of the different mortars used were tested for printed and conventionally mold-cast conditions under different loading directions (parallel and perpendicular to the printed layers). Basically, this study figured out four different mixes with different workabilities and five different printing methods. So, the following conclusions are drawn:

- Non printed samples dominated when tested at 28 days in regards to the printed ones. However, perpendicular samples always showed the lowest compressive strengths.
- Printed samples act more homogeneously when increasing the workability of the mortar used. In other words, the compressive strength of parallel printed samples converge toward those of non-printed elements as the workability increases.
- The concept of printing over an actual steel bar has been shown to be feasible and effective.
- 3D printed elements gave more or less the same pull-out strength as for non-printed elements, except for the case where the steel bar is inserted after printing.
- The printing direction did not majorly affect the capability of the element to withstand tensile loads applied over the steel bar.
- PerpM1 and ParaM2 were the most qualified printing methods because of their practicalities. Undeniably, all other methods were also acceptable.

- Based on the results of this research, as long as the material is considered printable and independently of the mix's workability, a strong link between concrete and steel will still be developed, and the pull-out strength would still be significant.

At the end, all the results and conclusions are based on tests done over manually printed samples. In a next step, the same study will be conducted over samples fabricated using an automated printer to validate more these results and conclusions. Simultaneously, different variables are going to be introduced and different parameters will be tested apart of the link between steel and concrete. Certainly, one of the targeted subjects to be investigated is the effect of the layer's geometry on the failing mode of pull-out specimens.

Acknowledgment:

The authors would like to acknowledge the financial support by Partenariats Hubert Curien (PHC) CEDRE program PROJET N° 42287YD, and the Supply of material from Carrières du Boulonnais, Eqiom, and Chryso.

References:

- [1] ASTM International, “F2792-12a - Standard Terminology for Additive Manufacturing Technologies,” *Rapid Manuf. Assoc.*, pp. 10–12, 2013.
- [2] B. Berman, F. G. Zarb, and W. Hall, “3-D printing : The new industrial revolution,” *Bus. Horiz.*, vol. 55, no. 2, pp. 155–162, 2012.
- [3] H. D. Lam CXF, Mo XM, Teoh SH, “Scaffold development using 3D printing with a starch-based polymer,” *Mater Sc Eng C*, vol. 20, no. 1, pp. 49–56, 2002.
- [4] A. R. Wegrzyn TF, Golding M, “Food layered manufacture: a new process for constructing solid foods,” *Trends Food Sci Technol*, vol. 27, no. 2, pp. 66–72, 2012.
- [5] J. Buchli, M. Giftthaler, N. Kumar, M. Lussi, T. Sandy, K. Dör, and N. Hack, “Digital in situ fabrication - Challenges and opportunities for robotic in situ fabrication in architecture , construction , and beyond,” *Cem. Concr. Res.*, 2018.
- [6] N. Labonnote, A. Rønquist, B. Manum, and P. Rütther, “Additive Construction : state of the art , challenges and opportunities,” *Autom. Constr.*, 2016.
- [7] S. Lim, R. A. Buswell, T. T. Le, S. A. Austin, A. G. F. Gibb, and T. Thorpe, “Developments in construction-scale additive manufacturing processes,” *Autom. Constr.*, vol. 21, no. 1, pp. 262–268, 2012.
- [8] B. Khoshnevis, “Automated construction by contour crafting - Related robotics and information technologies,” *Autom. Constr.*, vol. 13, no. 1, pp. 5–19, 2004.
- [9] B. Nematollahi, M. Xia, and J. Sanjayan, “Current Progress of 3D Concrete Printing Technologies,” *Proc. 34th Int. Symp. Autom. Robot. Constr.*, pp. 260–267, 2017.
- [10] T. T. Le, S. A. Austin, S. Lim, R. A. Buswell, R. Law, A. G. F. Gibb, and T. Thorpe, “Hardened properties of high-performance printing concrete,” *Cem. Concr. Res.*, vol. 42, no. 3, pp. 558–566, 2012.
- [11] M. Xia, B. Nematollahi, and J. Sanjayan, “Printability , accuracy and strength of geopolymer made using powder-based 3D printing for construction applications,” *Autom. Constr.*, vol. 101, pp. 179–189, 2019.
- [12] D. Lowke, E. Dini, A. Perrot, D. Weger, C. Gehlen, and B. Dillenburger, “Particle-bed 3D printing in concrete construction – Possibilities and challenges,” *Cem. Concr. Res.*, vol. 112, pp. 50–65, 2018.
- [13] T. A. M. Salet, F. P. Bos, R. J. M. Wolfs, and Z. Ahmed, “3D concrete printing – a structural engineering perspective 3D Concrete Printing – A Structural Engineering Perspective,” *High Tech Concr. Where Technol. Eng. Meet*, 2018.
- [14] D. Asprone, C. Menna, F. P. Bos, T. A. M. Salet, and J. Mata-falcón, “Rethinking reinforcement for digital fabrication with concrete,” *Cem. Concr. Res.*, 2018.
- [15] B. Nematollahi, P. Vijay, J. Sanjayan, A. Nazari, M. Xia, V. N. Nerella, and V. Mechtcherine, “Effect of polypropylene fibre addition on properties of geopolymers made by 3D printing for digital construction,” *Materials (Basel)*, vol. 11, no. 12, 2018.

- [16] S. Christ, M. Schnabel, E. Vorndran, J. Groll, and U. Gbureck, "Fiber reinforcement during 3D printing," *Mater. Lett.*, vol. 139, pp. 165–168, 2015.
- [17] M. Hambach and D. Volkmer, "Properties of 3D-printed fiber-reinforced Portland cement paste," *Cem. Concr. Compos.*, vol. 79, pp. 62–70, 2017.
- [18] B. Panda, S. Chandra Paul, and M. Jen Tan, "Anisotropic mechanical performance of 3D printed fiber reinforced sustainable construction material," *Mater. Lett.*, vol. 209, pp. 146–149, 2017.
- [19] I. Farina, F. Fabbrocino, G. Carpentieri, M. Modano, A. Amendola, R. Goodall, L. Feo, and F. Fraternali, "On the reinforcement of cement mortars through 3D printed polymeric and metallic fibers," *Compos. Part B Eng.*, vol. 90, pp. 76–85, 2016.
- [20] J. Mata-Falcon, P. Bischof, and W. Kaufmann, "Exploiting the Potential of Digital Fabrication for Sustainable and Economic Concrete Structures," *First RILEM Int. Conf. Concr. Digit. Fabr. – Digit. Concr. 2018*, 2019.
- [21] B. Panda, Y. Wei Tay, S. Chandra Paul, K. Fai Leong, T. M. Jen, and I. Gibson, "Current Challenges and Future Perspectives of 3D Concrete Printing," *2nd Int. Conf. Prog. Addit. Manuf. (Pro-AM 2016)*, pp. 16–19, 2016.
- [22] F. Bos, R. Wolfs, Z. Ahmed, and T. Salet, "Additive manufacturing of concrete in construction: potentials and challenges of 3D concrete printing," *Virtual Phys. Prototyp.*, vol. 11, no. 3, pp. 209–225, 2016.
- [23] G. De Schutter, K. Lesage, V. Mechtcherine, V. N. Nerella, G. Habert, and I. Agusti-Juan, "Vision of 3D printing with concrete — Technical, economic and environmental potentials," *Cem. Concr. Res.*, pp. 1–12, 2018.
- [24] N. Hack and Willi Viktor Lauer, "Mesh Mould: Robotically Fabricated Metal Meshes as Concrete Formwork and Reinforcement," *Archit. Des.*, 2015.
- [25] P. Ayres, W. Ricardo, P. Nicholas, and T. J. Andersen, "SCRIM – Sparse Concrete Reinforcement in Meshworks," 2019.
- [26] F. P. Bos, Z. Y. Ahmed, R. J. M. Wolfs, and T. A. M. Salet, "3D Printing Concrete with Reinforcement," *fib Symp. High Tech Concr. Where Technol. Eng. Meet*, vol. 1, 2018.
- [27] F. P. Bos, Z. Y. Ahmed, E. R. Jutinov, and T. A. M. Salet, "Experimental exploration of metal cable as reinforcement in 3D printed concrete," *Materials (Basel)*, vol. 10, no. 11, 2017.
- [28] N. Khalil, G. Aouad, K. El Cheikh, and S. Rémond, "Use of calcium sulfoaluminate cements for setting control of 3D-printing mortars," *Constr. Build. Mater.*, vol. 157, pp. 382–391, 2017.
- [29] K. El Cheikh, S. Rémond, N. Khalil, and G. Aouad, "Numerical and experimental studies of aggregate blocking in mortar extrusion," *Constr. Build. Mater.*, vol. 145, pp. 452–463, 2017.
- [30] J. G. Sanjayan, B. Nematollahi, M. Xia, and T. Marchment, "Effect of Surface Moisture on Inter-Layer Strength of 3D Printed Concrete," *Constr. Build. Mater.*, vol. 172, pp. 468–475, 2018.

- [31] T. Marchment, M. Xia, E. Dodd, J. Sanjayan, and B. Nematollahi, “Effect of Delay Time on the Mechanical Properties of Extrusion-based 3D Printed Concrete,” *Proc. 34th ISARC Int. Assoc. Autom. Robot. Constr.*, pp. 240–245, 2017.
- [32] M. J. Al-Shannag and A. Charif, “Bond behavior of steel bars embedded in concretes made with natural lightweight aggregates,” *J. King Saud Univ. - Eng. Sci.*, vol. 29, no. 4, pp. 365–372, 2017.
- [33] ACI Committee 408, “ACI 408R-03 Bond and Development of Straight Reinforcing Bars in Tension,” *Am. Concr. Inst.*, pp. 1–49, 2003.
- [34] M. Haskett, D. J. Oehlers, and M. S. Mohamed Ali, “Local and global bond characteristics of steel reinforcing bars,” *Eng. Struct.*, vol. 30, no. 2, pp. 376–383, 2008.
- [35] V. Mechtcherine, J. Grafe, V. N. Nerella, E. Spaniol, M. Hertel, and U. Füssel, “3D-Printed Steel Reinforcement for Digital Concrete Construction – Manu-Fecture, Mechanical Properties and Bond Behaviour [Under Review],” *Constr. Build. Mater.*, vol. 179, pp. 125–137, 2018.
- [36] V. N. Nerella, H. Ogura, and V. Mechtcherine, “Incorporating reinforcement into digital concrete construction,” *Proc. IASS Symp. 2018, Creat. Struct. Des. July 16-20, 2018, MIN, Boston, USA*, no. July, pp. 1–8, 2018.
- [37] S. C. Paul, Y. W. D. Tay, B. Panda, and M. J. Tan, “Fresh and hardened properties of 3D printable cementitious materials for building and construction,” *Arch. Civ. Mech. Eng.*, vol. 18, no. 1, pp. 311–319, 2018.
- [38] P. Feng, X. Meng, J. F. Chen, and L. Ye, “Mechanical properties of structures 3D printed with cementitious powders,” *Constr. Build. Mater.*, vol. 93, pp. 486–497, 2015.
- [39] V. N. Nerella and V. Mechtcherine, “Studying printability of fresh concrete for formwork free Concrete on-site 3D Printing technology,” 2016.
- [40] D. De Koker, “Manufacturing processes for engineered cement-based composite material products,” *M.Sc. thesis, Stellenbosch Univ. South Africa*, 2004.
- [41] B. Panda, S. C. Paul, N. A. N. Mohamed, Y. W. D. Tay, and M. J. Tan, “Measurement of tensile bond strength of 3D printed geopolymers mortar,” *Meas. J. Int. Meas. Confed.*, vol. 113, pp. 108–116, 2018.

Mechanical Assessment of Concrete - Steel Bonding in 3D Printed Elements

Bilal BAZ^{1,2}, Georges AOUAD¹, Philippe LEBLOND³, Omar Al-MANSOURI^{2,3},
Melody D'HONDT³, Sébastien REMOND⁴

¹ Faculty of Engineering, University Of Balamand, UOB, Al Koura, Lebanon

² IMT Lille Douai, LGCgE – GCE, F-59508 Douai, France

*³ Université Paris-Est, Centre Scientifique et Technique du Bâtiment (CSTB), 84 avenue Jean Jaurès,
Champs-Sur-Marne, 77447 Marne-la-Vallée Cedex 2, France.*

⁴ Univ Orléans, Univ Tours, INSA CVL, LaMé, EA 7494, France

Key words: Pull-out – Bond Strength – 3D Printing – Additive Manufacturing – Thixotropy

Abstract:

Digital construction of concrete elements using 3D printing technology has been undergoing an exponential growth in terms of research activities and demonstration projects. Though, most researches focused on the behavior of the cementitious materials used in 3D printing, without deeply immersing in the reinforcement of printed elements. In this paper, a detailed experimental program is presented to characterize the quality of the bond developed between concrete and steel bars through a series of pull-out tests. These tests are performed over printed and non-printed samples as well. When printed, the layers orientation, whether parallel or perpendicular to the steel bar is taken into consideration. Hence, it was found that a highly thixotropic material did not undermine the developed bond between printed concrete and rebar. In addition, vibrated concrete (non-printed) gave better resistance to pull-out stresses succeeded by the parallel then the perpendicular samples. Yet, the overall performance of 3D printed concrete in terms of the bond generated with steel could be rated as satisfactory.

1-Introduction

3D printing is a novel production method defined by the ASTM as being “the process of joining materials to make parts from 3D model data, usually layer upon layer” [1]. Lately, the application of 3D printing in the construction field has been widely developed, and it brought attention in both academic and industrial applications [2]. This new technique presents significant benefits in terms of higher quality products, faster production, higher geometrical freedom, and lower cost [3]-[6]. Practically, mortar layers are successively deposited in order to produce the intended element or

structure. However, the mortar used makes a challenging subject [7]. It has to be sufficiently workable to be pumped, and stiff enough to resist the imposed loads once the layer gets deposited [8]. In addition. It must gain sufficient strength to withstand the loads coming from subsequent layers, within a short period of time. In fact, the ability of the material to behave properly is linked to its rheology [9]. Herein, a balance should be always maintained between the structural build-up rate of the cement-based material and the increasing loads [10]. Indeed, the most important rheological factor affecting the material's behavior is its static yield stress. It must be high enough to ensure the stability of the printed element [11]. Hence, the strength gain corresponds to the structural build-up of the material, causing a continuous increase of the static yield stress over time [12]. This time dependent phenomenon represents a rheological characteristic termed thixotropy [12]. Roussel et al. [11] proposed a linear model based on the structuration rate " A_{thix} " of the material, to describe the static yield stress " τ_0 " evolution with time " t " (Eq. 1). Whereas Perrot et al. [13] offered an exponential model that implements a critical characteristic time " t_c " alongside (Eq. 2).

$$\tau_{0(t)} = \tau_{0,0} + A_{thix}t \quad [11] \text{ (Eq. 1)}$$

$$\tau_{0(t)} = A_{thix}t_c \left(e^{t_{rest}/t_c} - 1 \right) + \tau_{0,0} \quad [13] \text{ (Eq. 2)}$$

Usually, the measurements of the yield stress are carried using either rotational, or plate rheometers [14]. Though, despite their attractiveness, most rheometers are not adapted for materials containing aggregates such as mortar [15]. In fact, the yield stress of mortars is commonly measured using easier methods, such as the slump-flow test [16], the inclined plate test [17], and different penetration tests [18] [19] (cone plunger, Vicat plunger, etc.).

Apart from the material's rheology and requirements, most of the printing techniques focus on the placement of concrete regardless of the incorporation of reinforcement. Therefore, the application of 3D printed elements in concrete structures was almost limited for partitioning works and unreinforced masonry [20]-[22]. Over and above, the lack of reinforcement prevents the production of concrete elements having sufficient ductility and tensile capacity. Hence, in order for this technique to reach maturity, reinforcement has to be also integrated in the fabrication process itself. Accordingly, different reinforcing approaches were developed by several companies

and research institutes such as, Swinburne University of Technology, ETH Zurich, TU/e University, WinSun , ApisCore and many others [23]-[34].

Currently, most of the existing 3D printing techniques are neither feasible nor practical to be adopted for mass production, but if so, there is a lot of limitations that cease their progress and limit their potentials. For example, in the case of fiber reinforcing methods, the presence of fibers might generate a weakness between superposed layers, because they might not cross the horizontal joints properly, leaving extra voids [20]. Eventually, fibers are not capable of totally replacing continuous bars in terms of load bearing capacity in most of the structural requirements, because fiber reinforced elements are limited in strength and ductility [35]. In this paper a simpler reinforcing method has been adopted, described by integrating conventional steel bars between layers, during the printing process. However, the particular rheological properties of the printable material, as well as the nature of this technology that do not allow any type of external vibration impose many queries concerning the bond between concrete and the reinforcement. In addition, unlike conventional concrete elements, a more specific factor that would certainly influence the behavior of a printed section, is the layer direction with respect to the steel bar and acting loads. This is of high importance and should never be neglected because previous researches showed that these elements have anisotropic properties that should be considered [32], [36]-[38].

Typically, the pull-out test is a method used to determine the bond strength between steel bars and the surrounding material. Many factors affect the failing mechanism of the pull-out samples, mainly the volume of the surrounding concrete and confining conditions [39]. In unconfined condition a concrete splitting is more likely to occur resulting from the longitudinal proliferating cracks caused by the wedging action of the bar ribs. However, in confined conditions, the pull-out failure is generally governed by a de-bonding of the bar and concrete due to the fact of preventing the cracks propagation by the surrounding material [40], [41]. The resistance against pull-out forces is majorly dictated by the concrete quality, level of confinement, and most importantly the degree of compaction and the quality of the bond around the reinforcement [42], [43]. Indeed, the distinctive key parameter affecting the bond quality in printed concrete, is the fact of eliminating external vibration due to the absence of molds in 3D printing.

In this context, the aims of this research are first, to investigate the effect of a highly thixotropic material on the bond generated between 3D printed concrete and the steel bar, and second, understand the effect of the printing direction with respect to the bar on the developed bond. A proper comparison between the behavior of printed and conventionally casted samples is held to

demonstrate the potential of 3D printing technology.

2-Materials and methods

2.1- Mix design and material characterization

2.1.1- Mortar's composition

The mix used in this research has an average 28 days compressive strength of 60 MPa and flexural tensile strength of 13 MPa according to the European standard placing method NF EN 196-1 [44]. It is made of an Ordinary Portland Cement Type 1 (CEM I 52.5 N), with a water to cement ratio of 0.51. A limestone filler is used (Filler/Cement = 0.33). As well, this mix contains crushed limestone sand having a particle size distribution comprised between 0 and 2 mm including 19% smaller than 63 μm (Sand/Cement = 1.72). A High Range Water Reducer having a phosphonate base is utilized, with 31% \pm 1.5% dry content being 0.81% of the cement weight. In addition, a commercially used Viscosity Modifying Agent powder is added to the mix and it is equal to 0.4% of the cement weight.

2.1.2- Mixing procedure

The material's mixing has been done using a 5 liter mixer. The mixing procedure adopted consisted of dry mixing all solid ingredients first for 120 sec at a speed of 60 RPM. Then after, water and HRWR were gradually added within 30sec while keeping on the same mixing speed. Directly after pouring all the liquids, the speed was increase to 124 RPM for the next 90 sec. The mix was then left at rest for 60 sec. At the end, the mixing was launched again for 120 sec at high speed (124 RPM). It should be noted that all mixes have been done at room temperature ($\approx 22^{\circ}\text{C} \pm 2^{\circ}\text{C}$) to minimize the difference between batches.

2.1.3- Printability assessment

The preliminary evaluation of the material's printability has been systematically carried out based on visual inspections, when initially developing the mix. The printing was done manually, using a laboratory gun device, having a circular nozzle of 1 cm diameter, similar to the one used in [18], [45], [46]. The extrudability has been assessed by the ability of the material to get smoothly out of the nozzle without showing any discontinuity in the layer or nozzle's blockage. As for the

buildability of the mix, it has been primarily qualified by printing the largest number of superposed layers in a straight wall shape of 20 cm.

2.1.4- Flow table test

The workability of the developed mix has been measured as per the standard test method for flow of hydraulic cement mortar (ASTM C1437-15) [47]. The testing procedure consisted of filling half of the conical mold first, placed at the center of the flow table. The mold was uniformly tamped 20 times to insure a proper filling, with limited entrapped air voids. Then after, the remaining half was filled and the mold was tamped again. The excessive material was cut off to provide a plane surface. At the end, the mold was carefully lifted away, and the table was dropped 25 times within 15 sec, then the spread diameter of the material was measured.

2.1.5- Fall cone test

In this research, it was decided to use the Fall cone penetrometer to measure the static yield stress evolution of the mix, as per the European standard “NF EN ISO 17892-6” [48]. A steel alloy 30° cone weighting 80 g and having a smooth surface has been used. An additional 100 g was further added to the system to ensure a significant penetration in the material. The sample’s preparation consisted of placing the mix inside a circular steel container having a diameter of 30 cm and 5 cm deep. The container was then placed on a jolting table for 30 shocks. This was done to properly fill the container and remove the entrapped air bubbles. After finishing, the surface of the container has been gently sawn to cut off excessive material. The material was left at rest to settle for 120 sec. After then, the tip of the cone was positioned at the surface of the material. Afterwards, the cone was released for 5 sec ± 1 sec to penetrate well, and the penetration depth “h” was recorded. This procedure has been repeated every 150 sec over the course of 1320 sec (22 min), and a 5 cm distance was left between successive penetrations. The measurements were replicated three times, each on a different batch.

The static yielded stress was derived from the penetration depth of the cone using Eq. 3, where: " τ " is the calculated yield stress (Pa), " F " is the force generated by the mass of the cone (N), " h " is the penetration depth (mm), and " θ " is the angle of the cone used (degrees).

$$\tau = \frac{F \cos \theta^2}{\pi h^2 \tan \theta} \quad [49] \text{ (Eq. 3)}$$

In this research the linear model proposed by Roussel et al. [11] was adopted. However, the initial yield stress " $\tau_{0,0}$ " at $t = 0$ was neglected because its magnitude is insignificant when compared to the shear stress developed when the mix is at rest. Therefore, the static yield stress was presented in a simplified form, as shown in Eq. 4.

$$\tau_{0(t)} = A_{thix} t \quad [11] \text{ (Eq. 4)}$$

2.2- Specimen preparation for the pull-out test

2.2.1- Bar's geometry

The steel bars used have an indented surface geometry, and a representative nominal diameter (d_b) of 8 mm. The nominal design yield strength is equal to 500 N/mm², and the actual yield strength is equal to 626 N/mm², conforming to the European Standard requirements of indented steel bars EN 10080 [50]. Precisely, the surface geometry of the bars has three equally distributed rows of indentations as shown in Fig. 1. The corresponding variable are summarized in table 1.

Table 1: Surface geometry specifications of the indented bars

Inclination " β "	Spacing " c "	Width " b "	Depth " t "	Sum of gaps " Σe "
35°	3.2 mm	1.6 mm	0.8 mm	6 mm

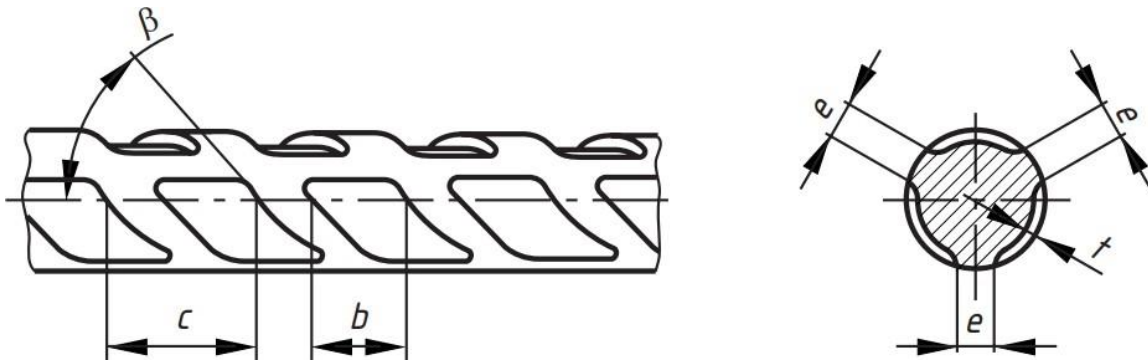


Figure 1: Illustration of an indented bar [50]

2.2.2- Mixing procedure

A uniform mixing procedure was adopted and always done at room temperature ($\approx 22^\circ \text{C}$) to minimize the difference between batches. An 80 liter mixer was used. All solid ingredients were dry mixed gently for around 2 min at a speed of 20 RPM. Then, water and High Range Water

Reducer were added gradually. The mixing process takes around 10 min with an increase in the mixing speed up to 100 RPM. During mixing, the walls of the mixer's bowl were scrapped using a large spatula to ensure that all materials are properly mixed. After finishing, the material was collected and directly placed inside the printer's pump.

2.2.3- Samples manufacturing

Two different sample categories were manufactured for the pull-out tests. The first category consists of conventionally mold-cast (non-printed) samples, taken as references. The second category includes printed samples with two different layer orientations, either parallel or perpendicular to the steel bar. Six samples are made for each condition.

First of all, an effective embedment depth of $5d_b$ equal to 4 cm is adopted for all samples of both categories. This is in accordance with the principle of the standard pull-out test proposed by the European Standard EN 10080 - Annex D [50]. Besides, an adhesive tape was wrapped at both sides of the bar (0.5 cm from each side) to break its adhesion with concrete, set the exact embedment depth needed and overcome the stress concentrations generated at the limits of the embedment depth. The non-printed samples were made by placing and vibrating mortar inside small polystyrene molds of $4 \times 4 \times 5$ cm with the bar passing through. On the other hand, the samples of the second category were printed using an automated 3-axis gantry printer having a circular nozzle of 1.9 cm diameter (Fig. 2). The standoff distance of the nozzle, corresponding to its vertical position above the printing surface was fixed to 1 cm, thus each printed layer has a height of 1 cm. Moreover, the printing speed was equal to 6.4 cm/sec, and it was adjusted in a way to produce a layer's width ranging between 5 and 5.5 cm. The printing path was traced in a way to produce parallel and perpendicular samples in a single run. The followed path and steel bars layout are shown in Fig. 3 and Fig. 4. Three layers were printed first, then the bars were placed in their proper locations, depending on the layers direction (Fig. 4). Each bar was slightly pushed down in a way that half of its diameter is merged in the layer below. Both ends (extremities) of the bar rely on supports to insure its stability and keep it strictly horizontal all over the layer's surface, without further drowning when depositing the next layers on top (Fig. 4). Then after, three more layers were printed on top of the bars, to end up having a total number of six layers.

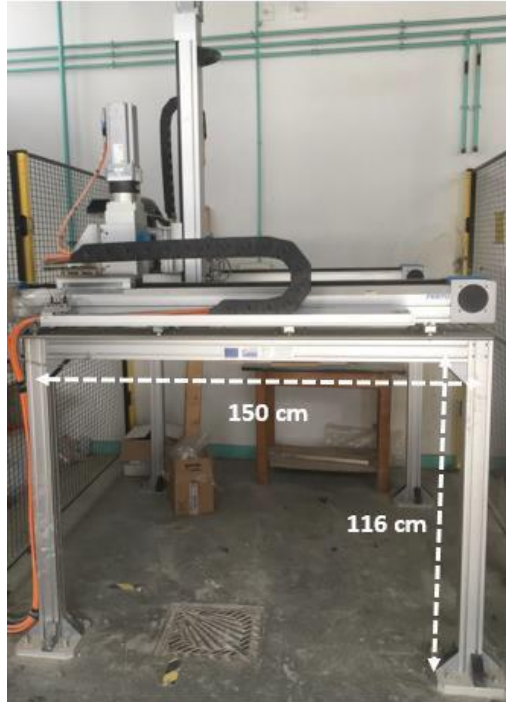


Figure 2: 3-axis gantry printer

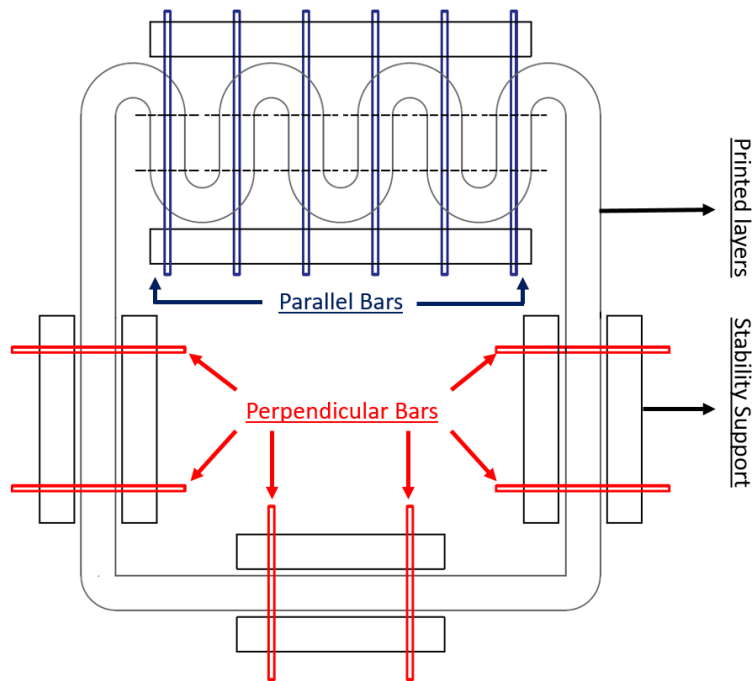


Figure 3: Conceptual printing path and bars layout



Figure 4: 3D printed Pull-out samples

It should be noted that the layers were printed successively with an actual time gap equal to 57 sec imposed by the corresponding printing speed. No intended delay was additionally introduced, in order to avoid any possibility of having cold-joint effect leading to a weakness in the adhesion between consecutive layers. Furthermore, the placing of the bars was done directly after the deposition of the 3rd layer to insure that both layers covering the bars have the same rheological characteristics when they come in contact with the bar's surface. The continuity in depositing superposed layers is of major importance since the mortar used is highly thixotropic. At the end, the samples were cut down properly and the redundant material was removed directly after printing (when the material is still fresh) as it can be seen in Fig. 5. This was done so the material can rebuild its internal structure in case of any disturbance while cutting the samples. Otherwise did, if the samples were cut after the material hardens, the cutting action may create micro-cracks, and hence, the bond between steel and concrete will be negatively affected. Over and above, the distance between bars was left large enough to avoid damaging the core samples, and to keep the curved edges and “modified” areas far from the steel bars. Afterwards, the samples were left to cure in ambient conditions.



Figure 5: Parallel and Perpendicular printed samples after being Cut

After 7 days of curing, the steel bars were cut from one side, and the printed and non-printed elements were top centered in polystyrene cube molds of 15×15×15 cm dimensions. The molds were then filled with a different mortar mix to insure a good confinement of the printed segment (Fig. 6). Indeed, the confined conditions favors pull-out failure of the bar to exclusively quantify the bond generated between steel and concrete. Alternatively stated, the degree of confinement and surrounding of the bar is one of the most important parameters that dictate the failure mode. Thus, a strong confinement of the samples has to be provided in order to avoid the splitting of the concrete cube, and insure a pull-out failure.

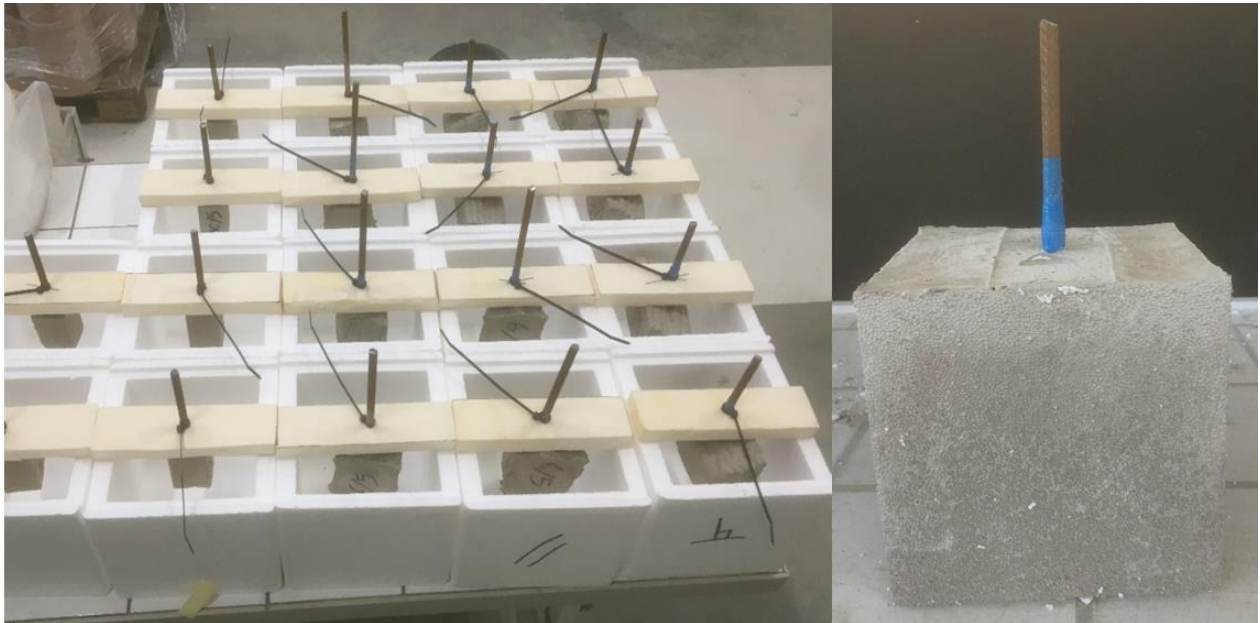


Figure 6: Confined Pull-out samples

2.3- Mechanical characterization of the bond strength and testing procedure

The applied load rate was equal to 0.05 mm/sec. This load rate has been chosen in a way that the failure occurs between the first and the third minutes of the test, as specified by the European Organization for Technical Assessment (EOTA) Technical Report 048 for the testing details of post-installed fasteners in concrete [51]. However, a customized setup system was developed for this research exclusively (Fig. 7). This system allowed to overcome the imperfections and deformity of the samples surface caused by the casting process by filling the voids with a fine sand, and therefore to provide a uniform load distribution. In practice, the sand was used as an alternative method for the neoprene pad caps, which are not able to cover such large defects.

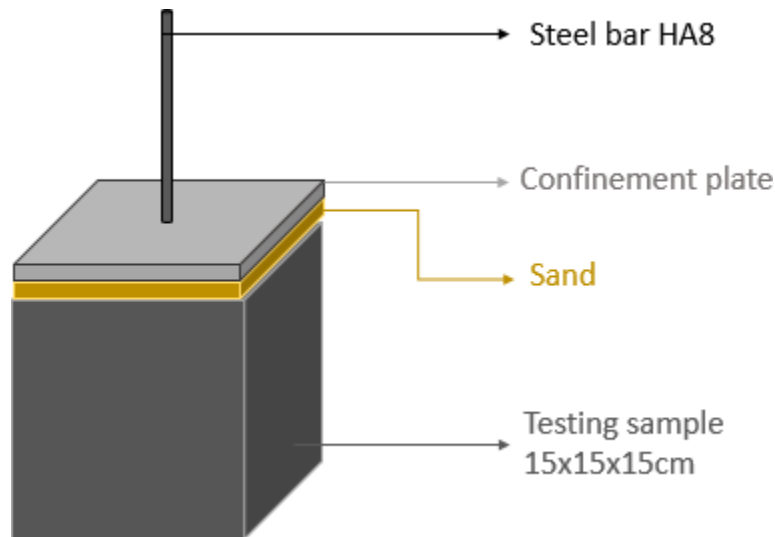


Figure 7: Setup illustration

Fig. 8 shows the actual pull-out sample with the assembled setup. Wood curbs were fixed all around the surface edges of the cube, creating a formwork of 5 mm depth to hold the sand particles. A steel plate having a thickness of 1 cm was grooved at the middle to allow for the steel bar to pass through. This was done to secure additional confinement for the concrete surrounding the bar when being pulled to avoid concrete cone failure, and ensure a definitive slipping failure mode. The drilled hole has a diameter of 12 mm corresponding to the bar's diameter (d_b) plus 4 mm (d_b+4) as specified by the EOTA TR 048 [51]. At the end, the whole system was fixed to the base of the testing machine using threaded rods and connectors, and the steel bar was gripped by the machine's clamp.

All results were calculated using the following equation:

$$\tau = \frac{F}{\pi d_b l_e} \text{ (Eq. 5)}$$

Where:

τ = experimental bond strength (MPa)

F = ultimate axial tension force (N)

d_b = nominal rebar diameter (mm)

l_e = embedment length (mm)



Figure 8: Pull-out testing system

3- Results and discussion

3.1- Flow table and fall cone results

First of all, the spreading diameter of the mix measured using the flow table was equal to 14.5 cm. Fig. 9 shows the evolution of the material's yield stress in function of time for all three trials and their average. It highlights that the increase of the yield stress is almost linear during the first 22 min. In this period, Roussel's model predicted the structural build-up of the material, and this was confirmed by the corresponding correlation factor (R^2) equal to 0.934. The yield stress linearly increased from 620 Pa straight up to 6828 Pa. The corresponding thixotropic index A_{thix} describing the slope of the resulting curve was equal to 5.17, which indicated that the material is highly thixotropic. This was determined based on the ranges defined by Roussel [11] to classify self-compacting concrete (SCC) according to their proper A_{thix} values. Roussel figured out that any mix showing an A_{thix} value strictly above 0.5 Pa/sec ($A_{thix} > 0.5$ Pa/sec) is considered highly thixotropic. In the literature, it can be found that most of the materials used for 3D printing are highly thixotropic. For example, Perrot et al. [8] developed a mix having a structuration rate of 0.9

Pa/sec. Kruger et al. [52], [53] developed different printable mixes having an A_{thix} ranging between 0.6 Pa/sec and 1.08 Pa/sec. Panda et al. [54] developed several mixes with an average A_{thix} value of 1.65 Pa/sec and 2.54 Pa/sec. Besides, Wangler et al. [3] point out that a material having an A_{thix} of 2 Pa/sec would result in a good printability performance. Here, it should be noted that the material used in this study has been designed to develop a significantly high structuration rate, compared to what has been presented in the literature. This was done to investigate the ultimate consequences on the bond quality between concrete and the steel bar, which an extremely thixotropic material may lead to. Eventually, a lower thixotropic material would systematically result in a reduced impact and better bonding.

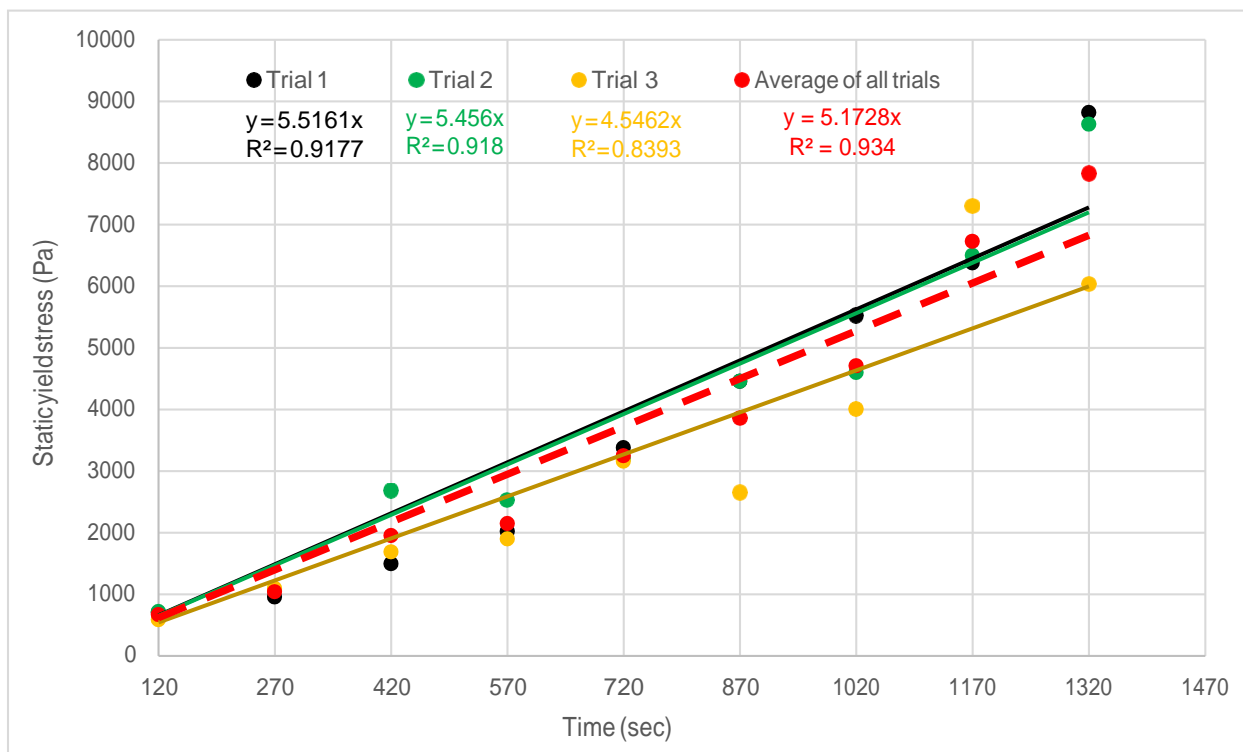


Figure 9: Yield stress variation in function of time

3.2- Pull-out results

Table 2 shows the actual pull-out stress (MPa) of each sample in all conditions (Non-printed, Parallel and Perpendicular). Fig. 10 shows the average result of the pull-out test of each sample corresponding to all conditions, in terms of actual stress and relative strength (%) with respect to the reference elements. The results showed a reasonable standard deviation for each case, indicating the reproducibility and consistency of the adopted method.

It can be clearly seen that the conventionally casted samples dominated, followed by the parallel then the perpendicular printed samples, generating a resistance against pull-out stresses of 18.7 MPa, 16.2 MPa and 14.5 MPa respectively. Accordingly, it was found that when the printed layers are parallel to the steel bar, a strength reduction of 13% in the pull-out capacity occurs, whereas, when the printed layers are perpendicular to the steel bar, a reduction up to 22% takes place. Despite this variance, it can be approved that even when a highly thixotropic mortar mix is used for printing, the material is still able to fill the spaces between the indentations of the bar, due to the pressure exerted when printing, and therefore ensure a good covering and provide a strong bond with the bar's surface.

Table 2: Detailed pull-out results

	Pull-Out Stress (MPa)	Average (MPa) (Std. Dev.)
Non-Printed	20.5	18.7 (2.1)
	20.5	
	17.4	
	20.8	
	16.2	
	17.0	
Parallel	14.9	16.2 (1.9)
	18.0	
	13.5	
	17.1	
	18.1	
	15.4	
Perpendicular	17.0	14.5 (2.0)
	13.5	
	11.9	
	14.3	
	16.9	
	13.6	

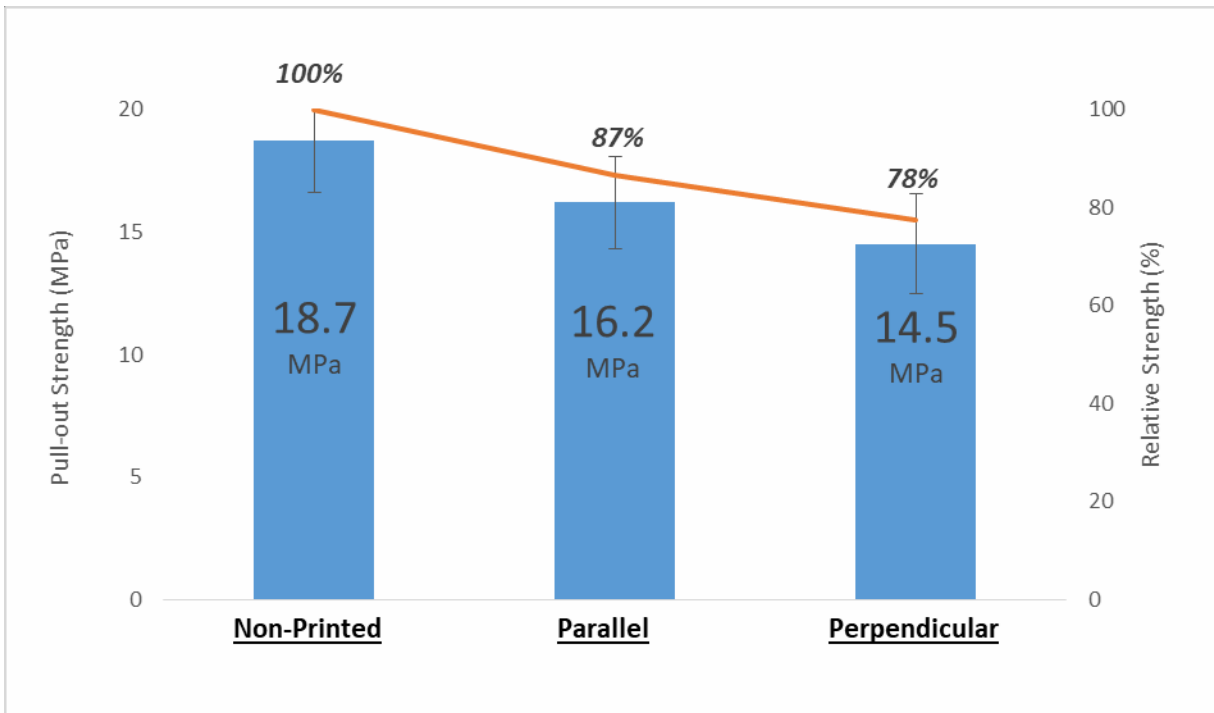


Figure 10: Graphical presentation of the average and relative pull-out strength

Fig. 11-13 represent the load-displacement curves of the steel bars for non-printed, parallel, and perpendicular samples respectively. In general, the resistance against pull-out forces is provided by three major mechanisms: chemical adhesion, friction, and mechanical interlocking. During the first stage, just before reaching the peak load, the bonding forces are provided by the chemical adhesion occurring at the interface between concrete and the bar, due to the hardening of cement. However, after failure, the bond forces between concrete and the bar correspond to the frictional and mechanical interactions. Herein, as it can be relatively seen in all load-displacement graphs, the same mode of failure occurred whether for printed or conventionally casted samples. Initially, a linear response took place short before reaching the peak load (the slope of the increasing load remains constant). Hereafter, the load kept on increasing but in a slower rate for a short period, and the curve exhibited a non-linear response until reaching the peak load. At that instant, the curve showed a plateau during which the slip kept on increasing for a constant bond strength. Finally, a constant decrease of the load began with a remarkable increase in the bar's slippage. At this stage, the acting load corresponded to the residual bond strength caused by the frictional and mechanical interactions between the bar and surrounding concrete.

Despite the mode of variation of the resulting curves, the highest average load was attained by the non-printed samples, followed by the parallel then the perpendicular printed ones (as shown earlier in Table 2 and Fig. 10). Besides, Fig. 12 representing the non-printed samples showed that the slopes of the increasing loads were the highest. The corresponding displacements of the bars before reaching the peak loads were way below 0.5 mm, which is the lowest displacement attained (until failure) in comparison with printed samples. Whereas in the case of printed elements, the corresponding displacements of the bars when the peak loads were reached floated around 0.5 mm. Alongside, the decreasing rates of the loads after failure (slopes of the curves) were slower than for parallel and perpendicular printed samples. These facts indicated that the bond developed between non-printed concrete and steel bars exhibit a stiffer behavior when compared to printed samples. As for the case of both printing conditions (Fig. 12, 13), the overall areas below the curves in the case of parallel samples were greater than for perpendicular samples. Indeed, the residual strength is mainly dictated by the confining forces acting over the bar being pulled. These differences imply that the parallel samples display stiffer behavior than perpendicular samples, as well as a stronger confinement of the bars. Hence, these findings confirm and further explain the variations between non-printed, parallel, and perpendicular samples.

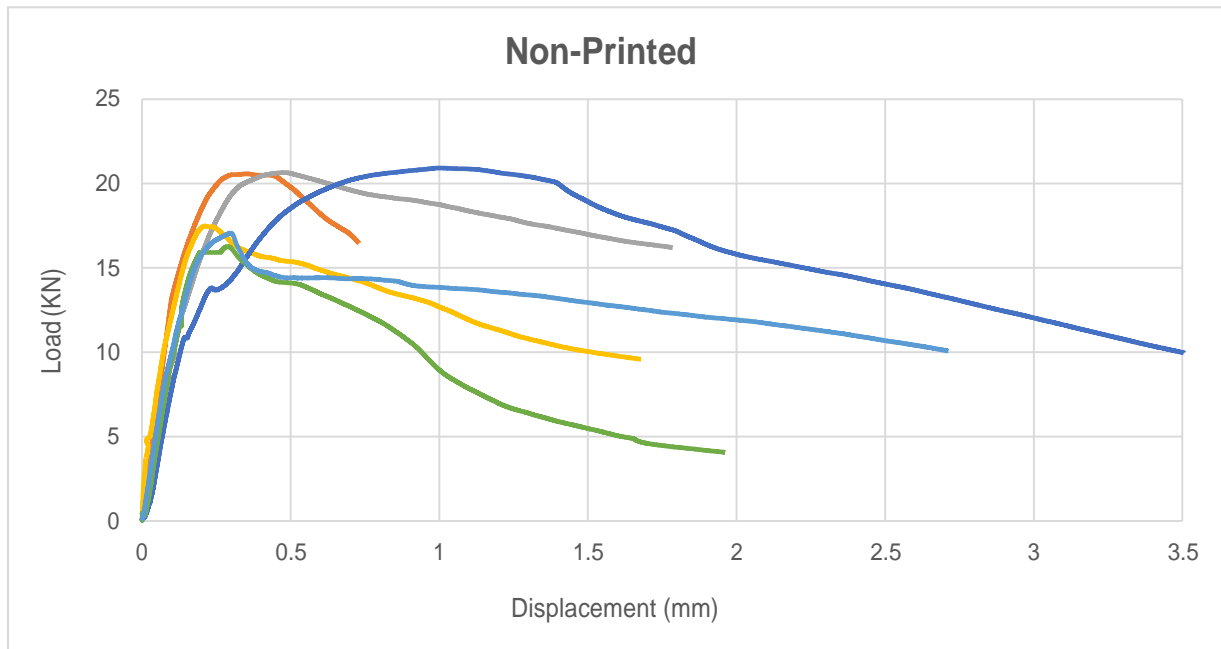


Figure 11: Load-displacement relationship for non-printed samples

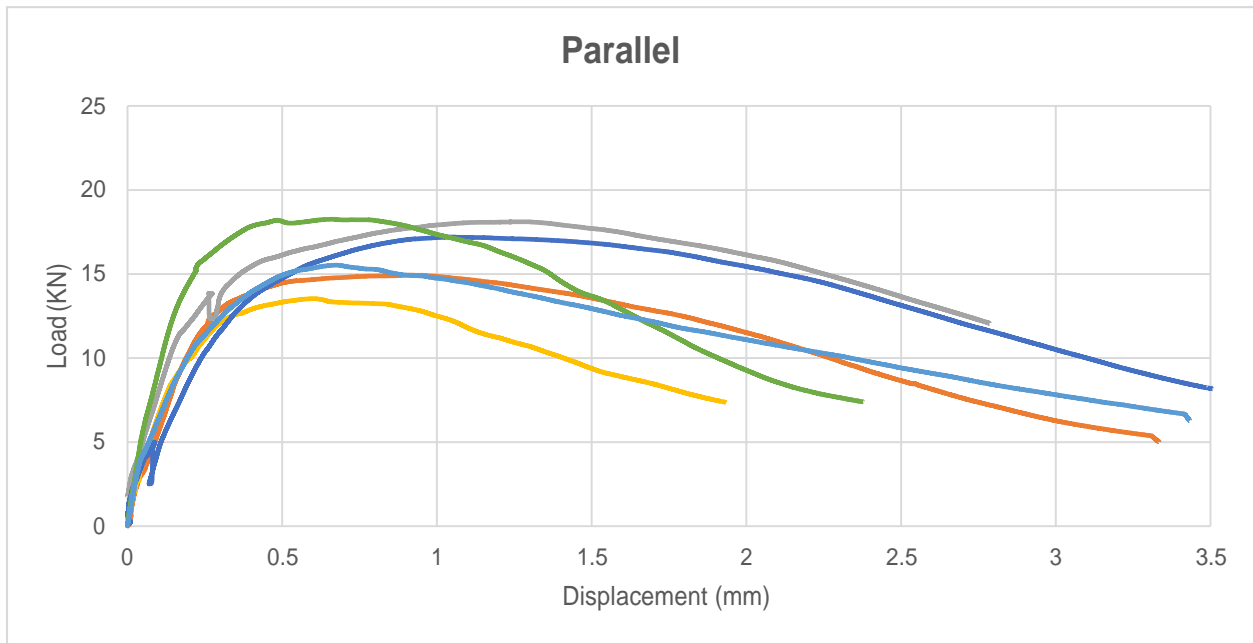


Figure 12: Load-displacement relationship for parallel samples

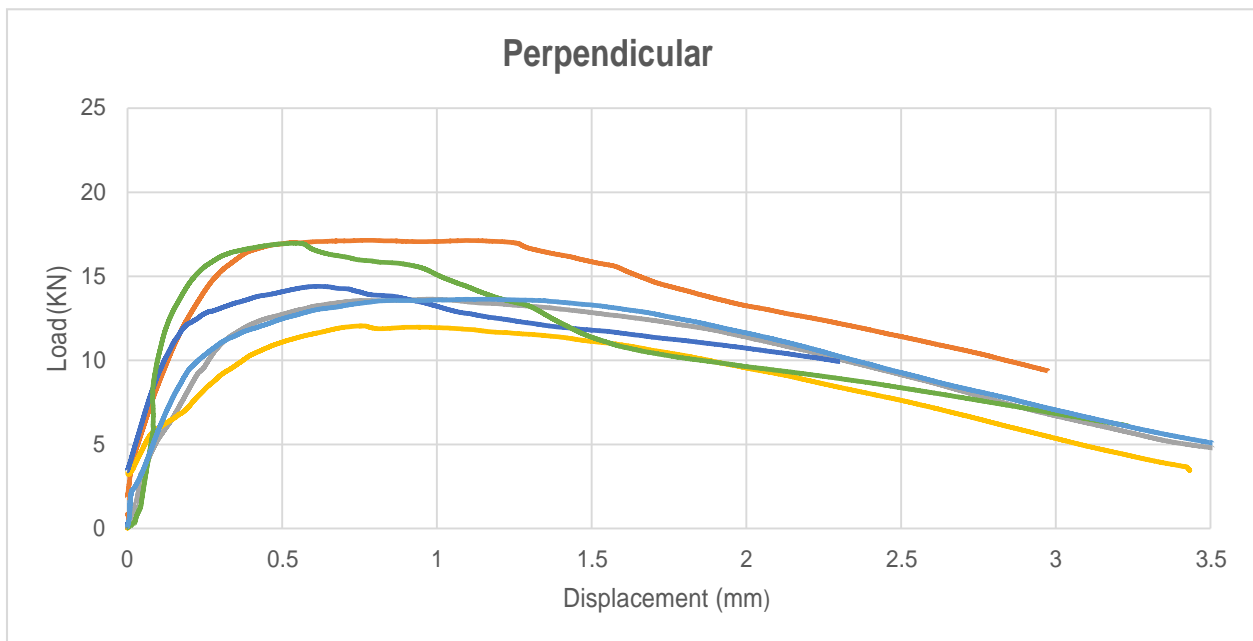


Figure 13: Load-displacement relationship for perpendicular samples

Fig. 14 shows an example of a broken printed sample. This figure allows a visual inspection of the bond generated between the steel bar and concrete. However, the presence of macroscopic voids can be clearly observed at the interface level, between printed layers. Fig. 15 schematically illustrates how these voids are produced. Precisely, they were created at the instant when the layer being printed splits off from the subsequent one, then when they couple back after the printer's

nozzle passes over the bar. Besides, other voids arose as well because of the absence of external vibration. All these irregularities induced a smaller contact surface between concrete and steel. Though, this fact explains and clarifies the difference in the pull-out results between conventionally casted and printed samples.

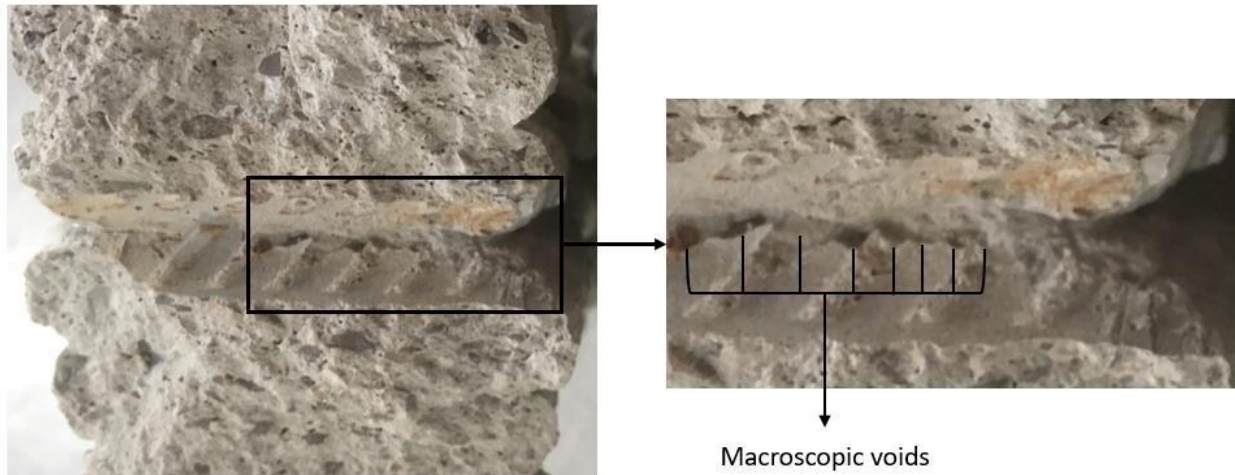


Figure 14: Broken printed element showing macroscopic voids

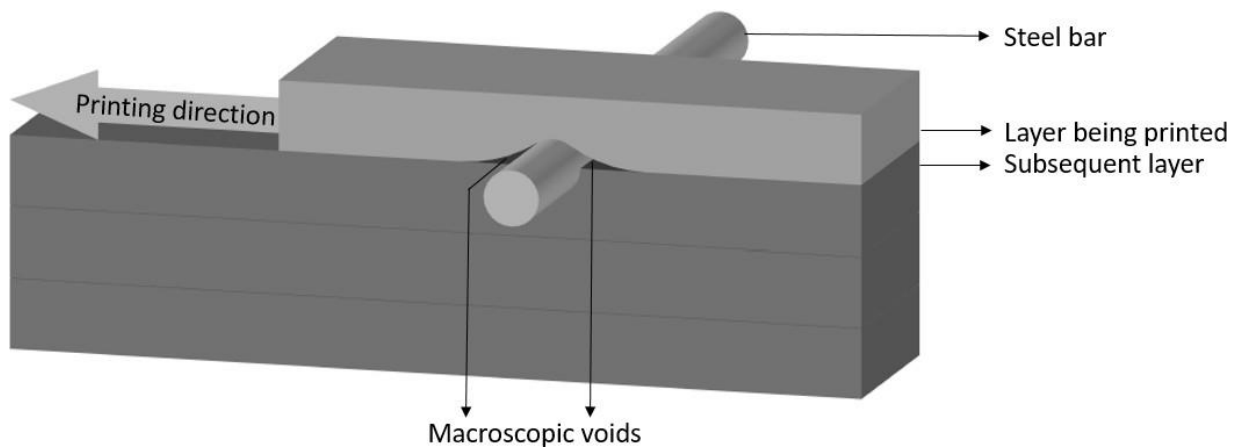


Figure 15: Schematic illustration of the voids creation

The difference between parallel and perpendicular samples can be attributed to the formation of larger voids in the case of perpendicular samples, caused by the splitting action of layers across the steel bar (as explained in the section 3.2 § 5). The volume of the material extruded out of a 1.9 cm nozzle fixed to a height of 1cm above the printing surface (standoff distance) is always constant along the printing path. Though, when the nozzle passes over the bar, an instantaneous change of the local nozzle's height occurs. Herein, the actual standoff distance is suddenly reduced to 0.6

cm, which is equal to the actual standoff distance (1 cm) minus half of the bar's diameter (0.4 cm) (Fig. 16). At this level, while the volume of the extruded material is maintained constant, the area designated to initially accommodate for the material is reduced. This reduction causes a higher squeezing of the material against the surface of the bar below, right before the material overflows. Hence, a higher printing pressure is exerted over the surface of the bar due to the temporary decrease of the nozzle's standoff distance.

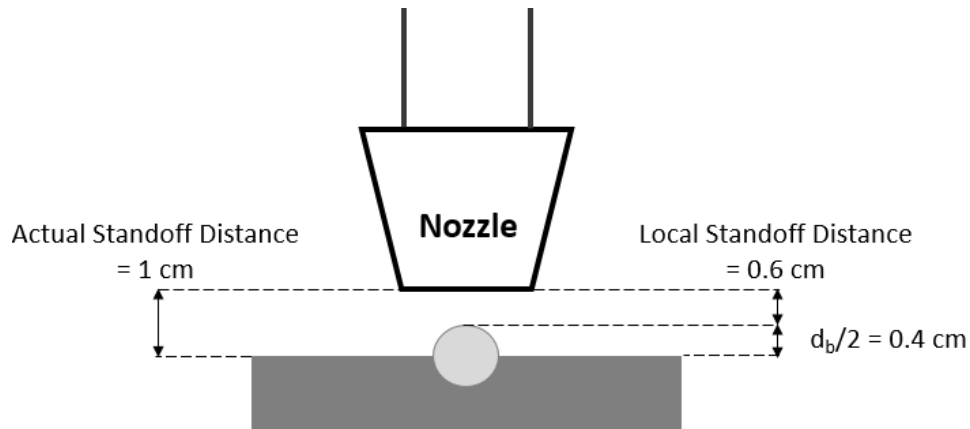


Figure 16: Nozzle's standoff distance variation

Particularly, the resulting printing pressure exerted over the bar largely differs between parallel and perpendicular samples, which therefore affects the degree and strength of confinement of the bar itself. Fig. 17 shows an illustration of the resulting pressure gradient over the bars for parallel and perpendicular samples respectively. It can be clearly observed that for the case of parallel sample, all the embedment depth of the bar is under maximum printing pressure. Herein, the maximum pressure zone, highlighted in red, represents the bar's surface area directly below the printer's nozzle, corresponding to a standoff distance of 0.6 cm. However, as the material spreads away, the resulting pressure starts to decrease gradually until it reaches the minimum at the layer extremities. The orange zone describes the area below the nozzle, at a standoff distance equal to 1 cm, and the yellow zone depicts the spread material outside the nozzle's projection. Correspondingly, a lower pressure results in a less dense material, and weaker internal structure. In contrast, the pressure variation largely influences the bond strength generated in the case of perpendicular sample. In this case, only 1.9 cm of the bar's embedment depth is subjected to the maximum pressure, corresponding to the nozzle's opening diameter, whereas, the rest carries a lower charge. As a matter of fact, the mortar's confinement in parallel samples is stronger than for

perpendicular ones. Therefore, it can be confirmed that the bonding conditions of a steel bar with the printed layer is affected by the printing direction.

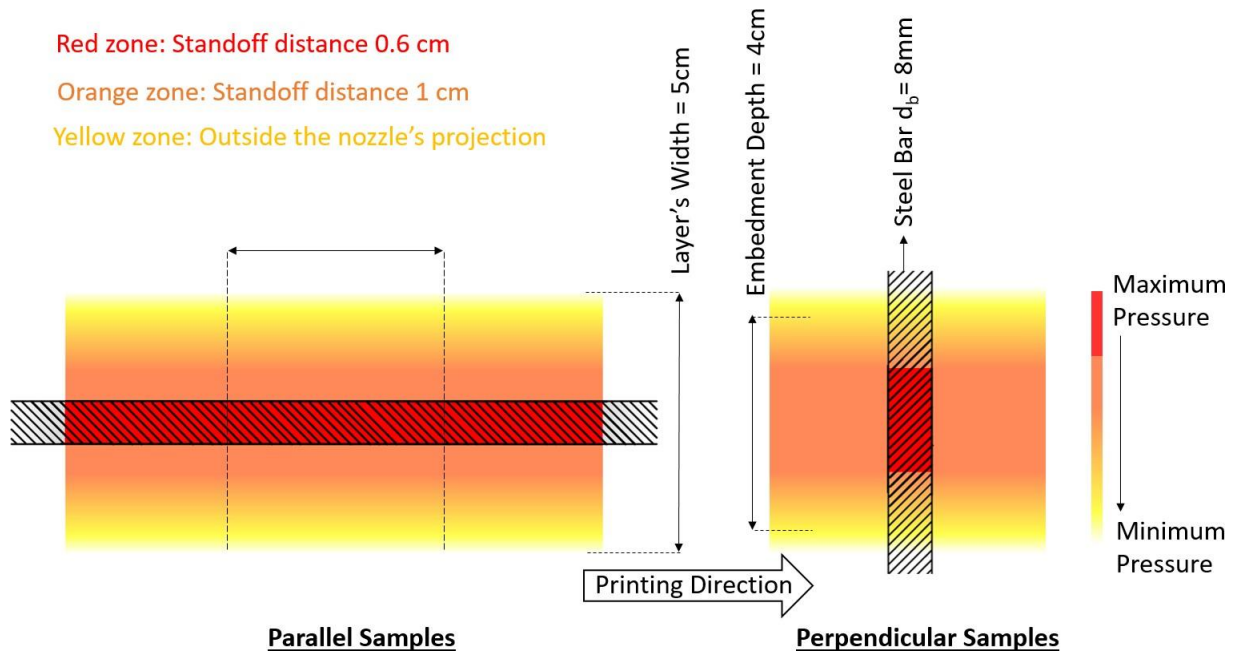


Figure 17: Pressure gradient over steel bars

As previously mentioned, this research was a continuation of a preceding project, where BAZ et al. [46] adopted a similar methodology for testing the bond generated between steel and concrete for mold casted and printed objects, based on a series of pull-out tests. In the former study, BAZ et al. used a lab gun device simulating the printer's work to produce the samples, and it was considered as a first step in this context. In addition, different printing methods and mortar workabilities were investigated. They defined four printing approaches, two parallel (ParaM1 & ParaM2) and two perpendicular (PerpM1 & PerpM2). The closest parallel method previously used to the current one was ParaM2, which was made by printing a bed layer first, then placing the bar at the center of it. On the other hand, the closest perpendicular method to the currently adopted approach was PerpM2. This method was done by printing simultaneously two adjacent layers, with the bar positioned perpendicularly in between. As for the printable material used in the current work, the mix was designed to have a spreading identical to Mix1 of the previous study to provide a proper comparison between results. Specifically, ParaM2 showed almost the same pull-out capacity of a non-printed element, equivalent to a 98%. Besides, PerpM2 gave a lower resistance against pull-out stresses making only 79% of the resistance achieved by the non-printed samples.

Though, in the present case, the same sequence of printing conditions is manifested, but with more explicit results. Namely, in both studies, non-printed samples dominated, followed by the parallel and perpendicular ones respectively. Hence, despite the printing method, the parallel printed layers always develop a better bond with steel bars. In addition, it is worth mentioning that the lab gun device can be used as a representative printing method for preliminary studies.

4- Conclusion:

The article at hand has presented an experimental research aiming to characterize the quality of the bond generated between concrete and a steel bar, based on the mechanical behavior of 3D printed elements under different printing conditions. First, a rheological characterization of the printable material has been carried out using the fall-cone penetrometer to track its structuration rate over time, showing that the used mortar is a highly thixotropic material. Second, a series of pull-out tests was done over printed and non-printed concrete samples to assess the bond generated between steel bars and concrete, and to further understand the effect of the printed layer's direction with respect to the steel bar on the pull-out capacity.

The variance in the bond strength between mold-casted, 3D printed parallel, and 3D printed perpendicular samples is primarily attributed to the casting method and layers direction with respect to the steel bar. It can be clearly observed that the resistance against pull-out forces dominated in mold casted elements. A better bond is always generated with the bar because of the externally applied vibration, eliminating most of the voids inside the bulk material. Besides, samples made of layers that are printed parallel to the steel bar outperformed those made of layers perpendicular to the bar (87% and 78% of the strength of vibrated samples respectively). Indeed, non-printed samples exhibited a stiffer and more rigid behavior compared to printed samples. Similarly, parallel printed samples showed a stiffer response when compared to the perpendicular printed ones. Despite the fact, these findings assure that a good bond is generated between concrete and steel even in printed elements. Yet, the major contributor of this difference is the variation of the resulting stresses applied over the mortar when being printed, caused by the printing process and parameters. These variations lead to a better confinement and stronger bond with the bar when the layers are printed parallel. Herein, this variation depends on the pumping pressure, and the layer's width with respect to the printer's nozzle. Therefore, convenient reduction/safety factors

still need to be applied to the printing method adopted in order to counterbalance the shortage of the bond strength.

Finally, the results of this work establish a wider research framework to optimize the conventional reinforcing techniques in the field of 3D concrete printing. Hence, it would be interesting to reconsider the same research project, but by focusing on the appropriate dimensions (geometry) of the printed layer.

Acknowledgment:

The authors would like to acknowledge the financial support by Partenariats Hubert Curien (PHC) CEDRE program PROJET N° 42287YD, and the Supply of material from Carrières du Boulonnais, Eqiom, and Chryso.

References:

- [1] ASTM International, “ISO/ASTM 52900:2015 Additive manufacturing — General principles — Terminology,” 2015.
- [2] J. H. Lim, B. Panda, and Q. Pham, “Improving flexural characteristics of 3D printed geopolymer composite with in-process steel cable reinforcement reinforcement,” *Construction and Building Materials*, vol. 178, pp. 32–41, 2018.
- [3] T. Wangler, E. Lloret, L. Reiter, N. Hack, F. Gramazio, M. Kohler, B. Mathias, D. Benjamin, J. Buchli, R. Nicolas, R. Flatt, and A, “Digital Concrete : Opportunities and Challenges,” *RILEM Technical Letters*, vol. 1, pp. 67–75, 2016.
- [4] M. Sakin and Y. C. Kiroglu, “3D Printing of Buildings: Construction of the Sustainable Houses of the Future by BIM,” *Energy Procedia*, vol. 134, pp. 702–711, 2017.
- [5] B. Nematollahi, M. Xia, and J. Sanjayan, “Current Progress of 3D Concrete Printing Technologies,” *Proceedings of 34th International Symposium on Automation and Robotics in Construction*, pp. 260–267, 2017.
- [6] X. Zhang, I. Flood, Y. Zhang, H. I. Moud, and M. Hatami, “A Cost Model to Evaluate the Economic Performance of Contour Crafting,” *Computing in Civil Engineering 2019: Visualization, Information Modeling, and Simulation - Selected Papers from the ASCE International Conference on Computing in Civil Engineering 2019*, no. June, pp. 618–625, 2019.
- [7] J. Buchli, M. Gifftthaler, N. Kumar, M. Lussi, T. Sandy, K. Dör, and N. Hack, “Digital in situ fabrication - Challenges and opportunities for robotic in situ fabrication in architecture, construction, and beyond,” *Cement and Concrete Research*, vol. 112, pp. 66–75, 2018.
- [8] A. Perrot, D. Rangeard, and A. Pierre, “Structural built-up of cement-based materials used for 3D- printing extrusion techniques,” *Materials and Structures*, vol. 49, pp. 1213–1220, 2016.
- [9] N. Roussel, “Rheological requirements for printable concretes,” *Cement and Concrete Research*, vol. 112, pp. 76–85, 2018.
- [10] Y. Weng, M. J. Tan, and S. Qian, “Rheology and Printability of Engineered Cementitious Composites-A Literature Review,” *2nd International Conference on Progress in Additive Manufacturing (Pro-AM 2016) 16-19 May 2016, Singapore*, 2016.
- [11] N. Roussel, “A thixotropy model for fresh fluid concretes : Theory , validation and applications,” *Cement and Concrete Research*, vol. 36, pp. 1797–1806, 2006.
- [12] N. Roussel and G. Ovarlez, “The origins of thixotropy of fresh cement pastes,” *Cement and Concrete Research*, vol. 42, no. 1, pp. 148–157, 2012.
- [13] A. Perrot, A. Pierre, and V. Picandet, “Prediction of lateral form pressure exerted by concrete at low casting rates,” *Materials and Structures*, vol. 48, no. 7, pp. 2315–2322, 2015.

- [14] P. Banfill, D. Beaupré, F. de L. Frédéric Chapdelaine, P. Domone, L. Nachbaur, T. Sedran, O. Wallevik, and J. E. Wallevik, “Comparison of concrete rheometers : International tests at LCPC (Nantes , France) in October , 2000,” 2017.
- [15] J. E. Wallevik, “Relationship between the Bingham parameters and slump,” *Cement and Concrete Research*, vol. 36, no. 7, pp. 1214–1221, 2006.
- [16] S. E. Chidiac, F. Habibbeigi, and D. Chan, “Slump and Slump Flow for Characterizing Yield Stress of Fresh Concrete,” *International Concrete Abstracts Portal*, vol. 103, no. 6, pp. 413–418, 2016.
- [17] A. F. Omran, K. H. Khayat, and Y. M. Elaguab, “Effect of SCC mixture composition on thixotropy and formwork pressure,” *journal material Journal of Materials in Civil Engineering*, vol. 24, no. 7, pp. 876–888, 2012.
- [18] N. Khalil, G. Aouad, K. El Cheikh, and S. Rémond, “Use of calcium sulfoaluminate cements for setting control of 3D-printing mortars,” *Construction and Building Materials*, vol. 157, pp. 382–391, 2017.
- [19] M. Rubio, M. Sonebi, and S. Amziane, “3D printing of fibre cement-based materials: fresh and rheological performances,” *Proceedings of 2nd ICBBM (PRO 119), 21–23 June 2017*, pp. 284–291, 2017.
- [20] V. Mechtcherine, J. Grafe, V. N. Nerella, E. Spaniol, M. Hertel, and U. Füssel, “3D-Printed Steel Reinforcement for Digital Concrete Construction Manufacture, Mechanical Properties and Bond Behaviour,” *Construction and Building Materials*, vol. 179, pp. 125–137, 2018.
- [21] J. Mata-Falcon, P. Bischof, and W. Kaufmann, “Exploiting the Potential of Digital Fabrication for Sustainable and Economic Concrete Structures,” *First RILEM International Conference on Concrete and Digital Fabrication – Digital Concrete 2018*, 2018.
- [22] R. N. P. Van Woensel, T. Van Oirschot, M. J. H. Burgmans, M. Mohammadi, Ph D, and K. Hermans, “Printing Architecture: An Overview of Existing and Promising Additive Manufacturing Methods and Their Application in the Building Industry,” *The International Journal of the Constructed Environment*, vol. 9, no. 1, pp. 57–81, 2018.
- [23] S. Lim, R. A. Buswell, T. T. Le, S. A. Austin, A. G. F. Gibb, and T. Thorpe, “Developments in construction-scale additive manufacturing processes,” *Automation in Construction*, vol. 21, no. 1, pp. 262–268, 2012.
- [24] E. Lloret, A. R. Shahab, M. Linus, R. J. Flatt, F. Gramazio, M. Kohler, and S. Langenberg, “Complex concrete structures: Merging existing casting techniques with digital fabrication,” *CAD Computer Aided Design*, vol. 60, pp. 40–49, 2015.
- [25] P. Ayres, W. R. L. da Silva, P. Nicholas, T. J. Andersen, and J. P. Greisen, “SCRIM – Sparse Concrete Reinforcement in Meshworks,” *Robotic Fabrication in Architecture, Art and Design 2018*, pp. 207–220, 2019.
- [26] T. Marchment and J. Sanjayan, “Mesh reinforcing method for 3D Concrete Printing,” *Automation in Construction*, vol. 109, 2020.

- [27] N. Hack, W. V. Lauer, F. Gramazio, and M. Kohler, “Mesh Mould: Robotically Fabricated Metal Meshes as Concrete Formwork and Reinforcement,” *FERRO-11: Proceedings of the 11th International Symposium on Ferrocement and 3rd ICTRC International Conference on Textile Reinforced Concrete*, pp. 347–359, 2015.
- [28] S. Christ, M. Schnabel, E. Vorndran, J. Groll, and U. Gbureck, “Fiberreinforcement during 3D printing,” *Materials Letters*, vol. 139, pp. 165–168, 2015.
- [29] F. P. Bos, Z. Y. Ahmed, R. J. M. Wolfs, and T. A. M. Salet, “3D Printing Concrete with Reinforcement,” *fib Symposium, High Tech Concrete: Where Technology and Engineering Meet*, vol. 1, 2018.
- [30] E. Lloret Fritschi, L. Reiter, T. Wangler, F. Gramazio, and R. J. Kohler, Matthias; Flatt, “Smart Dynamic Casting: Slipforming With Flexible Formwork - Inline Measurement and Control,” *second concrete innovation conference*, 2017.
- [31] M. Hambach and D. Volkmer, “Properties of 3D-printed fiber-reinforced Portland cement paste,” *Cement and Concrete Composites*, vol. 79, pp. 62–70, 2017.
- [32] B. Panda, S. Chandra Paul, and M. Jen Tan, “Anisotropic mechanical performance of 3D printed fiber reinforced sustainable construction material,” *Materials Letters*, vol. 209, pp. 146–149, 2017.
- [33] D. Asprone, F. Auricchio, C. Menna, and V. Mercuri, “3D printing of reinforced concrete elements: Technology and design approach,” *Construction and Building Materials*, vol. 165, pp. 218–231, 2018.
- [34] G. De Schutter, K. Lesage, V. Mechtcherine, V. N. Nerella, G. Habert, and I. Agusti-Juan, “Vision of 3D printing with concrete — Technical, economic and environmental potentials,” *Cement and Concrete Research*, vol. 112, pp. 25–36, 2018.
- [35] D. Asprone, C. Menna, F. P. Bos, T. A. M. Salet, J. Mata-falcón, and W. Kaufmann, “Rethinking reinforcement for digital fabrication with concrete,” *Cement and Concrete Research*, vol. 112, pp. 111–121, 2018.
- [36] G. Ma, J. Zhang, L. Wang, Z. Li, and J. Sun, “Mechanical characterization of 3D printed anisotropic cementitious material by the electromechanical transducer,” *Smart Materials and Structures*, vol. 27, no. 7, 2018.
- [37] K. Kim, S. Park, W. S. Kim, Y. Jeong, and J. Lee, “Evaluation of shear strength of RC beams with multiple interfaces formed before initial setting using 3D printing technology,” *Materials*, vol. 10, no. 12, p. 1349, 2017.
- [38] A. Kazemian, X. Yuan, E. Cochran, and B. Khoshnevis, “Cementitious materials for construction-scale 3D printing: Laboratory testing of fresh printing mixture,” *Construction and Building Materials*, vol. 145, pp. 639–647, 2017.
- [39] M. Haskett, D. J. Oehlers, and M. S. Mohamed Ali, “Local and global bond characteristics of steel reinforcing bars,” *Engineering Structures*, vol. 30, no. 2, pp. 376–383, 2008.
- [40] F. P. Bos, Z. Y. Ahmed, E. R. Jutinov, and T. A. M. Salet, “Experimental exploration of metal cable as reinforcement in 3D printed concrete,” *Materials*, vol. 10, no. 11, 2017.

- [41] M. J. Al-Shannag and A. Charif, “Bond behavior of steel bars embedded in concretes made with natural lightweight aggregates,” *Journal of King Saud University - Engineering Sciences*, vol. 29, no. 4, pp. 365–372, 2017.
- [42] Fédération Internationale du Béton, *Bond of Reinforcement in Concrete, State-of-Art-Report*. 2000.
- [43] J. Cairns, “Bond and anchorage of embedded steel reinforcement in the fib Model Code 2010,” *4th International fib Congress 2014: Improving Performance of Concrete Structures, FIB 2014 - Proceedings*, no. 1, pp. 262–264, 2014.
- [44] “AFNOR NF EN 196-1, Methods of testing cement - Part 1 : determination of strength,” 2006.
- [45] K. El Cheikh, S. Rémond, N. Khalil, and G. Aouad, “Numerical and experimental studies of aggregate blocking in mortar extrusion,” *Construction and Building Materials*, vol. 145, pp. 452–463, 2017.
- [46] B. A. BAZ, G. AOUAD, and S. REMOND, “Effect of the Printing Method and Mortar’s Workability on Pull-Out Strength of 3D Printed Elements,” *Construction and Building Materials*, vol. 230, 2020.
- [47] ASTM C1437-15, “Standard Test Method for Flow of Hydraulic Cement Mortar,” 2015.
- [48] CEN (European Committee for Standardization), “EN ISO 17892-6: Geotechnical investigation and testing - laboratory testing of soil - part 6: Fall cone test,” 2017.
- [49] P. Estellé, C. Michon, C. Lanos, and J. L. Grossiord, “De l’ intérêt d’ une caractérisation rhéologique empirique et relative,” *Rhéologie*, vol. 21, pp. 10–35, 2012.
- [50] EN 10080:2005, “Steel for the reinforcement of concrete - Weldable reinforcing steel - General,” 2005.
- [51] (EOTA) European Organisation of Technical Assessment, “TR 048 - Details of Tests for Post-installed Fasteners in Concrete,” 2016.
- [52] P. Kruger, S. Zeranka, and G. van Zijl, “An ab initio approach for thixotropy characterisation of (nanoparticle-infused) 3D printable concrete,” *Constr. Build. Mater.*, vol. 224, pp. 372–386, 2019.
- [53] K. Pj, S. Cho, S. Zeranka, and V. Z. Gpag, “Multi-physics approach for improved thixotropy of cement-based materials for 3DPC,” *1st International Conference on 3D Construction Printing Swinburne University of Technology, Melbourne, Australia*, pp. 1–8, 2018.
- [54] B. Panda, S. Ruan, C. Unluer, and M. J. Tan, “Improving the 3D printability of high volume fly ash mixtures via the use of nano attapulgite clay,” *Composites Part B: Engineering*, vol. 165, pp. 75–83, 2019.

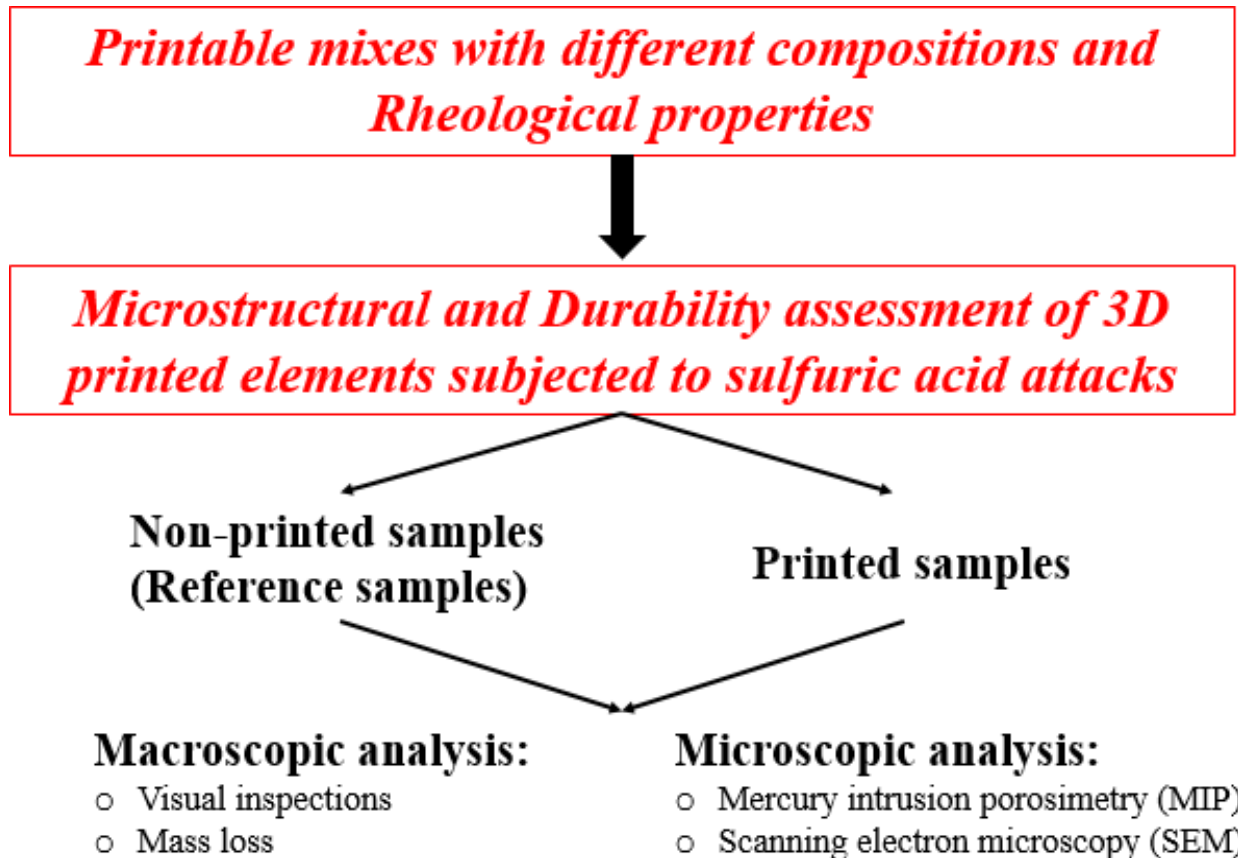
CHAPTER 4 : DURABILITY ASSASSMENT OF 3D PRINTED ELEMENTS IN FUNCTION OF THE MATERIAL'S RHEOLOGY AND EXPOSED ENVIRONMENTS

The application of 3D printing technology has become even more popular in the construction field. However, 3D printed elements were introduced to a developed field of applications, where they are continuously exposed to aggressive environments, especially in the infrastructure industry [169] [168]. In particular, the production technique that is based on layers stacking threatens the durability of the printed element. Alternatively stated, the fact of layers superposition might induce weaknesses in the bond generated between successive layers. These weaknesses might arise from the rheological and thixotropic properties of the printable mix, caused by the material's composition. Thus, this fact can generate a weak plane creating preferential pathways for chemicals intrusion [206].

The present chapter is an extent of the anticipated research plan and objectives set at the beginning of the thesis. It provides a comparative experimental investigation of the material's microstructure between printed and non-printed concrete samples, as well as the behavior of 3D printed elements when subjected to different concentrations of sulfuric acids and the consequences on its internal structure; in particular, the inter-layer bond quality between superposed layers. Alternatively stated, this preliminary study aims to investigate the overall effect of 3D printing technique on the quality of the link between successive layers through an accelerated process. Herein, three different mixes were selected out of the ones previously developed in chapter 2. It is referred to these mixes by Mix A, Mix B, and Mix C, and they represents respectively Mix 7, Mix 13 and Mix 14 of chapter 2. These mixes have different compositions and thixotropic behaviors. Precisely, Mix A is considered as the reference mix, Mix B has a higher content of limestone filler, and Mix C has a lower W/C ratio. These material variables, in particular the water content, influence the microstructure of the mix itself, and therefore its rheological properties. In its turn, the material's rheology affects the quality of the bond between successive layers. Indeed, in the case of a printed element, the durability would not be only affected by the internal structure of the bulk material, but by the inter-layer conditions as well. Besides, the tested elements were subjected to different concentrations of sulfuric acid (H_2SO_4) environments, mainly 1% and 3%, for an exposure duration of 56 days. This assessment has been done over a macroscopic and microscopic

scale. The macroscopic analysis was limited to the naked eye visual inspections and mass loss measurements, whilst the microscopic exploration consisted of mercury intrusion porosimetry (MIP) and scanning electron microscopy (SEM) analyses.

The simplified methodology chart of the work carried out in this chapter is shown below.



The results of this work were submitted for publication as a journal article in Construction and Building Materials, entitled “Durability assessment and microstructural analysis of 3D Printed concrete exposed to sulfuric acid environments”, by Bilal BAZ, Georges AOUAD, Joelle KLEIB, David BULTEEL, and Sébastien REMOND.

Durability assessment and microstructural analysis of 3D Printed concrete exposed to sulfuric acid environments

Bilal BAZ^{1,2}, Georges AOUAD¹, Joelle KLEIB², David BULTEEL², Sébastien REMOND³

¹ Faculty of Engineering, University Of Balamand, UOB, Al Koura, Lebanon

² IMT Lille Douai, LGCgE – GCE, F-59508 Douai, France

³ Univ Orléans, Univ Tours, INSA CVL, LaMé, EA 7494, France

Abstract

Additive manufacturing techniques are being more adopted in the construction field, and they are rapidly developing. However, it is expected that layers superposition imposes several limitations on the performance of 3D printed structures. In this regard, an efficient concrete structure should not only present reliable mechanical performances, but also appropriate durability performance against weathering. This paper presents an experimental study aiming to compare 3D printed elements to casted ones on a macro and micro scale, as well as their resistance against sulfuric acid attacks. Herein, three different mortar mixes having different thixotropic properties were used, and two solution concentrations were employed, one containing 1% sulfuric acid and the other containing 3%. At first, a visual observation of the degraded samples and their mass loss were held. Then, a microstructural characterization was performed through mercury intrusion porosimetry (MIP) and scanning electron microscopy (SEM) analyses. Still, not any printed element has cracked at the inter-layer level. Moreover, on a microscopic level, the MIP results showed that all samples of different compositions have an equal total porosity. However, the pore size distribution and their morphology largely differs between printed and non-printed specimens. The pore sizes are more spread in printed specimens. As for the SEM results, it can be clearly seen that no interface have revealed the formation of a weak plane that might even threaten the durability of the printed elements. Yet, a strong link between superposed layers has been developed, even when using materials having different rheological properties; and the overall specimen acted as a monolithic body without showing any signs of discontinuity or superposition effects.

Keywords: 3D printing – Durability – Mortar – Rheology – Thixotropy – Microstructural analysis – Porosity – Sulfuric acid.

1- Introduction

Nowadays, 3D printing is experiencing an exponential increase in terms of research and application activities, and it is continuously advancing [1][2][3][4][5]. Above all, 3D printing has been widely developed in the construction field [6], where it presented significant benefits in terms of higher geometrical freedom of concrete products, as well as faster production and lower cost [7][8][9][10].

Additive manufacturing has a remarkable impact on concrete manufacturing. Its application has evolved from printing prototypes and laboratory scale objects to the manufacturing of fully functional concrete elements [11][12]. Recently, 3D printing of concrete elements has been applied in the infrastructure construction industry, which could bring in significant improvements to the field [13][14]. Over and above, 3D printing was introduced to a more critical field of applications, where printed structures are continuously exposed to aggressive environments. For example, Winsun released the very first 3D printed river revetment wall, over 500 meters long [15]. Similarly, XtreeE has used 3D printing technology to reproduce natural coral reefs, using normal concrete material, as well as water collectors for drainage systems [16].

Despite that, daily applications still seem far away because of the conservative practices in this field [3]. They are persisting challenges in penetrating the market due to the lack of compliance with building codes [17]. In addition, some technical challenges need to be overcome to trigger all the opportunities offered by 3D printing techniques in the building sector, such as reinforcement incorporation to provide sufficient tensile capacity and ductility for the intended applications [18][19][20][21]. Though, in order to consider 3D printing as a successful construction practice, high quality properties of the final product have to be targeted. In other words, the design of concrete elements should be based on different requirements [22], mainly specified by the structural stability and ability to bear and transfer loads [23], the durability against environmental effects [24], and the aesthetic needs [25]. Indeed, for a broader field of applications, not just the physical and mechanical properties of printable materials need to be assessed, but the durability needs to be addressed as well. This is said because the life cycle assessment of constructions is majorly affected by the materials production [26], enabling them to reach a reasonable service life in natural or industrial exposure conditions [3].

The lack of performance testing protocols of 3D printed elements makes the analogy between printed and casted concrete elements obscure. All structural and durability design standards consider concrete as a homogeneous material [27], which might not be always applicable for 3D printed elements. In fact, these elements have anisotropic behavior due their particular production identity [28][29][30]. Thus, the current standards need to be revised and adapted for structures having anisotropic properties.

The properties of hardened cement paste are majorly influenced by its microstructure, and the way in which the material is casted [31]. The induced heterogeneities and interfaces caused by the process represent a major challenge [32]. The effect of weak interfaces between successive layers on the mechanical properties of 3D printed elements has been widely reported in the literature [33][34][35][36][37]. This weakness is due to the layered concept creating extra voids between successive layers, with more porous properties of the layers themselves, in addition to the anisotropic characteristics [3]. Having said that, the quality of the bond generated between superposed layers is mostly influenced by the rheological and thixotropic properties of the material used [38][39]. Alongside, the same printing parameters affecting the mechanical and rheological properties of concrete in its fresh and hardened states, affect the durability properties. These parameters are mainly the printing speed and pumping pressure [34]. For example, a higher print-time interval decrease the adhesion between successive layers due to the water evaporation causing a lower surface moisture content and possibly a weaker bond between layers [39]. In addition, an increase in the printing speed introduces bigger pores [40]. Alongside, a lower printing pressure induces a higher surface roughness due to the kinetic energy of the sand particles causing more voids formation [41]. In some cases, air bubbles present inside the layer itself might escape due to the pressure exerted by subsequent layers and stay entrapped at the interface level. Therefore, a weak link between successive layers would threaten the durability of printed elements, due to the creation of another preferential ingress path for aggressive substances from the surrounding environment. Alternatively stated, the chemical diffusion through interfaces can be faster than that in bulk concrete, which may jeopardize the durability of the structure. In addition, this matter would increase the corrosion rate of the reinforcing steel bars placed between layers. However, the current focus on the material properties concerning the durability aspect is still limited [27].

Durability characteristics correspond to the ability of the material to resist different environmental exposures for a long period of time, without significant deterioration [42]. Concerning the durability of concrete material, it depends on many factors, mainly cement type and content, water to cement (W/C) ratio [43], curing conditions and compaction [44]. Indeed, some of these aspects are not relevant for 3D printed elements, especially those related to compaction, which is not applicable in the field of additive manufacturing.

Typically, it is known that ordinary Portland cement has little resistance to acid attacks, because of its high alkalinity [45][46]. Therefore, acids can easily deteriorate concrete in various ways. Notably, sulfuric acid (H_2SO_4) is one of the most harmful acids to act on concrete materials due to its combined effect of acid and sulphate attack [47]. It reacts with the calcium hydroxide (CH) of the hydrated cement paste, and produces gypsum. Yet, the decomposition of concrete under acid attack depends mainly on concrete porosity and acid concentration [48].

This study is based on an experimental analysis of concrete samples exposed to sulfuric acid environments. Though, it is less common for a 3D printed structure to be subjected to high concentrations of acid attacks; however, the reason behind using it is because of being very corrosive, and thus, it would considerably accelerate the corrosion rate of concrete samples. However, the objective of this research is to investigate the microstructural properties of 3D printed concrete elements and their resistance against sulfuric acid attacks, in comparison to non-printed samples. In particular, it aims to qualify the interfaces and bonding efficiency between successive layers. Hence, it aims to draw a better perception regarding whether a printed element acts homogeneously as a casted object, or as a stack of concrete layers. Herein, three mixes compositions having different thixotropic properties were used, and all specimens whether printed or not, were studied on a macroscopic and microscopic scale.

2- Materials and Methods

The experimental program presented in this research covers two phases. The first phase corresponds to the materials development and rheological characterizations, whereas the second one describes the production and preparation of the specimens used for the durability assessment.

2.1- Mix design and material characterization

2.1.1- Raw Materials

All developed mixes consist of an Ordinary Portland Cement Type 1 (CEM I 52.5 N), having a density of 3.1g/cm^3 and $8.2\ \mu\text{m}$ median particle diameter “D₅₀”, (The chemical and mineralogical composition is shown in table 1.), CBCALC 80 μm limestone filler with a density of 2.7g/cm^3 and $5.7\ \mu\text{m}$ D₅₀, CHRYSO®Fluid Optima 100 high range water reducer (HRWR) having a phosphonate base with $31\% \pm 1.5\%$ dry content, commercially used BELITEX® ADDICHAP viscosity modifying agent (VMA) powder, and a crushed limestone sand having a particle size distribution of 0 to 2 mm including 19% smaller than $63\ \mu\text{m}$ and a density of $2.7\ \text{g/cm}^3$.

Table 1: Chemical and mineralogical composition of cement

Compounds	Concentration (%)
CaO	63.8
SiO ₂	20.0
Al ₂ O ₃	5.3
Fe ₂ O ₃	3.0
SO ₃	3.0
MgO	0.9
K ₂ O	0.9
Na ₂ O	0.5
P ₂ O ₅	0.3
TiO ₂	0.3
MnO	< 0.1
NiO	< 0.1
CuO	< 0.1
ZnO	0.1
SrO	0.1
ZrO ₂	< 0.1

2.1.2- Mortar compositions

Three mixes having different thixotropic characteristics were used in this study. The aim of testing more than one composition was to exclusively investigate the overall effect of 3D printing techniques on the quality of the link between successive layers, which is majorly affected by the material’s rheological properties.

These mixes compositions are shown in table 2. Mix A is considered as reference, Mix B contains a higher amount of limestone filler, and Mix C has a lower water to cement ratio (W/C).

Table 2: Relative mixes compositions

	Sand (S/C)	Filler (F/C)	Water (W/C)	VMA % (VMA/C)	HRWR % (HRWR/C)
Mix A	1.72	0.33	0.51	0.40	0.81
Mix B	2.02	0.54	0.60	0.47	0.95
Mix C	1.72	0.33	0.41	0.40	1.52

2.1.3- Mixing procedure

For the development of the mixes used, a 5 liters mixer was used, and the mixing procedure was done at room temperature ($\approx 22^{\circ}\text{C} \pm 2^{\circ}\text{C}$) to minimize the difference between batches.

The same mixing procedure adopted by Baz et al. [49] was followed, and it consisted first of dry mixing all solid ingredients for 120 sec at a speed of 60 RPM. Water and HRWR were added gradually afterwards, during 30 sec, while keeping on the same mixing speed. Then after, the mixing speed was increased to 124 RPM for 90 sec. Once finished, the mix is left at rest for 60 sec. At the end, the material's mixing was resumed for 120 sec at 124 RPM.

2.1.4- Printability assessment

The printability of the developed mixes has been systematically assessed, based on visual inspections. Initially, the printing has been done manually using a laboratory gun device equipped by a circular nozzle of a 1 cm diameter, as in El Cheikh et al. [50]. Herein, the extrudability of the mortar was evaluated based on its ability to get out of the nozzle smoothly, without any discontinuity in the layer or blockage of the nozzle.

2.1.5- Mechanical performance of mortars

The mechanical performance of the newly developed mixes was systematically evaluated by measuring the compressive strength of casted (non-printed) samples at 38 days (the age when the samples were submerged in the sulfuric acid solutions for the first time). Three trials of each mix were tested at a load rate of 144 KN/min.

2.1.6- Rheological characterization using the fall-cone test

The fall-cone penetrometer has been used to measure the evolution of the static yield stress over a certain period of time, as per the European standard "NF EN ISO 17892-6" [51]. Hereby, a 30°

steel cone having a smooth surface and weighting 80 g has been used. 100 g were further added to the system to ensure a significant penetration of the cone in the material [49].

The material was put in a circular steel container having a diameter of 30 cm and a depth of 5 cm. The container was then put over a jolting table for 30 shocks to insure a proper filling, and to remove any entrapped air bubbles. Then after, the surface of the container was gently sawn, and the excessive materials were cut off. The material was then left at rest for 120 sec. Once done, the tip of the cone was placed at the surface of the material, then it was released to fall under its own weight for $5 \text{ sec} \pm 1 \text{ sec}$, and the penetration depth " h " was recorded. This procedure was repeated every 150 sec over a time span of 1320 sec (22 min). 5 cm were left between a penetration and another. Besides, the measurements were repeated three times, each on a different batch.

The static yield stress was derived from the penetration depth of the cone, and it was calculated using Eq. 1. In this equation, " τ " corresponds to the calculated yield stress (Pa), " F " represents the force generated by the mass of the cone (N), " h " is the penetration depth (mm), and " Θ " is the angle of the cone used (degrees).

$$\tau = \frac{F \cos \theta^2}{\pi h^2 \tan \theta} \text{ [52] (Eq. 1)}$$

The linear model proposed by Roussel et al. [53] was adopted. However for this research, the initial yield stress " $\tau_{0,0}$ " at $t = 0 \text{ sec}$ was neglected because it has an insignificant magnitude relative to that developed when the mix is at rest. In fact, the total yield stress was presented in a simplified form following Eq. 2.

$$\tau_{0(t)} = A_{\text{thix}} t \text{ [53] (Eq. 4)}$$

2.2- Specimens preparation for the submersion in sulfuric acid solutions

2.2.1- Mixing procedure

A uniform mixing procedure was adopted for the production of all samples from different mixes. It was always done at room temperature ($\approx 23^\circ\text{C}$) to minimize the difference between batches. A DITO-SAMA 80 liters BMXE80 mixer was used. First, all solid ingredients were dry mixed for about 2 min at a low speed (20 RPM). Then after, water and HRWR were added gradually. After adding all liquids, the mixing speed was progressively increased to 100 RPM. The overall mixing

process took around 10 min. During the mixing time, the walls of the mixer's bowl were scrapped using a large spatula to ensure that all materials were properly mixed. After finishing, the material was collected and directly placed inside the printer's pump.

2.2.2-Samples manufacturing

Two different sample categories were made for each mix composition. The first category included casted samples, taken as references. The second category included printed samples. First, the reference samples were casted inside 4×4×16 cm molds, in a single pour, without external vibration. This is to simulate the bulk material of each printed layer which can never be vibrated. Second, printed samples were done using an automated 3-axis gantry printer having a circular nozzle of 1.9 cm diameter (Fig. 1). Hence, the difference in the production of reference samples is the absence of multiple layers and pumping pressure.

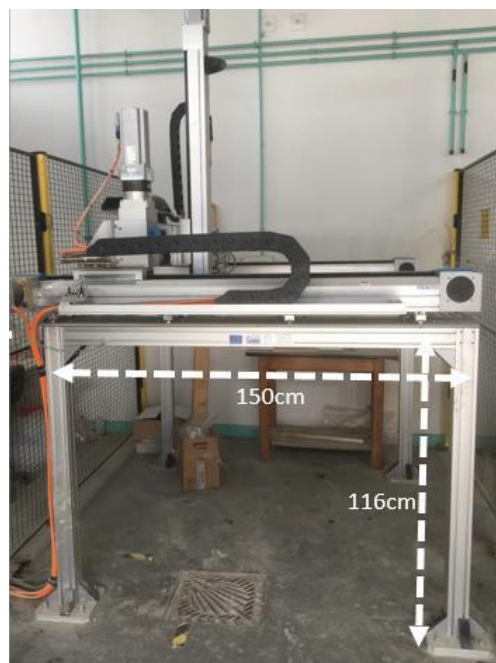


Figure 1: 3-axis gantry printer

The standoff distance of the nozzle was fixed to 1 cm, in order to obtain a 1 cm thick layers. Moreover, the printing speed was set to 6.4 cm/sec, and it was adjusted in a way to print a layer having a width ranging between 5 and 5.5 cm. Fig. 2 shows a printed sample of each mix. All samples made out of the same mix have the same number of superposed layers. It must be mentioned that, the layers were printed successively with a time gap of 15 sec, corresponding to the applied printing speed (No additional time gap has been intentionally added). After finishing,

the samples were directly cut down (when the material is still in its fresh state). All samples were left to cure in ambient conditions during the first 24 h.



Figure 2: Printed sample of each mix

After 24 h, non-printed samples were de-molded and kept at 100% RH at a temperature $\approx 20 \pm 2^\circ$ C for 38 days. Then after, all printed and non-printed samples were cut down properly to make $4 \times 4 \times 2$ cm specimens (Fig. 3). At the end, all samples were placed inside the oven for 6 days at 50 C to cease the hydration process.

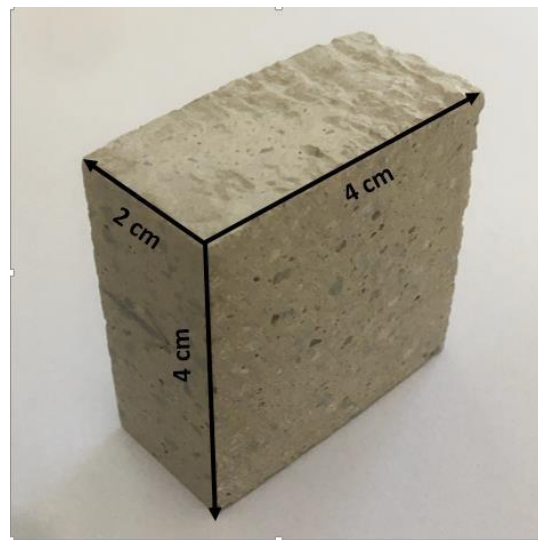


Figure 3: Testing sample

It should be noted here that printed samples were initially cut down, and only the core samples were subjected to acidic environment, to qualify exclusively the interface properties resulting from the layers superposition. In other words, this is done to eliminate first the vulnerable interfaces between consecutive layers generating concentration ports for acid ingress. Second, to guarantee that micro-cracks no longer exist at the surfaces. This issue must be taken seriously, because in 3D

printing, concrete elements are more susceptible to micro-cracks caused by the plastic shrinkage and temperature strains, due to the absence of formworks.

2.3- Sulfuric acid exposure

The Sulfuric acid (H_2SO_4) used has an initial concentration of 98%. Two samples of each production method and mix design were submerged in a bath of 1% and 3% sulfuric acid solution separately (the choice of these concentrations was based on the literature [45][54]). The volume of the solution was equal to four times the volume of submerged solid, as suggested by the standard test method for mortars exposed to sulfate attack (ASTM C1012/C1012M – 18b) [55]. The specimens were laid on plastic supports, inside hermetic plastic containers to prevent any evaporation (Fig. 4). The storage temperature was maintained at $22 \pm 2^\circ C$, and the solution was renewed at 3, 7, 14, 21, 28, and 42 days.



Figure 4: Specimens of the same mix placed inside a plastic container

2.4- Macroscopic characterization

All samples were gently cleaned using a brush and dried using paper towels before each solution renewal. This process was done to remove poorly adhered corroded material. Then after, a visual assessment of the corroded samples caused by the damage progression on the concrete elements surfaces was carried out, and the mass loss of each sample was recorded, during each solution renewal.

2.5- Microscopic characterization

2.5.1- Mercury Intrusion Porosimetry (MIP)

The description of the pore structure and their distribution play an important role when studying the durability of cementitious materials. In general, these pores are classified into macro-pores, capillary pores, and gel pores. However, there is no common agreement on the ranges describing the boundaries of each pore size [56]. In addition, until now there is no test or method that could measure the entire pore structure at once [41]. However, in this study it was decided to measure the pore size distribution using the Mercury Intrusion Porosimetry (MIP) for all non-degraded samples.

To study the porosity of all samples, printed and non-printed specimens having the dimensions of 1×1×1 cm were obtained from the core of the original ones. It should be mentioned that for the printed samples, the specimens were carefully taken in a way to insure the presence of an inter-layer inside of it. The masses of the tested samples ranged between 2.5 g and 3 g.

2.5.2- Scanning Electron Microscopy (SEM)

The Scanning Electron Microscopy (SEM) was used to characterize and visualize the inside of the degraded and non-degraded samples, and to explore the microstructural characteristics of all specimens. Herein, only degraded samples that were submerged in a solution of 1% acidic concentration were analyzed, because those who were attacked by a solution containing 3% acid were severely deteriorated.

The tested samples were cut off from the original ones. The size of each sample to be visualized was equal to 1.5×1.5 cm×“thickness of the sample” (the thickness of non-degraded samples is equal to 2 cm, whereas the thickness of degraded samples ranges between 1.7 cm and 1.9 cm depending on the degree of corrosion). Then after, these samples were impregnated with a low viscosity epoxy resin under vacuum, and cured for 24 h until the resin is fully hardened. Afterwards, the impregnated specimens were polished and coated with a carbon coating.

Fig. 5(a) shows the tested specimen extracted out of the original sample, and Fig. 5(b) shows a front view of one cut side, as well as the observation directions. All observations were conducted over the cut surfaces to visualize the inside of the element and not the degraded surfaces. For the non-printed samples (whether degraded or not), a random cut side was observed by the SEM since

there is no layers to be perceived. However in this study, special care was taken to visualize the internal structure of the printed samples in order to locate the inter-layer, if any is still existing after the complete setting and hardening of the material. For the non-degraded printed samples, the layers direction was known, and the SEM observation was carried over the correct cut side. Though, because of the complete surface deterioration of the degraded printed samples subject to sulfuric acid attack, all signs indicating the layers direction were ruined. Therefore, horizontal and vertical observations were done over both cut sides of the same sample.

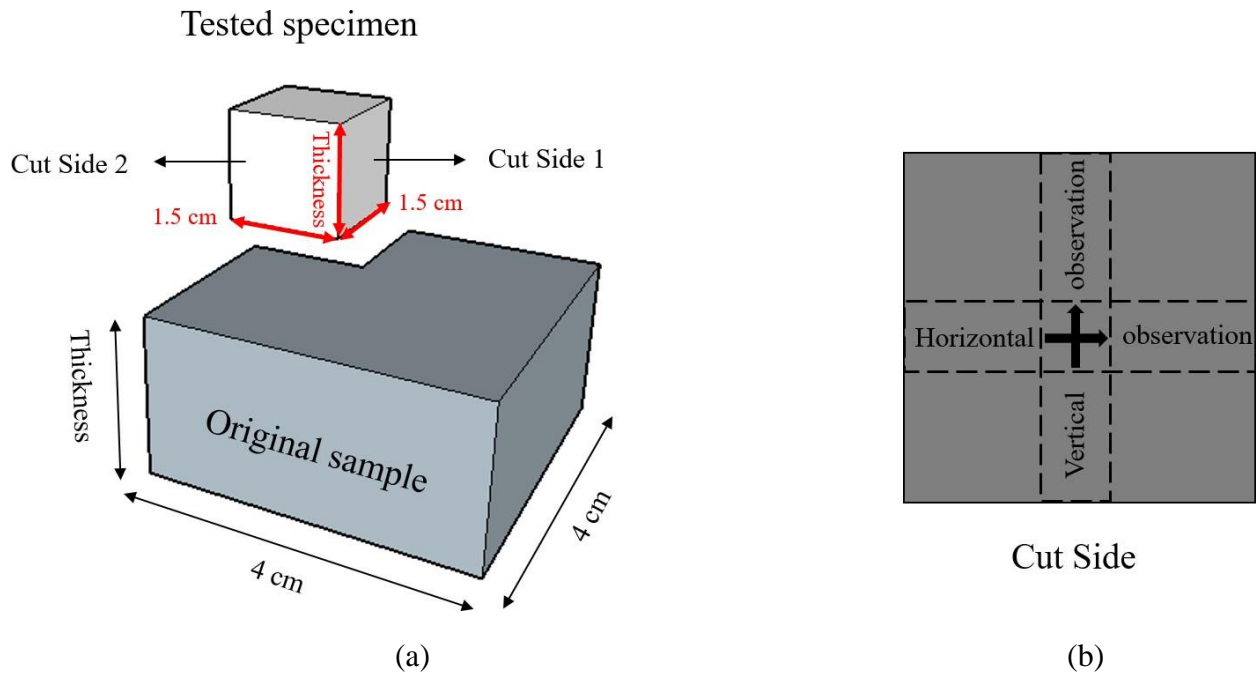


Figure 5: Schematic illustration of SEM samples

3- Results and discussion

3.1- Mechanical performance of mortars

Mix A, Mix B, and Mix C gave a compressive strength equal to 48 MPa, 57 MPa, and 73 MPa respectively. Herein, the resistance attained by Mix C was the highest among other mixes, because it has the lowest water to cement ratio. However, it was anticipated that Mix A yields a higher strength than Mix B because it has a lower limestone filler content. This is further detailed by Baz et al. [49].

3.2- Fall-cone and thixotropy results

Fig. 6, Fig. 7 and Fig. 8 show the yield stress evolution in function of time for Mix A, Mix B, and Mix C with their standard deviations respectively. These results pointed out that for all mixes the yield stress is almost linear during the first 1320 sec. For that given period, Roussel’s model predicted a reasonable structural build-up rate of the material, and this was further confirmed by the corresponding correlation factors (R^2) for each mix. Though, the equivalent thixotropic index “ A_{thix} ” describing the slope of the curves was equal to 2.85, 5.17, and 17.23 for Mix A, Mix B, and Mix C respectively. Hence, these mixes representing different A_{thix} values cover a wide range of materials having various rheological properties used for 3D printing applications. Therefore, the findings of this research could be applied over a broader range of printable material.

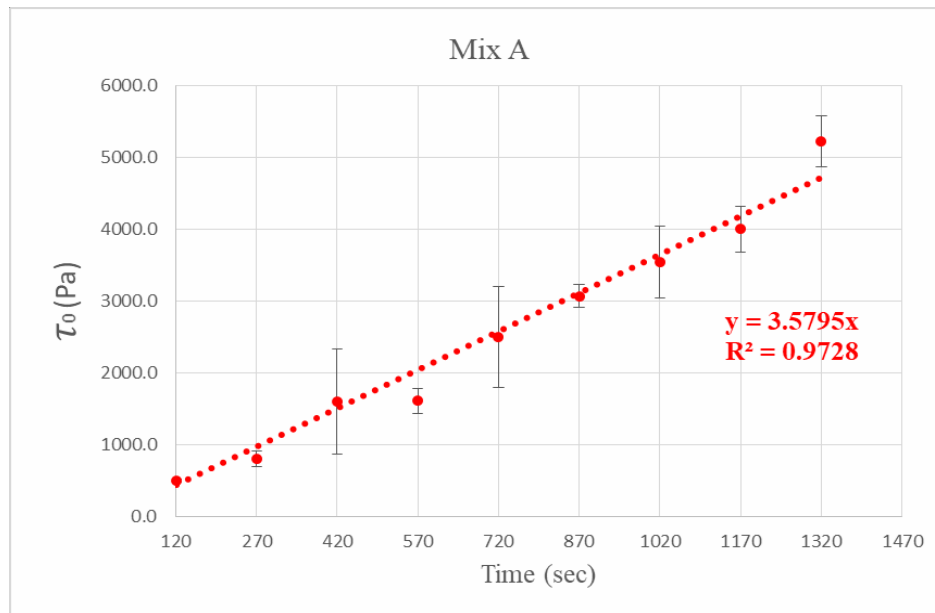


Figure 6: Yield stress variation in function of time for Mix A

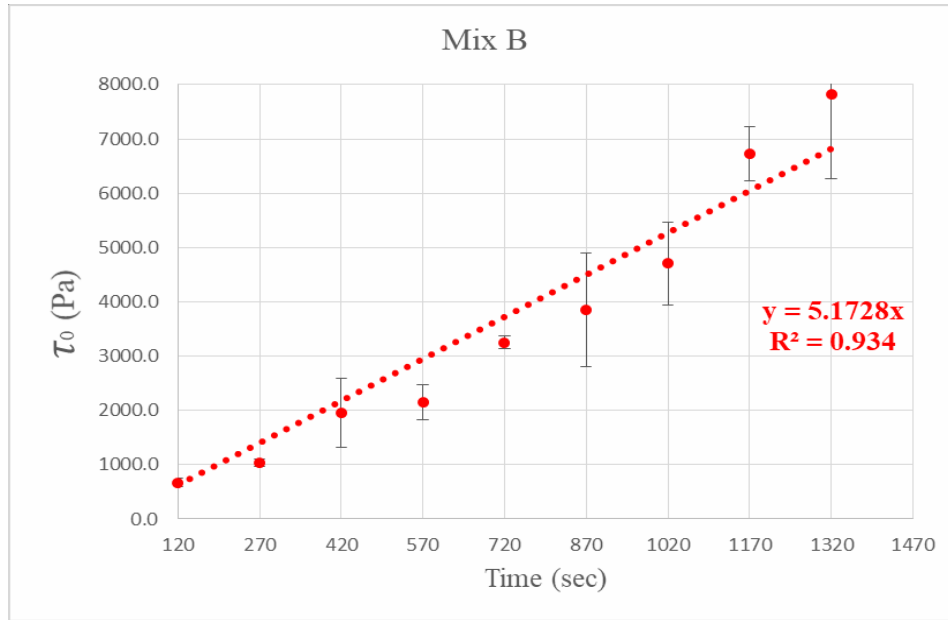


Figure 7: Yield stress variation in function of time for Mix B

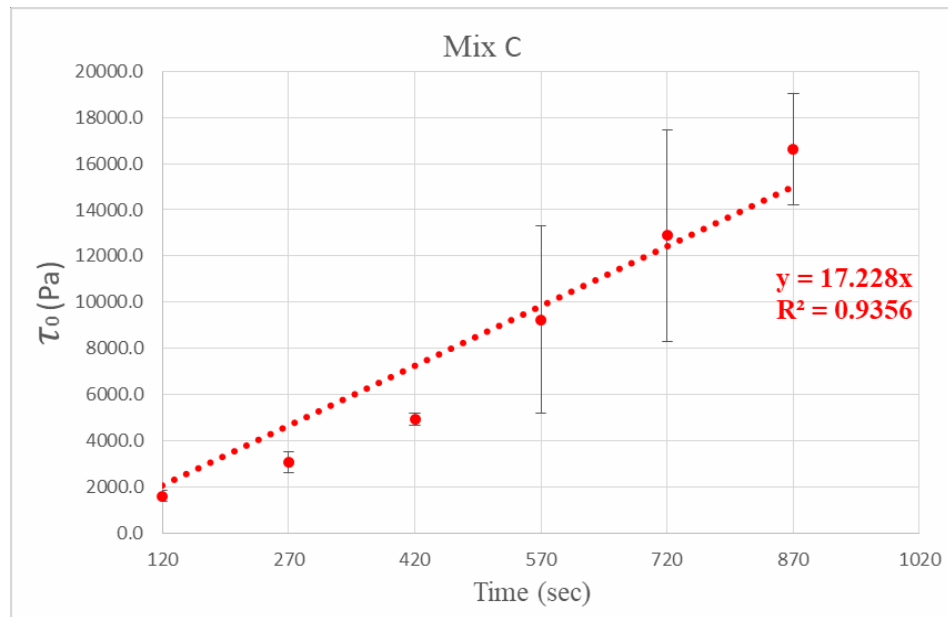


Figure 8: Yield stress variation in function of time for Mix C

3.3- Macroscopic analysis and results

3.3.1- Shape deterioration and visual assessment

Fig. 9 and Fig. 10 visually show the progression of damage on the surface of concrete samples exposed to a 3% and 1% acidic solution at different ages respectively. It can be clearly seen that after 3 days of continuous immersion, printed and non-printed concrete samples from all mixes started to show a mild corrosion, characterized by a slight spoiling of the cement paste. However,

as the immersion period increases, the material's loss became greater and more significant, especially with the higher concentration of sulfuric acid in the solution. Thus, after 56 days of immersion the samples presented a very porous surface structures, in addition to a more significant corrosion and spoiling of the paste leading to an irregular shape and smaller size of the specimens. Over and above, it can be noticed that the printed and non-printed samples of all mixes were in general equally deteriorated for each submersion condition. Herein, the printed and non-printed samples showed a thinner section with much more exposed aggregates when compared to shorter immersion periods. Though, it must be mentioned that for the case of all printed samples of all mixes, no inter-layer was observed and no cracks appeared at that level.

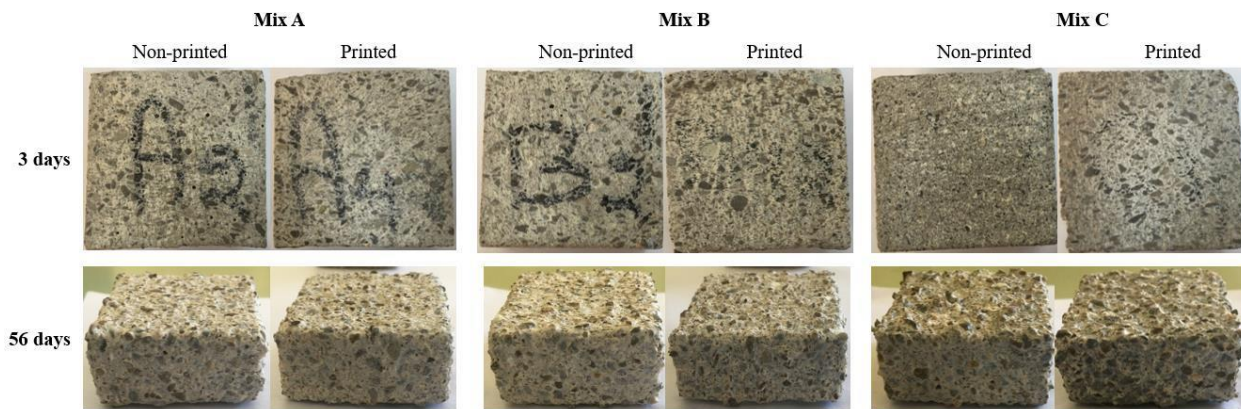


Figure 9: Progressive damage of printed and non-printed samples in 1% acidic solution

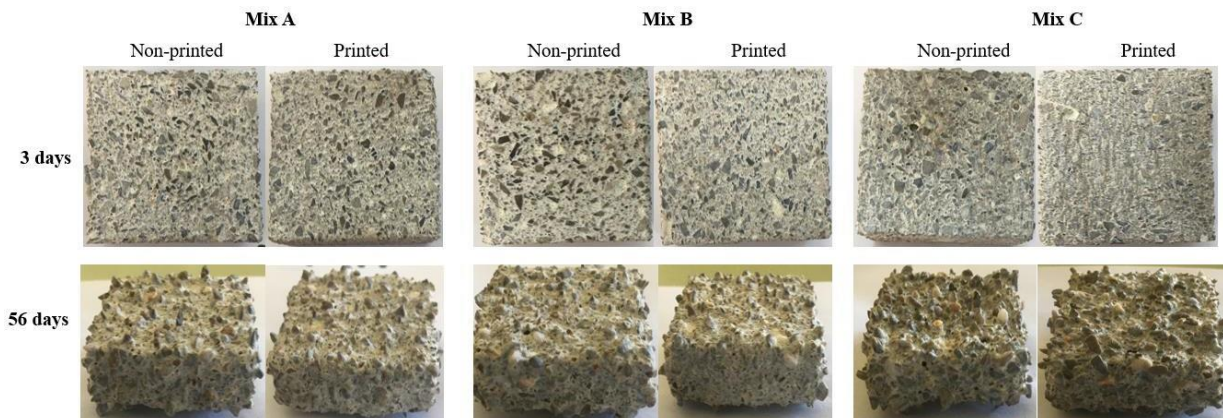


Figure 10: Progressive damage of printed and non-printed samples in 3% acidic solution

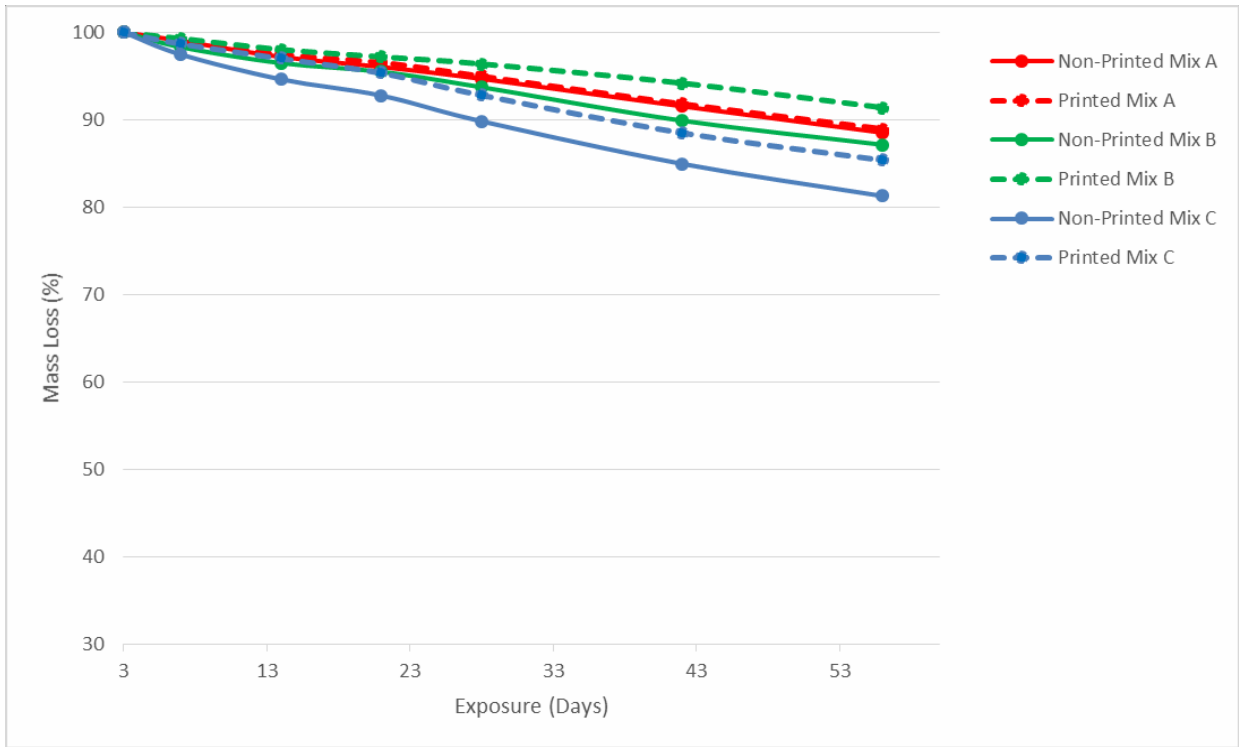
3.3.2- Mass Loss

Fig. 11 (a) and Fig. 11 (b) show the change in mass relative to the initial weight of the specimens measured after 3 days of immersion for all samples when subjected to 1% and 3% acidic solutions

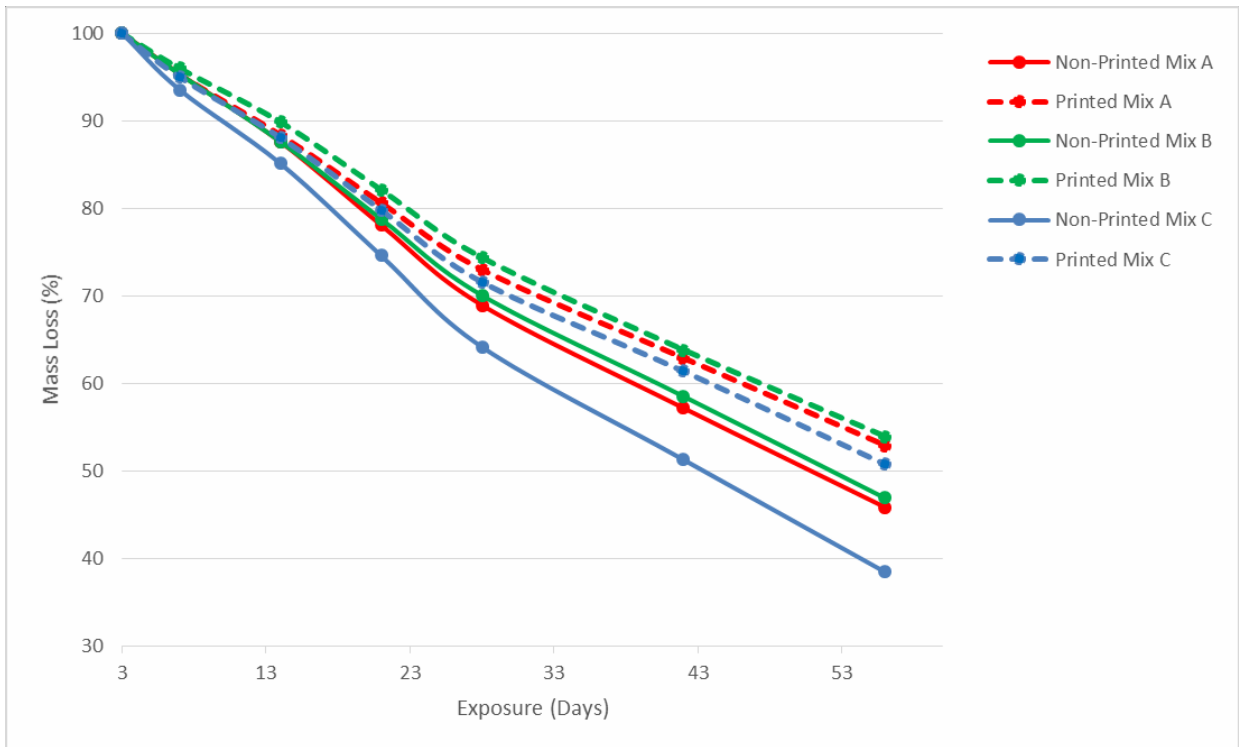
respectively. A continuous decrease of mass in all samples in different conditions is always observed for all mixes. However, the mass loss of the samples submerged in sulfuric acid having a concentration of 1% was much lower than the samples put in a solution having a concentration of 3%. Yet, the rate of decrease in non-printed samples was systematically higher than that of the printed ones.

In particular, Mix C showed the highest mass loss among other mixes. Though, it is not a matter of higher A_{thix} value, instead, it is majorly related to the water to cement ratio. Thus, as a matter of fact, this variance was not obvious between Mix A and Mix B because they both have the same water content, but only different limestone filler content. Particularly, previous studies found that a decrease in the water to cement ratio results in an increase of mass loss [43]. This happens even if a mix having a lower water to cement ratio is relatively denser and has fewer pores. However, knowing that a denser structure better prevents the absorption of sulfuric acid toward the inside of the sample, but still it presents an abundant amount of hydrates. Thus, as time progress the acid reacts with the cement paste over a larger concrete surface causing much more significant deterioration [43].

As for the current study, it can be said that 3D printed elements were strong enough to resist further deterioration and mass loss. Hence, this gives an indication that the inter-layers did not allow the solution to further penetrate inside the element, and therefore to react and ruin a larger surface of the specimen.



(a)



(b)

Figure 11: Mass loss of printed and non-printed concrete samples exposed to a solution containing (a) 1% and (b) 3% sulfuric acid

3.4- Microscopic analysis and results

3.4.1- Mercury Intrusion Porosimetry results

Table 3 shows the total porosity for all mixes and conditions. The total porosities of printed and non-printed samples, for all mixes were comparable. The non-printed samples made of Mix A, Mix B, and Mix C, had a porosity equal to 13.58%, 13.74%, and 11.23% respectively. Alongside, the total porosity of the printed samples of, Mix A was equal to 13.11%, Mix B equal to 12.89%, and Mix C equal to 11.67%. However, the distribution of pores differed largely between printed and non-printed specimens, as can be observed in Fig. 12-14. Figures 12(a), 13(a), 14(a) show the cumulative pores volume between 1 μm and 0.01 μm , whereas Figures 12(b), 13(b), 14(b) show the total amount of pores between 1 μm and 0.1 μm , and less than 0.1 μm independently.

Table 3: Total Porosity

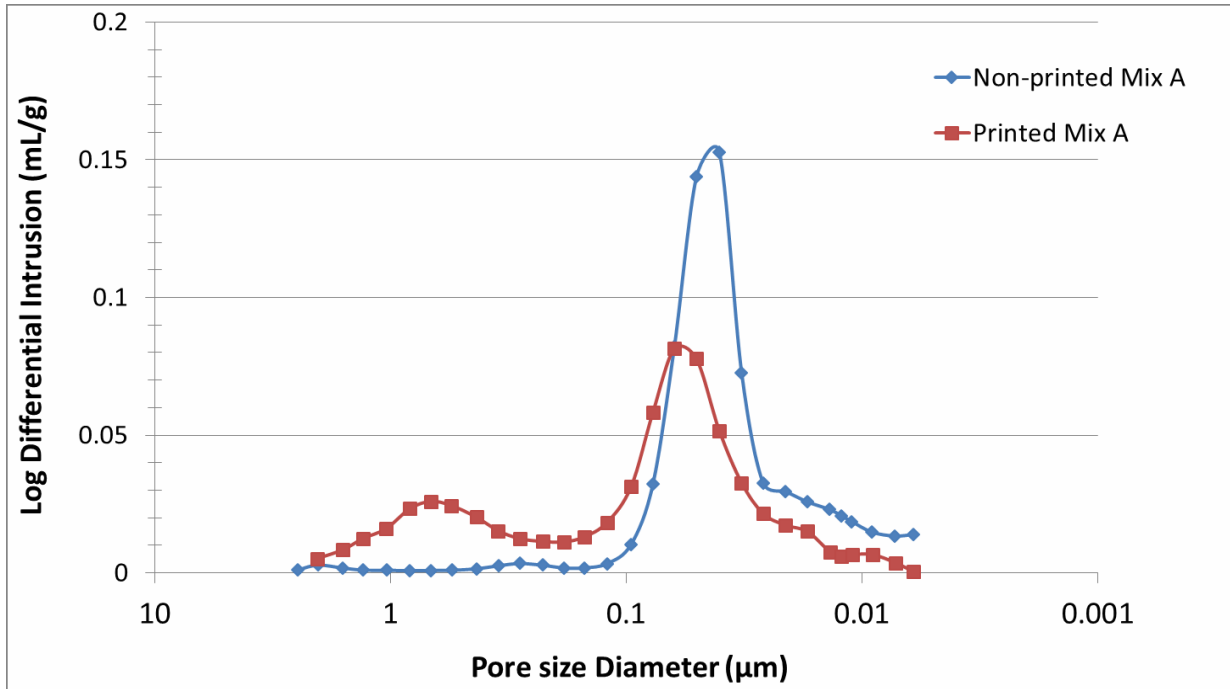
	Mix A		Mix B		Mix C	
	Non-printed	Printed	Non-printed	Printed	Non-printed	Printed
Total Porosity (%)	13.58	13.11	13.74	12.89	11.23	11.67

Despite the variance in the pore size distribution found among mixes between non-printed and printed samples, the target of this particular study is to provide a comparison between both types of samples within each mix individually. Hence, when comparing the results of the non-printed specimens to those of the printed ones in all mixes, it can be clearly seen that the non-printed samples show a much higher concentration of pores having diameters less than 0.1 μm . On the other hand, the results of printed samples of all mixes indicated the presence of a larger concentration of pores ranging between 1 μm and 0.1 μm , which are negligible in the non-printed ones.

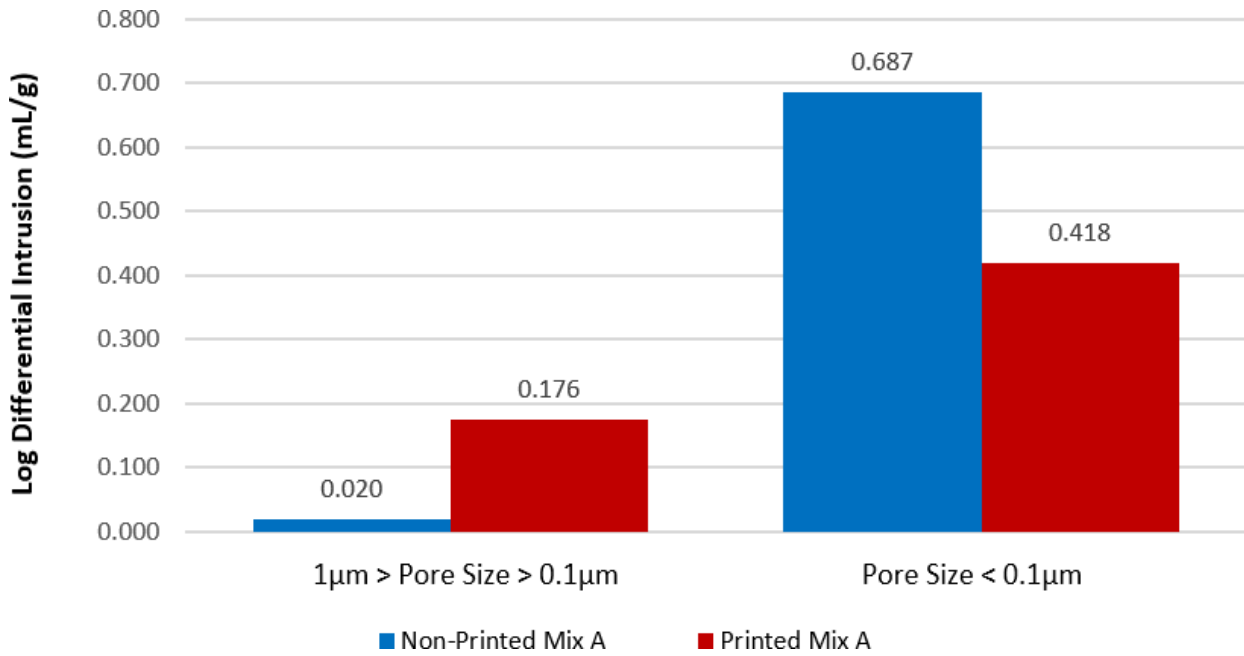
Based on the results of the MIP analysis, exposing the differences in the pore size distribution between printed or non-printed samples while having almost the same total porosity; this difference can be attributed to the external pressure exerted over the material when being printed [57]. As previously mentioned in section 2.2.2, non-printed samples were not vibrated on purpose, to get closer as much as possible of the material's internal structure inside of each printed layer that is not subject to any type of vibration. Thus, the only difference between the two production methods is the pumping pressure put over the deposited layers. Yet, the extruded material is subject

to high shearing stresses, causing a deflocculation of the material's internal structure, leading to a better rearrangement of the small particles including cement grains. Hence, this fact decreases the concentration of pores having a diameter smaller than 0.1 μm .

Few studies concerning the durability aspects and the effect of the pore size distribution were found in the literature, still no one provided a comparison between the different production methods (printed and non-printed). Schrofl et al. [58] discussed the increasing capillary water intake with respect to the increasing time gap between layers deposition. They found that a time gap up to 13 min was short enough to avoid preferential capillary suction at the inter-layer level. However, a time gap of 24 h would certainly give rise to quick capillary suction through the interfaces because of the formation of more accessible pores. Similarly, Van der Putten et al. [59] found that no additional porosity is induced while not having additional time gap between layers deposition. However, a much denser matrix is formed due to the low porosity found in samples with no time gap, which in its turn is caused by the material's compaction performed by the layer being printed over the one underneath. Bran-Anleu et al. [60] investigated the chloride penetration in 3D printed specimens for different interval times, and found that the penetration rate is significantly higher for longer time gaps due to the formation of additional voids between superposed layers. Hence, these previous findings support the results of this research.

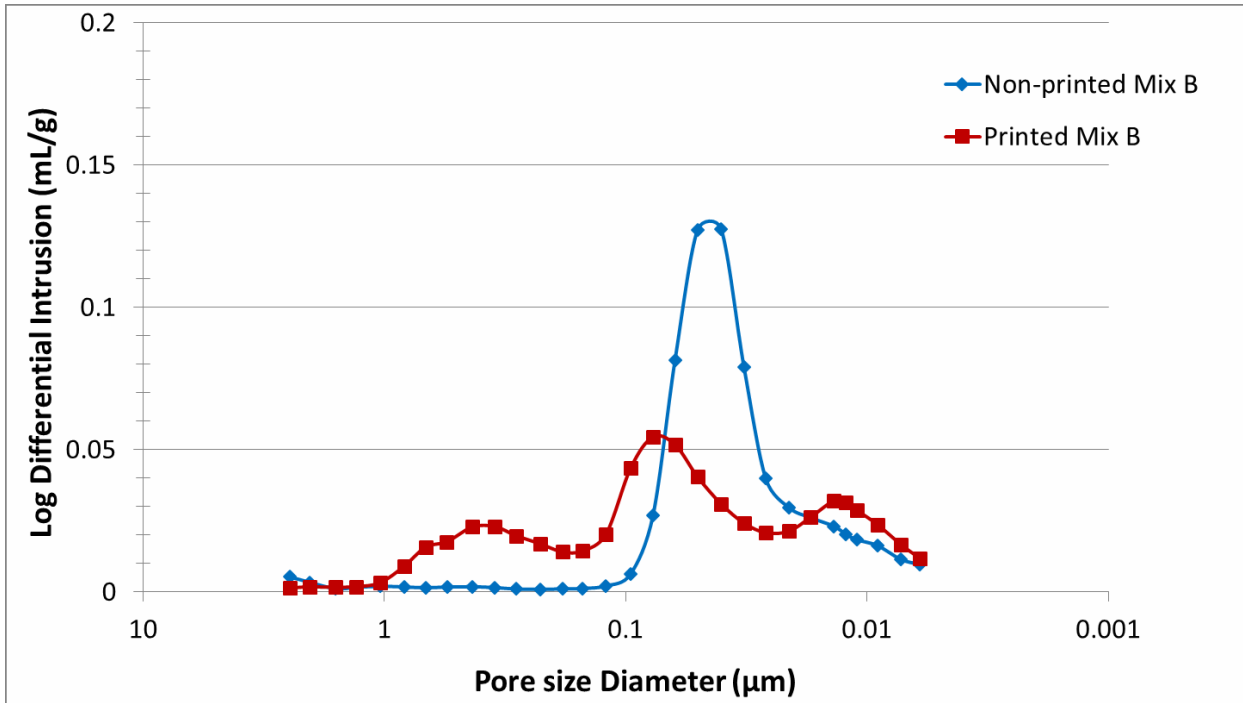


(a)

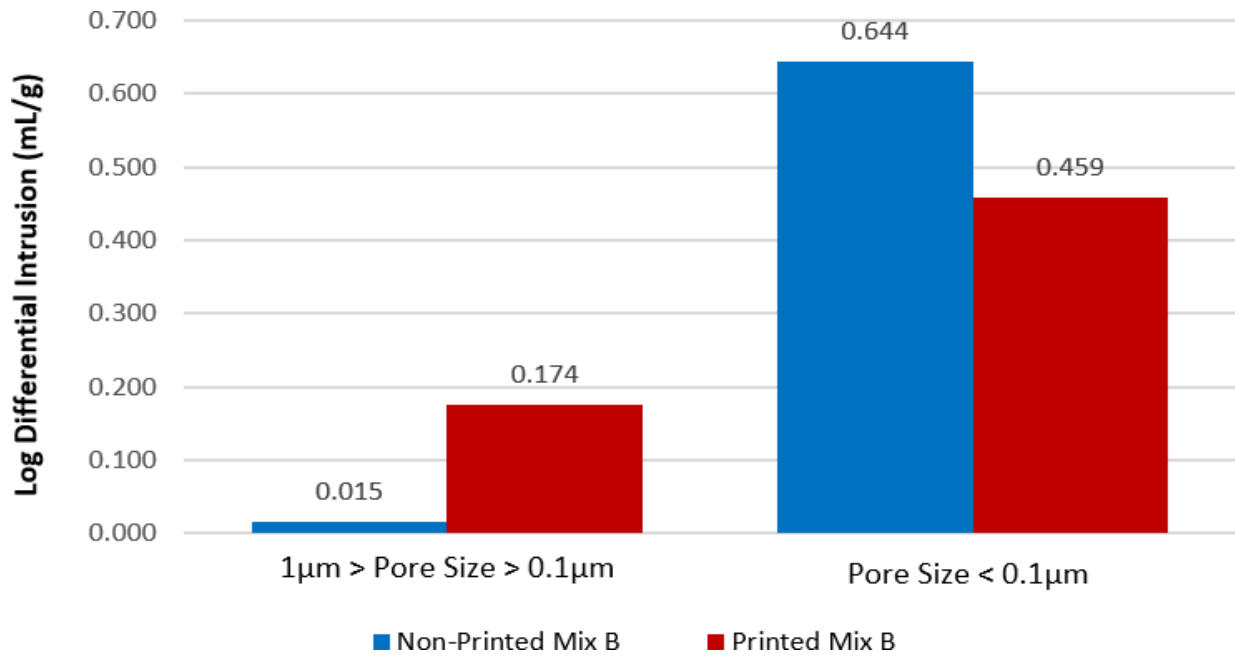


(b)

Figure 12: Pore size distribution of printed and non-printed elements *Mix A*

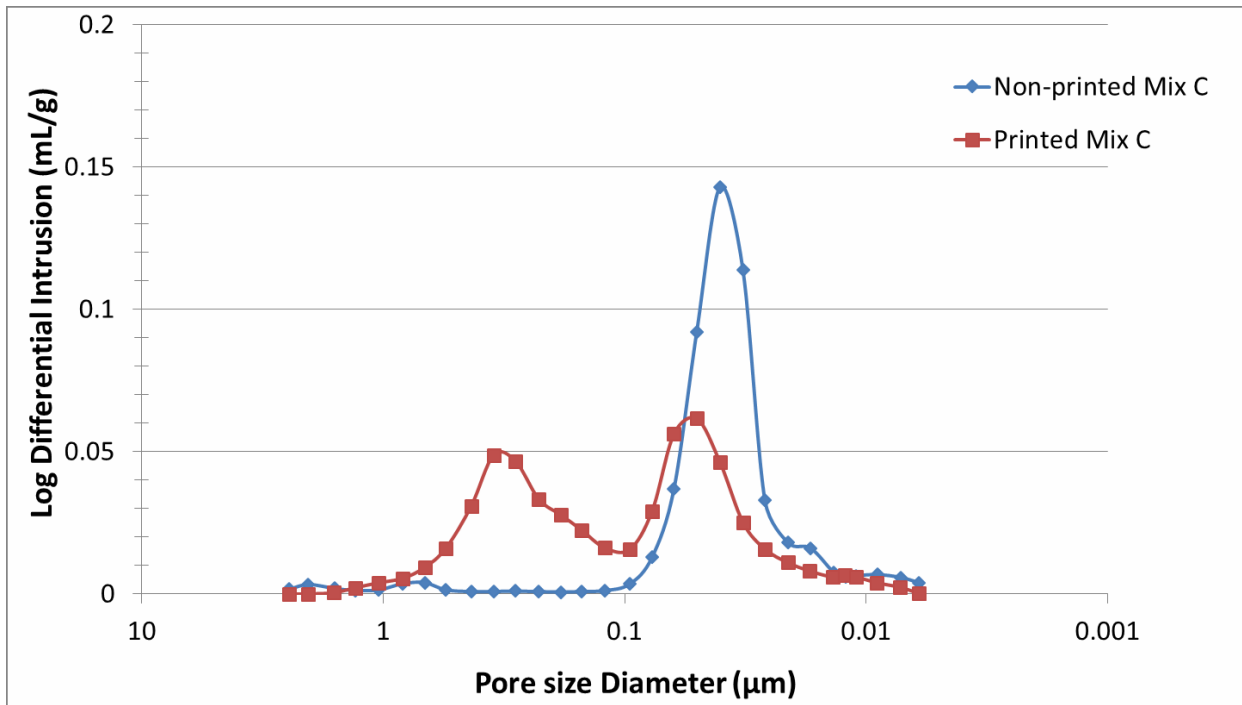


(a)

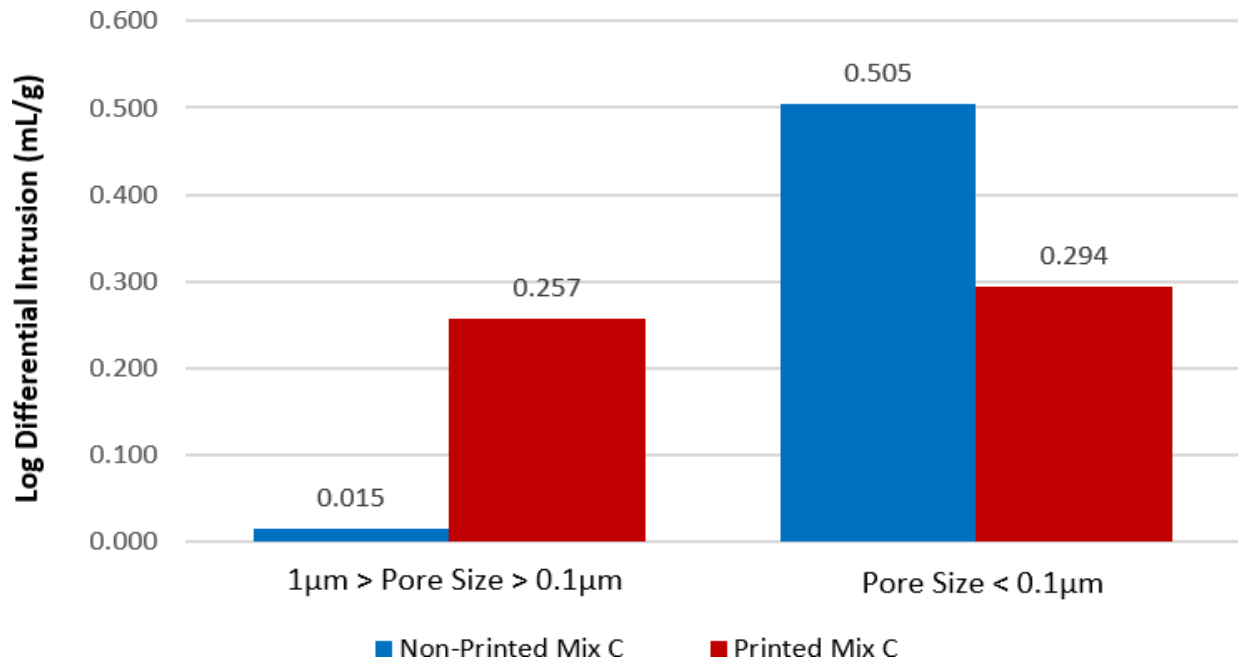


(b)

Figure 13: Pore size distribution of printed and non-printed elements *Mix B*



(a)



(b)

Figure 14: Pore size distribution of printed and non-printed elements *Mix C*

3.4.2- Scanning Electron Microscopy results

Based on the external appearance and shape of the printed elements shown in Fig. 2, it was decided to start by visualizing the specimens of Mix A. The printed layers are much more exposed than those of Mix B and Mix C. Therefore, it was presumed that if any inter-layer is to be identified, it has to be more visible in Mix A rather than other mixes.

Herein it should be noted that all presented figures are a collection of 38 independent SEM pictures that were organized and rearranged altogether to render a full image of the cut surface under display.

Fig. 15 shows the microstructure of a non-degraded and non-printed sample using Mix A, whereas Fig. 16 shows the microstructure of a non-degraded printed sample, at the cut side where the inter-layer must be located. It can be seen from Fig. 16 the presence of spherical pores of different volumes. This indicates that the larger pores are entrapped air bubbles, only caused by the production method, which did not use any vibration in this case. On the other hand, the majority of the pores in a printed sample (Fig. 16) have an irregular and deformed shape, unlike those found in the non-printed sample (Fig. 15). In fact, the void deformations in printed samples are caused by the external pressure applied on the material when being extruded. Besides, it can be also seen that the concentration of medium pores ($1\mu\text{m} > \text{Pore size} > 0.1\mu\text{m}$) is higher than in the non-printed sample, and this is previously confirmed by the MIP results in section 3.4.1.

Above all, if we take a deeper look over Fig. 16, no inter-layers can be identified. The pores do not present a continuous pattern over the cut surface, neither in the horizontal nor the vertical directions. As well, no crack lines were recognized that can provide any information about a weak plane. Even more, it is worth mentioning that the printing direction did not dictated a certain orientation of the sand grains. In addition, there cannot be seen any thin strip of continuous cement paste which could unveil the contact plane between the subsequent layer and the upper one. This fact gives an indication that the superposed layers merged well, and the sand grain crossed the inter-layers. Hence, this might be due to the kinetic energy of the suspended sand particles owing to the pumping pressure.

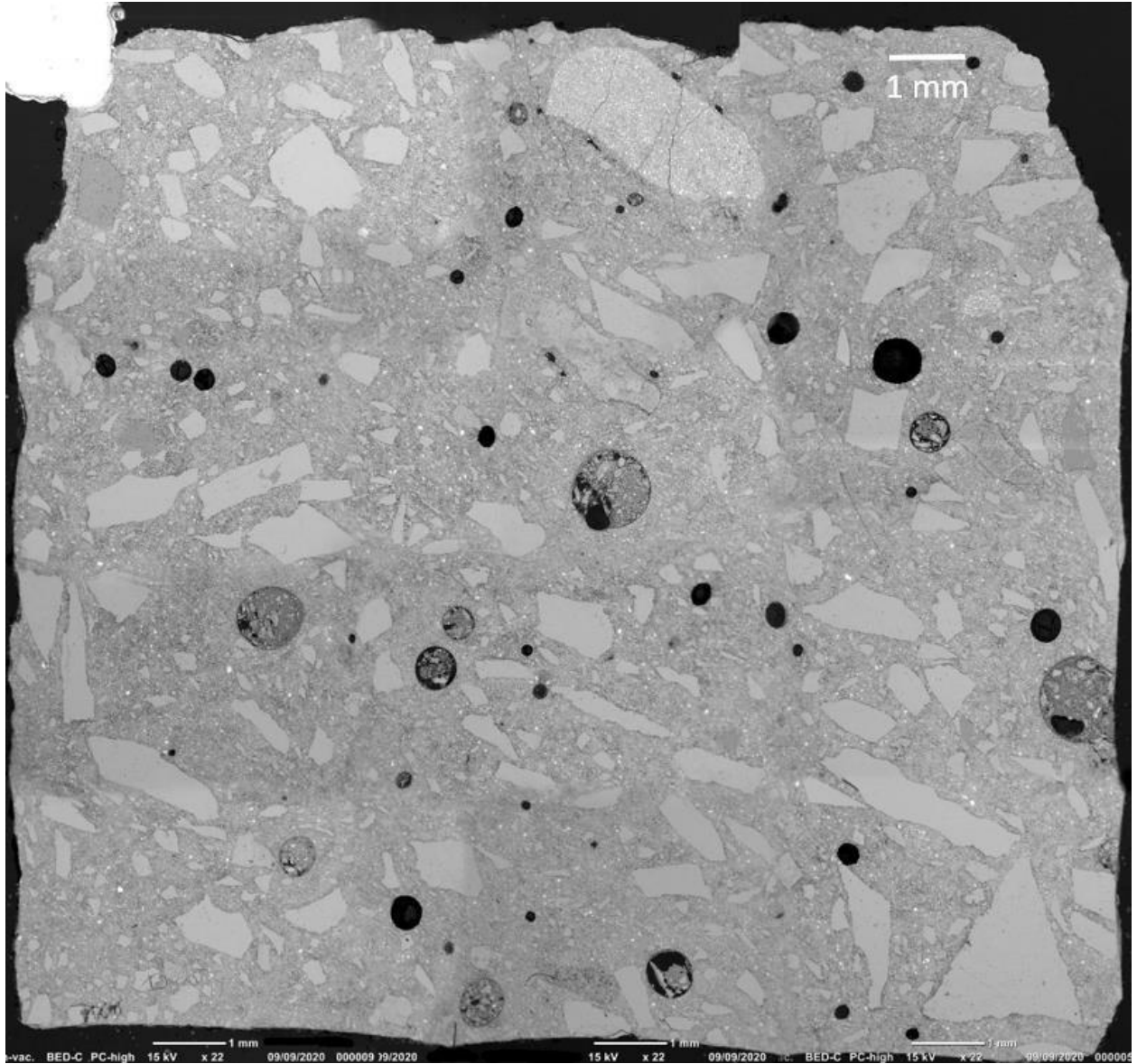
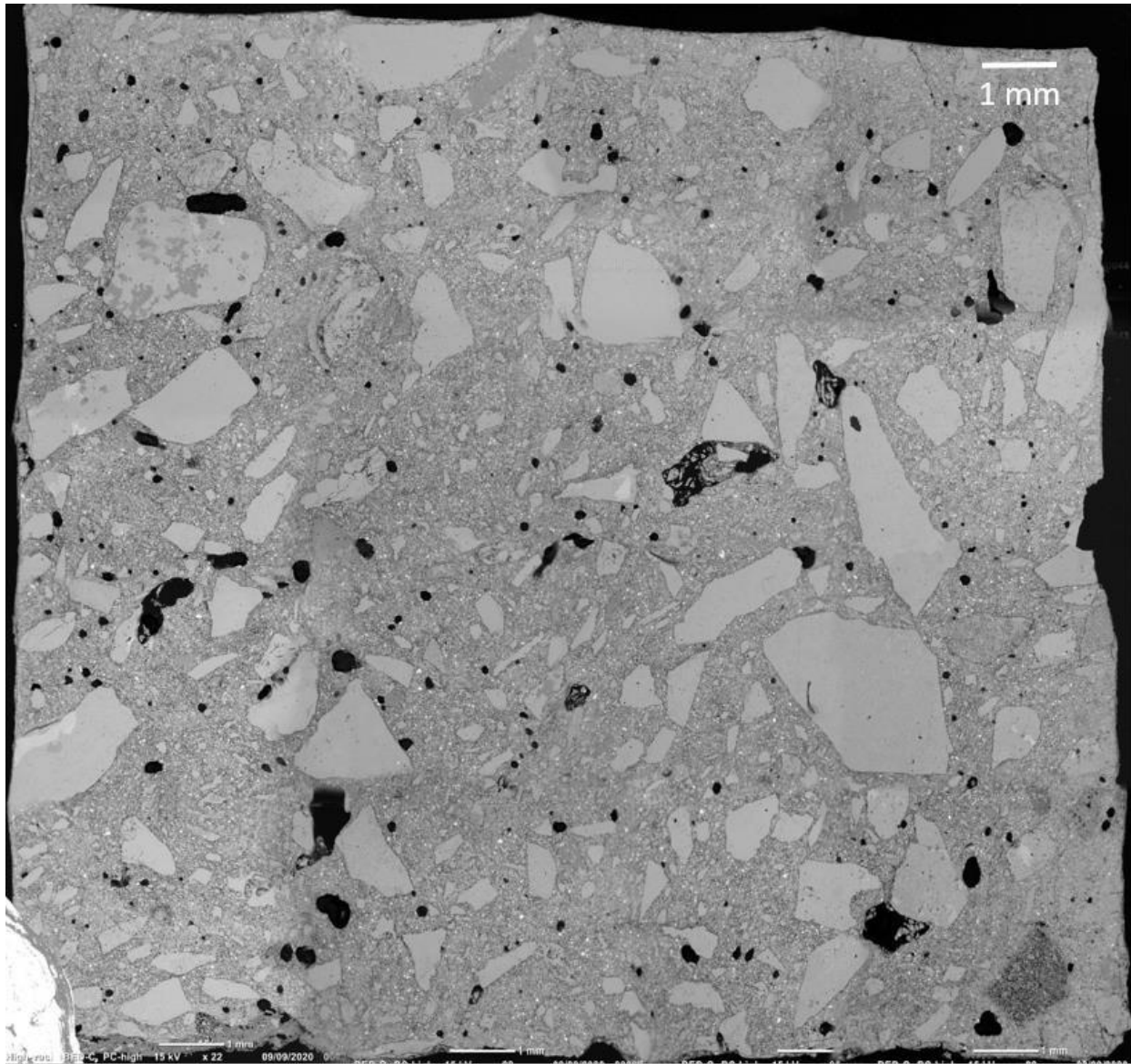


Figure 15: Microstructure of the non-degraded / non-printed sample *Mix A*



*Figure 16: Microstructure of the non-degraded / printed sample **Mix A***

Concerning the degraded samples, Fig. 17 shows the microstructure of the non-printed sample of Mix A after 56 days of acid exposure. The same interpretation reported on the non-degraded sample of Fig. 15 applies over the degraded one. Except that, in the case of degraded sample, the outer surface in contact with the solution has been damaged, as well as the smallest pores located near the surfaces in contact with the surrounding environment and reached by the acid solution ingress, were closed due to the precipitation of gypsum (small white dots) caused by the sulfate contained in the sulfuric acid (Fig. 18).

Fig. 19 and Fig. 20 show the microstructure of cut side 1 and cut side 2 respectively of the tested specimen extracted from the degraded printed element after 56 days of acid exposure (the two sides were observed for the reason previously explained in section 2.5.1). Still, even in a degraded printed sample, the inter-layers are not spotted neither at cut side 1, nor at cut side 2. This fact confirms that the inter-layer are not weak planes that create a preferential path for the solution's ingress into the concrete element. Herein, it can be said that the printed element acted like a monolithic body, and had a homogeneous microstructure.

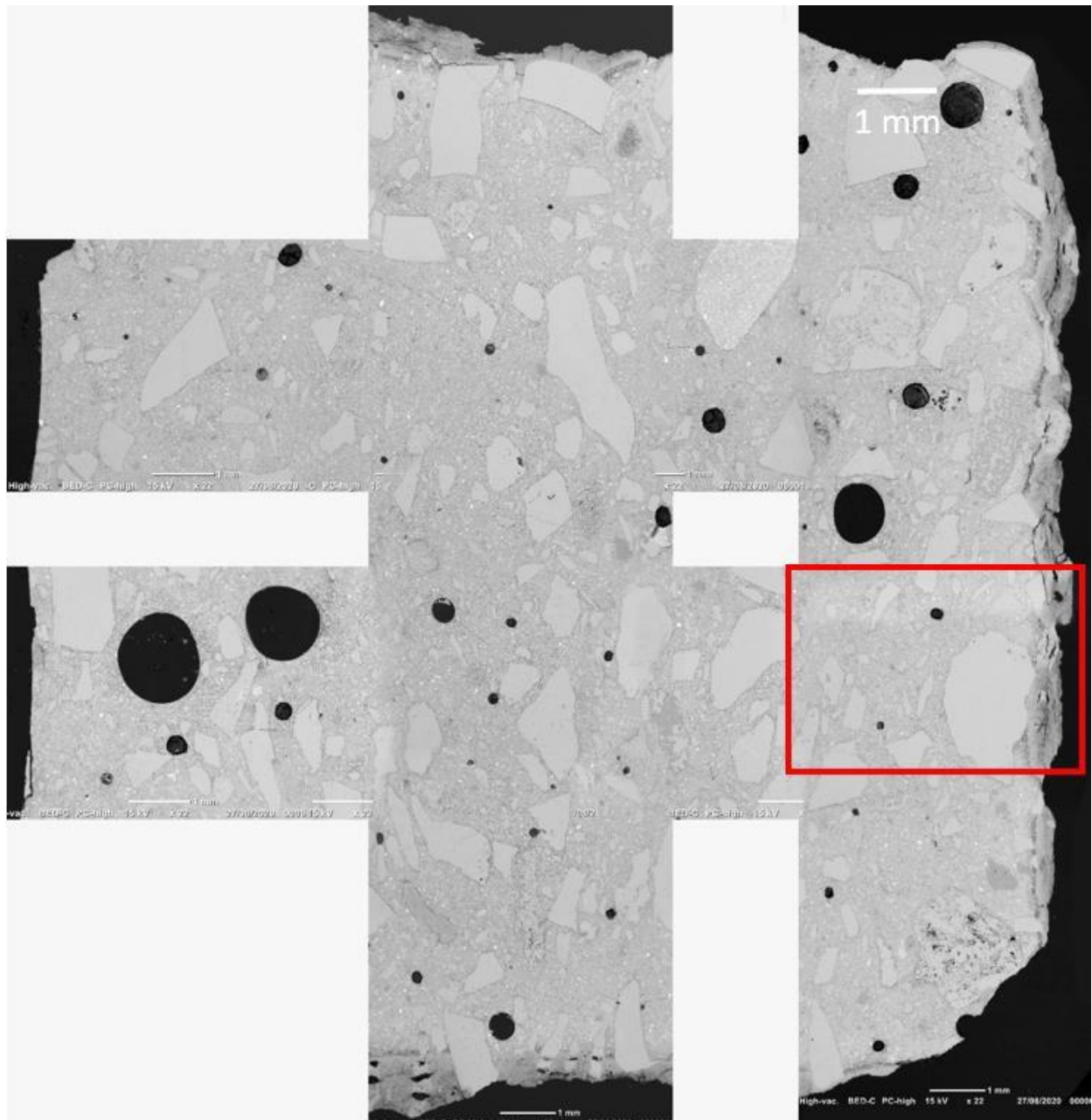
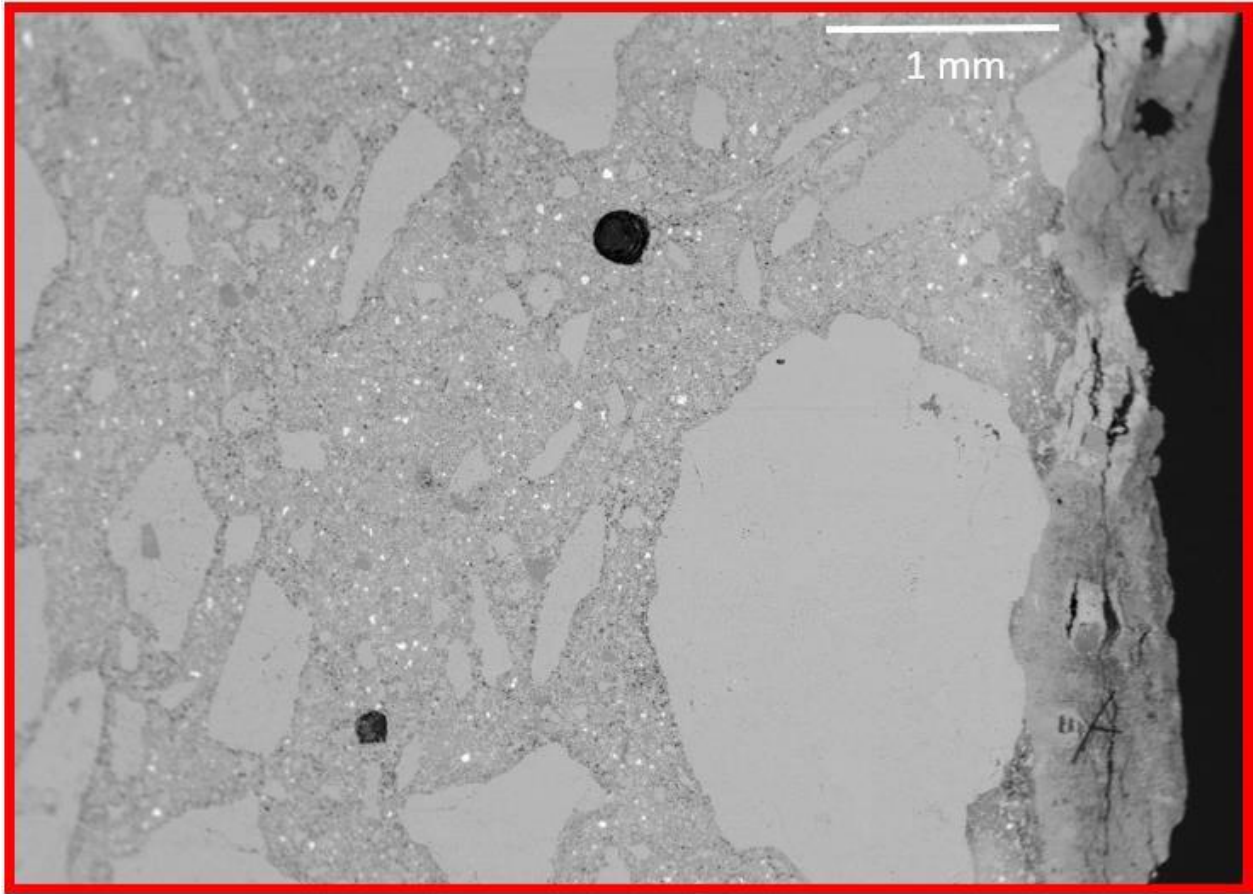


Figure 17: Microstructure of the degraded / non-printed sample after 56 days of exposure **Mix A**



*Figure 18: Closer view of the zone attained by the acid and the gypsum precipitation **Mix A***

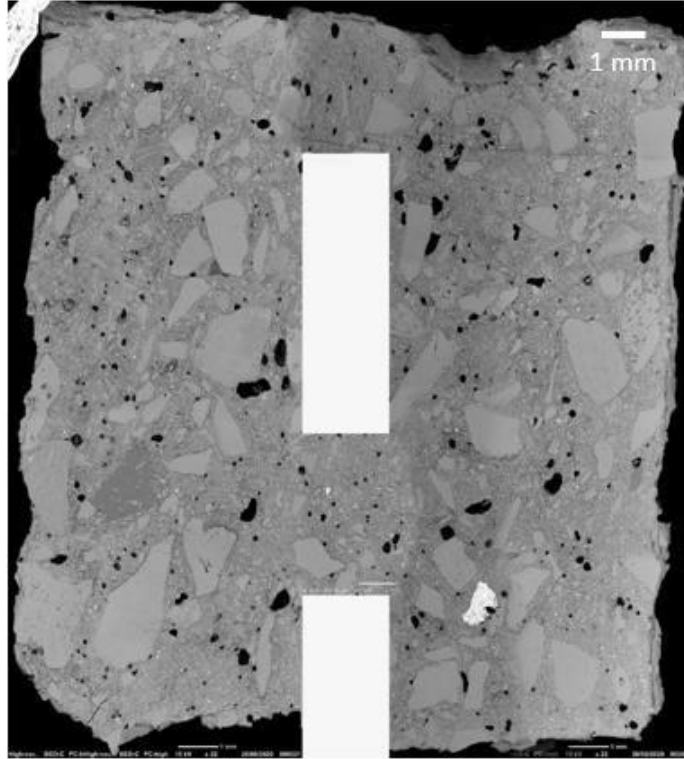


Figure 19: Microstructure of the degraded / printed sample Cut side 1 after 56 days of exposure **Mix A**

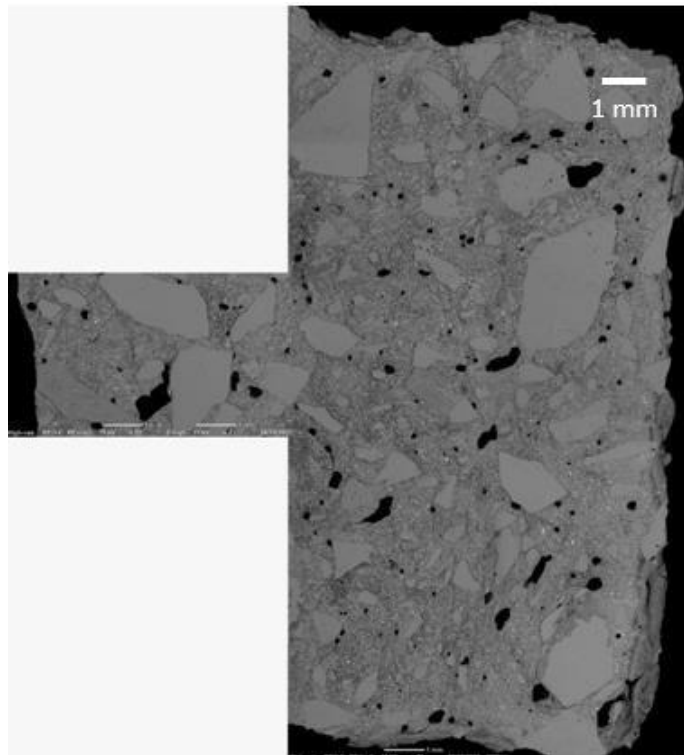


Figure 20: Microstructure of the degraded / printed sample Cut side 2 after 56 days of exposure **Mix A**

The findings of the SEM observations performed over all sample conditions (degraded / non-degraded, printed / non-printed) of Mix A were sufficient to figure out that no layers are going to appear in the rest mixes.

Overall, all these results including those of the MIP analysis confirmed the argument presented by De Koker [57] that in a printed concrete element, the concrete matrix could be denser than in a non-printed one, because of the external pressure exerted over the material when being extruded. Hence, this fact results in a stronger resistance against the degradation of the paste.

4- Conclusion and perspectives

This article presents an experimental research aiming to characterize the microstructural properties of 3D printed concrete elements in regard to non-printed ones. In particular, a durability assessment has been carried out over three printable mortar mixes having different thixotropic properties. Herein, these samples were subjected to two sulfuric acid solutions of 1% and 3% concentrations for 56 days continuously.

First, a rheological characterization of the mortars used was carried out using the fall-cone penetrometer. The measurements revealed that the mixes under investigation covered a wide range of materials with different thixotropic properties.

Second on a macroscopic scale, a visual assessment was carried out for all samples of both exposures. It was found that the printed and non-printed samples were equally deteriorated. However, those submerged in a 3% acid solution were much more degraded. Alongside, the mass loss of all samples caused by the acid attack was recorded. The rate of mass loss between printed and non-printed samples of all mixes was almost the same, but still, the non-printed ones degrades slightly faster in most cases. This happened because of the presence of a larger number of accessible pores (for the same total volume of porosity) exposing a larger surface of paste. Nevertheless, printed samples did not fail at the inter-layer level or showed any cracks over that plane.

Third on a microscopic scale, only the samples of all mixes that were submerged in a solution of 1% acid concentration were analyzed. This is done because the samples subject to 3% acid concentration were almost totally degraded. The porosity of all non-degraded samples, whether printed or not, were measured by the mercury intrusion porosimetry (MIP). The total porosity of

printed and non-printed samples of each mix separately was almost the same, however the pores size distribution varied a lot between printed and non-printed conditions. Generally, printed samples of all mixes presented a higher volume of pores having a diameter ranging between 1 μm and 0.1 μm . Despite that, non-printed samples showed the highest content of pores smaller than 0.1 μm . Besides, a scanning electron microscopy (SEM) visualization has been done over the degraded and non-degraded samples, in particular for Mix A that shows the highest level of surface roughness among all other mixes. The SEM images confirmed the previous findings, and it clarified the pores size distribution triggered by the MIP. In addition, despite of the material's thixotropic behavior, superposed layers are still able to merge together without showing any sign of layer stacking. Moreover, even when the printed samples were subjected to sulfuric acid attack, the inter-layers did not form weak planes for the solution ingress. Thus, the printed elements behaved as a monolithic body without showing any discontinuity in its internal structure that could threaten its durability.

Finally, it was perceived that the printing pressure applied over the material when being extruded has a fundamental effect of the material's internal structure. Hence it would be interesting to reconsider the same research context but by focusing on the effect of the printing parameters on the pore size distribution of a printed element, as well as their consequences on its durability against aggressive environments.

Acknowledgment:

The authors would like to acknowledge the financial support by Partenariats Hubert Curien (PHC) CEDRE program PROJET N° 42287YD, and the Supply of material from Carrières du Boulonnais, Eqiom, and Chryso.

- [1] M. Stefanoni, U. Angst, and B. Elsener, “Corrosion challenges and opportunities in digital fabrication of reinforced concrete,” 1st RILEM International Conference on Concrete and Digital Fabrication, Zurich, Switzerland., 2018.
- [2] P. Wu, J. Wang, and X. Wang, “A critical review of the use of 3-D printing in the construction industry,” *Automation in Construction*, vol. 68, pp. 21–31, 2016.
- [3] G. De Schutter, K. Lesage, V. Mechtcherine, V. N. Nerella, G. Habert, and I. Agustí-Juan, “Vision of 3D printing with concrete — Technical, economic and environmental potentials,” *Cement and Concrete Research*, vol. 112, pp. 25–36, 2018.
- [4] N. Labonnote, A. Rønquist, B. Manum, and P. Rütther, “Additive Construction: state of the art , challenges and opportunities,” *Automation in Construction*, vol. 72, no. 3, pp. 347–366, 2016.
- [5] J. Buchli, M. Gifftthaler, N. Kumar, M. Lussi, T. Sandy, K. Dör, and N. Hack, “Digital in situ fabrication - Challenges and opportunities for robotic in situ fabrication in architecture, construction, and beyond,” *Cement and Concrete Research*, vol. 112, pp. 66–75, 2018.
- [6] J. J. Biernacki, J. W. Bullard, G. Sant, K. Brown, F. P. Glasser, S. Jones, T. Ley, R. Livingston, L. Nicoleau, J. Olek, F. Sanchez, R. Shahsavari, P. E. Stutzman, K. Sobolev, and T. Prater, “Cements in the 21 st century: Challenges, perspectives, and opportunities,” *Journal of the American Ceramic Society*, vol. 100, no. 7, pp. 2746–2773, 2017.
- [7] T. Wangler, E. Lloret, L. Reiter, N. Hack, F. Gramazio, M. Kohler, B. Mathias, D. Benjamin, J. Buchli, R. Nicolas, R. Flatt, and A., “Digital Concrete : Opportunities and Challenges,” *RILEM Technical Letters*, vol. 1, pp. 67–75, 2016.
- [8] M. Sakin and Y. C. Kiroglu, “3D Printing of Buildings: Construction of the Sustainable Houses of the Future by BIM,” *Energy Procedia*, vol. 134, pp. 702–711, 2017.
- [9] B. Nematollahi, M. Xia, and J. Sanjayan, “Current Progress of 3D Concrete Printing Technologies,” *Proceedings of 34th International Symposium on Automation and Robotics in Construction*, pp. 260–267, 2017.
- [10] X. Zhang, I. Flood, Y. Zhang, H. I. Moud, and M. Hatami, “A Cost Model to Evaluate the Economic Performance of Contour Crafting,” *Computing in Civil Engineering 2019: Visualization, Information Modeling, and Simulation - Selected Papers from the ASCE International Conference on Computing in Civil Engineering 2019*, no. June, pp. 618–625, 2019.
- [11] J. H. Lim, B. Panda, and Q. Pham, “Improving flexural characteristics of 3D printed geopolymer composite with in-process steel cable reinforcement reinforcement,” *Construction and Building Materials*, vol. 178, pp. 32–41, 2018.

- [12] F. Bos, R. Wolfs, Z. Ahmed, and T. Salet, “Additive manufacturing of concrete in construction: potentials and challenges of 3D concrete printing,” *Virtual and Physical Prototyping*, vol. 11, no. 3, pp. 209–225, 2016.
- [13] S. Z. Jones, J. Vickers, T. Wangler, and P. Zavattieri, “Additive Manufacturing Processes for Infrastructure Construction : A Review,” vol. 141, no. September, pp. 1–13, 2019.
- [14] S. Bukkapatnam, J. Mander, S. Paal, Z. Pei, and L. Zeng, “Workshop Report—NSF Workshop on Additive Manufacturing (3D Printing) for Civil Infrastructure Design and Construction,” National Science Foundation (NSF), Alexandria, VA., 2017.
- [15] “Winsun completes world’s first, 500 meters long, 3D printed river revetment wall.” [Online]. Available: <https://www.3dprintingmedia.network/winsun-completes-worlds-first-3d-printed-river-revetment-wall-in-largest-construction-3d-printing-project-yet/>.
- [16] “In the Face of Climate Change: Saving Coral Reefs with 3D Printing.” [Online]. Available: <https://www.engineering.com/3DPrinting/3DPrintingArticles/ArticleID/17809/In-the-Face-of-Climate-Change-Saving-Coral-Reefs-with-3D-Printing.aspx>.
- [17] D. Asprone, C. Menna, F. P. Bos, T. A. M. Salet, J. Mata-falcón, and W. Kaufmann, “Rethinking reinforcement for digital fabrication with concrete,” *Cement and Concrete Research*, vol. 112, pp. 111–121, 2018.
- [18] B. BAZ, G. AOUAD, and S. REMOND, “Effect of the Printing Method and Mortar’s Workability on Pull-Out Strength of 3D Printed Elements,” *Construction and Building Materials*, vol. 230, p. 117002, 2020.
- [19] V. Mechtcherine, J. Grafe, V. N. Nerella, E. Spaniol, M. Hertel, and U. Füssel, “3D-Printed Steel Reinforcement for Digital Concrete Construction Manufacture, Mechanical Properties and Bond Behaviour,” *Construction and Building Materials*, vol. 179, pp. 125–137, 2018.
- [20] R. N. P. Van Woensel, T. Van Oirschot, M. J. H. Burgmans, M. Mohammadi, Ph D, and K. Hermans, “Printing Architecture: An Overview of Existing and Promising Additive Manufacturing Methods and Their Application in the Building Industry,” *The International Journal of the Constructed Environment*, vol. 9, no. 1, pp. 57–81, 2018.
- [21] B. Baz, G. Aouad, P. Leblond, O. Al-mansouri, D. Melody, and S. REMOND, “Mechanical assessment of concrete – Steel bonding in 3D printed elements,” *Construction and Building Materials*, vol. 256, p. 119457, 2020.
- [22] D. Lowke, E. Dini, A. Perrot, D. Weger, C. Gehlen, and B. Dillenburger, “Particle-bed 3D printing in concrete construction – Possibilities and challenges,” *Cement and Concrete Research*, vol. 112, pp. 50–65, 2018.

- [23] V. N. Nerella, H. Ogura, and V. Mechtcherine, “Incorporating reinforcement into digital concrete construction,” Proceedings of the IASS Symposium 2018, Creativity in Structural Design, July 16-20, 2018, MIN, Boston, USA, pp. 1–8, 2018.
- [24] R. A. Buswell and W. R. L. De Silva, “3D printing using concrete extrusion : a roadmap for research,” Latex templates, pp. 1–29, 2018.
- [25] W. Gao, Y. Zhang, D. Ramanujan, K. Ramani, Y. Chen, C. B. Williams, C. C. L. Wang, Y. C. Shin, S. Zhang, and P. D. Zavattieri, “The status , challenges , and future of additive manufacturing in engineering,” Computer-Aided Design, vol. 69, pp. 65–89, 2015.
- [26] I. Agustí-juan and G. Habert, “Environmental design guidelines for digital fabrication,” Journal of Cleaner Production, vol. 142, pp. 2780–2782, 2017.
- [27] Y. Tosun and R. Şahin, “DEVELOPMENTS OF 3D CONCRETE PRINTING PROCESS,” international civil engineering and architecture conference (ICEARC’19) TRABZON / TURKEY, 2019.
- [28] B. Panda, S. Chandra Paul, and M. Jen Tan, “Anisotropic mechanical performance of 3D printed fiber reinforced sustainable construction material,” Materials Letters, vol. 209, pp. 146–149, 2017.
- [29] G. Ma, J. Zhang, L. Wang, Z. Li, and J. Sun, “Mechanical characterization of 3D printed anisotropic cementitious material by the electromechanical transducer,” Smart Materials and Structures, vol. 27, no. 7, 2018.
- [30] S. C. Paul, Y. W. D. Tay, B. Panda, and M. J. Tan, “Fresh and hardened properties of 3D printable cementitious materials for building and construction,” Archives of Civil and Mechanical Engineering, vol. 18, no. 1, pp. 311–319, 2018.
- [31] E. Gallucci, K. Scrivener, A. Groso, M. Stampanoni, and G. Margaritondo, “3D experimental investigation of the microstructure of cement pastes using synchrotron X-ray microtomography (μ CT),” Cement and Concrete Research, vol. 37, no. 3, pp. 360–368, 2007.
- [32] M. Moini, J. Olek, B. Magee, P. Zavattieri, and J. Youngblood, “Additive Manufacturing and Characterization of Architected Cement-based Materials via X-ray Micro-Computed Tomography,” 1st RILEM International Conference on Concrete and Digital Fabrication, ETH, Zurich, 2018.
- [33] A. V Rahul, M. Santhanam, H. Meena, and Z. Ghani, “Mechanical characterization of 3D printable concrete,” Construction and Building Materials, vol. 227, 2019.
- [34] R. J. M. Wolfs, F. P. Bos, and T. A. M. Salet, “Hardened properties of 3D printed concrete: The influence of process parameters on interlayer adhesion,” Cement and Concrete Research, vol. 119, pp. 132–140, 2019.

- [35] Y. Wei, D. Tay, Y. Wei, D. Tay, G. Heng, A. Ting, Y. Qian, B. Panda, and M. J. Tan, “Time gap effect on bond strength of 3D-printed concrete,” *Virtual and Physical Prototyping*, pp. 1–10, 2018.
- [36] B. Zareiyani and B. Khoshnevis, “Interlayer adhesion and strength of structures in Contour Crafting - Effects of aggregate size, extrusion rate, and layer thickness,” *Automation in Construction*, vol. 81, pp. 112–121, 2017.
- [37] B. Zareiyani and B. Khoshnevis, “Effects of interlocking on interlayer adhesion and strength of structures in 3D printing of concrete,” *Automation in Construction*, vol. 83, pp. 212–221, 2017.
- [38] A. Akbar, S. Javid, P. Ghoddousi, G. G. Amiri, and K. Donyadideh, “A new photogrammetry method to study the relationship between thixotropy and bond strength of multi-layers casting of self- consolidating concrete,” *Construction and Building Materials*, vol. 204, pp. 530–540, 2019.
- [39] J. G. Sanjayan, B. Nematollahi, M. Xia, and T. Marchment, “Effect of Surface Moisture on Inter-Layer Strength of 3D Printed Concrete,” *Construction and Building Materials*, vol. 172, pp. 468–475, 2018.
- [40] J. Van Der Putten, G. De Schutter, and K. Van Tittelboom, “The Effect of Print Parameters on the (Micro) structure of 3D Printed Cementitious Materials,” *RILEM Bookseries* 19, pp. 234–244, 2019.
- [41] J. Van Der Putten, M. Deprez, V. Cnudde, and G. De Schutter, “Microstructural Characterization of 3D Printed Cementitious Materials,” *MDPI Materials*, vol. 12, no. 18, 2019.
- [42] P. K. Mehta and P. J. M. Monteiro, “Concrete: Microstructure, Properties and Materials,” 3rd ed. McGraw-Hill, New York, 2006.
- [43] E. Hewayde, M. Nehdi, E. Allouche, and G. Nakhla, “Effect of Mixture Design Parameters and Wetting-Drying Cycles on Resistance of Concrete to Sulfuric Acid Attack,” *JOURNAL OF MATERIALS IN CIVIL ENGINEERING*, vol. 19, no. 2, pp. 155–163, 2007.
- [44] “BS EN 206:2013 Concrete — Specification , performance , production and conformity,” 2014.
- [45] L. Gu, T. Bennett, and P. Visintin, “Sulphuric acid exposure of conventional concrete and alkali-activated concrete : Assessment of test methodologies,” *Construction and Building Materials*, vol. 197, pp. 681–692, 2019.
- [46] S. Barbhuiya and D. Kumala, “Behaviour of a Sustainable Concrete in Acidic Environment,” *MDPI Sustainability*, vol. 9, no. 1556, 2017.

- [47] E. Mene'ndez, T. Matschei, and F. P. Glasser, "Sulfate Attack of Concrete," *Performance of Cement-Based Materials in Aggressive Aqueous Environments*, RILEM State-of-the-Art Reports 10, 2013.
- [48] K. Kawai, S. Yamaji, and T. Shinmi, "Concrete Deterioration Caused by Sulfuric Acid Attack," *10DBMC International Conférence On Durability of Building Materials and Components LYON [France]*, 2005.
- [49] B. A. BAZ, S. Remond, and G. Aouad, "Influence of the mix composition on the thixotropy of 3D printable mortars," *Magazine of Concrete Research*, 2020.
- [50] K. El Cheikh, S. Rémond, N. Khalil, and G. Aouad, "Numerical and experimental studies of aggregate blocking in mortar extrusion," *Construction and Building Materials*, vol. 145, pp. 452–463, 2017.
- [51] CEN (European Committee for Standardization), "EN ISO 17892-6: Geotechnical investigation and testing - laboratory testing of soil - part 6: Fall cone test," 2017.
- [52] P. Estellé, C. Michon, C. Lanos, and J. L. Grossiord, "De l' intérêt d' une caractérisation rhéologique empirique et relative," *Rhéologie*, vol. 21, pp. 10–35, 2012.
- [53] N. Roussel, "A thixotropy model for fresh fluid concretes : Theory , validation and applications," *Cement and Concrete Research*, vol. 36, pp. 1797–1806, 2006.
- [54] A. Luisa, T. Torres, and M. Isabel, "Concrete degradation mechanisms by sulfuric acid attack," *Magazine of Concrete Research*, vol. 71, no. 7, pp. 1–13, 2018.
- [55] "ASTM C1012/C1012M – 18b Standard Test Method for Length Change of Hydraulic-Cement Mortars Exposed to a Sulfate Solution," pp. 1–9, 2018.
- [56] F. Gong, D. Zhang, E. Sicut, and T. Ueda, "Empirical Estimation of Pore Size Distribution in Cement , Mortar , and Concrete," *Materials in civil engineering*, vol. 26, no. 7, 2014.
- [57] D. De Koker, "Manufacturing processes for engineered cement-based composite material products," M.Sc. thesis, Stellenbosch University, South Africa, 2004.
- [58] C. Schr and V. N. Nerella, "Capillary Water Intake by 3D-Printed Concrete Visualised and Quantified by Neutron Radiography," *First RILEM International Conference on Concrete and Digital Fabrication – Digital Concrete 2018*, pp. 217–224, 2018.
- [59] J. Van Der Putten, G. De Schutter, and K. Van Tittelboom, "The Effect of Print Parameters on the (Micro)structure of 3D Printed Cementitious Materials," *First RILEM International Conference on Concrete and Digital Fabrication – Digital Concrete 2018*, pp. 234–244, 2018.
- [60] P. C. Bran Anleu, T. Wangler, and R. J. Flatt, "Chloride Ingress Through Cold Joints in Digitally Fabricated Concrete by micro-XRF Mapping," *First RILEM International Conference on Concrete and Digital Fabrication – Digital Concrete 2018*, 2018.

GENERAL CONCLUSION

This research concentrates on linking the fresh state properties of 3D printable materials to the hardened state properties of 3D printed elements. Initially, the experimental program goes over the formulation of printable concrete mixes and their rheological characterization. In particular, the rheological representation of the newly developed mixes was mostly concerned by their thixotropic behavior over a certain period of time, which is the principal aspect to be assessed for a 3D printable material. Afterwards, the outcomes of the rheological characterization were correlated to the hardened state properties of 3D printed concrete elements, namely their mechanical performance and structural capacity. Therefore, the methodical objectives of this work were first, to understand the effect of some chemical and mineral admixtures on the thixotropic behavior of 3D printable mortars. The second objective was to investigate how the rheological properties of the fresh material would affect the bond generated between reinforcing steel bars and the printed layers; and subsequently, the influence of the layers direction with respect to the bar on the quality of the developed bond. The third objective was to characterize the microstructure of a printed material and study the durability performance of 3D printed concrete elements when subjected sulfuric acid attack.

At first, four different categories of 3D printable mixes were developed, each having a specific material variable. These variables were the high range water reducer (HRWR) concentration, the viscosity modifying agent (VMA) concentration, the limestone filler content, and the water content. Primarily, all mixes were manually tested for printability (extrudability and buildability) using a laboratory device, simulating the work of an actual 3D printer. Later on, their rheological properties were carried out using the fall-cone penetrometer, which provides the actual yield stress of the mix, calculated based on the penetration depth of the cone. Herein, the yield stress measurements were recorded every 2.5 min over the course of 22 min. The linear model proposed by Roussel to describe the structuration rate of the material has been adopted, and the results were properly associated to the structuration rate (A_{thix}) and thixotropic behavior of each category of mixes independently. Indeed, this model was capable of simulating and predicting the actual thixotropic behavior of the materials, except for the category having different VMA concentrations. In addition, the results of this research showed that all of the material variables

influence the structuration rate of the mixes, but in a different order of magnitude. The HRWR, limestone filler and water, decreases the structuration rate of the material as their proportions increase in the mix, whereas, the VMA does not, it slightly increases it.

Concerning the effect induced by the material's fresh state properties on the hardened state properties of 3D printed elements, mechanical tests have been performed over 3D printed elements in order to qualify the bond generated between printed concrete layers and steel bars. This was done to investigate the effect of the material's rheology on the mechanical and structural performance of a printed element. With this in view, a series of pull-out tests has been performed over 3D printed elements under different printing conditions. At first, a preliminary study has been performed over manually printed concrete elements using a laboratory device. For this case, four mixes were used, having each a different workability. In addition, different printing methods were considered to produce the samples. Two different methods were adopted to print layers parallel to the steel bar (ParaM1 and ParaM2), and two other methods to print perpendicular layers to the bar (PerpM1 and PerpM2), as well as a separate method consisting of inserting the bar inside of a previously printed element (when the material is still fresh). Besides, conventionally mold casted samples were also tested, and they represented the reference model. The strategy undertaken in this project showed that 3D printed concrete samples gave a significant pull-out strength, but still slightly lower than the non-printed ones. In other words, the concrete layers in printed elements, whether parallel or perpendicular, are capable of developing a strong bond with the bar, close enough to the reference case. Taking ParaM1 as a representative sample of the parallel condition, it was found that the relative bond strength with respect to the non-printed elements varied between 0.8 and 0.95 following the mortar's workability. As for the perpendicular samples condition, taking the case of PerpM1, the relative bond strength ranged between 0.9 and 1 depending on the mortar's workability. Therefore, the printing direction did not majorly affect the quality of the bond. Conversely, a marginal and very weak bond strength was developed between printed concrete layers and the inserted bar after the layers have been printed. At the same time, the results showed that the material's workability does not majorly influence the quality and strength of the bond generated between concrete and steel bars.

In the same context, a more viable approach has been realized to produce 3D printed concrete samples, and qualify the bond between printed layers and steel bars. Accordingly, parallel and

perpendicular samples were printed using an automated 3-axis gantry printer. However, only one material has been used, having a high thixotropic behavior. The results of these samples exposed better the difference in the bond found between printed and mold casted samples in general, and parallel and perpendicular printed samples in particular. Consequently, the non-printed samples always dominated. Besides, the parallel samples outperformed the perpendicular ones. Hence, reduction factors of 0.87 and 0.78 need to be applied over parallel and perpendicular samples respectively. Though, even with the presence of these differences between samples, the developed bond can be always considered acceptable for all cases. As for the effect of the material's rheology, it can be confirmed that even a thixotropic material can still provide good confinement of the bar, thus, a printable material having a lower thixotropy would eventually result in a better bonding.

Overall, this experimental research showed that the manual printing technique can be used as a representative printing method for preliminary studies. Additionally, the results confirmed that the implementation of 3D printed reinforced concrete elements for structural application is a promising approach in the construction field, yet, it still requires further investigation and optimization in order to be fully acknowledged.

Last but not least, based on the findings of the microstructural characterization of 3D printed concrete elements, and their durability performance against sulfuric acid attacks, it is believed that the total porosity do not vary between printed and non-printed conditions. However, the pore size distribution and their morphology largely differs. It is more spread in printed samples. These facts are all attributed to the pumping pressure exerted over the material when being printed. Over and above, a strong inter-layer bonding is always found as long as a good combination between printing parameters is maintained (pumping pressure vs printing speed). Hence, the printed elements act as monolithic bodies without showing any weakness due to the layers superposition. Yet, printed specimens have the same ability to resist chemical attacks as non-printed ones. The inter-layers are strong enough to prohibit the creation of preferential pathways for chemical ingress to the inside of the element.

PERSPECTIVES

Despite the importance of all what has been done in this thesis, and the valuable outcomes that it brought to the field of construction and 3D printing in particular, there is still much more topics and issues to be investigated in order to provide a comprehensive understanding of this new construction technique.

In this study, the thixotropic properties of printable mortars were initially investigated. Though, it would be even more advantageous if the failure mode of a freshly printed elements is correlated to the rheological and thixotropic properties of the material used. Hence, the findings can be then associated to the execution aspect to anticipate the best method that has to be adopted for the production of 3D printed reinforced concrete elements.

As from a structural point of view, there is still a lot of basic testing protocols and parameters that should be assessed, starting by those prescribed for conventional reinforced concrete, such as the flexural strength, shear and bending moment capacity, and deflection of beams. It would be also relevant to study the adequacy of hybrid reinforcement of 3D printed elements, for example, by combining the best out of FRP sheets, in-mixed fibers, and conventional reinforcing bars. Alongside, convenient reduction / safety factors still need to be drafted and applied to all printed structures, depending on the printing method adopted, in order to counterbalance the shortage of the overall process (layers superposition, interface weaknesses, layers directions, etc.). Meanwhile, substantial effort must be put in to adapt the existing standards and codes to the newly developed construction technique. By that far, it can be started by focusing on the most effective combination (ratio) between the layer's geometry and bar size, to reach out the best mechanical capacity and structural integrity of the printed element, as well as the best protection of the reinforcing bars for a better durability.

Referring to the durability and microstructural assessment of 3D printed elements, and after studying the resistance of different printable mixes not having the same rheological properties against sulfuric acid attacks, it is needed to further expand the research frame in the field of durability. Chapter 4 was an extent of the anticipated research plan. However, because of time constraints, the study has been limited to the previously mentioned experimentations. Still and all, a protracted experimental program is still to be followed in a later time, and it will include a thermogravimetric analysis (TGA) and Micro-Computed Tomography (micro-CT).

Besides, even if no inter-layers were found in the current study, there will be always other cases where 3D printed elements are going to be subjected to weaknesses caused by the layers superposition. These weaknesses would certainly arise either due to the implementation of inadequate printing parameters, or other material compositions and rheological properties. Thereby, this fact threatens the embedded reinforcement, especially those located at the interface levels. Consequently, it would be essential to relate the fact of layers superposition and durability of 3D printed concrete elements to the corrosion of steel bars embedded in printed elements. This is fundamentally recommended in order to monitor the overall deterioration and performance degradation of 3D printed reinforced concrete, which is one of the major causes of failure in concrete structures. Apart from that, regarding the overall microstructure of concrete within a printed element in comparison to non-printed ones, a better understanding of the pore size distribution and their shape configurations must be carried out. In particular, the effect of the pumping pressure over these extents, since it is one of the most influencing printing parameters over a wide range of macro and micro properties.

For last, the accelerated drying and hardening rate of 3D printable mortars required for its buildability properties, is the initial contributor to the shrinkage of 3D printed concrete. In fact, this matter leads to the creation of micro-cracks and deformations in the printed element. Indeed, such issues negatively affect the overall performance of the printed element, on both mechanical and durability levels. Therefore, it would be essential to find a proper method to give the printed element a higher ability to resist all types of shrinkage.

REFERENCES

- [1] S. Mario, “The Art of Construction: Projects and Principles for Beginning Engineers and Architects,” *Chicago: Chicago Review Press*, 1990.
- [2] M. Vatan, “Evolution of Construction Systems : Cultural Effects On Traditional Structures and Their Reflection On Modern Building Construction,” 2018.
- [3] G. R. H. Wright, “Ancient Building Technology,” *Materials*, vol. 2, 2005.
- [4] H. J. Wu, “Modern Western Architecture,” *China Building Industry Press, 1st edition*, 1997.
- [5] J. Wu, H. Wei, and L. Peng, “Research on the Evolution of Building Technology Based on Regional Revitalization,” 2019.
- [6] A. Camões and R. M. Ferreira, “Technological evolution of concrete : from ancient times to ultra high-performance concrete,” pp. 1571–1578, 2010.
- [7] N. Labonnote, A. Rønnquist, B. Manum, and P. Rüther, “Additive Construction: state of the art , challenges and opportunities,” *Automation in Construction*, vol. 72, no. 3, pp. 347–366, 2016.
- [8] J. Buchli, M. Giftthaler, N. Kumar, M. Lussi, T. Sandy, K. Dör, and N. Hack, “Digital in situ fabrication - Challenges and opportunities for robotic in situ fabrication in architecture, construction, and beyond,” *Cement and Concrete Research*, vol. 112, pp. 66–75, 2018.
- [9] J. Mata-Falcon, P. Bischof, and W. Kaufmann, “Exploiting the Potential of Digital Fabrication for Sustainable and Economic Concrete Structures,” *First RILEM International Conference on Concrete and Digital Fabrication – Digital Concrete 2018*, 2018.
- [10] G. De Schutter, K. Lesage, V. Mechtcherine, V. N. Nerella, G. Habert, and I. Agusti-Juan, “Vision of 3D printing with concrete — Technical, economic and environmental potentials,” *Cement and Concrete Research*, vol. 112, pp. 25–36, 2018.
- [11] ASTM International, “ISO/ASTM 52900:2015 Additive manufacturing — General principles — Terminology,” 2015.
- [12] B. Berman, F. G. Zarb, and W. Hall, “3-D printing : The new industrial revolution,” *Business Horizons*, vol. 55, no. 2, pp. 155–162, 2012.
- [13] J. D. Prince, “3D Printing: An Industrial Revolution,” *Journal of Electronic Resources in Medical Libraries*, vol. 11, no. 1, pp. 39–45, 2014.
- [14] I. Hager, A. Golonka, and R. Putanowicz, “3D Printing of Buildings and Building Components as the Future of Sustainable Construction?,” *Procedia Engineering*, vol. 151, pp. 292–299, 2016.
- [15] R. A. Buswell, A. Thorpe, R. Soar, and A. Gibb, “Design , data and process issues for

- mega-scale rapid manufacturing machines used for construction,” *Automation in Construction*, 2008.
- [16] ElenaBs and Alamy, “3D printing house technology with 3D printer and connected computer transmitting data and process information, construction industry innovation, isome - Image ID: 2AFYEW4.” [Online]. Available: <https://www.alamy.com/>.
- [17] J. G. Sanjayan, B. Nematollahi, M. Xia, and T. Marchment, “Effect of Surface Moisture on Inter-Layer Strength of 3D Printed Concrete,” *Construction and Building Materials*, vol. 172, pp. 468–475, 2018.
- [18] M. Sakin and Y. C. Kiroglu, “3D Printing of Buildings: Construction of the Sustainable Houses of the Future by BIM,” *Energy Procedia*, vol. 134, pp. 702–711, 2017.
- [19] M. Valente, A. Sibai, and M. Sambucci, “Extrusion-Based Additive Manufacturing of Concrete Products : Revolutionizing and Remodeling the Construction Industry,” 2019.
- [20] G. Vantighem, W. De Corte, E. Shakour, and O. Amir, “Automation in Construction 3D printing of a post-tensioned concrete girder designed by topology optimization,” *Automation in Construction*, vol. 112, no. April 2019, p. 103084, 2020.
- [21] O. Kontovourkis, G. Tryfonos, C. Georgiou, G. Tryfonos, and C. Georgiou, “Robotic additive manufacturing (RAM) with clay using topology optimization principles for toolpath planning : the example of a building element,” *Architectural Science Review*, vol. 62, no. 4, pp. 1–14, 2019.
- [22] R. Kutylowski and M. Szwechłowicz, “Special kind of multimaterial topology optimization,” *Archives of Civil and Mechanical Engineering*, vol. 13, no. 3, pp. 334–344, 2013.
- [23] G. Vantighem, M. Steeman, V. Boel, and W. D. E. Corte, “Multi-physics topology optimization for 3D-printed structures,” 2018.
- [24] N. A. J. Bartels and T. F. . Houben, “STRUCTURAL OPTIMIZATION FOR 3D PRINTING,” 2016.
- [25] K.N. Jha, “Formwork for Concrete Structures,” *Tata McGraw Hill Education Private Limited*, 2012.
- [26] H. Al Jassmi, F. Al Najjar, and A. H. I. Mourad, “Large-Scale 3D Printing: The Way Forward,” *IOP Conference Series: Materials Science and Engineering*, vol. 324, no. 1, 2018.
- [27] Arnaud Perrot, *3D Printing of Concrete: State of the Art and Challenges of the Digital Construction Revolution*. 2019.
- [28] P. Poullain, E. Paquet, S. Garnier, and B. Furet, “On site deployment of 3D printing for the building construction – The case of YhnovaTM,” *MATEC Web of Conferences*, vol. 163, p. 01001, 2018.
- [29] “The Manufacturers of 3D Printed Houses.” [Online]. Available: <https://www.3dnatives.com/en/3d-printed-house-companies-120220184/>.

- [30] L. X., “Tower-type 3D (three-dimensional) printer and printing method thereof,” *CN103786235A*, 2014.
- [31] B. P., W. R.L., and TUMMINO M., “A concept for rapidly-deployable cable robot search and rescue systems,” *ASME 2005 International Design Engineering Technical Conferences and Computers and Information in Engineering Conference*, pp. 589–598, 2005.
- [32] P. Bosscher, R. L. Williams, L. S. Bryson, and D. Castro-Lacouture, “Cable-suspended robotic contour crafting system,” *Automation in Construction*, vol. 17, no. 1, pp. 45–55, 2007.
- [33] T. A. Newspaper, “To celebrate the Bauhaus centennial, German researchers show off new robot printer.” [Online]. Available: <https://archpaper.com/2019/09/bauhaus-centennial-german-researchers-new-robot-printer/>.
- [34] B. Khoshnevis, “Automated construction by contour crafting - Related robotics and information technologies,” *Automation in Construction*, vol. 13, no. 1, pp. 5–19, 2004.
- [35] D. Lowke, E. Dini, A. Perrot, D. Weger, C. Gehlen, and B. Dillenburger, “Particle-bed 3D printing in concrete construction – Possibilities and challenges,” *Cement and Concrete Research*, vol. 112, pp. 50–65, 2018.
- [36] B. Nematollahi, M. Xia, and J. Sanjayan, “Current Progress of 3D Concrete Printing Technologies,” *Proceedings of 34th International Symposium on Automation and Robotics in Construction*, pp. 260–267, 2017.
- [37] T. T. Le, S. A. Austin, S. Lim, R. A. Buswell, R. Law, A. G. F. Gibb, and T. Thorpe, “Hardened properties of high-performance printing concrete,” *Cement and Concrete Research*, vol. 42, no. 3, pp. 558–566, 2012.
- [38] A. Peters, “This village for the homeless just got a new addition: 3D-printed houses.” [Online]. Available: <https://www.fastcompany.com/90476220/why-stranger-things-heartthrob-finn-wolfhard-hit-pause-and-then-play-again-on-his-music-career>.
- [39] J. Belezina, “D-Shape 3D printer can print full-sized houses,” 2012. [Online]. Available: <http://newatlas.com/d-shape-3d-printer/21594/>.
- [40] V. Mechtcherine, J. Grafe, V. N. Nerella, E. Spaniol, M. Hertel, and U. Füssel, “3D-Printed Steel Reinforcement for Digital Concrete Construction Manufacture, Mechanical Properties and Bond Behaviour,” *Construction and Building Materials*, vol. 179, pp. 125–137, 2018.
- [41] P. Wu, J. Wang, and X. Wang, “A critical review of the use of 3-D printing in the construction industry,” *Automation in Construction*, vol. 68, pp. 21–31, 2016.
- [42] F. Bos, R. Wolfs, Z. Ahmed, and T. Salet, “Additive manufacturing of concrete in construction: potentials and challenges of 3D concrete printing,” *Virtual and Physical Prototyping*, vol. 11, no. 3, pp. 209–225, 2016.
- [43] S. E. E. Profile, “DEVELOPMENTS OF 3D CONCRETE PRINTING PROCESS,” *International civil engineering and architecture conference 2019 ICEARC’19*

TRABZON/TURKEY, 2019.

- [44] M. A. Alzarrad and S. Elhouar, “3D Printing Applications in Construction from The Past and into The Future 3D Printing Applications in Construction from The Past and into The Future,” no. August, 2019.
- [45] W. Gao, Y. Zhang, D. Ramanujan, K. Ramani, Y. Chen, C. B. Williams, C. C. L. Wang, Y. C. Shin, S. Zhang, and P. D. Zavattieri, “The status , challenges , and future of additive manufacturing in engineering,” *Computer-Aided Design*, vol. 69, pp. 65–89, 2015.
- [46] J. J. Biernacki, J. W. Bullard, G. Sant, K. Brown, F. P. Glasser, S. Jones, T. Ley, R. Livingston, L. Nicoleau, J. Olek, F. Sanchez, R. Shahsavari, P. E. Stutzman, K. Sobolev, and T. Prater, “Cements in the 21st century: Challenges, perspectives, and opportunities,” *Journal of the American Ceramic Society*, vol. 100, no. 7, pp. 2746–2773, 2017.
- [47] B. Ahuja, M. Cornelius, and H. Karg, “Additive manufacturing in production : challenges and opportunities,” no. March, 2015.
- [48] D. Asprone, C. Menna, F. P. Bos, T. A. M. Salet, J. Mata-falcón, and W. Kaufmann, “Rethinking reinforcement for digital fabrication with concrete,” *Cement and Concrete Research*, vol. 112, pp. 111–121, 2018.
- [49] Y. Tosun and R. Şahin, “DEVELOPMENTS OF 3D CONCRETE PRINTING PROCESS,” *international civil engineering and architecture conference (ICEARC'19) TRABZON / TURKEY*, 2019.
- [50] B. Panda, S. Chandra Paul, and M. Jen Tan, “Anisotropic mechanical performance of 3D printed fiber reinforced sustainable construction material,” *Materials Letters*, vol. 209, pp. 146–149, 2017.
- [51] G. Ma, J. Zhang, L. Wang, Z. Li, and J. Sun, “Mechanical characterization of 3D printed anisotropic cementitious material by the electromechanical transducer,” *Smart Materials and Structures*, vol. 27, no. 7, 2018.
- [52] N. Roussel, “Rheological requirements for printable concretes,” *Cement and Concrete Research*, vol. 112, pp. 76–85, 2018.
- [53] Y. Zhang, Y. Zhang, W. She, L. Yang, G. Liu, and Y. Yang, “Rheological and harden properties of the high-thixotropy 3D printing concrete,” *Construction and Building Materials*, vol. 201, pp. 278–285, 2019.
- [54] K. S. Kim, “Rheological Property Criteria for Buildable 3D Printing Concrete,” pp. 1–21, 2019.
- [55] M. Rubio, M. Sonebi, and S. Amziane, “FRESH AND RHEOLOGICAL PROPERTIES OF 3D PRINTING BIO- CEMENT-BASED MATERIALS To cite this version : HAL Id : hal-01576188,” 2017.
- [56] H. A. Barnes, J. F. Hutton, and K. Walters, “An Introduction to Rheology,” *Elsevier*, 1989.
- [57] D. Jiao, C. Shi, Q. Yuan, X. An, Y. Liu, and H. Li, “Effect of constituents on rheological

- properties of fresh concrete-A review,” *Cement and Concrete Composites*, vol. 83, pp. 146–159, 2017.
- [58] L. Reiter, T. Wangler, N. Roussel, and R. Flatt, “The role of early age structural buildup in digital fabrication with concrete,” *Cement and Concrete Research*, 2018.
- [59] N. Roussel and G. Ovarlez, “The origins of thixotropy of fresh cement pastes,” *Cement and Concrete Research*, vol. 42, no. 1, pp. 148–157, 2012.
- [60] P. Estellé, C. Lanos, Y. Mélinge, and A. Perrot, “Couette Rheometry from Differential Approach: Comparative Study and Experimental Application,” *THE XV INTERNATIONAL CONGRESS ON RHEOLOGY: The Society of Rheology 80th Annual Meeting, Aug 2008, Monterey, United States.*, pp. 1396–1398, 2008.
- [61] R. Carlos and V. Coelho, “Lattice Boltzmann Method for Bosons and Fermions,” p. 125, 2014.
- [62] H. quoc Nguyen and D. N. Ngoc, “Incompressible Non-Newtonian Fluid Flows,” *CONTINUUM MECHANICS – PROGRESS IN FUNDAMENTALS AND ENGINEERING APPLICATIONS*, 2012.
- [63] A. Olivas, F. Chiara, F. William, and B. Toman, “Re-Certification of SRM 2492 : Bingham Paste Mixture for Rheological Measurements,” *National Institute of Standards and Technology Special Publication 260-182*.
- [64] I. M. Krieger and T. J. Dougherty, “A mechanism for non-Newtonian flow in suspensions of rigid spheres,” *Trans. Soc. Rheol.*, vol. 3, pp. 137–152, 1959.
- [65] F. C.F., “Concrete Rheology: Knowledge and challenges ,” *2nd International RILEM Symposium on Advances in Concrete Through Science and Engineering (Quebec, Canada)*, 2006.
- [66] E.-A. Brujan, *Cavitation in Non-Newtonian Fluids with biomedical and bioengineering applications*. 2010.
- [67] P. Coussot and C. Ancey, “Rheophysical classification of concentrated suspensions and granular paste,” *Phys. Rev. Lett.*, pp. 4445–4457, 1999.
- [68] R. B. Bird, D. Gance, and B. J. Yarusso, “The rheology and flow of viscoplastic materials,” *Chem. Eng.*, vol. 1, pp. 1–70, 1982.
- [69] J. Mewis and A. J. B. Spaul, “Rheology of concentrated dispersions,” *Adv. Colloid Interface Sci*, vol. 6, pp. 173–200, 1976.
- [70] C. Atzeni, L. Massidda, and U. Sanna, “Comparison between rheological models for Portland cement pastes,” *Cem. Concr. Res*, vol. 15, pp. 511–519, 1985.
- [71] A. Papo, “Rheological models for cement pastes,” *Mater. Struct.*, vol. 21, pp. 41–46, 1988.
- [72] K. Vance, A. Arora, G. Sant, and N. Neithalath, “Rheological evaluations of interground and blended cement-limestone suspensions,” *Construction and Building Materials*, vol. 79, pp. 65–72, 2015.

- [73] D. P. Bentz, S. Z. Jones, I. R. Bentz, and M. A. Peltz, “Towards the formulation of robust and sustainable cementitious binders for 3-D additive construction by extrusion,” *Construction and Building Materials*, vol. 175, pp. 215–224, 2018.
- [74] J. E. Wallevik, “Relationship between the Bingham parameters and slump,” *Cement and Concrete Research*, vol. 36, no. 7, pp. 1214–1221, 2006.
- [75] F. De Larrard and N. Roussel, “Flow Simulation of Fresh Concrete under a Slipform Machine,” *Road Materials and Pavement Design*, 2011.
- [76] V. H. Nguyen, S. Remond, and J. L. Gallias, “Influence of cement grouts composition on the rheological behaviour,” *Cement and Concrete Research*, vol. 41, no. 3, pp. 292–300, 2011.
- [77] A. Perrot and D. Rängeard, “Prediction of the ram extrusion force of cement-based materials,” *applied rheology*, 2014.
- [78] F. De Larrard, C. F. Ferraris, and T. Sedran, “Fresh concrete : A Herschel-Bulkley material,” vol. 31, no. September, pp. 494–498, 1998.
- [79] M. Jolin, J. Lemay, N. Ginouse, and B. Bissonnette, “THE EFFECT OF SPRAYING ON FIBER CONTENT AND SHOTCRETE PROPERTIES,” *Engineering Conferences International, Shotcrete for Underground Support XII, Singapore Metro ConsultingEds, ECI Symposium Series*, 2015.
- [80] Y. Weng, M. J. Tan, and S. Qian, “Rheology and Printability of Engineered Cementitious Composites-A Literature Review,” *2nd International Conference on Progress in Additive Manufacturing (Pro-AM 2016) 16-19 May 2016, Singapore*, 2016.
- [81] E. ST, M. NS, F. CF, and F. DW., “Influence of the shape and roughness of inclusions on the rheological properties of a cementitious suspension,” *Cement and Concrete Composites*, vol. 30, pp. 393–402, 2008.
- [82] V. K, K. A, S. G, and N. N., “The rheological properties of ternary binders containing portland cement, limestone, and metakaolin or fly ash,” *Cement and Concrete Research*, vol. 52, pp. 196–207, 2013.
- [83] M. N, K. K, P. M, and J. C., “Aqueous CaCO₃ dispersions as reference systems for early-age cementitious materials,” *Colloids Surf Physicochem Eng Asp*, vol. 11, 2006.
- [84] N. Khalil, G. Aouad, K. El Cheikh, and S. Rémond, “Use of calcium sulfoaluminate cements for setting control of 3D-printing mortars,” *Construction and Building Materials*, vol. 157, pp. 382–391, 2017.
- [85] H. V. A. and Ferraris C.F, “The Use of Nomenclature in Dispersion Science and Technology,” *NIST Recommended Practice Guide*, 2001.
- [86] S. E. Chidiac, F. Habibbeigi, and D. Chan, “Slump and Slump Flow for Characterizing Yield Stress of Fresh Concrete,” *International Concrete Abstracts Portal*, vol. 103, no. 6, pp. 413–418, 2016.
- [87] N. Roussel, “Correlation between Yield Stress and Slump : Comparison between

- Numerical Simulations and Concrete Rheometers Results,” no. March, 2014.
- [88] A. F. Omran, K. H. Khayat, and Y. M. Elaguab, “Effect of SCC mixture composition on thixotropy and formwork pressure,” *Journal material Journal of Materials in Civil Engineering*, vol. 24, no. 7, pp. 876–888, 2012.
- [89] S. P. JIANG, J. C. MUTIN, and A. NONAT, “STUDIES ON MECHANISM AND PHYSICO-CHEMICAL PARAMETERS AT THE ORIGIN OF THE CEMENT SETTING. I. THE FUNDAMENTAL PROCESSES INVOLVED DURING THE CEMENT SETTING,” *Cement and Concrete Research*, vol. 25, no. 4, pp. 779–789, 1995.
- [90] V. N. Nerella and V. Mechtcherine, “Studying printability of fresh concrete for formwork free Concrete on-site 3D Printing technology,” 2016.
- [91] T. T. Le, S. A. Austin, S. Lim, R. A. Buswell, A. G. F. Gibb, and T. Thorpe, “Mix design and fresh properties for high-performance printing concrete,” *Materials and Structures/Materiaux et Constructions*, vol. 45, no. 8, pp. 1221–1232, 2012.
- [92] R. Wolfs, “3D printing of concrete structures,” *Master Architecture, Building and Planning, Eindhoven University of Technology, Department of the Built Environment*, 2015.
- [93] A. Perrot, D. Rängeard, and A. Pierre, “Structural built-up of cement-based materials used for 3D- printing extrusion techniques,” *Materials and Structures*, vol. 49, pp. 1213–1220, 2016.
- [94] D. M. Kirchmajer, R. G. Iii, and M. Panhuis, “An overview of the suitability of hydrogel-forming polymers for extrusion-based 3D-printing,” *Journal of Materials Chemistry B*, vol. 3, pp. 4105–4117, 2015.
- [95] R. N., C. P., and O. G., “La Pierre Liquide: des puits de potentiel au chantier,” *Rhéologie*, vol. 13, pp. 41–51, 2008.
- [96] R. B. Bird, D. Gance, and B. J. Yarusso, “The rheology and flow of viscoplastic materials,” *Rev. Chem. Eng.*, vol. 1, pp. 1–70, 1982.
- [97] T. Wangler, E. Lloret, L. Reiter, N. Hack, F. Gramazio, M. Kohler, B. Mathias, D. Benjamin, J. Buchli, R. Nicolas, R. Flatt, and A., “Digital Concrete : Opportunities and Challenges,” *RILEM Technical Letters*, vol. 1, pp. 67–75, 2016.
- [98] W. R. Schowalter and G. Christensen, “Toward a rationalization of the slump test for fresh concrete: Comparisons of calculations and experiments.,” *Rheology*, vol. 42, pp. 865–870, 1998.
- [99] N. Roussel, “Rheological requirements for printable concretes,” *Cement and Concrete Research*, vol. 112, pp. 76–85, 2018.
- [100] R. J. M. Wolfs, F. P. Bos, and T. A. M. Salet, “Early age mechanical behaviour of 3D printed concrete : Numerical modelling and experimental testing,” *Cement and Concrete Research*, vol. 106, pp. 103–116, 2018.

- [101] L. K. Mettler, F. K. Wittel, R. J. Flatt, and Hans J. Herrmann, “Evolution of strength and failure of SCC during early hydration,” *Cement and Concrete Research*, vol. 89, pp. 288–296, 2016.
- [102] G. Ovarlez and N. Roussel, “A physical model for the prediction of lateral stress exerted by self-compacting concrete on formwork,” *Materials and Structures/Materiaux et Constructions*, vol. 39, no. 286, pp. 269–279, 2006.
- [103] N. Roussel, “A thixotropy model for fresh fluid concretes : Theory , validation and applications,” *Cement and Concrete Research*, vol. 36, pp. 1797–1806, 2006.
- [104] ROUSSEL N., “Steady and transient flow behaviour of fresh cement pastes,” *Cement and Concrete Research*, vol. 35, no. 9, pp. 1656–1664, 2005.
- [105] A. Perrot, A. Pierre, and V. Picandet, “Prediction of lateral form pressure exerted by concrete at low casting rates,” *Materials and Structures*, vol. 48, no. 7, pp. 2315–2322, 2015.
- [106] L. T. and P. A., “Non-linear modeling of yield stress increase due to SCC structural build-up at rest,” *Cement and Concrete Research*, vol. 92, pp. 92–97, 2017.
- [107] V. Mechtcherine, F. P. Bos, A. Perrot, W. R. Leal, V. N. Nerella, S. Fataei, R. J. M. Wolfs, M. Sonebi, and N. Roussel, “Extrusion-based additive manufacturing with cement-based materials – Production steps , processes , and their underlying physics : A review,” *Cement and Concrete Research*, vol. 132, 2020.
- [108] B. Panda, S. Ruan, C. Unluer, and M. J. Tan, “Improving the 3D printability of high volume fly ash mixtures via the use of nano attapulgite clay,” *Composites Part B: Engineering*, vol. 165, pp. 75–83, 2019.
- [109] W. L. da Silva, J.-N. B. H. Fryda, P.-A. Andreani, and T. Andersen, “Evaluation of early-age concrete structural build-up for 3D concrete printing by oscillatory rheometry,” *Advances in Additive Manufacturing, Modeling Systems and 3D Prototyping. AHFE 2019, Advances in Intelligent Systems and Computing*, vol. 975, pp. 35–47, 2019.
- [110] M. Rubio, M. Sonebi, and S. Amziane, “3D printing of fibre cement-based materials: fresh and rheological performances,” *Proceedings of 2nd ICBBM (PRO 119), 21–23 June 2017*, pp. 284–291, 2017.
- [111] Y. Zhang, Y. Zhang, G. Liu, Y. Yang, M. Wu, and B. Pang, “Fresh properties of a novel 3D printing concrete ink,” *Construction and Building Materials*, vol. 174, pp. 263–271, 2018.
- [112] A. Kazemian, X. Yuan, E. Cochran, and B. Khoshnevis, “Cementitious materials for construction-scale 3D printing: Laboratory testing of fresh printing mixture,” *Construction and Building Materials*, vol. 145, pp. 639–647, 2017.
- [113] A. Perrot and D. Rangeard, “Extrusion criterion for firm cement-based materials,” no. May 2014, 2009.
- [114] Z. Toutou, N. Roussel, and C. Lanos, “The squeezing test : a tool to identify firm cement-based material ’ s rheological behaviour and evaluate their extrusion ability,” vol. 35, pp.

- 1891–1899, 2005.
- [115] H. Kheli, A. Perrot, T. Lecompte, D. Rangeard, and G. Ausias, “Prediction of extrusion load and liquid phase filtration during ram extrusion of high solid volume fraction pastes,” vol. 249, pp. 258–268, 2013.
- [116] G. J. Z. K, and K. W, “Possible optimisation of pastes and the according apparatus in process engineering by mri flow experiments,” *Chemical Engineering and Processing: Process Intensification*, vol. 42, pp. 517–534, 2003.
- [117] R. BD, M. P, B. F, R. S, M. Y, L. C, and C. P, “Internal flow characteristics of a plastic kaolin suspension during extrusion,” *Internal flow characteristics of a plastic kaolin suspension during extrusion, Journal of the American Ceramic Society*, vol. 95, pp. 494–501, 2012.
- [118] G. J, K. W, and P. M, “Extrusion of pastes with a piston extruder for the determination of the local solid and fluid concentration, the local porosity and saturation and displacement profiles by means of nmr imaging,” *Rheologica Acta*, vol. 41, pp. 134–143, 2002.
- [119] B. MA and B. J, “Evaluation of liquid phase migration in pastes and gels,” *Industrial & Engineering Chemistry Research*, vol. 51, pp. 1774–1781, 2012.
- [120] “University of Stuttgart Investigating Reinforcement of 3D Printed Concrete.” [Online]. Available: <https://www.morgen-filament.de/university-of-stuttgart-investigating-reinforcement-of-3d-printed-concrete/>.
- [121] R. J. M. Wolfs and A. S. J. Suiker, “Structural failure during extrusion-based 3D printing processes,” *The International Journal of Advanced Manufacturing Technology*, 2019.
- [122] A. S. J. Suiker, “Mechanical performance of wall structures in 3D printing processes : Theory , design tools and experiments,” *International Journal of Mechanical Sciences*, vol. 137, pp. 145–170, 2018.
- [123] D. Marchon and R. J. Flatt, *Impact of chemical admixtures on cement hydration*. Elsevier Ltd, 2015.
- [124] K. Pj, S. Cho, S. Zeranka, and V. Z. Gpag, “Multi-physics approach for improved thixotropy of cement-based materials for 3DPC,” *1st International Conference on 3D Construction Printing Swinburne University of Technology, Melbourne, Australia*, pp. 1–8, 2018.
- [125] I. Aiad, S. A. El-Aleem, and H. El-Didamony, “Effect of delaying addition of some concrete admixtures on the rheological properties of cement pastes,” *Cement and Concrete Research*, vol. 32, no. 11, pp. 1839–1843, 2002.
- [126] C. Hu and F. De Larrard, “The rheology of fresh high-performance concrete,” *Cement and Concrete Composites*, vol. 26, no. 2, pp. 283–294, 1996.
- [127] E. P. Koehler and D. W. Fowler, “Development of a portable rheometer for fresh Portland cement concrete,” *ICAR Rep.*, pp. 103–105, 2004.
- [128] P. F. G. Banfill, “Additivity effects in the rheology of fresh concrete containing water-

- reducing admixtures,” *Construction and Building Materials journal*, vol. 25, pp. 2955–2960, 2011.
- [129] J. Gołaszewski, “INFLUENCE OF MORTAR VOLUME ON THE RHEOLOGICAL PROPERTIES OF FRESH HIGH PERFORMANCE CONCRETE,” 2008.
- [130] F. J. Rubio-Hernández, A. Adarve-Castro, J. F. Velázquez-Navarro, N. M. Páez-Flor, and R. Delgado-García, “Influence of water / cement ratio , and type and concentration of chemical additives on the static and dynamic yield stresses of Portland cement paste,” *Construction and Building Materials*, vol. 235, p. 117744, 2020.
- [131] M. Rahman, M. H. Baluch, and M. A. Malik, “Thixotropic behavior of self compacting concrete with different mineral admixtures,” *Construction and Building Materials*, vol. 50, pp. 710–717, 2014.
- [132] R. S. Ahari, T. K. Erdem, and K. Ramyar, “Thixotropy and structural breakdown properties of self consolidating concrete containing various supplementary cementitious materials,” *Cement and Concrete Research*, vol. 59, pp. 26–37, 2015.
- [133] R. Saleh Ahari, T. Kemal Erdem, and K. Ramyar, “Effect of various supplementary cementitious materials on rheological properties of self-consolidating concrete,” *Construction and Building Materials*, vol. 75, no. 112, pp. 89–98, 2015.
- [134] G. H. Tattersall, “Workability and Quality Control of Concrete,” *London: E&FN Spon*, 1991.
- [135] K. Ma, G. Long, Y. Xie, and R. ZHU, “Rheological properties of compound pastes with cement-fly ash-limestone powder,” *J. Chin. Ceram. Soc.*, vol. 5, pp. 582–587, 2013.
- [136] K. Ma, G. Long, Y. Xie, and X. CHEN, “Factors on affecting plastic viscosity of cementfly ash-limestone compound pastes,” *J. Chin. Ceram. Soc*, vol. 11, pp. 1481–1486, 2013.
- [137] M. Bederina, M. Zoubir, and T. Bouziani, “Effect of Limestone Fillers the Physic-Mechanical Properties of Limestone Concrete,” *Physics Procedia*, vol. 21, pp. 28–34, 2011.
- [138] V. Bonavetti, H. Donza, G. Menéndez, O. Cabrera, and E. F. Irassar, “Limestone filler cement in low w/c concrete: A rational use of energy,” *Cement and Concrete Research*, vol. 33, no. 6, pp. 865–871, 2003.
- [139] S. Tsivilis, B. George, E. Chaniotakis, G. Grigoriadis, and D. Theodossis, “Properties and behavior of limestone cement concrete and mortar,” *Cement and Concrete Research*, vol. 30, no. 10, pp. 1679–1683, 2000.
- [140] Y. Qian, K. Lesage, K. El Cheikh, and G. De Schutter, “Effect of polycarboxylate ether superplasticizer (PCE) on dynamic yield stress, thixotropy and flocculation state of fresh cement pastes in consideration of the Critical Micelle Concentration (CMC),” *Cement and Concrete Research*, vol. 107, pp. 75–84, 2018.
- [141] K. H. Khayat, “Viscosity-Enhancing Admixtures for Cement-Based Materials - An Overview,” vol. 20, pp. 171–188, 1998.

- [142] A. V. Rahul, M. Santhanam, H. Meena, and Z. Ghani, “3D printable concrete: Mixture design and test methods,” *Cement and Concrete Composites*, vol. 97, pp. 13–23, 2019.
- [143] M. Palacios and R. J. Flatt, *Working mechanism of viscosity-modifying admixtures*. Elsevier Ltd, 2015.
- [144] “Guidelines for Viscosity Modifying Admixtures For Concrete,” 2006.
- [145] S. Daukšys and A. Klovas, “Calculation of plastic viscosity of concrete mixture using the modified empirical formula,” *FIB Conference: Sustainable Concrete: Materials and Structures*, no. 442, pp. 012–018, 2018.
- [146] J. Temitope, R. Combrinck, and W. Peter, “Measuring the thixotropy of conventional concrete : The influence of viscosity modifying agent , superplasticiser and water,” *Construction and Building Materials*, vol. 225, pp. 853–867, 2019.
- [147] R. A. Buswell and W. R. L. De Silva, “3D printing using concrete extrusion : a roadmap for research,” *Latex templates*, pp. 1–29, 2018.
- [148] D. Marchon, S. Kawashima, H. Bessaies-bey, S. Mantellato, and S. Ng, “Hydration and rheology control of concrete for digital fabrication : Potential admixtures and cement chemistry,” *Cement and Concrete Research*, vol. 112, no. December 2017, pp. 96–110, 2018.
- [149] D. P. Bentz, S. Z. Jones, M. A. Peltz, and P. E. Stutzman, “Mitigation of autogenous shrinkage in repair mortars via internal curing,” vol. 41, no. 4, pp. 35–39, 2015.
- [150] K. Kim, S. Park, W. S. Kim, Y. Jeong, and J. Lee, “Evaluation of shear strength of RC beams with multiple interfaces formed before initial setting using 3D printing technology,” *Materials*, vol. 10, no. 12, p. 1349, 2017.
- [151] T. D. Ngo, A. Kashani, G. Imbalzano, K. T. Q. Nguyen, and D. Hui, “Additive manufacturing (3D printing): A review of materials , methods , applications and challenges,” *Composites Part B*, vol. 143, no. December 2017, pp. 172–196, 2018.
- [152] E. K. Tschegg and S. E. Stanzl, “Adhesive power measurements of bonds between old and new concrete,” *Materials Scienc*, vol. 26, no. 5189–5194, 1991.
- [153] H. Beushausen and M. G. Alexander, “Bond strength development between concretes of different ages,” no. 1, pp. 65–74, 2008.
- [154] B. Zareiyan and B. Khoshnevis, “Interlayer adhesion and strength of structures in Contour Crafting - Effects of aggregate size, extrusion rate, and layer thickness,” *Automation in Construction*, vol. 81, pp. 112–121, 2017.
- [155] B. Zareiyan and B. Khoshnevis, “Effects of interlocking on interlayer adhesion and strength of structures in 3D printing of concrete,” *Automation in Construction*, vol. 83, pp. 212–221, 2017.
- [156] Y. Wei, D. Tay, M. Y. Li, and M. J. Tan, “Effect of printing parameters in 3D concrete printing : Printing region and support structures,” vol. 271, pp. 261–270, 2019.
- [157] Y. Wei, D. Tay, Y. Wei, D. Tay, G. Heng, A. Ting, Y. Qian, B. Panda, and M. J. Tan,

- “Time gap effect on bond strength of 3D-printed concrete,” *Virtual and Physical Prototyping*, pp. 1–10, 2018.
- [158] Z. Liu, M. Li, T. N. Wong, and M. J. Tan, “Towards additive manufacturing: Pumping flow rate with time-dependent material rheology in 3d cementitious material printing,” *Materials Science Forum*, vol. 941, pp. 2131–2136, 2018.
- [159] B. Panda, S. C. Paul, L. J. Hui, Y. W. D. Tay, and M. J. Tan, “Additive manufacturing of geopolymer for sustainable built environment,” *Journal of Cleaner Production*, vol. 167, pp. 281–288, 2017.
- [160] J. Van Der Putten, M. Deprez, V. Cnudde, and G. De Schutter, “Microstructural Characterization of 3D Printed Cementitious Materials,” *MDPI Materials*, 2019.
- [161] S. C. Paul, Y. W. D. Tay, B. Panda, and M. J. Tan, “Fresh and hardened properties of 3D printable cementitious materials for building and construction,” *Archives of Civil and Mechanical Engineering*, vol. 18, no. 1, pp. 311–319, 2018.
- [162] P. Feng, X. Meng, J. F. Chen, and L. Ye, “Mechanical properties of structures 3D printed with cementitious powders,” *Construction and Building Materials*, vol. 93, pp. 486–497, 2015.
- [163] D. De Koker, “Manufacturing processes for engineered cement-based composite material products,” *M.Sc. thesis, Stellenbosch University, South Africa*, 2004.
- [164] T. Marchment and J. Sanjayan, “Mesh reinforcing method for 3D Concrete Printing,” *Automation in Construction*, vol. 109, p. 102992, 2020.
- [165] R. J. M. Wolfs, F. P. Bos, and T. A. M. Salet, “Hardened properties of 3D printed concrete: The influence of process parameters on interlayer adhesion,” *Cement and Concrete Research*, vol. 119, pp. 132–140, 2019.
- [166] T. Marchment, M. Xia, E. Dodd, J. Sanjayan, and B. Nematollahi, “Effect of Delay Time on the Mechanical Properties of Extrusion-based 3D Printed Concrete,” *Proceedings of the 34th ISARC The International Association for Automation and Robotics in Construction*, pp. 240–245, 2017.
- [167] H. Lee, J. J. Kim, J. Moon, W. Kim, and E. Seo, “Correlation between pore characteristics and tensile bond strength of additive manufactured mortar using X-ray computed tomography,” *Construction and Building Materials*, vol. 226, pp. 712–720, 2019.
- [168] S. Bukkapatnam, J. Mander, S. Paal, Z. Pei, and L. Zeng, “Workshop Report—NSF Workshop on Additive Manufacturing (3D Printing) for Civil Infrastructure Design and Construction,” *National Science Foundation (NSF), Alexandria, VA.*, 2017.
- [169] S. Z. Jones, J. Vickers, T. Wangler, and P. Zavattieri, “Additive Manufacturing Processes for Infrastructure Construction : A Review,” vol. 141, no. September, pp. 1–13, 2019.
- [170] “Winsun completes world’s first, 500 meters long, 3D printed river revetment wall.” [Online]. Available: <https://www.3dprintingmedia.network/winsun-completes-worlds-first-3d-printed-river-revetment-wall-in-largest-construction-3d-printing-project-yet/>.

- [171] “In the Face of Climate Change: Saving Coral Reefs with 3D Printing.” [Online]. Available: <https://www.engineering.com/3DPrinting/3DPrintingArticles/ArticleID/17809/In-the-Face-of-Climate-Change-Saving-Coral-Reefs-with-3D-Printing.aspx>.
- [172] V. N. Nerella, H. Ogura, and V. Mechtcherine, “Incorporating reinforcement into digital concrete construction,” *Proceedings of the IASS Symposium 2018, Creativity in Structural Design, July 16-20, 2018, MIN, Boston, USA*, pp. 1–8, 2018.
- [173] I. Agustí-juan and G. Habert, “Environmental design guidelines for digital fabrication,” *Journal of Cleaner Production*, vol. 142, pp. 2780–2782, 2017.
- [174] S. H. Chowdhury, “Early Age Bond Strength of Reinforcing Bars in High Strength Concrete,” *4th International Conference on Structural Engineering and Construction Management 2013, Kandy, Sri Lanka*, pp. 78–89, 2013.
- [175] M. Słowik, “The analysis of failure in concrete and reinforced concrete beams with different reinforcement ratio,” *Archive of Applied Mechanics*, vol. 89, no. 5, pp. 885–895, 2019.
- [176] V. N. Nerella, H. Ogura, and V. Mechtcherine, “Incorporating reinforcement into digital concrete construction,” *Annual IASS Symposia: Creativity in structural design*, 2018.
- [177] R. N. P. Van Woensel, T. Van Oirschot, M. J. H. Burgmans, M. Mohammadi, Ph D, and K. Hermans, “Printing Architecture: An Overview of Existing and Promising Additive Manufacturing Methods and Their Application in the Building Industry,” *The International Journal of the Constructed Environment*, vol. 9, no. 1, pp. 57–81, 2018.
- [178] V. Mechtcherine, V. N. Nerella, and M. Hertel, “3D-PRINTED STEEL REINFORCEMENT FOR DIGITAL CONCRETE CONSTRUCTION – MANUFACTURE , MECHANICAL PROPERTIES AND BOND BEHAVIOUR,” 2018.
- [179] F. P. Bos, Z. Y. Ahmed, E. R. Jutinov, and T. A. M. Salet, “Experimental exploration of metal cable as reinforcement in 3D printed concrete,” *Materials*, vol. 10, no. 11, 2017.
- [180] B. K. H.-T. Y. Yeh, “Mega-scale fabrication by Contour Crafting,” *International Journal of Industrial and Systems Engineering*, vol. 1, no. 3, pp. 301–320, 2006.
- [181] S. Lim, R. Buswell, T. Le, R. Wackrow, S. Austin, A. Gibb, and T. Thorpe, “Development of a viable concrete printing process,” *Proc. 28th Int. Symp. Autom. Robot. Constr.*, pp. 665–670, 2011.
- [182] B. BAZ, G. AOUAD, and S. REMOND, “Effect of the Printing Method and Mortar’s Workability on Pull-Out Strength of 3D Printed Elements,” *Construction and Building Materials*, vol. 230, p. 117002, 2020.
- [183] N. Hack, W. V. Lauer, F. Gramazio, and M. Kohler, “Mesh Mould: Robotically Fabricated Metal Meshes as Concrete Formwork and Reinforcement,” *FERRO-11: Proceedings of the 11th International Symposium on Ferrocement and 3rd ICTRC International Conference on Textile Reinforced Concrete*, pp. 347–359, 2015.
- [184] P. Ayres, W. R. L. da Silva, P. Nicholas, T. J. Andersen, and J. P. Greisen, “SCRIM –

- Sparse Concrete Reinforcement in Meshworks,” *Robotic Fabrication in Architecture, Art and Design 2018*, pp. 207–220, 2019.
- [185] E. Lloret Fritschi, L. Reiter, T. Wangler, F. Gramazio, and R. J. Kohler, Matthias; Flatt, “Smart Dynamic Casting: Slipforming With Flexible Formwork - Inline Measurement and Control,” *second concrete innovation conference*, 2017.
- [186] I. Farina, F. Fabbrocino, G. Carpentieri, M. Modano, A. Amendola, R. Goodall, L. Feo, and F. Fraternali, “On the reinforcement of cement mortars through 3D printed polymeric and metallic fibers,” *Composites Part B: Engineering*, vol. 90, pp. 76–85, 2016.
- [187] F. P. Bos, E. Bosco, and T. A. M. Salet, “Ductility of 3D printed concrete reinforced with short straight steel fibers,” *Virtual and Physical Prototyping*, vol. 14, no. 2, pp. 160–174, 2019.
- [188] J. H. Lim, B. Panda, and Q. Pham, “Improving flexural characteristics of 3D printed geopolymer composite with in-process steel cable reinforcement reinforcement,” *Construction and Building Materials*, vol. 178, pp. 32–41, 2018.
- [189] D. Asprone, F. Auricchio, C. Menna, and V. Mercuri, “3D printing of reinforced concrete elements: Technology and design approach,” *Construction and Building Materials*, vol. 165, pp. 218–231, 2018.
- [190] P. O. Akadiri, E. A. Chinyio, and P. O. Olomolaiye, “Design of A Sustainable Building: A Conceptual Framework for Implementing Sustainability in the Building Sector,” pp. 126–152, 2012.
- [191] H. Yahya, K.; Boussabaine, “Quantifying environmental impacts and eco-costs from brick waste,” *J. Archit. Eng. Des. Manag*, vol. 6, pp. 189–206, 2010.
- [192] J. Pitt, M.; Tucker, M.; Riley, M.; Longden, “Towards sustainable construction: Promotion and best practices,” *Construct. Innov. Inf. Process Manag.*, vol. 9, pp. 201–224, 2009.
- [193] V. Kukadia and D. J. Hall, “Improving Air Quality in Urban Environments: Guidance for the Construction Industry,” *Building Research Establishment (BRE) Bookshop, CRC Ltd.: London, UK*, 2004.
- [194] A. Holton, I.; Glass, J.; Price, “Developing a successful sector sustainability strategy: Six lessons from the UK construction products industry,” *Corp. Soc. Responsib. Environ. Manag*, vol. 15, pp. 29–42, 2008.
- [195] G. K. C. Ding, “Sustainable construction—The role of environmental assessment tools,” *J. Environ. Manag*, vol. 86, pp. 451–464, 2008.
- [196] C. Kohtala, “Addressing sustainability in research on distributed production: an integrated literature review,” *Journal of Cleaner Production*, vol. 106, pp. 654–668, 2015.
- [197] S. Ford and M. Despeisse, “Additive manufacturing and sustainability: an exploratory study of the advantages and challenges,” *Journal of Cleaner Production*, vol. 137, pp. 1573–1587, 2016.

- [198] M. Kreiger and J. M. Pearce, “Environmental life cycle analysis of distributed three-dimensional 648 printing and conventional manufacturing of polymer products,” *ACS Sustainable Chemistry & Engineering*, vol. 1, pp. 1511–1519, 2013.
- [199] J. Faludi, C. Bayley, S. Bhogal, and M. Iribarne, “Comparing environmental impacts of additive 592 manufacturing vs traditional machining via life-cycle assessment,” *Rapid Prototyping Journal*, vol. 21, pp. 14–33, 2015.
- [200] I. Agustí-juan, F. Müller, N. Hack, T. Wangler, and G. Habert, “Potential benefits of digital fabrication for complex structures: Environmental assessment of a robotically fabricated concrete wall,” *Journal of Cleaner Production*, 2017.
- [201] S. A. O. Nair, S. Panda, M. Santhanam, G. Sant, and N. Neithalath, “A critical examination of the influence of material characteristics and extruder geometry on 3D printing of cementitious binders,” *Cement and Concrete Composites*, p. 103671, 2020.
- [202] M. G, L. Z, and W. L, “Printable properties of cementitious material containing copper tailings for extrusion based 3D printing,” *Construction and Building Materials*, vol. 20, no. 162, pp. 613–27, 2018.
- [203] L. TT, A. SA, L. S, B. RA, G. AGF, and T. T, “Mix design and fresh properties for highperformance printing concrete,” *Materials and Designstructure*, vol. 45, no. 8, pp. 1221–32, 2012.
- [204] C. Ness, J. Y. Ooi, J. Sun, M. Marigo, P. McGuire, H. Xu, and H. Stitt, “Linking particle properties to dense suspension extrusion flow characteristics using discrete element simulations,” *AIChE J.*, vol. 63, no. 7, pp. 3069–82, 2017.
- [205] M. Classen, J. Ungermann, and R. Sharma, “Additive Manufacturing of Reinforced Concrete— Development of a 3D Printing Technology for Cementitious Composites with Metallic Reinforcement,” *Applied sciences*, vol. 10, p. 3791, 2020.
- [206] A. Akbar, S. Javid, P. Ghoddousi, G. G. Amiri, and K. Donyadideh, “A new photogrammetry method to study the relationship between thixotropy and bond strength of multi-layers casting of self- consolidating concrete,” *Construction and Building Materials*, vol. 204, pp. 530–540, 2019.

Résumé Français:

La technique de construction la plus récente est basée sur une méthode automatisée pour produire des éléments en béton, connue sous le nom de fabrication additive ou impression 3D. Cette technique émergente devrait permettre à la construction de produire un approvisionnement plus rapide en logements, une réduction du coût de construction et, surtout, une meilleure efficacité des ressources en réduisant le nombre de travailleurs et la quantité de gaspillage produite. Cependant, cette technique est encore en phase de développement et elle a attiré l'attention dans les applications académiques et industrielles. Cependant, il existe encore de nombreuses limitations qui ne permettent pas la mise en œuvre efficace de cette technique dans le domaine de la construction.

L'impression 3D et son application réelle sont confrontées à de nombreux défis. Ces défis correspondent aux propriétés à l'état frais et durci du matériau cimentaire utilisé pour l'impression 3D, ainsi qu'aux stratégies de renforcement structurel nécessaires pour fournir une performance structurelle efficace en termes de ductilité et de capacité de traction.

Tout d'abord, concernant les enjeux imposés par le matériau utilisé pour l'impression 3D, il doit présenter deux caractéristiques primordiales, mais opposées, pour être considéré comme imprimable. Ces caractéristiques sont l'extrudabilité et la constructibilité. L'extrudabilité décrit la capacité du matériau à circuler dans les conduits du système et à sortir en continu de la buse sans la bloquer, ni présenter des problèmes de ségrégation. La constructibilité fait référence à la capacité de la couche imprimée à résister aux charges imposées provenant des couches suivantes sans se déformer. À cet égard, une compréhension du comportement rhéologique précoce du matériau doit être acquise, en particulier celui liés aux propriétés de constructibilité. La constructibilité est en effet l'aspect le plus fondamental d'un processus d'impression réussi. Parallèlement, elle a les conséquences les plus pénalisantes en cas de non-contrôle adéquat car il pourrait provoquer l'effondrement de tout l'élément. Techniquement, le phénomène rhéologique déterminant correspondant à la constructibilité est le comportement thixotrope, responsable du raidissement du matériau. Précisément, la thixotropie explique l'évolution du seuil de cisaillement du matériau avec le temps.

Un autre problème difficile qui ne peut jamais être omis est la stratégie de renforcement à utiliser pour les éléments imprimés en 3D pour une mise en œuvre efficace en tant qu'éléments structurels.

Pourtant, jusqu'à présent, le manque de ductilité et de capacité de traction causé par l'absence de renforcement, empêche ce mode de production de se situer parmi d'autres techniques de construction conventionnelles. En effet, de nombreuses approches ont été développées et différentes techniques de renforcement ont été exploitées pour déterminer la méthode de renforcement la plus adaptée qui réponde à toutes les contraintes imposées. Pourtant, les techniques de renforcement conventionnelles utilisant des barres d'armature ne peuvent jamais être abandonnées. Par conséquent, une bonne liaison entre l'acier et le béton doit toujours être assurée, malgré la technique ou l'approche utilisée pour son incorporation à l'intérieur de l'élément imprimé.

Outre tous les défis mentionnés précédemment, les performances de durabilité des éléments en béton imprimés en 3D doivent également être prises en compte. Ceci est également d'une grande importance car la technique d'impression 3D est introduite dans des domaines d'applications plus développés où les éléments imprimés peuvent être continuellement exposés à des environnements agressifs. Jusqu'ici, le concept de superposition de couches et l'existence d'interfaces entre couches successives pourraient créer des plans faibles au sein de l'élément imprimé. Ces faiblesses potentielles pourraient former des voies préférentielles pour l'entrée de produits chimiques à l'intérieur de l'élément à partir de son environnement. Ainsi, si cela se produisait, la dégradation du béton et la corrosion des armatures seraient certainement plus accélérées conduisant à toute la détérioration de l'élément imprimé.

Cette thèse traite en particulier de l'effet des propriétés du matériau à l'état frais sur l'état durci et les performances mécaniques des éléments imprimés en 3D. En d'autres termes, il vise à établir un lien entre les propriétés à l'état frais des matériaux imprimables 3D et les propriétés à l'état durci des objets imprimés en 3D. La première étape dans ce contexte a été de formuler de nouveaux mélanges imprimables et de tester leurs propriétés rhéologiques. En particulier, cette partie de l'étude examine l'influence de la composition du mélange sur la rhéologie du matériau en termes de variation du seuil de cisaillement dans le temps. La tendance et le mode de variation du taux de structuration (A_{thix}) en fonction de la composition du mélange est décrite. En fait, le taux de structuration fournit une indication cruciale sur la constructibilité du matériau, car il évoque sa rigidification sur une certaine période de temps. Afin d'assurer une bonne qualité d'impression, l'imprimabilité du matériau doit être soigneusement évaluée à une plus petite échelle avant de produire des lots plus importants. Par conséquent, dans cette recherche, quatre catégories de

mélanges, représentant chacune une variable matérielle, ont été étudiées. Ces variables sont les dosages en superplastifiant, en agent de viscosité, la teneur en filler calcaire et la teneur en eau. Ces facteurs ont été choisis parce qu'il est connu que le superplastifiant et l'agent de viscosité sont les adjuvants chimiques typiques à utiliser pour le contrôle rhéologique des matériaux à base de ciment; tandis que le calcaire est l'un des substituants les plus utilisés du ciment. Le dosage en eau a été systématiquement considéré en raison de son importance fondamentale dans toute conception de mélange. Ici, les mesures rhéologiques ont été effectuées à l'aide du pénétromètre à chute libre, et la profondeur de pénétration est corrélée au seuil de cisaillement. Les mesures ont été effectuées toutes les 150 secondes sur une durée de 1320 secondes.

Ici, les résultats ont montré que le modèle linéaire proposé par Roussel pour percevoir l'évolution du seuil de cisaillement avec le temps, décrit correctement le comportement thixotrope réel des mortiers mesurés à l'aide du pénétromètre à chute libre. Par ailleurs, une relation linéaire raisonnable est trouvée entre les taux de structuration et les variables matérielles. Cependant, toutes les variables n'ont pas la même influence et le même ordre de grandeur sur le taux de structuration du mélange. Précisément, le superplastifiant, le filler calcaire et la teneur en eau, diminuent la structuration à mesure que leur concentration augmente dans le mélange, alors que l'agent de viscosité l'augmente.

En dehors de cela, le comportement rhéologique des matériaux imprimables influence principalement l'intégrité structurelle de l'élément imprimé, en particulier la liaison entre l'acier et le béton. Cette liaison détermine la capacité d'un élément composite à se comporter de manière homogène comme un élément armé conventionnel monolithique. En principe, les propriétés rhéologiques du matériau imprimable affectent la qualité de la liaison générée entre les couches imprimées et les barres d'acier, ce qui à son tour affecte la capacité structurelle et les performances de l'élément lorsqu'il est soumis à des charges appliquées de l'extérieur. Ainsi, la seconde partie de cette thèse traite notamment la qualité de la liaison générée avec l'armature, à travers une série de tests d'arrachement réalisés sur élément imprimé et par rapport à ceux coulés de manière classique. Pour cela, deux techniques d'impression différentes sont adoptées pour produire les éléments imprimés, soit en utilisant une technique manuelle ou une imprimante à portique automatisée à 3 axes. Dans les deux cas, les paramètres variables sont la composition du matériau, les propriétés rhéologiques et thixotropes et la direction des couches par rapport à la barre d'acier, qu'elle soit

parallèle ou perpendiculaire à celle-ci. Précisément, dans le cas d'éléments imprimés manuellement, les objectifs sont d'étudier d'abord l'influence de la maniabilité du matériau et d'autre part, l'effet de la méthode d'impression sur la qualité de la liaison générée avec les barres d'acier. Ainsi, quatre mélanges imprimables différents sont développés, ayant chacun une maniabilité distincte. Ici, le processus d'impression manuel est effectué à l'aide d'un pistolet de laboratoire, simulant le travail effectué par une imprimante réelle. En outre, cinq conditions d'impression différentes sont étudiées au total. Au départ, deux méthodes pour chaque direction d'impression (deux parallèles et deux perpendiculaires) sont effectuées en imprimant directement sur la barre d'acier. Alors que la cinquième condition consiste à insérer la barre d'acier à l'intérieur de l'élément directement après son impression. En ce qui concerne les éléments imprimés produits à l'aide d'une imprimante à portique automatisée à 3 axes, le même cadre de travail est appliqué. Le premier objectif ici est d'étudier en particulier les conséquences qu'entraîne un matériau thixotrope sur la qualité de la liaison générée avec les barres d'acier. Alors que le deuxième objectif est d'identifier l'effet de la direction des couches par rapport à la barre d'acier sur la liaison développée. Cependant, un seul mélange est utilisé pour produire les échantillons imprimés. Le mélange est choisi parmi ceux initialement développés pour l'évaluation rhéologique et thixotropique des mortiers imprimables. Il a un comportement thixotrope très élevé, et il est délibérément sélectionné sur cette base afin de couvrir les résultats les plus néfastes qui pourraient survenir.

Les résultats de cette recherche montrent que la mise en œuvre de barres d'armature classiques, au niveau de l'interface entre les couches successives, est une méthode efficace et pratique pour le renforcement structurel d'éléments en béton imprimés en 3D. De plus, cela confirme que l'incorporation de renfort est capable d'améliorer la résistance globale des composants imprimés en 3D. Par conséquent, ils peuvent être utilisés comme éléments structurels intégraux. Plus précisément, les résultats ont montré que ni les propriétés rhéologiques du matériau imprimable utilisé, ni la direction des couches par rapport aux barres d'acier, n'affectent largement la qualité de la liaison générée entre les couches de béton imprimées et les barres d'acier. Cependant, malgré la méthode d'impression, que ce soit manuellement ou en utilisant l'imprimante à portique à 3 axes, la liaison dans les échantillons moulés de manière conventionnelle domine principalement. Les échantillons moulés offrent une meilleure résistance aux forces d'arrachement que les échantillons imprimés. Cela se produit en raison de la vibration appliquée de l'extérieur, qui n'est pas pratiquée

dans les éléments imprimés. Néanmoins, pour le cas particulier des éléments imprimés utilisant l'imprimante proprement dite, la variation de la qualité de liaison causée par la direction des couches était mieux provoquée. Ici, les échantillons imprimés en parallèle ont surpassé les échantillons imprimés perpendiculairement. Cependant, l'approche d'impression manuelle peut toujours être utilisée comme méthode d'impression représentative pour les études préliminaires.

Enfin, la troisième partie de cette thèse propose une étude expérimentale comparative de la microstructure du matériau entre des échantillons de béton imprimés et non imprimés, ainsi que du comportement des éléments imprimés en 3D lorsqu'ils sont soumis à différentes concentrations d'acide sulfurique. Cette étude montre les conséquences de l'attaque acide sur la structure interne d'un élément imprimé, en particulier la qualité de liaison inter-couches. Ici, trois mélanges différents sont sélectionnés parmi ceux développés au début de cette thèse, et ils ont des compositions et des comportements thixotropes différents. Par ailleurs, les éléments testés sont soumis à différentes concentrations d'acide sulfurique (H_2SO_4), principalement 1% et 3%, pendant 56 jours. Cette évaluation se fait à une échelle macroscopique et microscopique. L'analyse macroscopique est limitée aux inspections à l'œil nu et aux mesures de perte de masse, tandis que l'exploration microscopique consiste en des analyses de porosimétrie par intrusion de mercure (MIP) et de microscopie électronique à balayage (SEM).

Les résultats montrent que la porosité totale ne varie pas entre les conditions imprimées et non imprimées. Cependant, la distribution de la taille des pores et leur morphologie diffèrent largement, elle est plus étendue dans les échantillons imprimés. Ces faits peuvent être attribués à la pression de pompage exercée sur le matériau lors de l'impression. En plus, une forte liaison inter-couches est toujours trouvée tant qu'une bonne combinaison entre les paramètres d'impression est maintenue (pression de pompage vs vitesse d'impression). Ainsi, les éléments imprimés agissent comme des corps monolithiques sans montrer aucune faiblesse due à la superposition des couches. Les spécimens imprimés ont ainsi la même capacité à résister aux attaques chimiques que les spécimens non imprimés. Les couches intermédiaires sont suffisamment résistantes pour interdire la création de voies préférentielles pour l'entrée de produits chimiques à l'intérieur de l'élément.

Influence of the fresh state properties of 3D printable concrete on the steel-concrete bonding and durability

Summary: Currently, the latest technique being introduced to the construction field is known as Additive Manufacturing or 3D printing. Many challenges encounter this technique, notably the fresh and hardened state properties of the cementitious material used for 3D printing; and the reinforcement strategy to provide ductility and tensile capacity for structural elements.

This thesis deals with the effect of the material's fresh state properties on the hardened state and mechanical response of 3D printed elements. Initially, the work has started by formulating new printable mixes and testing their rheological properties; in particular their thixotropic behavior, depending on the material's yield stress variation over a certain period of time. After then, the results were linked to the mechanical and hardened state performance of 3D printed elements. Thus, a better understanding of the effect of certain chemical and mineral admixtures on the thixotropic behavior of the mix was carried out. Then, the relation between the material's rheology and thixotropic behavior with the bond developed between printed layers and reinforcing bars has been exposed, and the effect of the layers direction with respect to the steel bar on the quality of the bond was further assessed. At last, this research includes a microstructural characterization of 3D printed materials, as well as a durability assessment of the printed elements performance when subjected to sulfuric acid attacks.

More precisely, the yield stress evolution so-called thixotropic behavior was measured for different printable mixes over a certain period of time using the fall-cone penetrometer; and the effect of some chemical and mineral additives was considered. Herein, it was found that the material variables influence the structuration rate of the mix, but in different magnitudes. In particular, the addition of HRWR, Limestone filler and water content decrease the structuration rate of the material, whereas VMA increases it. Afterwards, the effect of the material's rheology, printing method and layers direction with respect to steel bar, on the developed link have been studied through a series of pull-out tests done over printed elements made either manually using a laboratory device or using an automated printer. Herein, different mixes with different workabilities and thixotropic behaviors were used. Alongside, concrete layers were printed either parallel or perpendicular to the steel bar. The overall results showed that printed samples were able to develop an acceptable bond strength in comparison with the mold casted specimens. Implicitly, these results indicated first that the manual printing can be considered as a preliminary testing method to simulate the work of an actual printer; second, the material's rheology did not majorly affect the bond with steel bars; third, parallel printed layers to the steel bar can still provide better bonding with it in comparison to that attained by the samples having perpendicular printed layers. As for the microstructural and durability assessment of 3D printed samples, different mixes were used to cover a wider range of material properties. Here, 3D printed samples were exposed to different concentrations of sulfuric acid, and the microstructure of the degraded and non-degraded samples was assessed. The results showed that concrete samples whether printed or not have the same performance when subjected to acid attack. In particular, printed samples did not show any sign of inter-layer weaknesses, neither at a micro nor macro scales. However, the only difference between a printed specimen and a non-printed one is that printed samples have a more spread pore size distribution and morphology, which is caused by printing parameters used.

Influence des propriétés à l'état frais des bétons imprimables sur la liaison acier-béton et sur la durabilité

Résumé: La fabrication additive ou impression 3D est la technique la plus récente introduite dans le secteur de la construction. De nombreuses questions restent posées, notamment la maîtrise des propriétés à l'état frais et durci du matériau utilisé; et la stratégie de renforcement pour fournir la ductilité et les capacités structurelles des éléments.

Cette thèse traite de l'effet des propriétés à l'état frais du matériau sur l'état durci et sur la réponse mécanique des éléments imprimés. Le travail a commencé par la formulation et la caractérisation rhéologique de nouveaux mélanges imprimables. La thixotropie des mortiers, c'est à dire de la variation du seuil de cisaillement au cours du temps, a été particulièrement étudiée et permet une meilleure compréhension de l'effet de certains adjuvants chimiques et minéraux sur la vitesse de structuration du mélange. Ensuite, la relation entre la rhéologie du matériau et la liaison développée avec les armatures a été explorée, en tenant compte de la direction des couches par rapport à la barre sur la qualité de la liaison. Enfin, cette recherche comprend une caractérisation microstructurale des matériaux imprimés, ainsi qu'une évaluation de la durabilité des éléments imprimés lorsqu'ils sont soumis à des attaques d'acide sulfurique.

Plus précisément, l'évolution du seuil de cisaillement a été mesurée pour différents mélanges imprimables sur une certaine période de temps à l'aide du pénétromètre à chute libre; et l'effet de certains additifs chimiques et minéraux a été examiné. Ici, il a été constaté que les paramètres de formulation influencent le taux de structuration du mélange, mais dans des amplitudes différentes. En particulier, l'ajout de superplastifiant, de filler calcaire et l'augmentation du dosage en eau diminuent le taux de structuration du matériau, alors que l'agent de viscosité l'augmente. Ensuite, l'effet de la rhéologie du matériau, de la méthode d'impression et de la direction des couches par rapport à la barre, sur la qualité de la liaison acier/béton imprimé a été étudié à travers des tests d'arrachement sur des éléments imprimés réalisés manuellement ou à l'aide d'une imprimante automatisée. Ici, différents mélanges avec des ouvrabilités et des comportements thixotropes différents ont été utilisés. Des couches parallèles et perpendiculaires à la barre ont été imprimées. Les résultats ont montré que les échantillons imprimés étaient capables de développer une contrainte d'adhérence acceptable par rapport aux échantillons moulés. Ces résultats indiquent également que l'impression manuelle peut être considérée comme une méthode d'essai préliminaire pour simuler le travail d'une imprimante; et que la rhéologie du matériau n'a pas eu d'effet majeur sur la liaison avec les barres. De plus des couches imprimées parallèlement à la barre présentent une meilleure liaison par rapport à celle obtenue pour les échantillons ayant des couches imprimées perpendiculairement. Concernant l'évaluation de la microstructure et de la durabilité des échantillons imprimés, différents mélanges ont été utilisés pour couvrir une large gamme de propriétés des matériaux. Ici, des échantillons imprimés ont été exposés à différentes concentrations d'acide sulfurique et la microstructure des échantillons dégradés et non dégradés a été évaluée. Les résultats ont montré que les échantillons qu'ils soient imprimés ou non, ont les mêmes performances contre une attaque acide. En particulier, les échantillons imprimés n'ont montré aucun signe de faiblesse entre les couches, ni à une échelle micro ni à une échelle macro. La différence majeure entre un échantillon imprimé et un échantillon coulé est que les échantillons imprimés ont une distribution et une morphologie de la taille des pores plus étalées, ce qui est causé par les paramètres d'impression utilisés.